ENTRAINMENT FROM FALLING LIQUID FILMS

J.S. ADAMS, B.E. (Hons.)

A Thesis submitted for the Degree of Doctor of Philosophy in March 1969. The investigation reported was carried out in the Chemical Engineering Department of the University of Adelaide from March 1964 to February 1969.

CONTENTS

SUMMARY

Droplet entrainment in two phase downwards annular flow of air and water in a 1.330 in. bore x 250 in. long tube has been studied. Three pressure levels were used. The air velocity was varied from 0 to 340 ft/sec at 5½ psia, from 0 to 370 ft/sec at 15 psia and from 0 to 160 ft/sec at 45 psia. The water rates ranged from 30 to 3500 lb/hr.

A porous wall injector to produce minimum droplet entrainment and a spray injector to produce maximum droplet entrainment were the two types of liquid injectors used. Droplet mass velocity profiles in the gas core were measured with a 0.075 in. bore traversing sampling probe. These traverses were made at levels 16, 61 and 245 inches below the injector for air velocities from 50 to 200 ft/sec, water flow rates from 300 to 2700 lb/hr and pressure levels of 15 psia and 45 psia. Liquid film flow rate measurements were made with a porous wall liquid extractor. Pressure gradient measurements and liquid volume fraction measurements were carried out as well.

Ciné films of the flow were taken at levels 11, 56 and 235 inches below the injector. From these films the velocities of, and the time intervals between, the disturbance waves were determined.

There was general agreement with the results of the Harwell group for two phase upwards flow. The

equilibrium between the flow of the liquid as droplets in the core and the flow of the liquid in the film on the tube wall was established very slowly. For a porous wall injector equilibrium was reached at the 245 inch level in runs at 50 ft/sec air velocity but not in runs at 100 ft/sec and higher air velocities. Equilibrium was established more quickly when the spray injector was used but the velocity profile was more asymmetrical. Far from the injector the droplet mass velocity profiles showed a maximum at the tube axis.

The experimental pressure gradients were plotted against a homogeneous "reduced" velocity. This permitted pressure gradients obtained at different flow rates and densities to be compared. The experimental frictional pressure gradient was up to twice the equivalent homogeneous pressure gradient at moderate, 100 ft/sec at 0.0712 lb/ft^3, air velocities but approached the homogeneous value at very high air velocities. When the spray injector was used the experimental pressure gradient was generally slightly lower than if the porous wall injector was used at the same flow conditions.

The liquid volume fractions at low gas flow rates were slightly less than predicted by the analysis of Dukler. This was probably because the liquid volume fractions were measured near the bottom of the test-section where the

liquid film flowed as fully developed disturbance waves. Dukler's analysis was based on a smooth liquid film.

The disturbance wave velocities ranged from 4 to 23 ft/sec. Increases in water flow rate, air velocity or air density all caused increases in the disturbance wave velocity. The theory of Hall Taylor and Nedderman (1968) was able to predict the trend of the data on the coalescence of disturbance waves as they travelled between the top two measurement levels.

It is proposed that droplet entrainment may arise from the growth and break-down of ripples near the crests of disturbance waves. This theory is able to predict the right sort of wavelength of the ripples and also to show that very large droplets have higher radial velocities than the smaller droplets which comprise the bulk of the droplet entrainment.

DECLARATION

This thesis contains no material which has been accepted for the award of any other degree or diploma in any University and, to the best of the author's knowledge and belief, the thesis contains no material previously published or written by another person, except where due reference is made in the text.

ACKNOWLEDGEMENT

The author wishes to thank Professor R.W.F. Tait for his supervision of this work and also the members of the Chemical Engineering Department of the University of Adelaide for their assistance. Thanks are also due to my wife and her family for assistance in the tedious task of reading and tabulating the ciné film data and the final typing of this Thesis.

1. INTRODUCTION

This work was begun in 1964 as an extension of work in the Department of Chemical Engineering, University of Adelaide (Messenger, 1964; Clegg, 1966) on heat transfer to falling liquid films which was then nearing completion. Messenger had measured local heat transfer coefficients for falling film evaporation on the outside of a vertical 1 in. O.D. x 18 in. heated length brass tube electrically heated internally by pyrotenax kumanal resistance windings. This tube was mounted in a 1½ in. nominal bore pyrex glass jacket. The test liquids were water, chloroform, methyl alcohol, ethyl alcohol and iso-propyl alcohol. The film flow and the cocurrent vapour flow could be independently varied. Clegg used a 1 in. O.D. electrically self-heated 18/8/Ti austenitic titanium stabilized stainless steel (B.S. Type EN58B) tube of heated length 32.45 in., also in a 1½ in. pyrex glass jacket. He extended Messenger's work on water, measuring both local heat transfer coefficients and pressure gradients. Both of these studies were restricted to the somewhat limited liquid and vapour flow rates for which no entrainment occurred. Hence it was decided that a study of entrainment from falling liquid films with cocurrent gas flow was a logical extension of the current work.

Because of the known similarity (Wallis, 1961) between the hydrodynamic behaviour of two-phase two component flow and film boiling in tubes, that is two-phase single component flow with heat addition, it seemed reasonable to expect that the mechanisms of entrainment formation and deposition and the general characteristics of flow with entrainment would also be related. A two-phase two component non-heated system was chosen in preference to either a two-phase heated or a two-phase unheated single component system because:-

(1) It would be possible to remove a sample of the mixture of gas and entrained droplets in the gas phase core by means of a sampling probe and thus obtain droplet mass velocity profiles. With a single component system condensation would make such a sampling probe unworkable.

(2) The Harwell Chemical Engineering group (Lacey, Hewitt and Collier, 1962) had indicated that a long length of test-section, perhaps up to 1000 diameters from the liquid injection point, was needed to establish equilibrium entrainment. This indicated that a long test section would have to be used; the simplest method would be to use an unheated test-section operating at atmospheric temperature.

(3) It was considered (Lacey, Hewitt and Collier, 1962; Hall Taylor, Hewitt and Lacey, 1963) that entrainment arose from "disturbance" or "roll" waves. This indicated that a transparent test section was required so that these waves could be studied photographically.

Requirements (2) and (3) indicated that as simple a test-section as possible, that is a tube, should be used in preference to the annular test-sections of Messenger and Clegg.

The survey of the literature showed that entrainment in two-phase downwards flow had been neglected in comparison with horizontal flow and upwards or "climbing film" flow in spite of its inherently simpler character. It was well known, see for example Parker and Grosh (1961), that at high gas velocities all these flows, for liquids which wet the tube wall, to which liquids this Thesis is restricted, develop a similar mist-annular character. This is to be expected for at high gas velocities the gravitational forces are small compared with frictional forces and inertia forces. In this flow structure there is a thin wavy liquid film on the tube wall (the annular film) and a core consisting of gas plus entrained liquid droplets.

As the gas velocity is reduced the gravitational forces become important. In horizontal flow the gravitational forces act at right angles to the frictional and inertia forces. At low gas velocities the flow changes to stratified flow where the gas flows above a wavy liquid film or, for high liquid flow rates, bubbly flow in which the gas phase is carried as bubbles in a continuous liquid phase.

In upwards flow the gravitational forces oppose the frictional and inertia forces. As the gas velocity is reduced the waves on the film become more pronounced and the film thickens. With further reduction in the gas velocity the flow gradually changes to slug flow in which the liquid phase is carried up the tube in slugs and the liquid film drains back down the tube between the slugs.

In downwards flow the gravitational forces and the frictional and inertia forces are in the same direction. The annular structure of the flow is retained, except for very high liquid flow rates when bridging across the tube occurs, right down to zero gas velocity.

Because downwards flow retained its annular structure over the whole range of gas velocities it was

expected that the mechanisms for entrainment formation might also remain much the same over this range. This was in contrast to upwards flow where it was known (Levy, 1963) that in the slug flow regime entrainment was probably formed through other mechanisms.

Since it was thought that droplet entrainment was closely linked with "disturbance" waves an important part of the experimental work would be the measurement of disturbance wave velocities and frequencies by means of ciné photography. Hold-up and pressure gradient measurements would also be required. These would be followed by the measurement of droplet mass velocity profiles and liquid film flow rates.

It was already apparent from the extensive work of the Harwell Chemical Engineering Group on upwards flow that further experimental work, such as direct film thickness measurements, would require a great deal more time and resources. Instead it was decided that it would be more fruitful to compare and combine the data obtained with the data of other workers, both for upwards and horizontal flow as well as for downwards flow, and then use this knowledge to attempt to obtain a greater insight into the mechanisms causing the formation and deposition of entrainment in two-phase flow.

2. REVIEW OF PREVIOUS AND RELATED WORK

The scope of this Thesis is such that it is necessary to review work on liquid film flow, both with and without gas flow, on waves, on atomization and on droplet formation as well as on two-phase annular flow itself.

2.1 Liquid Film Flow

The flow of thin liquid films has been extensively studied since the original work of Hopf (1910) and Nusselt (1916). In this review there is only space for an outline and reference should be made to reviews on this subject, such as those of Fulford (1964) and Whitaker (1964), for greater detail.

2.1.1 Smooth laminar film flow

For two dimensional laminar flow of an incompressible liquid film down a vertical flat plate the Navier-Stokes equations become:-

$$\rho_L \left[\frac{\partial u_L}{\partial t} + u_L \frac{\partial u_L}{\partial x} + v_L \frac{\partial u_L}{\partial y} \right] = - \frac{\partial p}{\partial x} + \mu_L \left[\frac{\partial^2 u_L}{\partial x^2} + \frac{\partial^2 u_L}{\partial y^2} \right] + \rho_L g \qquad \ldots\ldots (2.1)$$

$$\rho_L\left[\frac{\partial v_L}{\partial t} + u_L\frac{\partial v_L}{\partial x} + v_L\frac{\partial v_L}{\partial y}\right] = -\frac{\partial p}{\partial y} + \mu_L\left[\frac{\partial^2 v_L}{\partial x^2} + \frac{\partial^2 v_L}{\partial y^2}\right] \quad \ldots\ldots (2.2)$$

where u_L and v_L are the liquid velocities in the x (down the plate) and y directions (perpendicular to the plate) respectively, t is the time, μ_L the liquid viscosity, ρ_L the liquid density, p the pressure and g the acceleration due to gravity.* The flow system is sketched in Fig. 2.1 on page 8. For steady, non-wavy laminar flow, all derivatives with respect to t and x are zero and v_L is zero. In this case the equations reduce to

$$\left.\begin{aligned} 0 &= -\frac{dp}{dx} + \mu_L\frac{d^2u_L}{dy^2} + \rho_L g \\ 0 &= -\frac{dp}{dy} \end{aligned}\right\} \quad \ldots\ldots (2.3)$$

If τ_i is the interfacial shear stress at the free surface and h the liquid film thickness, then at the interface $y = h$ and $\frac{du_L}{dy} = \frac{\tau_i}{\mu_L}$. At the solid wall $y = 0$ and $u = 0$. Integration of equation (2.3) twice with these boundary conditions gives:-

$$u_L = \frac{y}{\mu_L}(h - \frac{y}{2})(-\frac{dp}{dx} + \rho_L g) + \frac{\tau_i y}{\mu_L} \quad \ldots\ldots (2.4)$$

---

* Complete nomenclature is given in Section 7 of this Thesis.

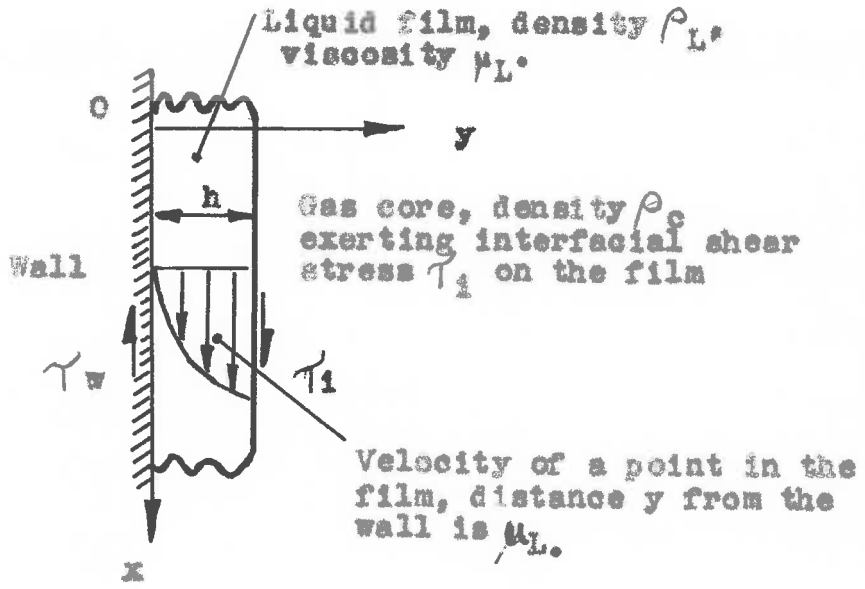

FIGURE 2.1: The Falling Liquid Film.

For axisymmetric flow in a tube equation (2.3) can be used in cylindrical coordinate form. For tube flow a force balance on the core gives:-

$$-\frac{dp}{dx} + \rho_c g = \frac{2\tau_i}{R-h} \qquad \ldots\ldots (2.5)$$

where ρ_c is the core density and R the tube radius. $R = \infty$ is the flat plate case. Substitution of equation (2.5) with $R = \infty$ in equation (2.4) gives:-

$$u_L = \frac{(\rho_L - \rho_c)gy(h - y/2)}{\mu_L} + \frac{\tau_i}{\mu_L} y \qquad \ldots\ldots (2.6)$$

A similar procedure gives the solution for axisymmetric flow:

$$u_L = \frac{1}{\mu_L}\left[(\rho_L-\rho_a)g + \frac{2\tau_i}{R-h}\right]\frac{R^2-r^2}{4} + \frac{(\rho_L-\rho_a)g}{2\mu_L}(R-h)^2 \ln\frac{r}{R} \qquad \ldots\ldots (2.7)$$

where r is the radial coordinate. Substitution of $y = h$ in equation (2.6) or $r = R-h$ in equation (2.7) gives the surface velocity u_{L_i}.

The volume flow rate per unit width of wall, Q_L, is:-

$$Q_L = \int_0^h u_L \, dh \qquad \ldots\ldots (2.8)$$

Substitution in equation (2.6) and integration gives:-

$$Q_L = \frac{(\rho_L-\rho_a)\,g\,h^3}{3\mu_L} + \frac{\tau_i h^2}{2\mu_L} \qquad \ldots\ldots (2.9)$$

Integration of equation (2.7) using $Q_L = \frac{1}{R}\int_{R-h}^{R} ur \, dr$ gives the axisymmetric flow solution:-

$$Q_L = \frac{(\rho_L-\rho_a)g}{16\mu_L R}\left[R^4 - 4R^2(R-h)^2 + 3(R-h)^4 - 4(R-h)^4 \ln\frac{R-h}{R}\right] + \frac{\tau_i h^2(2R-h)^2}{8\mu_L R(R-h)} \qquad \ldots\ldots (2.10)$$

This can be shown to reduce to equation (2.9) at $R = \infty$ by expansion in a series. For a flat plate, the average velocity, $\bar{u}_L = \frac{Q_L}{h}$, hence

$$\bar{u}_L = \frac{(\rho_L - \rho_c)gh^2}{3\mu_L} + \frac{\tau_i h}{2\mu_L} \qquad \ldots\ldots (2.11)$$

Now the wall shear stress, τ_w is given by:-

$$\tau_w = (\rho_L - \rho_c)gh + \tau_i \qquad \ldots\ldots (2.12)$$

Putting $T = \frac{\tau_w}{(\rho_L - \rho_c)gh}$, that is the ratio of the wall shear stress to the net weight of the liquid after allowing for the buoyancy of the core, then for a flat plate, the ratio of surface velocity to average velocity is:-

$$\frac{u_{L_1}}{\bar{u}_L} = \frac{T - \frac{1}{2}}{T/2 - 1/6} \qquad \ldots\ldots (2.13)$$

This ratio lies between 1.5 (for T = 1; free falling film flow) and 2 (for $T \gg 1$).

The flat plate solutions, equations (2.6), (2.9) and (2.11), can be used for flow down a plate inclined at an angle θ to the horizontal by replacing the gravitational factor, g, by its component parallel to the plate, g sin θ. For flow on or in an inclined tube the situation is more complex as the gravitational component normal to the tube axis gives the flow a

tangential component. Flow on a rod at small angles of inclination from the vertical has been studied by Butterworth (1967).

2.1.2 Wavy laminar film flow

The velocity of an infinitesimal disturbance on a laminar film can be found from continuity considerations by the method of Lighthill and Whitham (1955). This method assumes that there are no restoring forces on the disturbance. Consider a small disturbance of height δh above the liquid film moving with a velocity c. Then the change in the film flow rate, δQ_L, as the disturbance passes must equal the flow $c\delta h$ associated with the disturbance. In the limit, therefore,

$$c = \frac{dQ_L}{dh} \qquad \ldots\ldots (2.14)$$

For a laminar film on a flat plate this gives:

$$c = \frac{(\rho_L - \rho_c) g h^2}{\mu_L} + \frac{\tau_i h}{\mu_L} \qquad \ldots\ldots (2.15)$$

Hence the ratio of wave velocity to average velocity

$$c/\bar{u}_L = \frac{T}{T/2 - 1/6} \qquad \ldots\ldots (2.16)$$

This ratio lies between 3 (for $T = 1$) and 2 (for $T \gg 1$). Equation (2.16) was used by Cousins and Hewitt (1968b)

for upwards flow under high shear conditions, that is with $^{c}/\bar{u}_{L} = 2$.

The transition from smooth laminar to wavy laminar flow occurs at very low liquid flow rates for falling film flow on a vertical surface. For free falling film flow different workers have suggested values of Reynolds number N_{Re_L}, defined as $\frac{Q_L \rho_L}{\mu_L}$, between 0 and 7 for the transition. Kapitza (1948) was the first to attempt to explain free falling wavy laminar film flow by means of an oscillatory steady state solution of the equations of motion. He solved equation (2.1), omitting the $v_L \frac{\delta u_L}{\delta y}$ and the $\frac{\delta^2 u_L}{\delta x^2}$ terms. Bushmanov (1960) subsequently solved equation (2.1) with the $v_L \frac{\delta u_L}{\delta y}$ term included. The corrected Kapitza theory in Levich (1959, English translation 1962) gives $^{c}/\bar{u}_{L} = 3$ as a first approximation, in agreement with equation (2.16), and $^{c}/\bar{u}_{L} = 2.4$ when second order terms were included and a condition of minimum viscous energy dissipation applied. The theories of Benjamin (1957) and Hanratty and Hershmann (1961) also predict $^{c}/\bar{u}_{L} = 3$ as limiting cases.

Massot, Irani and Lightfoot (1966) obtained a linearised solution for equations (2.1) and (2.2) by a similar method to that of Kapitza, but including all terms. They were unable to find a linearized solution which satisfied both equations (2.1) and (2.2).

Neglecting the influence of equation (2.2) which was second order in comparison with equation (2.1), they found for a free falling film:-

$$N_{We_L} = \frac{3(3 - {}^{c}/\bar{u}_L)}{({}^{c}/\bar{u}_L - 3/2)(({}^{c}/\bar{u}_L)^2 - \frac{12}{5}({}^{c}/\bar{u}_L) + \frac{6}{5})} \quad \ldots\ldots (2.17)$$

where the Weber number,

$$N_{We_L} = \frac{\bar{u}_L^2 h \rho_L}{\sigma} = \frac{g^2 h^5 \rho_L^3}{9\mu_L^2} = N_{Re_L}^2 \cdot \frac{\mu_L^2}{h\sigma\rho_L} \quad \ldots\ldots (2.18)$$

and σ is the liquid-core interfacial tension. The core density, ρ_c, was assumed to be negligible in comparison with the liquid density, ρ_L. From equation (2.18) it can be seen that N_{We_L} is a strong function of the dimensionless flow rate N_{Re_L} but is also a weaker function of the film thickness at constant flow rate. For small values of N_{We_L}, that is small N_{Re_L} and hence thin films, equation (2.17) predicts ${}^{c}/\bar{u}_L = 3$. For large values of N_{We_L} it predicts ${}^{c}/\bar{u}_L = \frac{6}{5} + \frac{6}{25} = 1.689$, in agreement with the theory of Ishihara *et al.* (1961).

The experimental work reviewed by Fulford indicates that for free falling film flow on a vertical tube ${}^{c}/\bar{u}_L$ approaches 3 for very low Reynolds numbers, $N_{Re_L} \lesssim 10$. As N_{Re_L} is increased ${}^{c}/\bar{u}_L$ decreases to

about 1.7 at N_{Re_L} = 100. At higher Reynolds numbers $^{c}/\bar{u}_L$ increases again, however at these values of N_{Re_L} the flow is beginning to change to turbulent flow.

2.1.3 The visual appearance of film flow

Fulford cites the work of many investigators which show that as the Reynolds number is increased laminar wavy film flow changes gradually into turbulent wavy film flow. The transition begins, for a free falling film on a vertical flat plate, at N_{Re_L} from 250 to 400 and is complete at $N_{Re_L} \approx 800$. He sums up the general observations of free falling film flow as follows: 'At very low flow rates the film surface is completely smooth and mirror-like, troubled only occasionally by small random "dimples", which are rapidly damped out in the direction of flow of the film. At slightly larger Reynolds numbers, small, symmetrical, regular waves appear. The wave fronts are almost straight and perpendicular to the direction of flow. At still larger flow rates, the regular symmetrical waves tend to become less regular, and the cross section of the wave assumes the non-symmetrical shape usually described as a "roll" wave (Dressler, 1949) with a steep front and a long gently sloping tail. Frequently each roll wave is preceded by a number of small waves (termed "push" waves by Brauer

(1956)) which move as a group with the main wave. In this zone of flow the wave fronts are no longer straight at all times but show a tendency to form bulges or to split or overtake each other. ... As the liquid flow rate is increased a stage is reached when the main waves and their accompanying push waves have become so randomly mixed that the individual wave fronts can scarcely be distinguished and the surface appears to be covered with a mass of small jagged "turbulent" waves.'

2.1.4 The film thickness of free falling liquid films

Equation (2.9) can be written in dimensionless form by multiplying both sides by $\frac{\rho_L}{\mu_L}$. This gives, for a free falling film,

$$(3\,N_{Re_L})^{\frac{1}{3}} = h\left(\frac{g\rho_L^2}{\mu_L^2}\right)^{\frac{1}{3}} \left(\frac{\rho_L - \rho_g}{\rho_L}\right)^{\frac{1}{3}} \qquad \ldots\ldots (2.19)$$

Dukler (1959) termed the group on the right hand side the Nusselt film thickness parameter N_T. General conclusions which can be drawn from Fulford's review are:-

(1) The Nusselt equations (2.12 or 2.18) correctly predict the film thickness for smooth laminar flow. Indeed, the stereoscopic photography studies of small air bubbles in the film by Wilkes and Nedderman (1962) showed that the velocity profile was semi-parabolic, as

predicted by equation (2.6) with $\tau_i = 0$.

(2) For wavy laminar films the measurements of Portalski (1960, 1963, 1964) indicated that the mean thickness of a wavy film was 0.94 of the value predicted by the Nusselt equations. This was in agreement with the Kapitza theory which predicted a ratio of 0.93. The Kapitza theory is probably valid for Reynolds numbers up to 50.

(3) For turbulent film flow the experimental data are well fitted by the Brötz (1954) equation:

$$N_T = (3\ N_{Re_L}^2 / 590)^{\frac{1}{3}} \qquad \ldots\ldots (2.20)$$

Thus it can be seen that the exponent on N_{Re_L} increases from the theoretically predicted $^1/_3$ in the smooth laminar flow regime to $^2/_3$ in the turbulent flow regime.

2.1.5 Turbulent falling liquid films

The available theories of turbulent falling film flow neglect the wavy nature of the flow and obtain solutions for the case of smooth turbulent flow. An early approach is that of Levich (1948, and also in English in "Physico-Chemical Hydrodynamics", 1962) who deduced that for free falling film flow all turbulence must decrease to zero at the free surface. This led to

an expression for the average velocity,

$$\bar{u}_L = \left[\frac{gh}{K_1}\right]^{\frac{1}{2}} \ln\left\{\frac{\rho_L h}{u_L}\left[\frac{gh}{K_1}\right]^{\frac{1}{2}}\right\} \qquad \text{.....(2.21)}$$

where K_1 is a constant, whose value was not specified.

The fact that film flow undergoes a laminar-turbulent transition with increasing Reynolds number in a somewhat analogous manner to single phase full pipe flow suggests that the eddy diffusivity distribution and the velocity profile in turbulent film flow and in turbulent single phase pipe flow are also similar. That is, turbulent film flow, like turbulent single phase pipe flow, can be thought of as having a region of laminar flow near the solid wall, then a buffer region, then a region of turbulent flow far from the wall. Perhaps the most important of the analyses to date based upon this analogy is that originally proposed by Dukler and Bergelin (1952) and subsequently improved by Dukler (1959, 1960, 1961). This analysis allows for the effects of interfacial shear due to flow of the core, and, in addition, calculates heat transfer coefficients by assuming that the thermal eddy diffusivity, ϵ_H, and the momentum eddy diffusivity, ϵ, are equal. Hewitt (1961) subsequently applied Dukler's analysis to climbing film flow. Dukler's method has been used in this Department

by both Messenger (1964) and Clegg (1966) in their analyses of their results.

Near the wall, for $y^+ \lesssim 20$, Dukler used Deissler's (1950) expression for eddy diffusivity,

$$\epsilon = \epsilon_H = n^2 u_L y \left[1 - \exp\left(\frac{-n^2 u_L y \rho_L}{\mu_L}\right)\right] \quad \ldots\ldots (2.22)$$

For $y^+ > 20$ he used the von Kármán equation

$$\epsilon = \epsilon_H = \chi^2 \left|\frac{(du_L/dy)^3}{(d^2u_L/dy^2)^2}\right| \quad \ldots\ldots (2.23)$$

where y is the distance of a point in the film from the solid wall, and the dimensionless distance $y^+ = \frac{y u_L^* \rho_L}{\mu_L}$. The friction velocity $u_L^* = \sqrt{\frac{\tau_w}{\rho_L}}$, τ_w being the shear stress at the solid wall. Dukler used the same values of n and χ as had been suggested for single phase full pipe flow. He pointed out that this put a severe test on the Deissler expression, for even at Reynolds numbers many times greater than the laminar-turbulent transition Reynolds number the liquid film may still be very thin. Hence the wall region $0 \leqslant y^+ \leqslant 20$ can be a large fraction of the total film thickness. In dimensionless form equation (2.22) becomes:-

$$\frac{\epsilon \rho_L}{\mu_L} = \frac{\epsilon_H \rho_L}{\mu_L} = n^2 u_L^+ y^+ \left[1 - \exp(-n^2 u_L^+ y^+)\right] \quad \ldots\ldots (2.24)$$

where $u_L^+ = \frac{u_L}{u_*}$.

The shear stress, τ, at any point in the film depends on the combined effects of liquid viscosity and liquid turbulence, viz:-

$$\tau = (\mu_L + \epsilon \rho_L) \frac{du_L}{dy} \qquad \ldots\ldots\ldots\ldots(2.25)$$

In dimensionless form this is:-

$$\frac{\tau}{\tau_w} = \left(1 + \frac{\epsilon \rho_L}{\mu_L}\right) \frac{du_L^+}{dy^+} \qquad \ldots\ldots\ldots\ldots(2.26)$$

Now, τ is the wall shear stress, τ_w, minus the weight of the film between the wall and the point. Ignoring curvature of the wall this is a linear function of y, viz:-

$$\tau = \tau_w - (\rho_L - \rho_c) gy \qquad \ldots\ldots\ldots\ldots(2.27)$$

In ratio form this gives a linear function for y^+ :-

$$\frac{\tau}{\tau_w} = 1 - \frac{(\rho_L - \rho_c) gh}{\tau_w} \cdot \frac{y}{h} = 1 - \frac{s^3 y^+}{\eta} \qquad \ldots\ldots(2.28)$$

where $\eta = \frac{hu_L^* \rho_L}{\mu_L} = \frac{h\sqrt{\tau_w \rho_L}}{\mu_L}$, that is η is the value of y^+ at the free surface, and $s = \left[\frac{(\rho_L - \rho_c) gh}{\tau_w}\right]^{\frac{1}{3}} \approx \left[\frac{\rho_L gh}{\tau_w}\right]^{\frac{1}{3}}$ if $\rho_c \ll \rho_L$. Also, since for flow on a flat plate

equation (2.27) gives $\tau_i = \tau_w - (\rho_L - \rho_c)gh$, it follows that s^3 is related to the dimensionless ratio T used in equations (2.13) and (2.16) by

$$s^3 = \frac{1}{T} \qquad \ldots\ldots (2.29)$$

By substituting equations (2.24) and (2.28) into (2.26) Dukler obtained a non-linear equation, valid for the region $0 < y^+ \leqslant 20$, which he solved numerically on a computer obtaining graphs of u_L^+ versus y^+ for values $\frac{s^3}{\eta}$ from 1.0 to 0.000001. For the turbulent zone $y^+ > 20$, equation (2.23) in dimensionless form was used instead of equation (2.24).

η depends on the Reynolds number of the flow, since, ignoring curvature of the wall,

$$N_{Re_L} = \frac{\rho_L}{\mu_L} Q_L = \frac{\rho_L}{\mu_L} \int_0^h u_L \, dy = \int_0^{\eta} u_L^+ \, dy^+ \qquad \ldots\ldots (2.30)$$

At the liquid-core interface equation (2.28) gives:-

$$s^3 + \frac{\tau_i}{\tau_w} - 1 = 0 \qquad \ldots\ldots (2.31)$$

Combining the expressions for η and s so as to eliminate h gives $\eta = \frac{\tau_w^{3/2} s^3}{\rho_L^{\frac{1}{2}} g \mu_L}$. Substituting for τ_w from this expression and $\tau_i = \frac{R}{2}(-\frac{dp}{dx})$ from equation (2.5) [this

assumes $R-h \approx R$ and $\rho_G \ll \rho_L$] gives:-

$$s^3 + \frac{\beta}{\eta^{2/3}} s^2 - 1 = 0 \qquad \ldots\ldots (2.32)$$

where $$\beta = \frac{\tau_1}{(\rho_L g^2 \mu_L^2)^{\frac{1}{3}}} = \frac{R(-\frac{dp}{dx})}{2(\rho_L g^2 \mu_L^2)^{\frac{1}{3}}} \qquad \ldots\ldots (2.33)$$

By using equations (2.32), (2.33) and (2.30) Dukler was able to evaluate $\frac{s^3}{\eta}$ in terms of the pressure gradient and the liquid Reynolds number.

For small values of N_{Re_L} η approaches 0 and Dukler's equations (2.26 plus 2.28) can be integrated directly to give the laminar flow solution, equation (2.9). For free falling film flow, that is for $s = 1$, in spite of ignoring the wavy nature of the flow, the Dukler analysis predicts values of N_T close to the experimentally measured values up to $N_{Re_L} = 3000$. At very high Reynolds numbers the predicted values of N_T are too low. N_T has been defined in Section 2.1.4 (p 15).

However, it should be noted that the Dukler analysis has neglected the disturbance waves. These waves require a long flow section to grow to maturity. Hence N_T should decrease with increasing distance below the point of liquid injection.

Levy (1966) has suggested that the shear stress in the liquid film is due mainly to momentum transfer

by means of gas-liquid interfacial shear rather than momentum transfer through the interchange of droplets between the gas core and the liquid film.

Wicks (1967) has pointed out that the Dukler analysis has an allowance for the effect of the wavy interface in the pressure gradient term β. β depends on the total pressure gradient which includes the effect of the interfacial waves. Hence, if the transport properties of the liquid film, such as momentum and heat transfer, depend on the total pressure gradient then the Dukler analysis would be expected to predict the correct values of these properties regardless of whether the waves are present or not.

It should be noted that a later publication of Deissler (1955) gives $y^+ = 26$ rather than $y^+ = 20$ as the change over point from the Deissler to the von Kármán profile. Lee (1964) has modified the Dukler analysis to allow for the discontinuity in eddy diffusivities at $y^+ = 20$. Both these corrections are minor.

Anderson and Mantzouranis (1960a) used an improved form for equation (2.30) which allowed for curvature of the wall, viz:-

$$N_{Re_L} = \int_0^{\eta} \left(1 - \frac{y}{R}\right) u_L^+ \, dy^+ = \int_0^{\eta} \left(1 - \frac{\mu_L y^+}{R\sqrt{\tau_w \rho_L}}\right) u_L^+ \, dy^+$$

By using equation (2.34), together with the von Kármán (1939) universal velocity distribution, they obtained

graphs of η versus N_{ReL} with $\frac{\mu_L}{R\sqrt{\tau_w \rho_L}}$ as a parameter. They did not allow for any variation in shear stress across the film and for this reason their analysis is less accurate than that of Dukler. If the film is in laminar flow, then $u_L^+ = y^+$, and equation (2.34) can be integrated directly to give, ignoring curvature:-

$$N_{ReL} = \frac{1}{2}\eta^2$$

i.e. $$\Theta_L = \frac{\tau_w h^2}{2\mu_L} \qquad \ldots\ldots (2.35)$$

Dividing the correct equation, equation (2.9), by equation (2.35) gives a correction ratio which can be applied to the Anderson and Mantzouranis curves. This was done by Collier and Hewitt (1961) who applied the laminar correction ratio even to turbulent films. They used a similar procedure with the Calvert and Williams (1955) analysis, another analysis which neglected the shear stress variation across the liquid film.

2.2 Disturbance Waves

The waves described in the part of the previous section dealing with wavy laminar films are closely spaced ripples ($^1/_4$ - 2 inches apart) moving at a relatively low velocity. Another type of wave structure,

commonly termed disturbance waves, consists of waves up to several feet apart moving at higher velocities mostly in the range 4-15 ft/second.

Hall Taylor, Hewitt and Lacey (1963) carried out a photographic study of disturbance waves for upwards flow of air and water in a 22 ft. long x $1\frac{1}{4}$ inch bore vertical Perspex tube with the water injected through a porous section in the tube wall. For the annular flow regime they found that the character of the flow passed through several transitions as the water rate was increased, these transitions being independent of moderate changes in air rate.

At low water rates the tube "dewetted", that is the water failed to wet the whole tube surface and patches of rippling liquid film were interspersed with sections in which the water flowed as rivulets. At higher water rates the whole tube was wetted with a rippling liquid film.

As the water flow rate was increased further they found that pulses of disturbance waves began to appear in the film at values of the non-dimensional film thickness $\eta \simeq 12$. When $\eta \approx 18$ the rippling liquid film flow had entirely changed over to disturbance wave

flow. They pointed out that the work of Wicks and Dukler (1960) had indicated that there was a critical value of $\eta \simeq 16\text{-}18$ below which very little droplet entrainment into the gas stream occurred, and suggested that this showed that disturbance waves could well be a major source of droplet entrainment.

This was confirmed by the high speed ciné films of Cooper, Hewitt and Pinchin (1964). They found that the milky visual appearance of disturbance waves was due to their surface being covered with closely spaced ripples which scattered the incident light. The region between the disturbance waves was comparatively quiescent with few ripples. They found that droplets appeared to be entrained from the tips of the disturbance waves; the smaller droplets diffused into the gas core, whereas some of the larger ones fell back into the liquid film. Such droplet impingements gave rise to a circular ripple pattern travelling with and immediately preceding each disturbance wave. Wallis (1966) reached similar conclusions from a photographic study of cocurrent downwards air-water flow in an annulus with a $1\frac{1}{4}$ in. O.D. inner tube and a 4 in. bore outer tube, the water flow being on the outside of the inner tube. He also found that the disturbance waves had a steep front and a long gently sloping tail, the same shape as that which had

been found by Hanratty and Hershmann (1961) for horizontal cocurrent flow.

Nedderman and Shearer (1963) used a similar test-section to that of Hall Taylor, Hewitt and Lacey, but found that the transition point from "dewetted" to fully wetted flow was as much as a factor of 2 lower. They suggested that dewetting was due to the nature of the liquid-solid interface and to the state of cleanliness of the whole apparatus. Different values were found for the transition point depending on whether the water flow rate was being increased or decreased.

Nedderman and Shearer also found that the flow changed directly from the ripple flow regime to the disturbance wave regime without any intermediate pulse flow regime. They attributed this difference to the longer air calming length before the liquid injector in their apparatus. At high air flow rates this transition occurred at a constant water rate independent of small changes in air rate. This finding was in agreement with Hall Taylor, Hewitt and Lacey and also with Knuth (1954) who studied horizontal flow.

More extensive studies by Shearer (1964) and Hall Taylor and Nedderman (1968) have shown that the onset of disturbance waves is a function of the gas rate.

For the air-water system the onset occurred at $N_{Re_L} = 20$ corresponding to $\eta \approx 6.5$ for $N_{Re_G} = \frac{D \bar{u}_{Gs} \rho_G}{\mu_G} = 20000$ increasing to $N_{Re_L} = 75$ corresponding to $\eta \approx 13$ for $N_{Re_G} \geq 120000$. $\bar{u}_{Gs}$ is the gas superficial velocity. The same curve fitted the data from 0.625 in., 1.0 in. and 1.25 in. diameter tubes.

Hall Taylor and Nedderman found that the addition of the surface active agent Teepol to the water to reduce the surface tension to 35 dynes/cm. had little effect on the liquid Reynolds number for wave inception. However, the liquid viscosity had a marked effect. Using aqueous sucrose solutions they found that a 20 fold increase in viscosity compared with tap water resulted in a 5 fold increase in the liquid flow rate necessary for wave inception at $N_{Re_G} = 100000$. Lesser increases in viscosity required lesser increases in liquid flow rate.

2.2.1 Disturbance wave velocities

Hall Taylor, Hewitt and Lacey found that for higher water flow rates the wave velocity was independent of the water flow rate and increased at a decreasing rate as the air flow rate was increased. Shearer (1964) found that data from 0.625 in. and 1.25 in. tubes lay close to a common curve when he plotted the

wave velocity x tube diameter product versus Q_L, the liquid flow rate per unit perimeter of tube. Different curves were obtained at different air Reynolds numbers. Hall Taylor and Nedderman found that these curves also fitted their steam-water data. Nedderman and Shearer suggested that at a fixed water rate the mean wave velocity, $\bar{v}$, was approximately proportional to the square root of the air velocity relative to the waves. Hall Taylor and Nedderman found that the standard deviations of all their sets of velocity measurements in a 1.0 inch tube were about the same, and were independent of the variation in mean velocity from set to set.

2.2.2 Disturbance wave frequencies

Hall Taylor, Hewitt and Lacey (1963) and Wallis (1966) found that at a fixed air rate the frequency was approximately proportional to the water rate thus indicating that each wave transported about the same amount of water. However, Nedderman and Shearer found that this relationship did not hold over a wider range of flow rates.

Because of the variations in wave velocities as the waves move along the flow channel, they can approach one another and coalesce. This coalescence of

waves means that the frequency decreases with the distance from the injector, at first rapidly and then more slowly. Hall Taylor and Nedderman (1968) made extensive measurements of wave frequencies in the first few feet after the injector using electrical conductance probes to detect the waves. In their analysis they postulated that the waves leave the injector at equal intervals of time and that their velocities are normally distributed with a standard deviation Σ. They assumed that when the waves coincided they coalesced. Their final equation can be rearranged to show that the increase in the mean separation time between the waves at a distance ℓ downstream from the injector and the waves at the injector, $(\Delta t)_\ell - (\Delta t)_{inj}$, is equal to $\sqrt{\frac{8}{\pi}} \frac{\Sigma \ell}{\bar{v}^2}$. The mean separation time is the reciprocal of the frequency. They could not measure Σ near the injector. The value of Σ obtained from the velocity measurements further downstream had to be increased from the measured 0.485 ft/second to 0.67 ft/second to fit the frequency data.

Far from the injector Hall Taylor, Hewitt and Lacey (1963), Nedderman and Shearer (1963), and Hall Taylor and Nedderman (1968) all found evidence for preferred separation distances between the waves. This would tend to stabilize the waves and prevent further coalescence.

Instantaneous values of film thickness can be obtained by measuring the electrical resistance of the film between two electrodes set in the wall. This resistance is a non-linear function of the film thickness and the shape of the interface. The mathematics involved in converting the resistance measurement into a film thickness has been discussed by Wicks (1967). In his experimental work Wicks used an analyzer which could indicate both the frequency and the fraction of the total time that the film thickness exceeded any chosen value.

His wave crossing frequency versus film thickness curves show a steep rise, particularly at the higher air flow rates. This suggests that the waves move on a thin liquid film of relatively constant thickness. The frequency rises to a maximum, the value of which is a strong function of gas rate and then decreases at larger film thicknesses. His probability versus thickness curves show that the wave height can be up to 10 times the minimum film thickness.

2.3 Droplet Formation

It has already been pointed out that droplet formation or a great part of it is somehow associated with the disturbance waves. This section reviews

first, mechanisms of droplet formation and second, the available knowledge of droplet formation in two phase flow.

2.3.1 Mechanisms of droplet formation

The classical investigation of the break-up of liquid jets was by Rayleigh (1879). He found that the break-up of an inviscid liquid jet, that is a jet with negligible viscosity, begins when its length exceeds its circumference. Subsequently, Haenlein (1931) distinguished four regions of jet disintegration with increasing jet velocity. At low jet velocities, break-up occurs from dilatational waves, that is periodic oscillations in jet diameter. He confirmed Weber's (1931) theoretical prediction that the life of a jet before it broke up was independent of its velocity, that is the jet length is proportional to its velocity. These oscillations are due to the interaction of small disturbances and surface tension forces.

In the second region aerodynamic forces assist the break-up and the jet length does not increase linearly with velocity. In the third region the jet length is relatively constant but it has a periodic lateral sinuous motion. Aerodynamic forces are more important than surface tension forces. In the fourth

region high jet velocities cause the jet to break up as it leaves the nozzle.

The mechanism of the break-up of liquid sheets like the break-up of liquid jets depends on the relative magnitudes of surface tension, liquid inertia and aerodynamic forces. The theoretical expression of Squire (1953) for the exponential growth factor B of waves on a two dimensional liquid sheet moving at uniform velocity $\bar{u}_L$ through a stationary gas can be rearranged in the form:-

$$B = \frac{N\left[\frac{\sigma}{\rho_G h}\coth\frac{Nh}{2}\right]^{\frac{1}{2}}\left[N_{We_L} - Nh\left(\frac{\rho_L}{\rho_G} + \coth\frac{Nh}{2}\right)\right]^{\frac{1}{2}}}{\frac{\rho_L}{\rho_G} + \coth\frac{Nh}{2}} \qquad \ldots\ldots\ldots(2.36)$$

where B is in units of time $^{-1}$, N is the wave number $= \frac{2\pi}{\lambda}$ where λ is the wavelength, h is the film thickness and $N_{We_L} = \frac{h\bar{u}_L^2\rho_L}{\sigma}$ is the usual form of Weber number.

Equation (2.36) is valid if B is zero or positive; this is so if

$$N_{We_L} \geq Nh\left(\frac{\rho_L}{\rho_G} + \coth\frac{Nh}{2}\right) \qquad \ldots\ldots(2.37)$$

York, Stubbs and Tek (1953) made a similar analysis to that of Squire. Unlike Squire who considered symmetrical oscillations, that is waves in phase, on both sides of the liquid sheet, they considered waves on one side of the sheet only. Their expression for the growth factor can be put in a

form similar to equation (2.36) except that coth $\frac{Nh}{2}$ is everywhere replaced by tanh Nh.

The key growth expression is equation (2.37). If $N_{We_L} < Nh(\frac{\rho_L}{\rho_G} + \coth\frac{Nh}{2})$ wave growth does not occur, in fact the wave amplitude oscillates harmonically with time.

If $N_{We_L} = Nh(\frac{\rho_L}{\rho_G} + \coth\frac{Nh}{2})$, the wave amplitude increases linearly with time and if

$N_{We_L} > Nh(\frac{\rho_L}{\rho_G} + \coth\frac{Nh}{2})$, it increases exponentially with time.

If Nh is fairly small so that $\coth\frac{Nh}{2} \sim \frac{2}{Nh}$ and $\rho_G \ll \rho_L$ so that $\frac{\rho_L}{\rho_G} + \coth\frac{Nh}{2} \sim \frac{\rho_L}{\rho_G}$ equation (2.36) simplifies to:- $$B = \left[\frac{2N}{h\rho_L}\right]^{\frac{1}{2}}\left[\rho_G \bar{u}_L^2 - N\sigma\right]^{\frac{1}{2}} \quad \ldots\ldots\ldots(2.38)$$

The condition B=0 gives the maximum unstable wave number

$$N_{max} = \frac{\rho_G \bar{u}_L^2}{\sigma} \quad \ldots\ldots\ldots(2.39)$$

Differentiation of equation (2.38) gives the wave number for the maximum growth rate:- $$N_{opt} = \tfrac{1}{2} N_{max} \quad \ldots\ldots\ldots(2.40)$$

If the theory of York, Stubbs and Tek is used a different expression arises in place of equation (2.38) and although equation (2.39) remains the same the condition for maximum growth becomes:-

$$N_{opt} = \tfrac{3}{4} N_{max} \quad \ldots\ldots\ldots(2.41)$$

Hagerty and Shea (1955) considered both sides of the liquid sheet. When the disturbances on the two sides are out of phase by 180° a dilatational or symmetric wave forms; when they are in phase a sinuous or anti-symmetric wave forms.

Dombrowski, Hasson and Ward (1960) studied the spray pattern produced by a rectangular orifice fan nozzle. They found that the streamlines were straight and that the liquid velocity along a streamline was constant for given spray conditions and independent of liquid viscosity. The sheet thickness, h, was inversely proportional to the distance from the orifice, r. That is:-

$$K_2 = hr \qquad \ldots\ldots (2.42)$$

At low nozzle pressures the sheet thickness was a function of both the surface tension, σ, and a parameter proportional to $\sqrt{p_{inj}/\rho_L}$, where p_{inj} was the injector pressure. At high pressures it was unaffected by surface tension but still a function of $\sqrt{p_{inj}/\rho_L}$.

In a theoretical analysis of a fan spray which was an extension of the method of Squire (1953), Fraser, Eisenklam, Dombrowski and Hasson (1962) showed that if the most unstable wave length, λ_{opt}, caused the waves to

break into ligaments with a spacing of $\frac{1}{2}\lambda_{opt}$ which subsequently broke into equal sized droplets by the Rayleigh process for the break up of jets then the droplet size was given by:-

$$d = \text{const} \sqrt{\lambda_{opt} h_{br}} \qquad \ldots\ldots\ldots(2.43)$$

where h_{br} is the thickness of the liquid sheet at break up. They found that h_{br} was given by:-

$$h_{br}^3 = \frac{K_2^2 \rho_G^2 \bar{u}_L^2}{2\mathcal{E}^2 \rho_L \sigma} \qquad \ldots\ldots\ldots(2.44)$$

where $\mathcal{E} = \ln \frac{\text{wave amplitude at break up point}}{\text{wave amplitude at the orifice}}$ and is approximately constant for a given orifice. Substitution of equations (2.39), (2.40) and (2.44) into (2.43) gave:-

$$d = \text{cons} \left[\frac{\rho_L}{\rho_G}\right]^{\frac{1}{6}} \left[\frac{\sigma}{\rho_L \bar{u}_L^2}\right]^{\frac{1}{3}} \qquad \ldots\ldots\ldots(2.45)$$

since $\rho_L \bar{u}_L^2$ is proportional to the nozzle pressure it followed that d was inversely proportional to the cube root of the nozzle pressure. Nelson and Stevens (1963) in an experimental study of the droplets produced by swirl type spray nozzles showed that the droplet volumes were normally distributed.

In their study of atomization from spinning cups Fraser, Dombrowski and Routley (1963) observed both sinuous and dilatational waves. They observed two

mechanisms of disintegration:-

(1) At low speeds the sheet of liquid extended to form a thick rim which surface tension forces broke into irregular threads and thence into droplets.

(2) At high speeds aerodynamic forces controlled. Half wave lengths were torn off. These subsequently contracted to threads and thence into droplets.

2.3.2 Droplet break up in a gas stream

Hinze (1955) studied the break up of a liquid droplet in a fluid stream. He found that break up occurred when the droplet Weber number, $N_{We_d} = \frac{\rho_G u_G^2 d}{\sigma}$, exceeded a critical value. In the definition of droplet Weber number, ρ_G is the fluid density and u_G the local free stream velocity. The value of $(N_{We_d})_{crit}$ depended on the type of deformation and on the flow pattern around the droplet. For break up in a gas stream $(N_{We_d})_{crit}$ varied between 13 and ∞ depending on the way in which the relative velocity between the gas stream and the droplet varied with time and on a viscosity number, $N_{Vi} = \frac{\mu_L}{\sqrt{\rho_L \sigma d}}$. The lowest value of 13 is obtained for the sudden shock case and $N_{Vi} = 0$. Haas (1964) used two high speed ciné cameras 90° apart to obtain simultaneous photographs of mercury droplets

suddenly exposed to a high velocity air stream. In this system N_{V_l} is very small. He obtained $(N_{We_d})_{crit}$ = 11.2 in reasonable agreement with Hinze's theory.

2.3.3 The formation of droplets in two phase gas-liquid flow

Most of the studies on annular two phase gas-liquid flow with entrained droplets in the gas stream have looked at the overall system in which droplets are simultaneously being entrained from the liquid film into the gas core and redeposited back from the gas core into the liquid film. It is only recently that these two effects have been investigated separately.

Anderson and Mantzouranis (1960b) used a probe method to measure droplet entrainment for air-water flow up a 0.5 in. diameter vertical pipe. For their range of annular flow conditions they found experimentally that the droplet mass flow rate was proportional to the gas mass flow rate to the 2.6th power at a constant liquid mass flow rate and to the liquid rate to the 1.5th power at a constant gas rate.

Wicks and Dukler (1960) studied droplet entrainment in 1.025 inch and 2.945 inch diameter horizontal tubes using a fixed large diameter sampling probe. In their analysis they proposed that transport of entrained

liquid droplets by the gas core was analogous to the transfer of momentum, that is the pressure gradient, in the gas core. Martinelli and Lockhart (1949) had correlated the ratio of the two phase pressure gradient to the single phase pressure gradient. They found

$$\phi_G^2 = \frac{\left(-\frac{dp}{dx}\right)_{\text{two phase}}}{\left(-\frac{dp}{dx}\right)_{\substack{\text{gas alone at the same flow rate} \\ \text{as in the two phase flow}}}}$$

was a function of

$$X^2 = \frac{\left(-\frac{dp}{dx}\right)_{\substack{\text{liquid alone at the same flow rate} \\ \text{as in the two phase flow}}}}{\left(-\frac{dp}{dx}\right)_{\substack{\text{gas alone at the same flow rate as} \\ \text{in the two phase flow.}}}}$$

Wicks and Dukler suggested that

$$\psi_G^2 = \frac{\text{Droplet transport rate in two phase flow}}{\text{Mass transfer rate in single phase gas flow}}$$

was also a function of X^2. They suggested that the droplet transport rate depended on the droplet concentration in the core and a critical droplet Weber number, the Weber number being defined in terms of the relative gas and liquid velocity, $N_{We_d} = \frac{\rho_G(u_G-u_L)^2 d}{\sigma}$. They used Hinze's criterion for sudden shock injection of liquid into a gas stream, that is $(N_{We_d})_{crit} = 13$.

They use $(N_{We_d})_{crit} = 22$ for gentle injection of liquid.

They suggested that the single phase mass transfer rate was proportional to the pressure gradient, $(-\frac{dp}{dx})_G$, for gas flowing alone at the same flow rate. Hence they found that the dimensional droplet entrainment parameter, Γ, where

$$\Gamma = \frac{(N_{We_d})_{crit} \; E \; V_L}{(-\frac{dp}{dx})_G \; V_G} \qquad \ldots\ldots\ldots\ldots\ldots\ldots\ldots\ldots(2.46)$$

should be a function of X^2. In equation (2.46) E is the fractional entrainment, that is the fraction of the total liquid flow present as droplets in the gas core. V_L and V_G are the respective liquid and gas volume flow rates.

Collier and Hewitt (1961) applied the analysis of Wicks and Dukler to the data of Bennett and Thornton (1961) and found qualitative agreement over the range of X^2 for which Wicks and Dukler had obtained their data. They pointed out that Wicks and Dukler's analysis applied to droplet formation only, whereas E is based on net entrainment, that is it depends on the total effect of droplet formation and deposition. For high gas and liquid flow rates the liquid film flow rate was independent of the total liquid rate and inversely proportional to the gas flow rate. Their correlation, valid for $X > 0.08$, was:-

$$X = 0.069 \, \Gamma^{0.39} \qquad \ldots\ldots\ldots\ldots\ldots\ldots(2.47)$$

Subsequently, Gill, Hewitt and Lacey (1965) found that equation (2.47) was valid for liquid films with a non-dimensional film thickness $\eta > 16\text{-}18$. For $\eta < 16\text{-}18$,

$$X = \text{const.} \Gamma^{0.16} \qquad \ldots\ldots (2.48)$$

and the value of the constant depended on the actual value of X at the changeover point. They suggested that this changeover represented the point of inception of disturbance waves. Equations (2.47) and (2.48) successfully correlated data from both an annular slot liquid injector (using $(N_{We_d})_{crit} = 22$) and a multiple jet liquid injector (using $(N_{We_d})_{crit} = 13$). They pointed out that the correlation was only valid for air-water systems.

Charvonia (1959) suggested as a lower limit, below which droplet formation will not occur, that the liquid film should at least be partially turbulent, and as an upper limit that droplet formation must occur when the liquid film thickness reaches the thickness of the gas phase buffer layer.

If the turbulence sets in when the film is thicker than the laminar sub-layer, that is $\eta = \frac{h\, u^* \rho_L}{\mu_L} = 5$, then by substitution in equation (2.9),

$$N_{Re_L} = \frac{Q_L \rho_L}{\mu_L} = 25\left[\frac{1}{2} - \frac{1}{6}\frac{\rho_L g h}{\tau_w}\right] \qquad \ldots\ldots (2.49)$$

For large τ_w, that is $\frac{\rho_L g h}{\tau_w} \approx 0$, this means that turbulence sets in at $N_{Re_L} = 12.5$. Probably more realistic would be that appreciable turbulence sets in at $\eta = 8$ corresponding to $N_{Re_L} = 32$. Hence, Charvonia's minimum criterion implies that, for a given liquid, there is a minimum film flow rate below which droplet entrainment will not occur irrespective of the gas flow rate. Similarly, Charvonia's upper limit is principally a liquid flow rate criterion also.

The existence of a minimum liquid rate for entrainment was confirmed by Cousins, Denton and Hewitt (1965) who found that for vertical upwards flow in a 0.375 inch tube the minimum water rate for entrainment was about 10 lb/hr for high air velocities. 10 lb/hr of water corresponds to $N_{Re_L} \approx 50$ and falls between Charvonia's limits. Disturbance waves could definitely be seen at a water rate of 15 lb/hr. If the velocity profile in the liquid film is similar to the Deissler (1955) profile, then 10-15 lb/hr of water corresponds to $\eta \approx 12$-14 for high air velocities. This is in agreement with the results of Hall Taylor, Hewitt and Lacey (1963) and Nedderman and Shearer (1963) for air

and water in $1\frac{1}{4}$ inch tubes.

Cousins, Denton and Hewitt also found that, at least at the lower liquid rates, there was a minimum distance from the liquid injector before entrainment of droplets began; this probably corresponded to a minimum length necessary for the appearance of disturbance waves.

Some years earlier from experiments with the horizontal flow of air over relatively thick films of water and mineral oils van Rossum (1959) had found that there was a minimum air velocity below which entrainment of droplets did not occur no matter how thick the liquid film was. This velocity was given approximately by:-

$$\bar{u}_{G_{crit}}(\text{metres/sec}) \approx \frac{1}{4}\sigma\,(\text{dynes/cm}) \quad \ldots\ldots (2.50)$$

For thin films the minimum air velocity required to cause entrainment was higher.

Wallis (1962, 1966) measured fractional liquid entrainment in vertical flow as a function of gas velocity for air as the gas, and water and several silicone oils as the liquids. At higher gas rates and over the range 20% to 50% entrainment the curves obtained were approximately linear. He extrapolated the linear portion to zero entrainment to obtain a critical gas velocity for the onset of entrainment. However, his graphs indicate that

the lower part of the curve approaches zero entrainment asymptotically or nearly so and that there is up to 5% entrainment present at the intercept gas velocity. His empirical correlation for the intercept gas velocity, $\bar{u}_{G_{crit}}$, was:-

$$\bar{u}_{G_{crit}} = 2.46 \times 10^{-4} \frac{\sigma}{\mu_G} \sqrt{\frac{\rho_L}{\rho_G}} \quad \text{.....(2.53)}$$

He found that the direction of flow did not affect $\bar{u}_{G_{crit}}$

For air and water at atmospheric pressure and temperature Wallis' equation gives $\bar{u}_{G_{crit}}$ (metres/sec) = 0.38 σ(dynes/cm), which is about 50% higher than van Rossum found for horizontal flow. The results of this Thesis support van Rossum rather than Wallis. On page 153 there is a further discussion on the critical gas velocity for the onset of entrainment.

Wave growth and interface instability is possible between different layers of a stratified heterogeneous fluid which are in relative motion. This may occur even if the layers are in laminar flow (Ostrach and Koestel, 1965). Smith (1964) has pointed out that this instability, the Kelvin-Helmholtz (Kelvin, 1871) instability, applies just as much to a wavy

interface as to a smooth interface. By using the modification proposed by Miles (1959) this criterion can be applied to a gas-liquid interface using any chosen gas and liquid velocity profiles. The Kelvin-Miles wave velocity relationship in effect considers an energy balance along a fluid streamline. When the wave velocity becomes complex the wave motion is unstable.

Hanratty and Woodmansee (1965) suggested that the onset of droplet entrainment in horizontal two phase flow in a channel might be due to a Kelvin-Helmholtz instability of the three dimensional waves which were present at higher gas velocities. From their experimental work they concluded that this criterion could be correct for thick liquid films but that a higher gas velocity was needed for thin films.

Ostrach and Koestel (1965) found that wave growth and film break up could be brought about by a Kelvin-Helmholtz or a Tollmein-Schlichting instability. When a fluid is undergoing transition from laminar to turbulent flow a Tollmein-Schlichting instability can occur as a result of amplification by viscosity of infinitesimal disturbances in the fluid. It does not require a variation in density as does the Kelvin-Helmholtz instability. The criterion for the onset of this instability is that the Reynolds number exceeds a minimum critical value.

Ostrach and Koestel's criteria for the onset of each instability were:-

Tollmein-Schlichting: $$\frac{l\, u_{L_i} \rho_L}{\mu_L} = 1.6 \times 10^6 \quad \ldots (2.51)$$

Kelvin-Helmholtz: $$\frac{l \rho_L u_{L_i}^2}{\sigma} = 6.5 \times 10^5 \quad \ldots (2.52)$$

where l is the distance from the liquid injector. Equation (2.51) is a Reynolds number and equation (2.52) is a Weber number. The existence of a minimum distance before droplet entrainment begins was found by Gill, Denton and Hewitt (1965). They found that this minimum distance tended to zero at high liquid flow rates. High liquid flow rates correspond to higher surface velocities u_{L_i} and hence by both criteria, equation (2.52) in particular, l approaches zero.

Huyghe and Truong (1965) suggested that the key factor controlling droplet entrainment was the kinetic energy per unit volume of the core. Subsequently, Truong and Huyghe (1965) suggested that the kinetic energy per unit volume of the core, where the core was assumed to be a homogeneous mixture of gas and entrained droplets, should correlate (1 - E) where E is the fractional entrainment. Paleev and Filippovich (1966) suggested that 1 - E is correlated by $\rho_c \bar{u}_G^2 \left(\frac{\mu_L^2}{\sigma^2 \rho_L}\right)$,

which as Cousins and Hewitt (1968b) have shown, is of similar form to the correlation of Truong and Huyghe but includes a property group $\frac{\mu_L^2}{\sigma^2 \rho_L}$.

Wallis (1968) pointed out that the correlation of Paleev and Filippovich did not account for the minimum gas velocity required for entrainment to take place. Wicks (1968) suggested that Wallis' plots for incipient entrainment could be improved by plotting E versus $\bar{u}_G\sqrt{\rho_G}$ rather than E versus $\bar{u}_G$.

Wicks (1967) has shown that the maximum shear forces likely to be experienced by a droplet are near the interface, that is in the region of its formation. Hence droplet size is controlled by the formation mechanisms. Of course, coalescence and agglomeration of droplets could lead to an increase in size in the gas core.

2.4 Two Phase Annular Flow with Droplet Entrainment

2.4.1 Void fraction and film thickness

For two phase annular flow without droplet entrainment the whole of the liquid flow is in the liquid film. Then, if $\bar{h}$ is the average film thickness, the void fraction that is the gas volume fraction, α, is

given by:-

$$\sqrt{\alpha} = 1 - \frac{\bar{h}}{R} \qquad \ldots\ldots (2.54)$$

and $\bar{h}$ can be calculated by means of the Dukler (1959) analysis from the liquid flow rate and the pressure gradient.

If entrained liquid droplets are present then the situation is much more complex. The liquid volume fraction, $(1-\alpha)$, is the sum of the fractions of the tube cross-sectional area occupied by the film and the droplets. However, the amount of entrainment at any point depends not only on the local gas and liquid flow rates and physical properties, but also on the inlet conditions.

Gill, Hewitt, Hitchon and Lacey (1963) found that if the liquid is injected through a porous section of the wall, so that no entrainment is formed by the injector, then the equilibrium between the liquid film and the droplet core is only approached very slowly. They used upwards flow of air and water in a $1^1/4$ inch vertical tube and found that the droplet flow rate was still increasing 209 inches downstream from the injector. Working with an axial jet injector in which nearly total droplet entrainment was produced, that is

approaching the equilibrium from the other direction, Gill and Hewitt (1968) found a shorter length, about 60 diameters, was needed to reach equilibrium. Incidentally, these results show that entrainment correlations which neglect length such as the one used by Collier and Hewitt (1961) and Gill, Hewitt and Lacey (1965) can only be valid at the particular distance from the injector at which their samples were taken.

Not only the local droplet flow rate in the gas core but also the local pressure gradient depended on the type of liquid injector. The pressure gradient was lower with the injectors which produced a high degree of initial entrainment than with the porous wall and annular slot injectors which produced very little initial entrainment.

Gill and Hewitt found that the film flow rate predicted by applying the Dukler-Hewitt analysis using the experimentally measured pressure gradient and film thickness (obtained by a direct method) was about 20% more than the experimentally measured value. However, the changes in going from one type of injector to another were self-consistent.

This is not unexpected, for as has already been discussed in Section 2.1.5 in explaining why the

Dukler analysis predicts the experimental data so well, the major influence of the gas core on the liquid film is through the interfacial shear stress. The Dukler analysis allows for this by means of the pressure gradient parameter β. However, at present the entrainment flow rate, because it depends on local conditions, inlet conditions and the distance from the inlet, cannot be properly predicted.

2.4.2 Application of the Dukler analysis to the gas core

As the Dukler (1959, 1960, 1961) analysis works so well for the liquid film it would seem worthwhile to test it on the gas core also. Wicks (1967) has done this assuming that the eddy diffusivity equations for single phase flow could be applied to the gas core as well.

The von Kármán (1939) equation for the turbulent core in smooth pipe flow using the Deissler changeover point at $y^+ = 26$ is:-

$$u^+ = \frac{u}{u_*} = 3.8 + \frac{1}{\chi} \ln y^+ \qquad \ldots\ldots (2.55)$$

For flow in a rough pipe experimental data can be correlated by the equation:-

$$u^+ = \frac{u}{u^*} = A + \frac{1}{K} \ln \frac{y}{e} \qquad \ldots\ldots (2.56)$$

where A is a constant and e is the equivalent sand roughness. Experimental work has shown that K is unaltered by pipe roughness. Wicks cited the work of Hanratty and Lillelehet (1961a, 1961b) which suggested that for channel flow of a gas above a wavy liquid film the waves caused a displacement downwards of the straight line in the u^+ versus ln y^+ graph but did not change the slope, that is the value of K. Hence, Wicks considered that the waves had a similar effect on the gas core to that of a rough solid wall.

With the boundary conditions of equal gas and liquid interfacial shear stresses and equal gas and liquid velocities at the interface, Wicks found that at a given pressure gradient the gas flow rate predicted by applying the Dukler analysis to the gas core was considerably greater than, up to twice, the experimentally measured value. He tackled this anomaly by postulating that the gas interfacial shear was composed of a form drag, τ_{form}, as well as a gas interfacial frictional shear stress, τ_{fric}. Hence:-

$$\tau_i = \tau_{fric} + \tau_{form} \qquad \ldots\ldots (2.57)$$

Wicks proposed that $\frac{\tau_{form}}{\tau_i}$ and hence $\frac{\tau_{fric}}{\tau_i} = 1 - \frac{\tau_{form}}{\tau_i}$, should depend on the drag coefficient of the wavy interface. Accordingly, he plotted, using experimental data from Collier and Hewitt (1961), $\frac{\tau_{fric}}{\tau_i}$, calculated by applying the Dukler analysis to both the gas and liquid phases, against a wave Reynolds number based upon the root mean square wave height and a relative velocity between the gas phase near the wavy interface and the waves. This relative velocity was based upon $\frac{u_G^*}{\chi} = \frac{1}{K}\sqrt{\frac{\tau_i}{\rho_G}}$, where u_G^* is the gas core friction velocity at the interface, that is based upon τ_i and not τ_{fric}. This assumed that the gas velocity profile was logarithmic all the way to the gas-liquid interface. Then, using the curve obtained, Wicks was able to use the experimental total pressure gradients and liquid flow rates of other investigators to predict gas flow rates. He compared the predicted with the actual experimental gas flow rates and found reasonable agreement.

However, this approach is not very satisfactory because the gas form drag, τ_{form}, in fact swamps the gas frictional shear stress τ_{fric}. From Wicks' curve, $\frac{\tau_{form}}{\tau_{fric}} = \frac{\tau_i}{\tau_{fric}} - 1$, ranges from 3 at high gas flows, that is small waves and low wave Reynolds numbers, to 11 at medium gas flow rates, with a trend to even higher values at low gas flow rates. Consequently the Dukler

analysis does not contribute very much to the understanding of the nature of the gas core.

2.4.3 The velocity profile of the gas-droplet core

Gill, Hewitt, Hitchon and Lacey (1963) measured local droplet mass flow rates at varying distances from the injector for the upwards flow of air and water in a 1½ inch tube. The water was injected through a porous section of the tube wall. They also made impact pressure traverses with a Pitot tube. They assumed that the gas-droplet mixture behaved as a homogeneous fluid. Therefore the impact pressure, Δp_{im}, is

$$\Delta p_{im} = \tfrac{1}{2} \rho_c u_m^2 = \tfrac{1}{2} (G_G + G_{LE}) u_m \quad ....(2.58)$$

i.e. $$\Delta p_{im} = \tfrac{1}{2} (G_G + G_{LE}) \left[\frac{G_G}{\rho_G} + \frac{G_{LE}}{\rho_L} \right] \quad ....(2.59)$$

G_G and G_{LE} are the respective gas and droplet local mass velocities. ρ_c is the mean core density . $u_m = \left[\frac{G_G}{\rho_G} + \frac{G_{LE}}{\rho_L} \right]$ is the mean core velocity. G_{LE} (from the local droplet mass flow rate) and Δp_{im} were measured. Hence G_G and u_m could be calculated.

Gill, Hewitt, Hitchon and Lacey showed that integration of the local gas mass flow rate across the diameter of the core gave total gas flow rates in agreement with the input gas mass flow rate. They claimed that this justified the homogeneous fluid assumption. In fact it does not, for the gas velocity could be less than the droplet velocity at some points in the tube and greater than the droplet velocity at other points in the tube.

They found that the mean linear velocity, u_m, was a linear function of $\ln \frac{y}{R}$ from $\frac{y}{R} = 0.05$ to $\frac{y}{R} = 1.0$, that is from just beyond the tops of the waves to the tube axis, and thus in agreement with the form of equation (2.56) for single phase flow in a rough pipe. However, the value of K, instead of being 0.40 (von Kármán, 1939) or 0.36 (Deissler, 1955) as it is in single phase flow, was only about 0.22 (for u^* based on ρ_G) or 0.18 (for u^* based on ρ_c). This corresponded to a very much steeper gas velocity profile at a given value of the gas friction velocity. This is shown clearly by differentiation of equation (2.56):-

$$\frac{du}{dy} = \frac{u^*}{Ky}; \quad \text{i.e.} \quad \frac{du}{d(\ln y)} = \frac{u^*}{K} \qquad \ldots\ldots (2.60)$$

and u^* can be defined as $\sqrt{\frac{\tau_i}{\rho_G}}$ or $\sqrt{\frac{\tau_i}{\rho_c}}$.

Furthermore, there was no clear trend in K with distance from the injector; indeed examination of their graphs suggests that K is independent of the distance from the injector, and therefore probably substantially independent of droplet concentration. They concluded that the core velocity profile was determined primarily by the wavy liquid film.

In a subsequent paper Gill, Hewitt and Lacey (1964)

reported that for water rates up to about 200 lb/hr K was in the range 0.3 to 0.4, but at higher water rates it decreased rapidly falling to about 0.14 (based on ρ_c) at 1250 lb/hr of water. They showed that for water rates up to 200 lb/hr, that is for K approximately equal to the single phase value, the pressure gradient could be correlated in terms of an effective roughness height related to a relative film thickness, that is the liquid film thickness minus the gas phase boundary layer thickness. This method had been used earlier by Hartley and Roberts (1961). In the annular flow regime there was no systematic trend in K with air rate. Later measurements by Gill and Hewitt (1967) using an axial jet injector, which produced a greater amount of entrainment at all distances from the injector, gave linear velocity profiles of similar shape, confirming the conclusion that the core velocity profile was determined primarily by the wavy liquid film.

The effect of the liquid droplets themselves on the velocity profile could perhaps be similar to that of solid particles. For solid particles the situation is probably less complex for there is no moving wavy interface. Doig and Roper (1967) found that at low solids to air mass ratios the gas velocity profile was more peaked whereas at high solids to air mass ratios it was flatter

than the single phase velocity profile at the same gas rate. In the latter case there seemed to be a tendency to form a moving plug of high solids to air ratio in the core. This case is probably due to interparticle collision and is discussed in detail with reference to droplets in Appendix 5. Applied to gas-liquid flow these effects would tend to be swamped by the dominance of the interfacial waves.

2.4.4 Pressure gradient

Of the general two phase flow correlations for pressure gradient the consensus of opinion (Dukler, Wicks and Cleveland, 1964a; Pletcher and McManus, 1968) is that the Martinelli-Lockhart correlation (Martinelli and Lockhart, 1949) is still the best for two phase annular flow. It was derived for horizontal flow, and for vertical flow the correlation of Hughmark and Pressburg (1961) may be better. However, this latter correlation is very much an empirical one.

Dukler, Wicks and Cleveland (1964b) suggested a correlation based on applying similarity analysis to a two phase flow. A major parameter in their analysis was the ratio of the gas and liquid volume flow rates. However, the work of Gill and Hewitt (1967), which was

discussed in detail in Section 2.4.1, showed that for annular two phase flow with droplet entrainment the pressure gradient depended not only on the overall flow conditions but also on the amount of the liquid phase flowing in the film and in the core. It follows that more exact pressure gradient analyses will need to include a flow distribution parameter.

It has already been mentioned in the previous section that for low water rates, up to 200 lb/hour in a $1^1/4$ inch tube, Gill, Hewitt and Lacey (1964) were able to correlate the pressure gradient in terms of relative roughness height. Hoogendoorn and Welling (1965) also correlated their pressure gradient data for the horizontal flow of air and mineral oils in terms of relative roughness. They found that the roughness height required was 2.7 times the mean film thickness. Their data were obtained at low liquid to gas ratios, that is their correlation applied to similar conditions to the correlation of Gill, Hewitt and Lacey. Nedderman and Shearer (1965) correlated their pressure gradient data for the ripple flow regime, that is at gas velocities too low for droplet entrainment to be significant, in terms of roughness heights also.

Chiew and Ibele (1964) correlated their pressure gradient data in terms of the wave height above

the base layer of liquid remaining on the wall between the waves. They plotted their results in the form of a friction factor versus gas superficial Reynolds number at each liquid flow rate. They found a maximum friction factor at the gas Reynolds number corresponding to the onset of droplet entrainment. Similar curves were obtained by Clegg (1966).

These results are in agreement with those already mentioned of Gill and Hewitt (1967), who found that for a given two phase flow with droplet entrainment that if the amount of entrainment was increased and the film thickness decreased by using a spray injector then the pressure gradient was reduced.

Chien and Ibele found the criterion for the onset of entrainment to be a straight line sloping downwards on a log-log plot of liquid superficial Reynolds number versus gas superficial Reynolds number. However, the existence of minimum gas and liquid rates for droplet entrainment as discussed in Section 2.3.3 means that, at best, such a plot can only hold over the centre of the range.

2.4.5 The effect of wall oscillations on a single phase gas flow

Since the presence of interfacial waves does

so change the gas velocity profile then it follows that investigations of the energy transfer from a single phase gas flow to a wavy solid wall, both oscillating or steady, should be of help in elucidating the structure of the gas core in two phase flow.

Chang and Dukler (1964) showed that the results of Laird (1954), who studied the laminar flow of air through an oscillating flexible tube and found astonishing increases in friction factor - up to 100 times, could be correlated in terms of the dimensionless group $\frac{F\ a\ R}{\nu}$, viz:-

$$\frac{f_{mw}}{f_w} = 1 + C_1 \left(\frac{F\ a\ R}{\nu}\right)^3 \exp\left[C_2 \left(\frac{F\ a\ R}{\nu}\right)^2\right] \quad \ldots.(2.61)$$

where f_{mw} is the friction factor of the moving wall, f_w is the friction factor of the stationary wall, F is the frequency of the oscillation, R is the no oscillation tube radius, a, is the amplitude of oscillation about the no oscillation radius R, ν is the kinematic viscosity and C_1 and C_2 are constants.

Houze and Dukler (1965) studied the turbulent flow of air in a horizontal 18 in. wide x 1.5 in. deep channel, the floor of which could be oscillated mechanically to produce waves of wavelength 2.0 in., amplitude 0.025 in. and frequencies up to 20 cycles per

second. A hot wire anemometer with a two wire x-type probe was used to obtain the root mean square gas velocity fluctuations $\sqrt{\overline{u_G'^2}}$ and $\sqrt{\overline{v_G'^2}}$ and the time averaged correlation product $\overline{u_G' v_G'}$. The wall oscillation frequency showed up strongly in all energy spectra obtained. They found that the velocity fluctuations at a point in space were influenced not only by the motion of the wall below it, but also by low frequency oscillations induced upstream and being transported to it.

Instead of finding a nett transfer of energy from the gas to wall in excess of the stationary wall case as would be expected from Laird's results, they found there was a strong transfer of energy from the wall to the gas at the oscillation frequency. This meant that the total energy transfer from the gas to the wall was less than the stationary wall case. However, they considered that for smaller wavelengths and larger amplitudes of oscillation that there could be increased energy transfer to the wall.

Houze and Dukler concluded that the oscillation did cause marked changes in the gas phase sufficient to affect momentum, heat and mass transfer in a manner considerably different from a simple surface roughness

effect. This substantiated the similar conclusion Dukler and Hagiros (1961) had made based on pressure gradient and entrainment measurements in horizontal two phase flow.

2.4.6 Droplet motion between the film and the core

It has already been mentioned in reviewing the paper by Gill, Hewitt, Hitchon and Lacey (1963) that the droplets in the gas core move at the gas linear velocity. Gill, Hewitt and Lacey (1964) found that at points far from the injector the droplet concentration was approximately uniform across the core. Because the core behaved as a homogeneous fluid then the mean droplet concentration was proportional to the more easily measured volumetric flow ratio, that is the ratio of the volume flow rate of the entrained droplets to the gas volume flow rate. The volumetric flow ratio was independent of gas rate, provided total liquid entrainment was not being approached. They thought that the volumetric flow ratio was possibly proportional to $\sqrt{\rho_G}$.

At low liquid rates the fraction entrained increased as liquid rate was increased, for a given gas rate; at high liquid rates the rate of increase of the fraction entrained tended to zero, that is the fraction

entrained tended to a constant value or at least only increased slowly.

Quandt (1965) proposed a dye mixing method for measuring the droplet mass transfer coefficient between the film and the core. He showed that if the liquid film could be instantaneously and uniformly labelled with dye, then for the condition of equilibrium entrainment, that is the rate of deposition of droplets from the core equal to the rate of formation of droplets from the film, the rate can be expressed in terms of the dye concentration in the film and in the core at a point further downstream. Quandt's expression was for a rectangular channel. For a tube the derivation is given by Cousins, Denton and Hewitt (1965). They showed that within the limit of accuracy of most experiments any change in film flow rate can be neglected. Hence, the change in dye concentration in the film per unit length, $\frac{dC_f}{dx}$, can be expressed by:-

$$\frac{dC_f}{dx} = \frac{2\pi(C_d - C_f)(R-h)M_{tr}}{W_f} \qquad \ldots\ldots (2.62)$$

where C_d is the dye concentration in the droplets, h is the film thickness, R is the tube radius, W_f is the mass flow rate of the film and M_{tr} is the rate of transfer per unit wall area.

A mass balance on the dye stuff gives:-

$$C_m W_{LT} = C_f W_{LT}(1 - E) + C_d E W_{LT} \quad \ldots\ldots (2.63)$$

where C_m is the bulk mean dye concentration, E is the fractional entrainment and W_{LT} is the total liquid flow rate. Substituting for C_d from equation (2.63) into equation (2.62) gives:-

$$\frac{dC_f}{dx} = \frac{2\pi(R - y)M_{tr}}{E.W_f}(C_m - C_f) \quad \ldots\ldots (2.64)$$

Integrating:

$$\ln(C_f - C_m) = -\frac{2\pi(R - y)M_{tr}}{E(1 - E)W_{LT}} x + C_{ONST.} \ldots\ldots (2.65)$$

And at $x = 0$, $C_d = 0$, hence $C_f = \frac{C_m}{1 - E}$.

$$\therefore \quad \ln\left(\frac{C_f}{C_m} - 1\right) = \ln\frac{E}{1 - E} - \frac{2\pi(R - y)M_{tr}}{E(1 - E)W_{LT}} x \quad \ldots\ldots (2.66)$$

Hence a plot of $\ln\left(\frac{C_f}{C_m} - 1\right)$ versus x has an intercept $\ln\frac{E}{1 - E}$ and a slope $\frac{2\pi(R - y)M_{tr}}{E(1 - E)W_{LT}}$, and thus M_{tr} may be obtained. A mass transfer coefficient for droplet interchange, k_{in}, may be defined as:-

$$k_{in} = \frac{M_{tr} W_G}{W_{LE} \rho_G} \quad \ldots\ldots (2.67)$$

The experimental results of Cousins, Denton and Hewitt showed that Quandt's method of labelling the film, in which the dye solution was injected into the base of the film through a porous section of the wall, was not very satisfactory for the dye did not mix instantaneously into the film, but tended to remain at the base of the film. Samples removed from the base of the film short distances downstream had greater than the mean film dye concentration. Also, the surface layers of the film from which droplet entrainment was taking place had less than the mean film dye concentration at that level.

However, the method did give order of magnitude estimates for k_{gh} in the range 0.5 to 1.5 ft/second. These agreed with the experimental results of Alexander and Coldren (1951) and were also in agreement with deposition coefficients obtained by measuring the rate of build up of a new liquid film after completely removing the original film.

In more recent experiments, Cousins and Hewitt (1968a) injected the dye in the same way, but removed the whole of the liquid film in order to obtain the mean dye concentration. They obtained low values for E and k_{gh} consistent with poor mixing in the liquid film.

They used an isokinetic sampling probe based on the CISE design (Adorni et al., 1961) to measure gas and liquid mass velocities and to measure dye concentration in the gas core.

The results showed that near the injector the dye concentration in the droplets, C_d, was not uniform across the gas core, further invalidating Quandt's method. A uniform dye concentration across the whole tube was reached about 13 feet from the injector for a gas rate of 450 lb/hr in the $1^1/4$ inch vertical tube used. For a gas rate of 800 lb/hr about $14\frac{1}{2}$ feet was needed.

The droplet diffusivity calculated from the measured concentration gradient was somewhat less than the gas phase eddy diffusivity. They were able to calculate values of mass transfer coefficient, k_{th}, as a function of position across the tube. The values ranged from about 0.5 ft/sec. near the interface up to 3-5 ft/sec. near the tube axis. However, near the axis the method of calculating was invalid (giving $k_{th} = \infty$ at the axis).

Unidirectional droplet deposition rates have been measured by Cousins and Hewitt (1968b). They formed the droplets by entrainment from a liquid film;

then they removed the liquid film by suction through a porous section of the tube wall and studied the build-up of a new film from the deposited droplets.

The droplet deposition rate per unit wall area, M_d, can be thought of as depending on the concentration difference between the core and the wall, the concentration at the wall being zero. Hence

$$M_d = k_d \frac{W_{LE}}{\left(\frac{W_G}{\rho_G} + \frac{W_{LE}}{\rho_L}\right)} \approx k_d \frac{W_{LE}\rho_G}{W_G} \quad \ldots\ldots (2.68)$$

$\left[\frac{W_{LE}}{\rho_L} \ll \frac{W_G}{\rho_G}\right]$. k_d is the droplet mass transfer deposition coefficient. This equation is of the same form as equation (2.67). M_d is related to the change in droplet flow rate, viz:-

$$\frac{dW_{LE}}{dx} = -2\pi R M_d = -\frac{2\pi R k_d W_{LE}\rho_G}{W_G} \quad \ldots (2.69)$$

Rearranging and integrating:-

$$k_d = \frac{W_G}{2\pi R \rho_G (x_2 - x_1)} \ln \frac{(W_{LE})_1}{(W_{LE})_2} \quad \ldots (2.70)$$

where $(W_{LE})_1$ and $(W_{LE})_2$ are the respective entrainment flow rates at distances x_1 and x_2 from the film extractor.

They found that k_d was independent of upstream conditions, gas velocity, gas density and tube diameter, (for 3/8 inch and $1\frac{1}{4}$ inch tubes). The only variable

which affected k_d was the distance from the film removal point. Near the film removal point k_d was high and decreasing rapidly. It asymptotically approached a constant value further downstream. Photographic studies indicated that the high values of k_d near the film removal point were due to the deposition of large droplets possessing relatively high radial velocities. The range of values of k_d was from 0.2 to 1.0 ft/second, the higher values occurring close to the film removal point.

Cousins and Hewitt pointed out that the finding that k_d was independent of gas velocity was surprising. This suggests that the radial velocity of the droplets is largely independent of their axial velocity. In a turbulent single phase flow the mass transfer coefficient is proportional to $(u_G)^{0.8}$. Hence the effective radial velocity of the diffusing substance is nearly but not quite proportional to the mean axial velocity of the bulk flow.

Cousins and Hewitt suggested that the droplets were too large to be much affected by gas turbulent eddies. However, the simple analysis of Longwell and Weiss (1953) indicates that the ability of a droplet to follow a gas eddy is a very strong function of its size, approximately inversely proportional to the fourth power of its diameter. By making the rather doubtful

assumption that the drag force of an eddy on a droplet was given by Stokes' Law and also assuming that the gas velocity fluctuations were sinusoidal, Longwell and Weiss showed that:

$$\frac{\epsilon_d}{\epsilon_M} = \frac{1}{1 + \left(\frac{\pi(\rho_L - \rho_G)d^2 F}{9\,\mu_G}\right)^2} \qquad \ldots\ldots (2.71)$$

where ϵ_d is the droplet diffusivity, ϵ_M is the mass eddy diffusivity (assumed equal to the momentum eddy diffusivity) and F is the eddy frequency. Application of equation (2.71) to water droplets in an air stream gives $\epsilon_d/\epsilon_M \approx 0.4$ for 40 micron droplets in an 80 ft/second air stream in $1\frac{1}{4}$ inch tube. This is very approximate because the liquid film on the wall greatly alters the value of χ in the von Kármán equation (equation 2.23).

This suggests that droplets larger than about 50 microns are little affected by gas turbulence. In this category are the large droplets with high radial velocities which settled out near the film removal point. Their radial velocities could well be remnants of their initial radial injection velocity at formation.

The constant value of k_d which Cousins and Hewitt found far from the film removal point could well be due to smaller droplets which are partially affected by gas turbulence and have lost all "memory" of their radial

velocity of formation.

Hoogendoorn and Welling (1965) made separate measurements of atomization rate and equilibrium entrainment for the horizontal flow of air and mineral oils in 51 mm and 140 mm tubes. They obtained straight line graphs on log-log coordinates of atomization rate versus the flow rate per unit perimeter. The slope was a little less than 2. They also obtained straight line plots on log-log coordinates of the fraction atomized versus the liquid to gas mass flow rate ratio.

They postulated that the film atomization rate, M_a, was unaffected by the presence of droplets in the gas core. By making this assumption they were able to apply their atomization results to a flow with simultaneous deposition and atomization. They postulated that the deposition rate, M_d, was proportional to the droplet flow rate and inversely proportional to the tube diameter.

At equilibrium the deposition and atomization rates must be equal,

$$\therefore \quad M_a = M_d = \frac{1}{\pi D} b \frac{W_{LE}}{D} = \frac{b\, W_{LE}}{\pi D^2} \qquad \ldots\ldots (2.72)$$

where b is the droplet deposition coefficient.

Hoogendoorn and Welling found that for the 51 mm tube $b = 0.02 \pm 0.005$, and was independent of the air

velocity for $\frac{W_L}{W_G}$ from 0.04 to 0.2.

This result is apparently in conflict with the results of Cousins and Hewitt, for combination of equations (2.68) and (2.72) gives:-

$$k_d = b \frac{W_G}{\pi D^2 \rho_G} = b \frac{\bar{u}_{Gs}}{4} \qquad \ldots\ldots (2.73)$$

where $\bar{u}_{Gs}$ is the gas superficial velocity, that is the gas velocity if it flowed alone in the tube at the same flow rate as in the two phase annular flow. Hence Hoogendoorn and Welling's results imply that k_d is proportional to axial velocity.

To compare this result with the unidirectional deposition results of Cousins and Hewitt it is necessary to extrapolate their graphs of k_d to zero distance. This it is almost impossible to do. However, they do indicate that in a flow with simultaneous atomization and deposition the large droplets with high radial velocities could well make the major contribution to droplet exchange between the film and the core. If these droplets retain a remnant of their radial velocity of formation during the whole of their life in the core then the deposition rate will not be proportional to the droplet concentration in the core. However, Hoogendoorn and Welling's assumption that the deposition rate is

proportional to the droplet flow rate in the core fails to account for the constant value of k_d found far from the film removal point by Cousins and Hewitt.

2.4.7 Size and velocity measurements of droplets in the gas core

Size measurements have been made by Wicks (1967) and size and velocity measurements have been made by Cousins and Hewitt (1968b). Wicks used a needle probe method. The tip distance between two 0.052 inch diameter needles with 20° conical tips mounted on opposite sides of Wicks' 6 in. x 3/4 in. test section could be varied by means of a micrometer drive mechanism. The zero spacing could be checked with a modified microscope. He used an electronic counter to count the number of times the needle tips were bridged by liquid droplets. He showed that the kinetic energy of the average droplet (100 microns in diameter; 70 ft/second) greatly exceeded the sum of the surface energy and the viscous energy that could be taken up by the droplet in removing it from the tips. Hence, he claimed that the droplets could not adhere to the tips and render them inactive.

The count rate versus needle spacing curve obtained could be solved by numerical integration using

a digital computer to give the droplet size distribution. Wicks was able to fit his droplet size distribution with the upper limit modification of the log normal distribution. The upper limit modification was originally proposed by Mugele and Evans (1951) to account for the existence of a maximum stable droplet size. The equation is:-

$$\frac{d\,(\text{cumulative volume fraction of droplets greater than diameter } d)}{d\,\Omega} = \frac{\exp\left\{\left[-\ln\frac{\Omega}{A_1}\right]^2 / 2\Sigma^2\right\}}{\sqrt{2\pi}\,\Sigma\,\Omega} \quad \ldots\ldots (2.74)$$

where $$\Omega = \frac{d}{d_{max} - d} \quad \ldots\ldots (2.75)$$

and d is the droplet size, d_{max} is the maximum droplet size, Σ is the variance and A_1 is a constant. d_{max} is chosen to give the line of best fit. However, as Wicks points out, this is merely a convenient way of recording the data; it does not indicate the nature of the forces generating the droplets.

Wicks found that the volume median droplet size was almost independent of the water flow rate. It was a strong function of air velocity, decreasing linearly

with air velocity at velocities greater than 150 ft/ second. At lower air velocities the volume median droplet size lay well below this line. Wicks suggested that another mechanism of droplet formation might be operating in this region.

The maximum droplet size was also almost independent of water flow rate and a strong function of air velocity. The maximum droplet size lay in the range predicted by Hinze's theory (see Section 2.3.2) using $\frac{\rho_G u_G^2 d}{\sigma} = We_d = 22$ with u_G equal to $\frac{1}{2} \bar{u}_G$ and $\bar{u}_G$ respectively. The maximum droplet size was two to ten times the mean film thickness. Wicks considered that this meant that droplet formation was more complex than could be explained by a simple shearing off of the wave tips.

Cousins and Hewitt (1968b) formed the droplets by entrainment from a liquid film; then they removed the liquid film by suction through a porous section of the tube wall and studied the droplets photographically. Droplet sizes were obtained by direct measurement of the photographic images of droplets on still photographs taken at 5x magnification using a 0.2 microsecond spark source, illumination being from the rear. This method could be used to measure droplets down to 25 microns in

diameter. Smaller droplets were counted. The volume mean diameter ($\sqrt[3]{\overline{d^3}}$) ranged from 56 to 87 microns for a gas velocity of 93.5 feet per second and 44 to 53 microns for a gas velocity of 163 feet per second. There was a relatively long tail on the distribution, there being a few droplets up to 400 microns in size, corresponding to several hundred times the mean droplet volume.

The number of droplet impingements per unit area per unit time could be estimated by counting them on ciné film frames. This coupled with a measurement of the droplet deposition rate was used to give an independent estimate of the volume mean diameter. For measurements 3 inches downstream from the film removal point this gave values considerably higher than the value obtained from the still photographs. Further downstream the values were in good agreement. Cousins and Hewitt attributed this difference to the higher radial velocities of the larger droplets.

Cousins and Hewitt's photographic measurements gave values of the volume mean diameter far less than would be predicted from Wicks' curve. Thus for air velocities of 93.5 and 163 ft/second respectively Wicks' curve predicts mean diameters around 250 microns. Part of the difference is almost certainly due to the size of the test section; Cousins and Hewitt used a

3/8 inch diameter tube, Wicks used a 6 inch x 3/4 inch rectangular channel. At a given gas velocity there would be a much lower pressure gradient and interfacial shear stress in the larger test section. This lower interfacial shear stress could mean larger droplets. However, this explanation seems inadequate to explain the whole discrepancy. Possibly Wicks' method did not count all of the smaller droplets.

The axial velocity measurements of Cousins and Hewitt were made by direct measurements on the cine film photographs. They found that for a gas mean velocity of 93.5 ft/second the average droplet velocity was equal to the gas velocity. At 163 ft/second the average droplet velocity was a little less than the gas velocity. They found that the gas sub-layer near the interface had little retarding effect on the droplets and the droplets reached the liquid film on the wall with very little loss in velocity.

The droplet axial velocities were unaffected by the entrainment flow rates. This is not surprising as the droplet concentrations used by Cousins and Hewitt were so low that interference between the droplets would have been minimal. This is discussed in detail in Appendix 5.

2.5 Summary

The key facts upon which an understanding of droplet entrainment in two phase annular flow needs to be based are:-

(1) The mean film thickness of a wavy annular liquid film is predicted reasonably well by the Dukler analysis. This applies whether a cocurrent gas flow is present or not. If entrained droplets are present in the gas phase the Dukler analysis can be applied using the actual film flow rate.

(2) There is a minimum gas rate below which significant droplet entrainment does not occur.

(3) Droplets are entrained from the disturbance waves. If the liquid rate is too low for disturbance waves to form then there is no droplet entrainment even at high gas rates.

(4) The presence of the wavy liquid film steepens the gas velocity profile except at low liquid rates. At low liquid rates the pressure gradient can be explained reasonably well in terms of a wave relative roughness. At higher liquid rates this approach is inadequate.

(5) The local axial droplet velocity is approximately equal to the local axial gas velocity.

(6) It takes a long distance from the liquid injector to approach an equilibrium droplet concentration.

(7) The droplet radial velocities are a function of their size. Larger droplets apparently have higher radial velocities.

3. EXPERIMENTAL APPARATUS

3.1 Overall Design

The apparatus was similar in diameter and length to that which had been used at Harwell for upwards flow work (Lacey, Hewitt and Collier, 1962; Hall Taylor, Hewitt and Lacey, 1963). The apparatus was designed for downwards flow. A transparent test-section was used so that the disturbance waves could be studied photographically. As the study was to be on the mechanisms of entrainment formation and deposition, it was decided to use as simple a test-section geometry as possible, a tube. The use of a tube was expected to make it easier to obtain a symmetrical flow distribution. Difficulties with obtaining an even distribution of liquid on a flat plate had been experienced by Messenger (1964); he had had to abandon the flat plate and use an annular test-section. The dissertation of Wicks (1967) indicates that he had considerable trouble with an asymmetrical liquid distribution in his 6 inch x $^{3}/_{4}$ inch rectangular test-section.

The key dimension which controls the size of the equipment is the tube diameter. The factors encouraging the use of a larger diameter are:-

(i) The ease of measuring accurate velocity profiles with a larger traversing probe in a larger diameter tube.

(ii) The larger tube is likely to be closer in size to industrial evaporator tubes and boiler tubes.

(iii) The pressure gradient for a given gas velocity is less, and hence accelerational effects are less.

The factors encouraging the use of a smaller diameter are:-

(i) For a given maximum gas velocity the gas flow rate required is proportional to the square of the diameter.

(ii) About 200 diameters are required to get reasonably close to equilibrium entrainment. Gill, Hewitt, Hitchon and Lacey (1963) observed that for upwards flow in a $1\frac{1}{4}$ inch tube the entrainment flow rate was still increasing appreciably 209 inches downstream of the injector. Hence the height of the test-section needs to be proportional to its diameter.

The balancing of these factors led to the test-section size being based on Jobling 5510/38 (38 mm O.D., 2 mm wall) glass tubes, the chosen test-section diameter being 1.330 inches.

The apparatus was designed with recirculating gas and liquid loops so that it could be used for liquids other than water and gases other than air.

Gill, Hewitt, Hitchon and Lacey (1963) had reported on sampling probe measurements of droplet entrainment for upwards flow. For a porous wall injector, which produced practically zero initial entrainment, graphs of total droplet entrainment versus distance downstream from the injector showed an initial steep increase in droplet entrainment, and then a gradual flattening out to a slow rate of increase further downstream. As it was expected that a downwards flow system would behave in a similar manner the three sampling levels were designed to be at 15 inches, 5 feet and 20 feet below the injector.

Because of the expected relationship between disturbance waves and entrainment the three photographic levels were chosen as near to the sampling levels as possible. This approach was designed to measure the disturbance wave parameters over only a short length of tube in order to approximate point values. This approach was different from that of Hall Taylor, Hewitt and Lacey (1963) and Nedderman and Shearer (1963) who had both set up their cameras about 10 feet from the tube and observed the waves over a distance of 5 feet or so. These two groups

of workers used framing rates up to 64 pictures per second, whereas in this investigation the camera was much closer to the test-section and framing rates of up to 260 pictures per second were used.

The two film flow rate measuring stations were located close to the 5 foot and 20 foot sampling levels.

The average liquid volume fraction in the flow was measured by means of hold-up cocks, 9 feet apart at the bottom of the test-section. It was necessary to use a wide hold-up cock spacing to capture enough liquid for accurate measurement. In downwards flow the liquid volume fraction is generally small.

The flowsheet of the experimental apparatus is shown in Figure 3.1.

3.2 The Test Section

The test-section was supported between two 4 inch x 2 inch x 30 feet long steel channels mounted back-to-back 10 inches apart and cross-braced at 2 feet intervals. To isolate the test-section from external vibrations the channels were mounted on a 36 in. long x 22 in. wide x 20 in. high concrete block which was supported by 4 coil springs with a total spring rate of 650 lb/inch under the

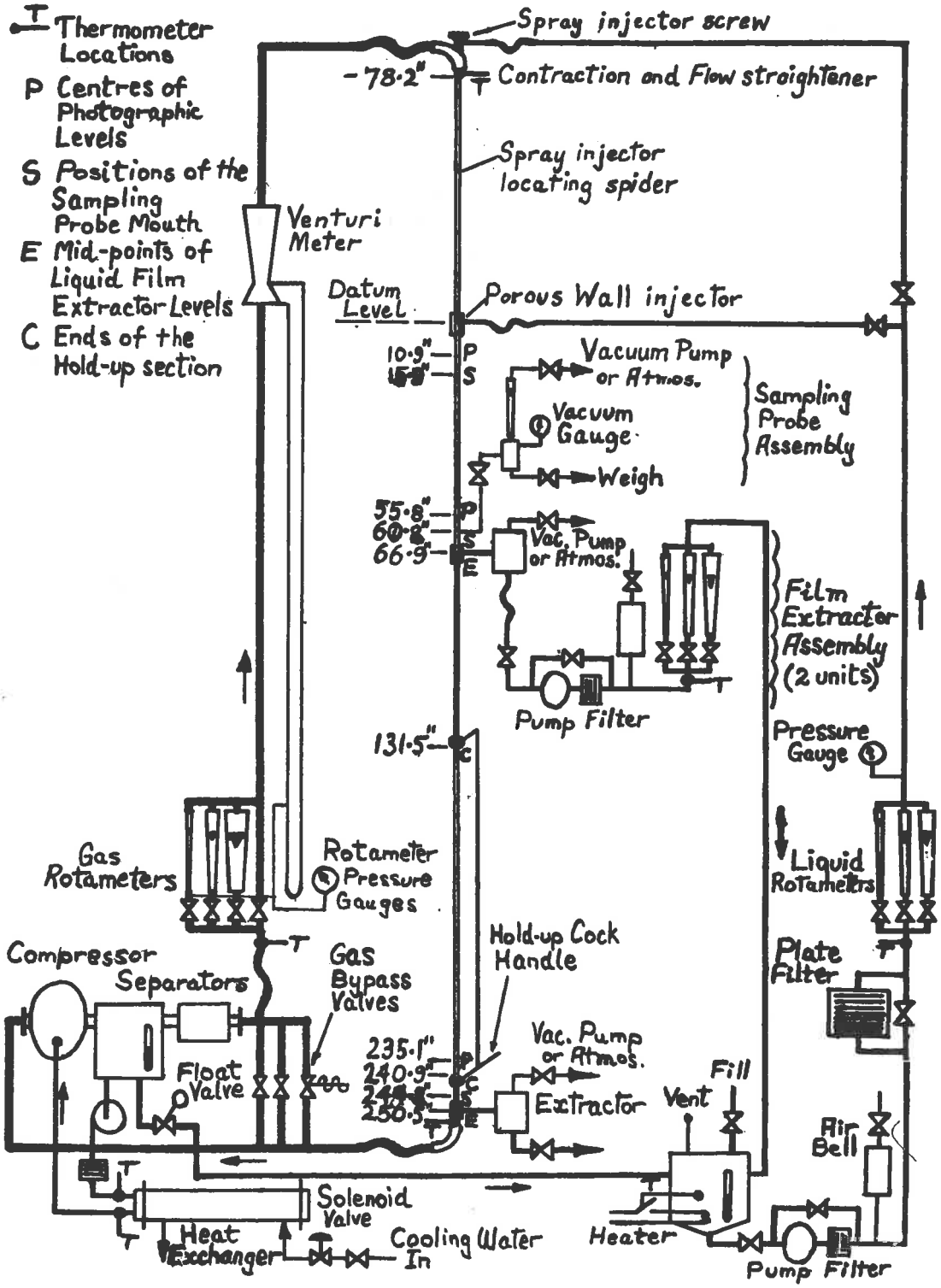

FIGURE 3.1: FLOWSHEET: ENTRAINMENT FROM FALLING LIQUID FILMS

load conditions. This gave a system with a natural frequency of 108 cycles per minute and with about 98% attenuation of the worst source of vibration, a nearby reciprocating compressor with a speed of 740 rpm under load. The vertical alignment of the channels and the test-section was adjusted and maintained by an assembly of horizontal coil springs between the channels and a support scaffold constructed from 1½ inch galvanised pipe at a level 22 feet above the top of the concrete base block.

Initially it had been planned to construct the test-section from lengths of $1\frac{1}{4}''$ bore perspex tubing. However, it was found that there was a great variation in the diameter of the tubes available. All the tubes in stock at several suppliers were measured and the members of the group with the smallest spread in diameter were purchased. The variation in diameter was still too large, so a reamer was constructed to bore the tubes to a constant diameter. Examination of the first tube reamed showed that this method was quite useless because the tube diameter altered after the reaming operation. As a result of this failure the use of perspex tubing was abandoned.

Fortunately, it was found that Jobling 5510/38

glass tubing, the closest larger glass size to $1\frac{1}{4}$ inch, had a much smaller spread in diameter. By grading, a group of tubes with a small diameter variation around a mean value of 1.330 inch was chosen. An important advantage of glass was that it could be used for a much wider range of liquids than perspex.

The test-section was built up so that adjacent tube ends had individually matched diameters. Included at the required levels were the necessary sampling probe sections, liquid injectors, liquid film extractors and hold-up cocks. The assembled test-section had a gas calming length of 78 inches. The working section was 250 inches long between the mid points of the porous wall injector and the bottom liquid extractor. As the test-section was on a vibration isolation mounting all connections to it were made with flexible hoses. The gas inlet and exit lines used 3 inch bore wire reinforced nitrile rubber hoses.

The glass tube ends were ground square and then joined by means of male and female socket joints, the female socket joints each containing two diametrically opposed 0.020 inch bore pressure tappings. The arrangement of a male and a female socket joint is shown in Figure 3.2a. This Figure also shows the location of the

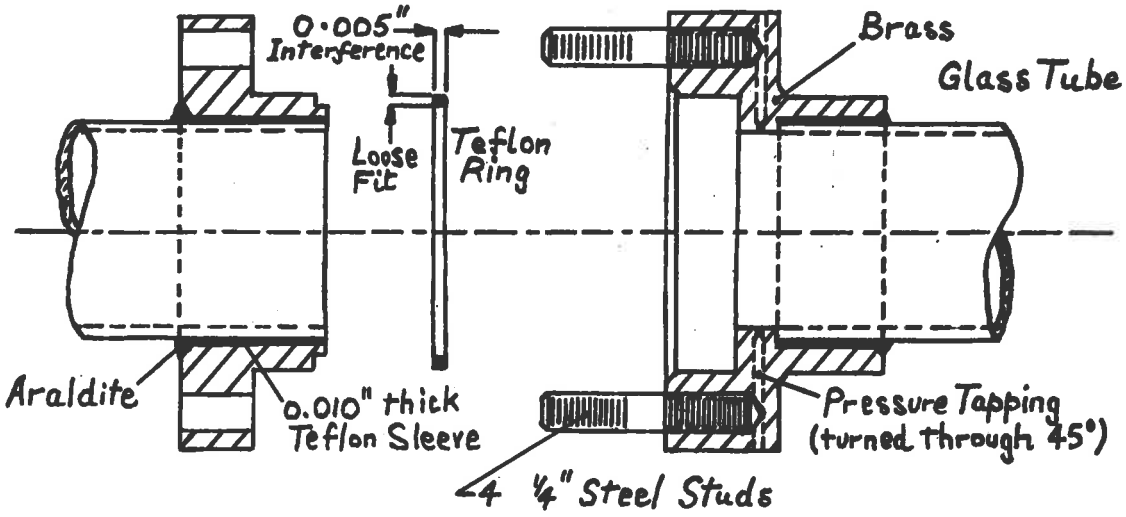

FIGURE 3.2a: CROSS-SECTION OF THE TUBE SOCKET JOINTS
($\frac{3}{4}$ size)

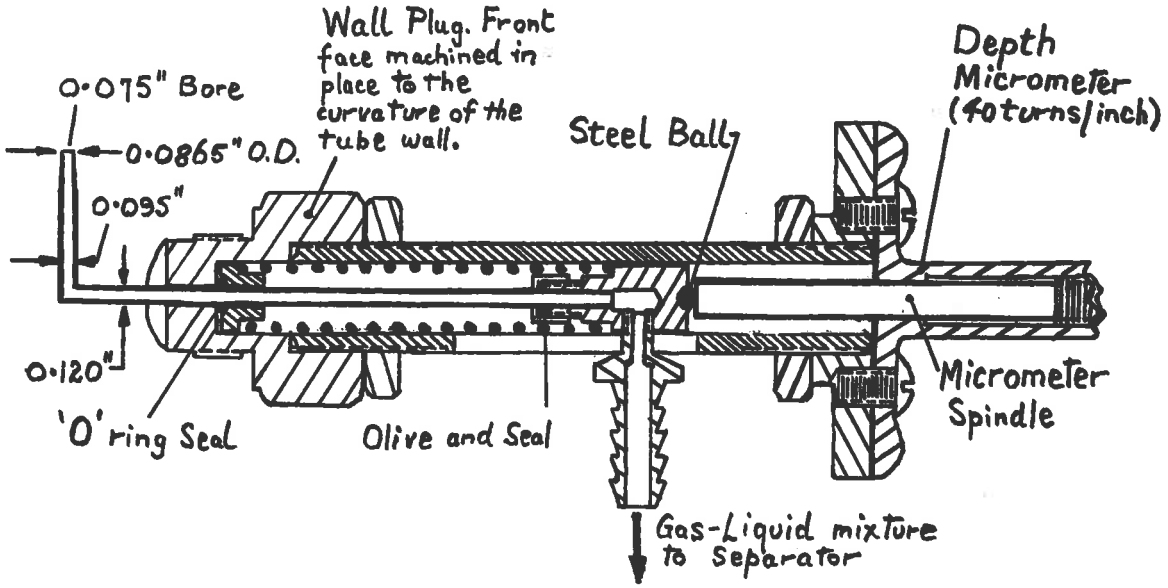

FIGURE 3.2b: DETAIL OF SAMPLING PROBE UNIT
($\frac{3}{4}$ size)

0.010 inch teflon spacer used to allow for eccentricities and irregularities in the tube outer surface. The location of the sampling probes, liquid injectors, liquid film extractors and hold-up cocks can be seen in Figure 3.1.

The Test-section Vertical Alignment

Even small deviations from vertical alignment can cause large asymmetries in the flow of both the droplets in the core (Gill, Hewitt, Hitchon and Lacey, 1963) and the liquid film (Butterworth, 1967). The test-section was aligned at each joint by using a plumb-bob hanging inside it as the vertical reference line.

Test-section Temperature

The test-section temperature was measured just before the gas calming length and just after the working section with calibrated 0-50°C mercury-in-glass thermometers with their bulbs in the flow stream. The temperature after the working section, being the temperature of the gas-liquid mixture, was taken to be the test-section temperature.

3.3 The Gas Circulating Loop

The gas was circulated by a Nash H5 rotary

compressor V-belt driven by a 50 HP Brook electric motor. For runs at 5½ and 15 psia test-section pressure, the compressor was driven at 1710 rpm giving gas velocities of up to 350 ft/second in the test-section. For runs at 45 psia test-section pressure, the compressor speed had to be reduced to 1460 rpm to prevent overloading the electric motor. This limited the gas velocity to about 160 ft/second.

The compressor could handle a mixed liquid and gas feed so that there was no need to separate the gas and liquid coming from the test-section. After the compressor there was a separating chamber which was followed by a wire mesh separator to remove entrained droplets from the gas stream. The compressor was always operated with its discharge above atmospheric pressure so that excess liquid flowed, controlled by a float operated valve, from the separating chamber to a lagged 10 gallon liquid sump.

The gas flow to the test-section was metered by a bank of three rotameters and a venturi meter. The venturi meter was in series with the rotameter bank. Its capacity was such that its useful range overlapped the top half of the range of the largest rotameter. Hence, in this range double checking was possible. The

gas pressure at the flow meters was measured by either of two calibrated 4 inch dial pressure gauges with ranges 0-30 psig and 0-60 psig, or by a 4 inch dial vacuum gauge with a range 0-30 inches of mercury. The gas temperature at the flow meters was measured by a calibrated 0-50°C mercury-in-glass thermometer with its bulb in the flow stream.

Excess gas was recirculated through a by-pass line. The by-pass line contained three valves in parallel. Two of these were for manual variation of the by-pass flow rate. The third, a 2 inch diameter spring-loaded relief valve, was for automatic by-pass control. When the test-section hold-up cocks were closed so that the fraction of liquid in the two-phase flow could be measured, the gas flow was completely stopped. The automatic opening of the by-pass relief valve prevented any damage to the equipment.

The compressor was cooled by circulating liquid from the separating chamber through a heat exchanger and back, re-entering the compressor at points near the compressor shaft sealing glands. An electrical relay was placed between the power supply of the electric motor driving the circulating pump and the power supply of the compressor so that if the pump power supply was interrupted the compressor was switched off. A solenoid valve was used to turn on the cooling water

flow to the heat exchanger automatically when the compressor was started. Figure 3.3 is a photograph of the compressor with the lower end of the test-section in the background.

3.4 The Liquid Circulating Loop

Liquid was pumped from the liquid sump by a McPherson G1 gear pump through a plate filter and rotameter bank to either of the two liquid injectors that were used. The temperature of the liquid in the sump could be raised to any preset temperature up to 50°C by means of a 2 KW immersion heater controlled by a "Jumo" thermometer and relay. In practice it proved more convenient to regulate the temperature of the entire system by manually altering the cooling water flow rate to the compressor heat exchanger.

The temperature of the liquid at the rotameter bank was measured by a 0-50°C mercury-in-glass thermometer. The liquid pressure was measured after the rotameters. This was necessary to detect any clogging of the pores of the porous wall injector.

3.5 The Liquid Injectors

Two types of injector were used, a porous wall injector to place the liquid on the wall of the test-

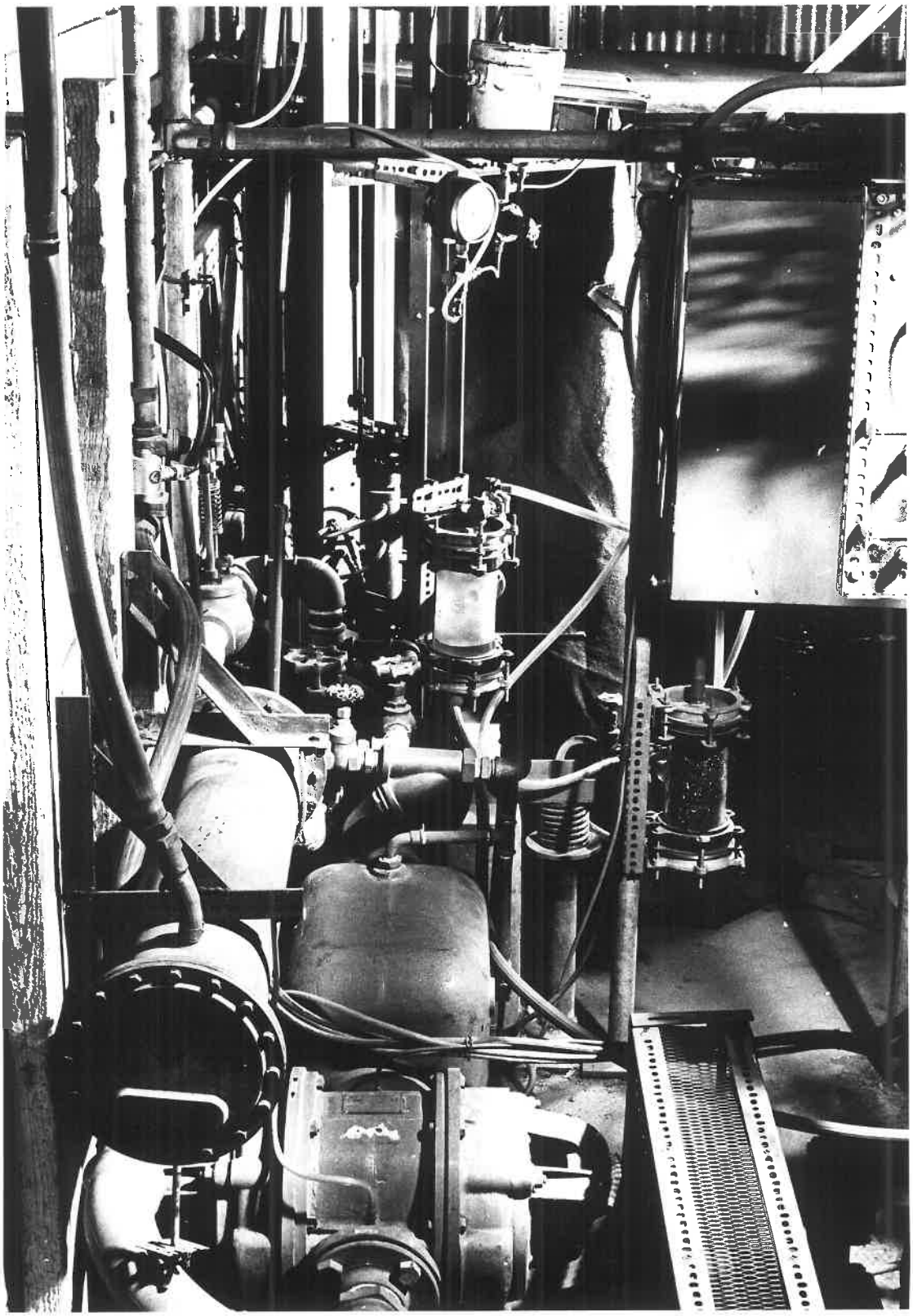

FIGURE 3.3: THE COMPRESSOR WITH THE LOWER END OF THE TEST-SECTION IN THE BACKGROUND.

section with minimum droplet entrainment, and a spray injector to inject as much liquid as possible into the gas stream. The spray injector head was located so that the spray liquid, if it moved in a straight line, would strike the tube wall half-way along the porous wall element.

(a) Porous wall injector. This was a 4 inch long x 2 inch outside diameter x 1.330 inch bore sintered Aluminium Oxide hollow cylinder mounted in the test-section. It was finished to the correct bore size with a diamond tipped boring bar. To ensure that the feed to the test-section wall was evenly distributed the porous element was mounted in a tangential entry feed chamber. A plate filter was included in the liquid circulating loop to reduce the incidence of clogging of the pores of the element. If the element did become clogged it could be cleared by a back-flushing procedure in which liquid was pumped into the test-section through the top liquid extractor unit with the hold-up cocks, which were lower down the test-section, closed. The back-flushing liquid flow rate through the porous wall injector could be increased by pressurizing the test-section.

(b) Spray injector. The spray injector head was at the bottom end of a 90 inch long x 0.5 inch outside diameter 16 gauge copper tube centrally located in the calming length of the test-section by means of a spider. The spray head consisted of a 50° included angle copper cone mounted on the end of a 0.125 inch outside diameter stainless steel tube. This tube was centrally located in the injector tube by spiders. It ran the whole length of the injector tube to an external screw head at the top. By turning the screw head the spray cone could be raised or lowered and the annular gap between the cone and the bevelled end of the copper injector tube varied so that the average velocity of the spray as it left the injector head remained constant at 15 ft/second for different liquid flow rates.

3.6 The Liquid Extractors

There were two of these, their midpoints being 66.7 inches and 250.5 inches below the midpoint of the porous wall injector. They were identical to the porous wall injectors but were operated in reverse. Because of the wavy nature of the film flow some gas came out with the extracted liquid. The gas and liquid were separated in a glass separating chamber located as near as possible to the extractor. The gas from the chamber

was exhausted to atmosphere or to a vacuum pump as required. The liquid was pumped through a rotameter bank back to the liquid sump.

3.7 The Hold-up Cocks

The fraction of liquid in the two-phase flow could be determined by rapidly and simultaneously shutting two hold-up cocks located at the lower end of the test-section 110.5 inches apart, giving a trapped length of 109.4 inches. The trapped liquid drained on to the top of the bottom cock and was measured with a ruler.

The automatic gas by-pass system has already been described. Automatic by-passing of the liquid was not needed for there was sufficient capacity in the length of test-section above the top hold-up cock. This gave sufficient time to close the hold-up cocks and then stop the liquid feed pump even when operating at the maximum liquid feed rate.

Figure 3.4 is a photograph of the spray injector, a porous wall injector or extractor and a hold-up cock.

3.8 Pressure Measurement

There was a total of 14 pressure measuring

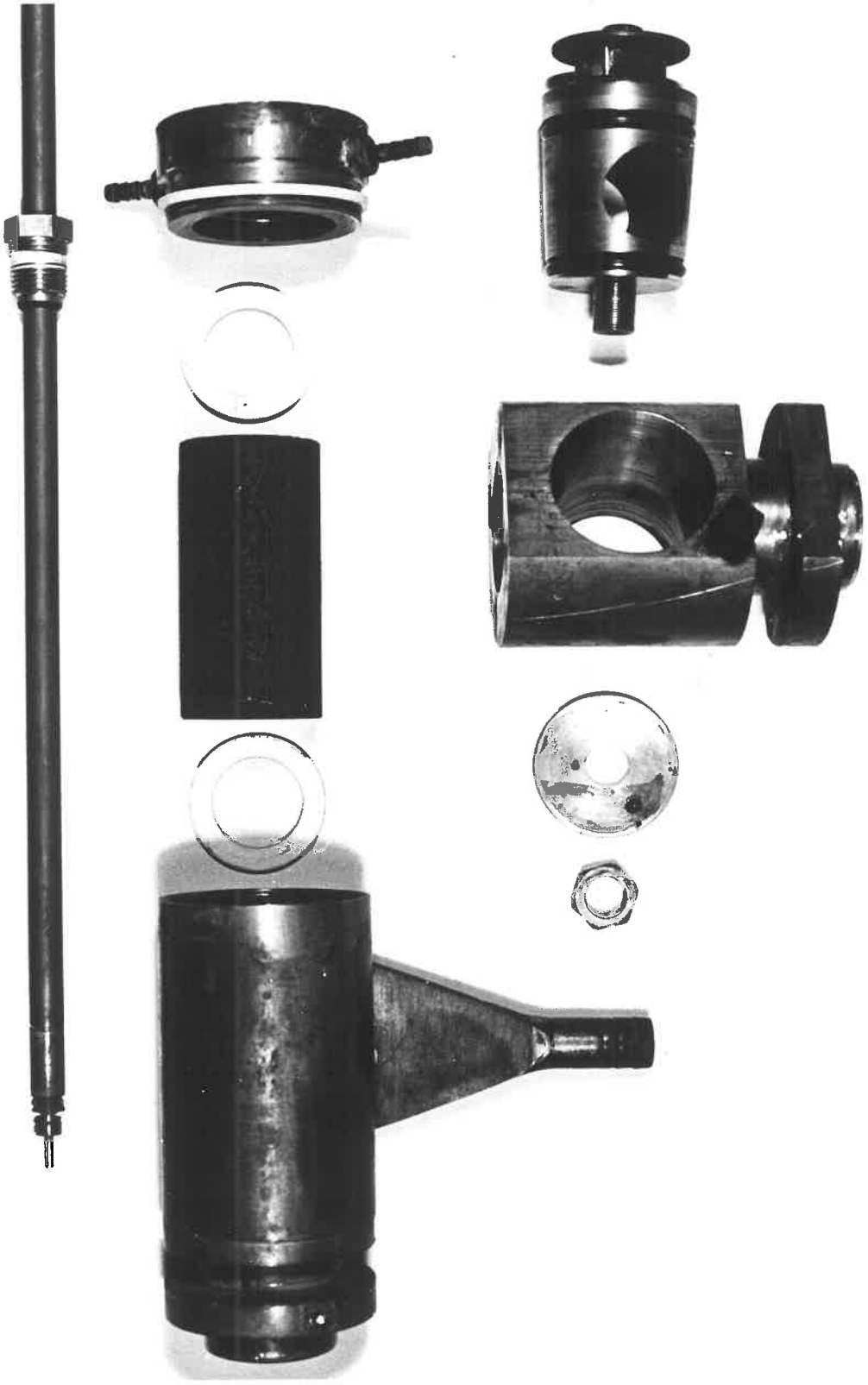

FIGURE 3.4 : THE SPRAY INJECTOR, THE POROUS WALL INJECTOR AND A HOLD-UP COCK.

stations in the test-section. They were located as follows:-

(i) 2 in each of the 3 porous wall units,

(ii) 1 in each of the 5 glass tube lengths,

(iii) 1 in each of the 3 sampling probe units.

The pressure measuring stations each consisted of two diametrically opposed holes, the last 0.125 inch of each hole being 0.020 inch in diameter. These holes were joined to a tee-piece fitted with a non-return valve and plug socket by means of flexible hoses. Six hoses with plug-in ends were provided to connect the tee-pieces to the measuring manometers. The use of non-return valves meant that the hoses could be easily moved from one measuring station to another. Solid plugs were plugged into the sockets of the stations not in use to guard against any leaky non-return valves.

The six transmission lines went to a switching manifold. As they entered the manifold they were purged with water from an air pressure driven water reservoir. The purge liquid has to be the same liquid as that used in the test-section. Water was used in all runs in this investigation. The reservoir was fitted with a loose diaphragm to limit absorption of air by the water. The purge rate was limited to about 8 lb/hr for

water by means of a length of 0.019 inch diameter capillary tubing. When the manometers were near the balance point an additional length of capillary tubing was switched in series to reduce the purge flow to about 1 lb/hr.

Three manometers were used:-

(i) An 8 foot long water over mercury manometer with one side open to atmosphere. This could measure pressures up to 40 psig. Absolute pressures up to 55 psia could be measured by adding the reading of this manometer to the atmospheric pressure measured with a Fortin barometer.

(ii)Two identical 4 feet long water over symmetrical tetrabromoethane ($CHBr_2.CHBr_2$) differential manometers. The density of tetrabromoethane saturated with water was measured and found to be 2.92 gm/ml. Hence the effective density of the liquid combination was 1.92 gm/ml and the differential manometers could measure pressure differences up to 3 psi.

3.9 Pressure Control of the Test-Section

As the air circulated in a closed loop the pressure in the test-section could be controlled quite simply by bleeding air into the air circulating loop from an external

source of air pressure. The pressure of the bleed air was controlled by an air regulating valve. This valve had an effective control range from 2 psig to 35 psig.

For the runs at 45 psia pressure at the bottom of the test-section the bleed air was admitted on the suction side of the compressor. The pressure control was good because there was little pressure loss in the short line between the bottom of the test-section and the compressor.

For the runs at 15 psia the bleed air had to be admitted upstream of the valves below the gas meters so that the bleed gas pressure was at least 2 psig (16.7 psia) and the pressure control valve could function properly. Pressure control was more difficult as adjustments in either gas or the liquid rate caused variations in the test-section pressure loss. These variations meant that compensating changes in the setting of the pressure control valve were needed to maintain a given pressure at the bottom of the test-section. For the runs at 5½ psia the bleed air was admitted at the discharge side of the compressor. The same control difficulties were experienced as at 15 psia.

3.10 The Sampling Probe Assembly

The droplet sampling probe assembly is shown in Figure 3.5. The unit was so designed that the probe unit could be screwed into any of three locations in the test-section after removing a double plug insert. This could be done without any dismantling of the rest of the test-section. The three positions of the probe mouth were at levels 15.9, 60.8 and 244.8 inches below the midpoint of the porous wall injector. The probe unit is drawn in Figure 3.2b. There were three wall plugs each matched to the wall at a particular level. When the sampling probe was not installed the hole for the probe tube was blocked with a second plug also matched to the wall contour.

The probe mouth had a bore of 0.075 inch and an outside diameter of 0.0865 inch. The bore of 0.075 inch corresponded to a test-section to probe cross-sectional area ratio of 314:1.

The probe was operated with an air velocity through its mouth of about 80-90% of the isokinetic velocity, this being the local mainstream air velocity. It is shown in Appendix 4 that under the sampling conditions used the overall mass capture efficiency of liquid droplets was 99% or better. Moreover, the capture

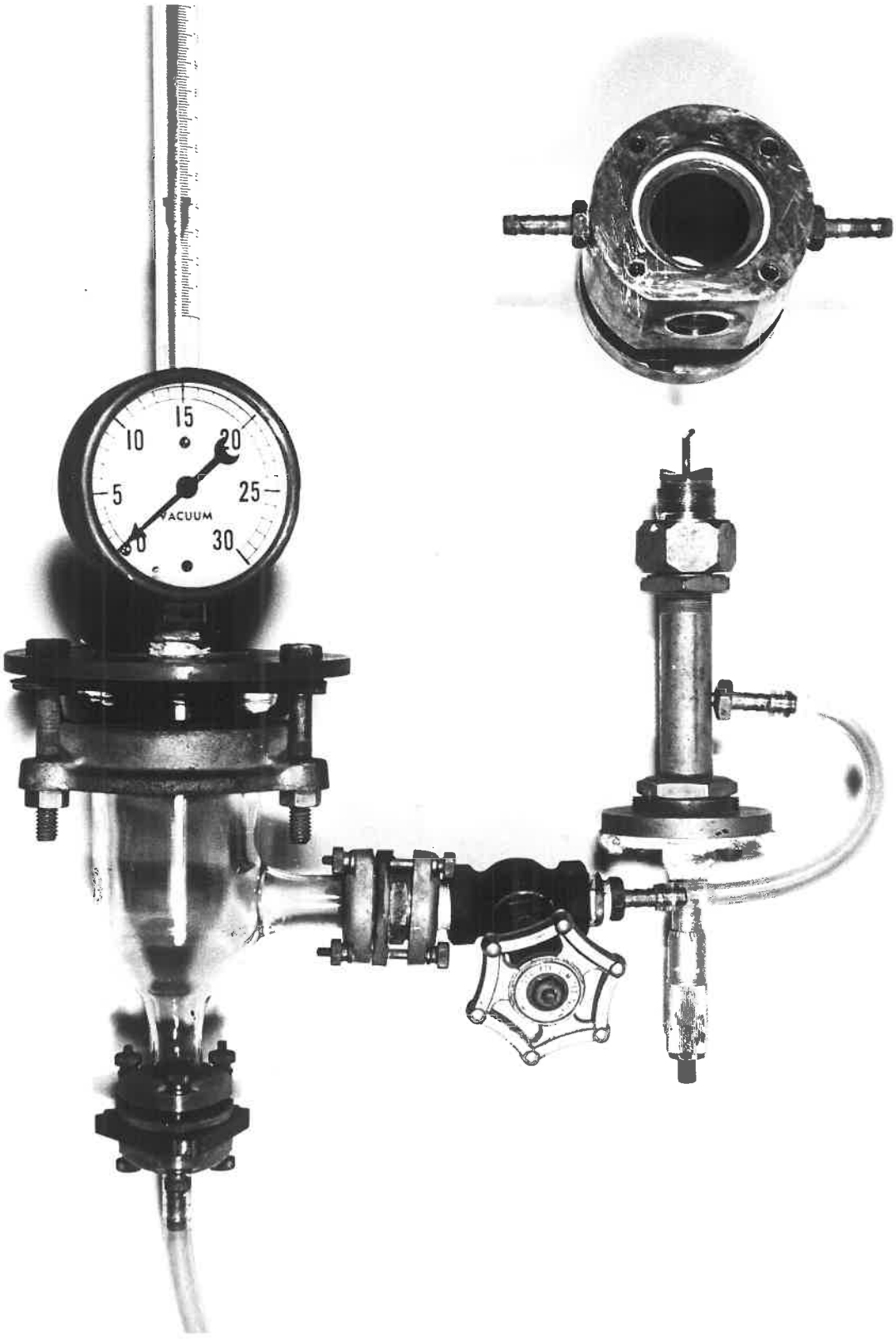

FIGURE 3.5 : THE SAMPLING PROBE ASSEMBLY.

efficiency is unaffected by quite wide variations in air take-off rate. This meant that the desired air take-off rate at any location of the probe mouth could be calculated to a sufficient degree of accuracy from the total air flow rate together with the experimental velocity profile of Gill, Hewitt, Hitchon and Lacey (1963) for upwards flow. This velocity profile was expected to be somewhat inaccurate for downwards flow. However it was considered that it would be more accurate than a single phase turbulent velocity profile. Even a single-phase turbulent velocity profile would have been sufficiently accurate because of the insensitivity of capture efficiency to air take-off rate.

After leaving the probe tube, the air and water droplets were separated in a 2 inch diameter glass chamber. The air passed from the chamber through a rotameter to atmosphere or to a vacuum pump as required. The water droplets collected in the bottom of the chamber, from whence they were drained off and weighed. The air flow rate was measured by means of the rotameter together with a vacuum gauge to measure the pressure in the separating chamber.

The probe could be traversed across the test-section by means of a 40 turns per inch micrometer screw,

and hence positioned to an accuracy of 0.0005 inch. The distance from the outer edge of the probe tube to the axis of the probe mouth was known and so the probe could be zeroed by screwing it across the test-section until it touched the far wall and then noting the reading on the micrometer drum.

3.11 The Photographic Equipment

All the ciné films were taken on Kodak Tri-X reversal film with a 16 mm Vinten camera. The camera was 33 inches from the test-section and mounted so that the long axis of the picture was parallel to the flow direction. A 1½ inch f/2 lens was used giving a field of view 9 inches long. A scale marked in half inches and a coded legend describing the flow were photographed with the test-section. The centres of the three photographic sections were at levels of 10.9, 55.8 and 235.1 inches below the midpoint of the porous wall injector.

The main illumination was indirect. A white card behind the test-section was illuminated by two 750 watt Quartz-Iodine lamps also behind the test-section and located above and below the camera field of view. Auxiliary illumination of the scale and the legend was with a 300 watt photoflood lamp. The camera arrangement

is shown in Figure 3.6.

Because the test section was viewed by transmitted light from a diffuse white card no direct reflections which could spoil the pictures were possible. The waves showed up as dark patches against the white background. There was a cylindrical lens effect caused by the tube curvature. This did not affect this investigation as all the measurements were in the axial direction. A detailed discussion of the problems in photographing a two-phase flow has been given by Cooper, Hewitt and Pinchin (1964) and more recently by Arnold and Hewitt (1967).

The camera was used with a $^{1}/_{10}$th shutter giving exposure times of $^{1}/_{10}$th of the reciprocal of the framing rate. The camera had 3 speeds, giving framing rates of about 60, 180 and 260 pictures per second respectively. The exact rate was obtained from timing marks put on the film at $^{1}/_{100}$th second intervals.

Measurement of the film data

A Leitz Wetzlar 35 mm film reader was modified to take spooled film. The projector and the mirror were repositioned further from the screen plane to increase the magnification. This meant that the unit had to be used in a darkened room. In the final assembly

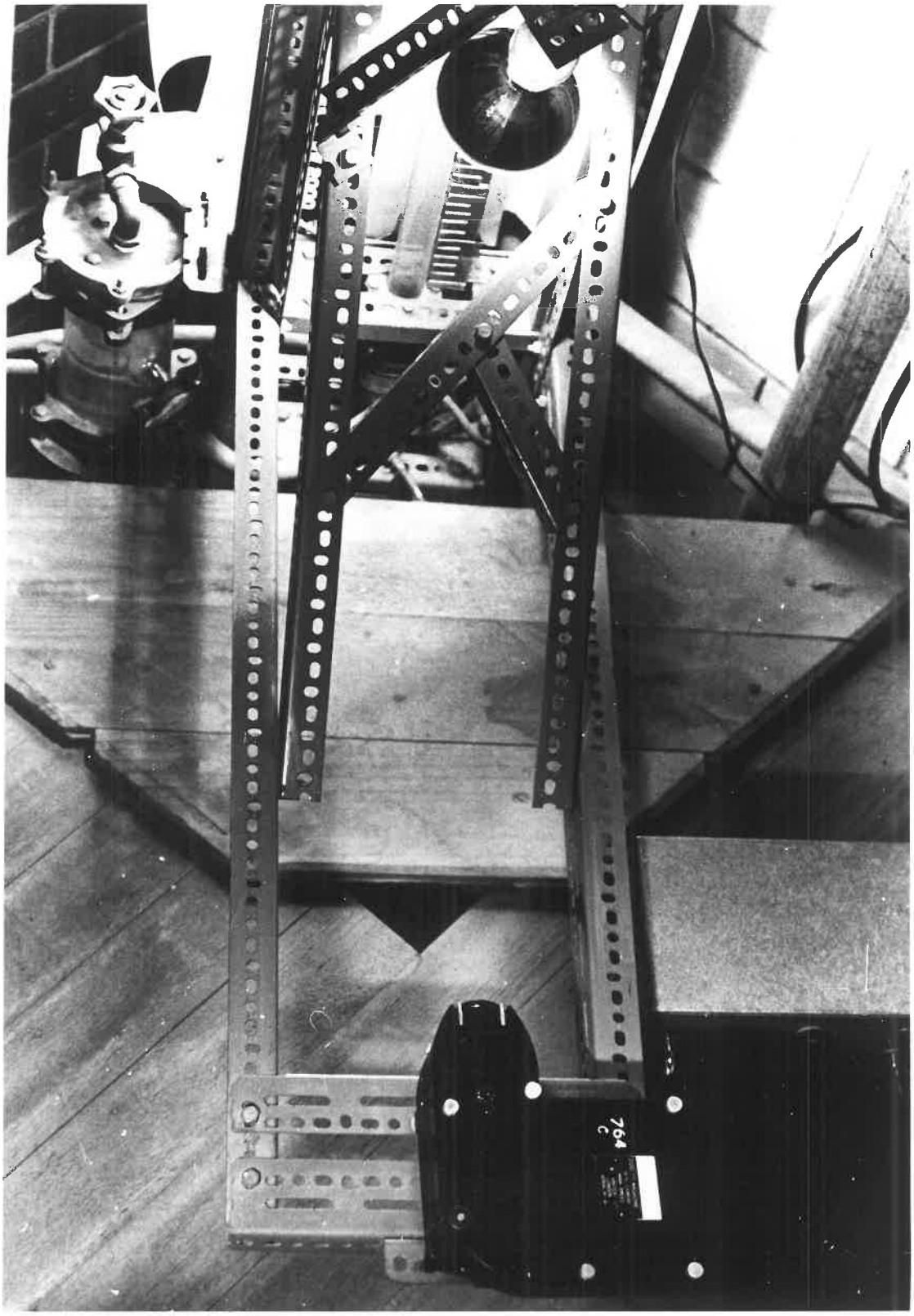

FIGURE 3.6: THE CINÉ CAMERA ARRANGEMENT.

three 16 mm frames could be seen simultaneously at about full size. The projected size was not critical as a scale had been photographed together with the flow.

4. EXPERIMENTAL WORK

A total of 233 experimental runs was carried out on the air-water system in the 1.330 inch diameter test-section. The air velocities at the 235" level ranged from 0 to 370 feet per second based on the total flow area. The water flow rates ranged from 30 to 3700 lb/hour. 30 of the runs were at 5½ psia test-section pressure, 112 at 15 psia and 91 at 45 psia, the test-section pressure being set in reference to the 245.2 inch level. Liquid volume fraction and pressure gradient measurements were made in some of the runs at each of these pressures.

Ciné films were taken in 203 of the runs. In the runs at 15 psia and 45 psia three photographic levels were used. The mid-points of these levels were 10.9, 55.8 and 235.1 inches below the injectors. In the runs at 5½ psia only the bottom photographic level was used.

In the 5½ psia series of runs only the porous wall injector was used whereas in the 15 psia and 45 psia runs both the porous wall injector and the spray injector were used. In the runs at 15 psia and 45 psia both sampling probe traverses and liquid film flow rate measurements were made. The sampling probe traverses were made at the 15.9, 60.8 and 244.8 inch levels. Liquid film flow rate measurements were made at two levels, the mid-points of the

liquid film extractors being 66.9 and 250.5 inches below the injectors. The experimental data are tabulated in Appendix 1.

Appendix 2 contains tables of air and water viscosities and densities over the pressure range and the temperature range of the experimental data.

Also tabulated in Appendix 1 along with other derived results to be explained later in this section are:-

(i) The air density at the 235 inch level calculated from the pressure at the 235 inch level and the density tables in Appendix 2.

(ii) The air superficial velocity at the 235 inch level, given by $\frac{G_G}{\rho_G}$, where G_G is the air mass flow rate in lb/ft^2 hr.

(iii) The liquid film Reynolds number $N_{Re_L} = \frac{W_L}{\pi D u_L}$ This assumes that all of the liquid flows in the liquid film.

4.1. Calibration of flow meters

Each liquid rotameter was calibrated at 5 cm scale intervals. The smaller rotameters in each bank were calibrated over the whole range and the largest rotameter in each bank was calibrated up to the maximum pump output flow rate. The calibrations were carried out by timing the flow of warm water, in the range 30°C to 40°C, into a weigh tank. It was known that this was the likely operating

temperature range. The measurements were corrected to the chosen standard temperature of 37.8°C (100°F) by means of the rotameter manufacturer's charts, and then standard calibration curves were drawn. Temperature correction factors were calculated from the manufacturer's charts.

Facilities were not available to calibrate the gas rotameters. Calibration curves for air saturated with water were constructed from the rotameter manufacturer's charts at intervals over a range of pressures from 6.70 psia to 50.0 psia at the standard temperature of 37.8° C. The true flow rate could be obtained from the closest calibration curve by multiplying by the square root of the density ratio. The venturi meter of bore 2.711 in. and throat 1.397 in. was constructed to specification B.S. 1042: 1943. It was installed after an 80 diameters long length of straight vertical 2.711 in. bore pipe. It was 90 diameters downstream of the flow control valve. The venturi meter calibration curves were drawn up using a discharge coefficient of 0.99.

As the rotameters and the venturi meter were in series it was possible to compare the upper half of the range of the largest rotameter (Rotameter Manufacturing Co. Metric 65K) with the lower part of the range of the venturi meter. The rotameter consistently indicated 1-2% less flow than did the venturi meter. It was

considered that the venturi meter was more accurate and hence over its useful range its reading was preferred to that of the 65K rotameter.

The float in the 65K rotameter was unstable at certain flow ranges tending to "spin" and "bounce". This was much reduced but not completely eliminated by installing a flow straightener made from ¼in. O.D. copper tubes between the control valve and the rotameter. During the course of the experimental runs the discrepancy between the rotameter and the venturi meter gradually increased, being in the range 2-3% at the end. This was almost certainly due to the breaking off of pieces of "koranite" from the metering edge of the rotameter float. Much of this increase in error occurred after a moderately large piece of "koranite" had broken off. All readings with the 65K rotameter after this occurrence were increased by 2% to compensate and give a more accurate measure of the true gas flow rate.

4.2. Operation of the equipment.

When the compressor had been started and air was circulating through the test section it was sometimes necessary to dry out the hollow gas rotameter floats. This was done by strongly throttling the air flow with the flow control valves. This meant that the air on the downstream side was appreciably below saturation and

hence the rotameter floats gradually dried out.

While this was being done the water was circulated at a moderate rate through the test section in order to come to temperature equilibrium. About an hour after start up the system pressure and the gas and liquid flow rates were set to their desired values.

When equilibrium was reached the gas and liquid flow rates, the system pressures and the system temperatures were recorded. Then the ciné film sequence was taken and liquid samples withdrawn with the probe. The sampling operation could take up to an hour at the lower droplet flow rates because up to 8 sampling positions were used and two samples were taken at each position. Then the gas and liquid flow rates and the system pressures and temperatures were recorded again. Finally, void fraction measurements and liquid film flow rate measurements were made. These were left until last because they both disturbed the flow considerably.

4.3. Difficulties with the experimental apparatus.

4.3.1. Sampling probe system.

The mechanical design of the double plug system was very good. It permitted easy removal of the probe and in addition the alignment marks allowed accurate replacement of the plugs. The only deficiency of the system was that it did not provide automatic vertical setting of the probe

mouth. This had to be done with a bore gauge for the bottom probe position and visually, by comparing with a vertical such as the edge of the test-section tube, for the top two probe positions.

4.3.2. Water circulating loop.

It was originally intended to use distilled water in the liquid circulating loop. However the water very quickly picked up finely divided rust from the cast iron compressor and separator. Most of this was removed by pumping the water through a plate type filter press, but there was still sufficient in the circulating water to make it pointless to use distilled water and so ordinary tap water was used.

4.3.3. Pressure measurement.

The choice of a liquid purge pressure measuring system was not very satisfactory. The problem was air bubbles coming out of solution. It was for this reason that a plastic diaphragm was used between the air and the water in the pressurised water supply tank. Distilled water was used to reduce the risk of clogging the capillary resistances.

4.4. Pressure and pressure gradient measurements.

The level 235 inches below the water injector was chosen as the bottom reference level because it was at the centre of the bottom photographic section.

The bottom pressure gradient was measured between points 188.6 and 245.2 inches below the injector. The bottom absolute pressure was measured at the 245.2 inch level for all runs except runs 31 to 37 inclusive. In these runs, the first runs carried out, the absolute pressure was measured at the 188.6 inch level. Similarly, the centre of the top photographic section, which was 11 inches below the injector, was chosen as the top reference level.

The total pressure gradient at any point is the sum of its frictional, accelerational and gravitational components, viz:-

$$\left(-\frac{dp}{dx}\right)_{tot} = \left(-\frac{dp}{dx}\right)_{fric} + \left(-\frac{dp}{dx}\right)_{acc} + \left(-\frac{dp}{dx}\right)_{grav} \qquad \ldots\ldots\ldots\ldots\ldots\ldots (4.1)$$

This equation is discussed in detail in Section 5 of this Thesis. For the small corrections required to correct the measured pressures and pressure gradients to the reference level values it is sufficient to regard $\left(-\frac{dp}{dx}\right)_{tot}$ as being proportional to $\left(-\frac{dp}{dx}\right)_{fric}$. For a given mass flow rate and assuming that the flow structure does not change then $\left(-\frac{dp}{dx}\right)_{fric}$ is proportional to the mixture velocity. This is approximately inversely proportional to the gas density and therefore the absolute pressure.

Thus:-

$$\left(-\frac{dp}{dx}\right)_{tot} \propto \frac{\text{constant}}{p} \qquad \ldots\ldots\ldots\ldots\ldots\ldots\ldots(4.2)$$

$$\text{Integrating : } \frac{1}{2}\left[p_1^2 - p_2^2\right] = \text{const.}\left[x_2 - x_1\right] \ldots\ldots\ldots(4.3)$$

$$\text{Hence} \qquad p_3^2 = p_1^2\left[\frac{x_2 - x_3}{x_2 - x_1}\right] + p_2^2\left[\frac{x_3 - x_1}{x_2 - x_1}\right] \ldots\ldots(4.4)$$

Equation (4.3) shows that, at least over a short distance, it is more accurate to consider p^2 rather than p to vary linearly with distance. By using equations (4.2), (4.3) and (4.4) relationships for the calculation of absolute pressures and point values of the total pressure gradient at the reference levels were derived. They were:-

$$p_{235} = \left[0.1802(p_{245.2} + 2.0404\Delta PB)^2 + 0.8198p_{245.2}^2\right]^{\frac{1}{2}} \qquad \ldots\ldots\ldots\ldots\ldots(4.5)$$

$$\left(-\frac{dp}{dx}\right)_{235} = \frac{0.2450\left[(p_{245.2} + 2.0404\Delta PB)^2 - p_{245.2}^2\right]}{\left[0.1802\ (p_{245.2} + 2.0404\Delta PB)^2 + 0.8198p_{245.2}^2\right]^{\frac{1}{2}}} \qquad \ldots\ldots\ldots\ldots\ldots(4.6)$$

$$p_{11} = \left[0.8615\ p_{2.9}^2 + 0.1385(p_{2.9} - 2.1089\Delta PT)^2\right]^{\frac{1}{2}} \quad \ldots\ldots(4.7)$$

$$\left(-\frac{dp}{dx}\right)_{11} = \frac{0.2371\left[p_{2.9}^2 - (p_{2.9} - 2.1089\Delta PT)^2\right]}{\left[0.8615\ p_{2.9}^2 + 0.1385(p_{2.9} - 2.1089\Delta PT)^2\right]^{\frac{1}{2}}} \quad \ldots\ldots(4.8)$$

where $p_{245.2}$ and $p_{2.9}$ were the absolute pressures at the 245.2 and 2.9 inch levels, ΔPB was the differential pressure between the 188.6 inch level and the 245.2 inch level, and ΔPT was the differential pressure between the 2.9 inch level and the 61.2 inch level both in ft water/ft tube. The expressions in the forms (4.5) to (4.8) could be evaluated directly on a programmable desk calculator. These calculated point values are tabulated under the derived results in Appendix 1.

4.4.1. Plotting of the pressure gradient data

In the first method chosen for plotting the pressure gradient data they were plotted in the dimensionless form feet of water per foot of tube against the air rate. Different curves were obtained for each liquid rate and each pressure. Comparison of the curves and insight into their nature was almost impossible with the data in this form. Reference lines for air flow alone calculated using a relative roughness of 0.0004 from the friction factor - Reynolds number curves in Foust et al. (1960) were added to give a basis for comparison. These lines were drawn for densities equal to the mean gas density at the 235

inch level for each of the three pressure levels. The mean gas densities were 0.0267 lb/ft^3, 0.0712 lb/ft^3 and 0.2193 lb/ft^3 respectively. These three reference lines could be made to lie near one another by plotting the calculated pressure gradients against a "reduced" gas velocity defined as $\bar{u}_G \left[\frac{\rho_G}{\rho_{ref}}\right]^{\frac{1}{2}}$, where ρ_{ref} is a reference density. This was chosen as the mean density of the medium pressure runs, 0.0712 lb/ft^3.

The three reference lines did not coincide because in a single phase flow the friction factor is a function of the Reynolds number and therefore also of the density. By trial and error it was found that the lines could be almost superimposed if a "reduced" gas velocity defined by $\bar{u}_G \left[\frac{\rho_G}{\rho_{ref}}\right]^{15/32}$ was used.

Plotting the experimental data against a reduced gas velocity resulted in different curves for the different liquid flow rates. It was finally decided to plot the data as if the two phase mixture behaved as a homogeneous fluid. The reduced velocity can be written in the form:-

$$\left[\frac{\bar{u}_G \rho_G}{\rho_{ref}}\right]^{15/32} \bar{u}_G{}^{17/32}$$

In terms of the liquid and gas mass flow rates G_L and G_G This is:-

$$\text{Reduced velocity} = \left[\frac{G_L + G_G}{0.0712}\right]^{15/32} \left[\frac{G_L}{\rho_L} + \frac{G_G}{\rho_G}\right]^{17/32} \qquad \text{.....(4.9)}$$

The reason a fractional power rather than a decimal power was used was that it could be easily handled on the desk calculator which could calculate repeated square roots rapidly.

The advantages of using a homogeneous reduced velocity instead of a simple air velocity are:-

(1) It permits data obtained at different densities, in particular the top and bottom pressure gradients, to be compared.

(2) At high gas velocities with total liquid entrainment the mixture should behave like a homogeneous gas. The departure from true homogeneous behaviour should be of interest.

4.4.2. The pressure gradient graphs.

The pressure gradient data obtained at a water flow rate of 1000 lb/hr are shown in Figure 4.1. Graphs of the data obtained at the other water flow rates are given in Appendix 3. The reference lines for air flow alone are also plotted. These are shown as a set of three lines which almost superimpose, the low pressure line having the least slope and the high pressure line the greatest slope. An additional reference line which is 2½ times (150% above) the standard reference set of lines is also plotted. It should be noted that these reference lines are frictional pressure gradients only and do not include accelerational and gravitational effects.

LEGEND

WATER RATE (LB/HR)	INJECTOR TYPE	SYSTEM PRESSURE	PRESSURE GRADIENT SYMBOL Δ11	PRESSURE GRADIENT SYMBOL Δ235	PRESSURE GRADIENT GRAPH Δ11	PRESSURE GRADIENT GRAPH Δ235
1000	Porous Wall	Low	○	●	– ——	——
1000	Porous Wall	Medium	□	■	– ——	——
1000	Spray	Medium	◇	◆	– – –	– –
1000	Porous Wall	High	△	▲	– ——	——
1000	Spray	High	▽	▼	– – ——	– –

Figure 4.1 TOTAL PRESSURE GRADIENT VERSUS REDUCED VELOCITY WATER RATE 1000 LB/HR.

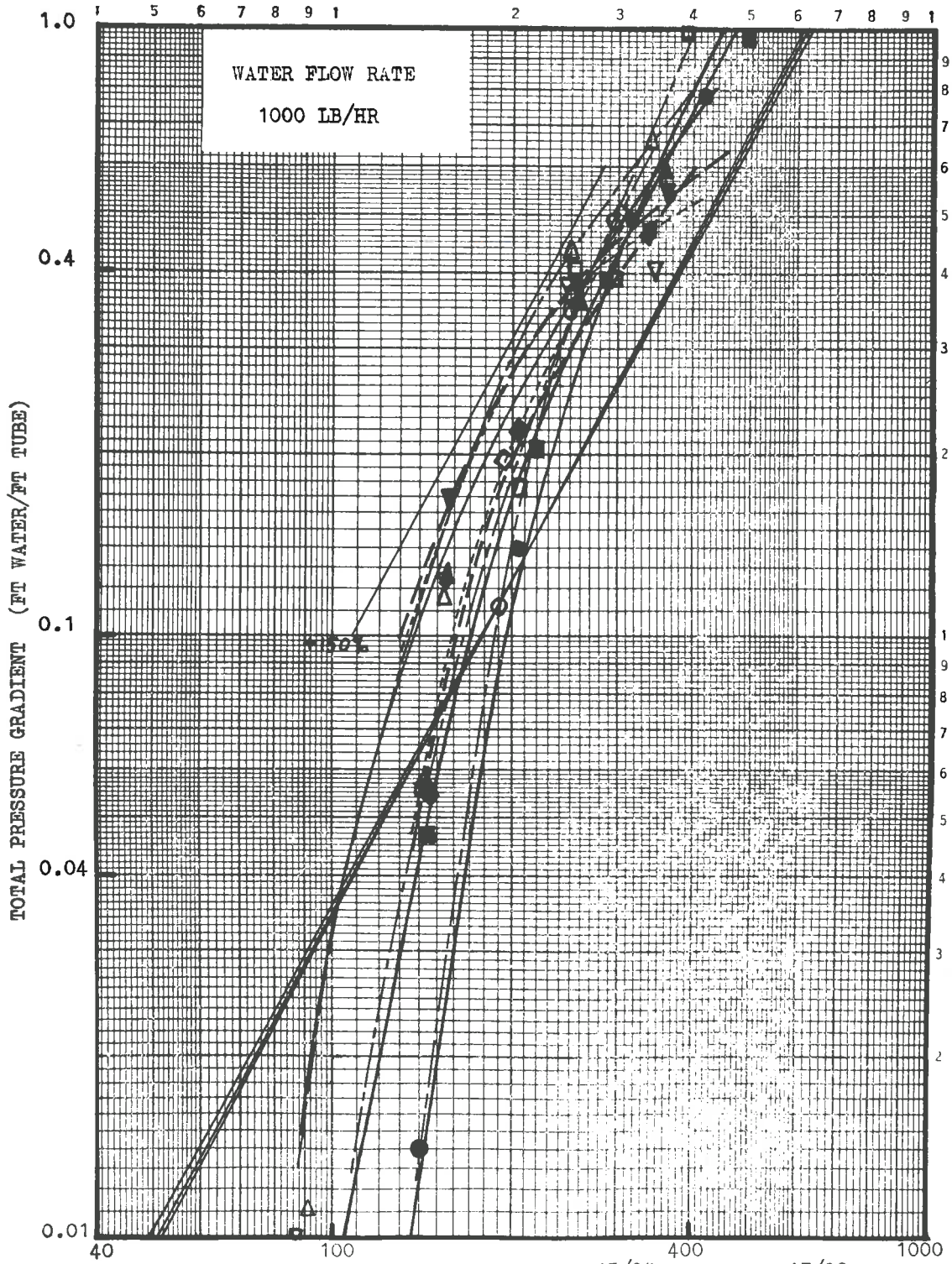

$$\text{REDUCED VELOCITY (FT/SEC)} = \frac{1}{3600}\left[\frac{G_L+G_G}{\rho_{ref}}\right]^{15/32}\left[\frac{G_L}{\rho_L}+\frac{G_G}{\rho_G}\right]^{17/32}$$

ρ_{ref} = 0.0712 LB/FT^3. G_L AND G_G IN LB/FT^{2}HR.

If it is assumed that equation (4.2) holds over the entire test section then values of the top and bottom pressure gradient can be calculated from the top and bottom absolute pressures. These values were used when the curves of best fit were drawn. They were particularly useful in showing up bad data points and also in indicating the likely deviation from the true value of points slightly in error.

The graphs are of considerable assistance in understanding the nature of the gas-liquid interaction in two phase flow. Only points arising directly from the graphs can be mentioned here. They are:-

(1) At moderate to high gas rates the curves lie substantially above and approximately parallel to the reference lines. The high pressure curves are furthest above, being about twice the reference value.

(2) At very high gas velocities the curves cross each other. The cross over is probably due to accelerational effects. The shape of the high pressure curves, which are least affected by accelerational effects, suggests that, if the accelerational component were removed, the curves would approach the reference lines.

(3) At low gas velocities there is little gas-liquid interaction and the curves fall below the reference line. In this region the curves become very steep and the use of a reduced velocity is unsatisfactory. It can be seen

from equation (4.9) that if G_L is at least several times G_G then the reduced velocity is approximately proportional to the square root of the gas velocity. It follows that graphs of pressure gradient versus reduced velocity will have about twice the slopes of graphs of pressure gradient versus gas velocity when plotted on logarithmic co-ordinates.

(4) Comparisons between curves at different liquid rates show that as the liquid rate is increased the portion of the curve approximately parallel to the reference lines occurs at higher pressure gradients. The maximum displacement of this portion of the curves above the reference lines occurs at the liquid rates of 600 and 1000 lb/hr.

(5) The differences between the pressure gradients produced by the porous wall injector and the spray injector at the bottom of the test-section were small. As has already been mentioned in Section 2.4.1 of the literature review the pressure gradient measurements of Gill and Hewitt (1968) indicated that an injector which produced a high degree of initial entrainment, such as a spray injector, would cause lower pressure gradients. Far from the injector these differences would be expected to be small. These results do show that in all cases the

spray injector produced a lower pressure gradient at the bottom of the test-section at high gas flow rates. At low gas rates the results showed that there was little difference between the two injectors. This is understandable because at low gas rates there is little entrainment anyway.

(6) Comparison between the top and bottom pressure gradients is difficult because of the differences in absolute pressures at the top and the bottom. As mentioned in point (1) increasing the pressure results in a displacement away from the reference line. The differences between the curves of the top and bottom pressure gradients are small except at low pressures and the higher liquid rates. Under these conditions the pressure gradients at the top are significantly greater than the pressure gradients at the bottom. This is particularly noticeable at the higher gas velocities. It is possibly due to the pressure gradient required to accelerate a relatively large mass of liquid up to a high gas velocity.

4.5. Liquid volume fraction measurements.

The measured liquid volume fractions are tabulated in Appendix 1 and are graphed against the liquid Reynolds number in Figure 4.2. below. In runs with liquid volume fractions less than 0.009 the liquid level was

LEGEND (Cont.)

MEAN SUPERFICIAL AIR VELOCITY AT 235 IN. LEVEL (FT/SEC)	MEAN AIR DENSITY AT 235 IN. LEVEL (LB/FT^3)	INJECTOR TYPE	LIQUID VOLUME FRACTION SYMBOL	LINE
0	0.2225	Porous Wall	▲	H00
20.2	0.2213	Porous Wall	▲	H20
51.1	0.2207	Porous Wall	▲	H51
51.1	0.2193	Spray	▼	HS51
104.0	0.2211	Porous Wall	▲	H104
102.8	0.2183	Spray	▼	HS103
161.4	0.2208	Porous Wall	▲	H161
(Point (5720, 0.047) is for 142 ft/sec, 0.2189 lb/ft^3)				
162.2	0.2182	Spray	▼	HS162

Figure 4.2. LIQUID VOLUME FRACTION VERSUS

DIMENSIONLESS LIQUID FLOW RATE , $N_{Re_L} = \frac{W_L}{\pi D \mu_L}$

LEGEND

MEAN SUPERFICIAL AIR VELOCITY AT 235 IN.LEVEL (FT/SEC)	MEAN AIR DENSITY AT 235 IN. LEVEL (LB/FT^3)	INJECTOR TYPE	LIQUID VOLUME FRACTION SYMBOL	LINE
0	0.0267	Porous Wall	●	L00
50.9	0.0269	Porous Wall	●	L51
104.5	0.0268	Porous Wall	●	L105
208.8	0.0268	Porous Wall	●	L209
(Point (2875, 0.049) is for 235 ft/sec, 0.0255 lb/ft^3)				
347.9	0.0275	Porous Wall	●	L348
0	0.0707	Porous Wall	■	M00
10.4	0.0711	Porous Wall	■	(curves co-incide)
20.7	0.0709	Porous Wall	■	M21
50.7	0.0709	Porous Wall	■	M51
51.3	0.0718	Spray	◆	MS51
98.3	0.0715	Porous Wall	■	M98
98.7	0.0719	Spray	◆	MS99
154.4	0.0701	Porous Wall	■	M154
204.8	0.0718	Porous Wall	■	M205
204.1	0.0711	Spray	◆	MS204
335.9	0.0726	Porous Wall	■	M336
(Point (6244, 0.035) is for 277 ft/sec, 0.0730 lb/ft^3)				

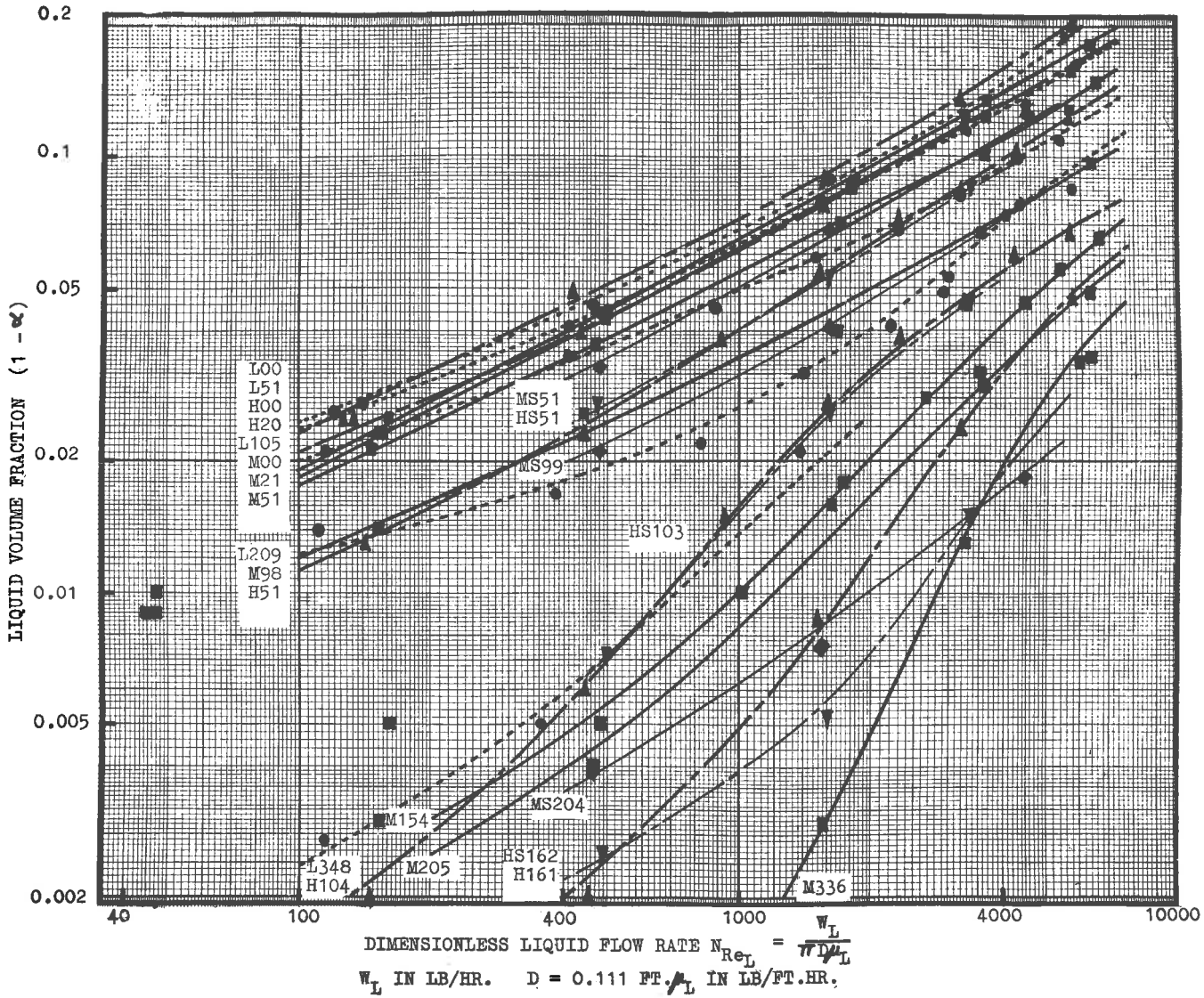
0.2
0.1
0.05
0.02
0.01
0.005
0.002
LIQUID VOLUME FRACTION (1 - ∝)
40
100
400
1000
4000
10000
L00
L51
H00
H20
L105
M00
M21
M51
L209
M98
H51
MS51
HS51
MS99
HS103
MS204
M154
L348
H104
M205
HS162
H161
M336
DIMENSIONLESS LIQUID FLOW RATE $N_{Re_L} = \frac{W_L}{\pi D \mu_L}$
W_L IN LB/HR. D = 0.111 FT. μ_L IN LB/FT.HR.

below the top of the body of the hold-up cock. Hence these measurements are of a lower order of accuracy than the rest. The curves are drawn for different values of the air superficial velocity and density. As would be expected the curves at zero gas velocity almost coincide. At zero gas velocity and the maximum liquid rate there was a tendency to "bridge over" at the highest pressure. This did not occur to the same extent at the lower pressures.

The data obtained at the lowest water flow rate, 30 lb/hr, fell considerably below the extrapolation of the curves based on the higher water flow rates. The 30 lb/hr runs were the first runs carried out and trouble was being experienced in preventing leakage around both hold-up cocks. This was subsequently cured by fitting 'O' rings to these cocks.

4.5.1. Effect of the spray injector on the liquid volume fraction.

In the runs at 50 and 100 ft/sec air velocity the spray injector caused a significantly lower liquid volume fraction at the lower liquid rates but practically no difference at the higher liquid rates. At the higher air velocities, 200 ft/sec (medium pressure) and 160 ft/sec (high pressure) the liquid volume fractions were unaltered

at the lower liquid rates but much less at the higher liquid rates. Under equilibrium conditions, that is when there are constant liquid flow rates in the film and in the core, with high gas velocities most of the liquid flow is in the core. This, together with the high pressure gradient, means that as equilibrium conditions are approached the liquid film is thin. However, because of the high gas velocity, the liquid volume fraction in the core will be small. Therefore, the total liquid volume fraction could still depend mostly on the liquid film thickness. Consequently, variations in film flow rate which are small compared with the total liquid flow rate could appreciably affect the total liquid volume fraction.

These results are substantiated by the core and film flow rate measurements reported in part 8 of this section. The measurements of the total liquid flow rate in the core at the bottom of the test-section show that there is no difference between the porous wall and the spray injector at a gas velocity of 50 ft/sec, but that the spray injector gives more entrainment at the higher gas velocities. This indicates that at high gas velocities there is significantly less flow in the liquid film, even at the bottom of the test-section, when the spray injector is used.

4.5.2. The liquid volume fraction with zero gas flow.

Comparison of the measured liquid volume fractions at zero gas rates with the values predicted by the Dukler analysis showed that the Dukler analysis predicted liquid volume fractions 10-15% high. This difference is probably due to the liquid volume fraction measurements being made far downstream from the injector in a region where the liquid was flowing as fully developed disturbance waves. The Dukler analysis assumes a uniform thickness liquid film.

The testing of various velocity profiles showed that the liquid volume fraction versus N_{Re_L} curve at zero gas flow could be reasonably well fitted by integration of the logarithmic velocity profile:-

$$u_L^+ = A + \frac{1}{\chi} \ln y^+ \qquad \text{.....(4.10)}$$

Allowing for curvature of the tube but ignoring the buoyancy of the core from equation (2.34)

$$N_{Re_L} = \int_0^{\eta} \left(1 - \frac{u_L}{R\sqrt{\tau_w/\rho_L}}\, y^+\right) u_L^+ \, dy^+ \qquad \text{.....(4.11)}$$

and

$$\tau_w = \rho_L g h \qquad \text{.....(4.12)}$$

$$\eta = \frac{h\sqrt{\tau_w \rho_L}}{\mu_L} = \frac{\rho_L}{\mu_L} h^{3/2} g^{\frac{1}{2}} \quad \text{.....(4.13)}$$

$$h = R(1-\sqrt{\alpha}) \quad \text{.....(4.14)}$$

where α is the gas volume fraction

Now $\frac{\mu_L}{R\sqrt{\tau_w \rho_L}} = \frac{h}{\eta R} = \frac{1-\sqrt{\alpha}}{\eta}$ and hence integration of equation (4.11) gives

$$N_{Re_L} = \frac{1}{K}\left(1-\tfrac{1}{2}(1-\sqrt{\alpha})\right)\eta \ln\eta - \frac{1}{K}\left(1-\tfrac{1}{4}(1-\sqrt{\alpha})\right)\eta + A\left(1-\tfrac{1}{2}(1-\sqrt{\alpha})\right)\eta \quad \text{.....(4.15)}$$

Fitting equation (4.15) to the experimental data gave $A = 3.1$ and $K = 0.22$. This was much less than the single phase flow value of 0.36 or 0.40. However, it should be noted that similar reductions in K occur in the gas phase of two phase flow. This has been reviewed in Section 2.4.3.

It is of interest to compare equations (4.10) and (4.15) with the expression of Levich (1948) for a free falling turbulent film given in equation (2.2.1). In non-dimensional form this is:-

$$N_{Re_L} = \frac{\bar{u}_L \rho_L h}{\mu_L} = \frac{\eta}{\sqrt{K_1}} \ln\left[\frac{\eta}{\sqrt{K_1}}\right] \quad \text{.....} \quad (4.16)$$

Equation (4.16) is obtained by integration of

$$u_L^+ = \frac{1}{\sqrt{K_1}} (1 + \ln \sqrt{K_1}) + \frac{1}{\sqrt{K_1}} \ln y^+ \quad \ldots\ldots\ldots (4.17)$$

Equation (4.17) is of similar form to equation (4.10). Putting $\sqrt{K_1} = 0.30$ fitted the experimental data approximately, but gave too steep a slope at the lower Reynolds numbers.

Application of the Dukler analysis to the zero gas flow case

If the shear stress varies linearly across the liquid film (equation 2.28) and the von Kármán equation is assumed to hold far from the solid wall, then integration by the method of Hewitt (1961) gives:-

$$\frac{du_L^+}{dy^+} = \frac{s^3/\eta}{2 \left(\text{Constant} - \sqrt{1 - \frac{s^3 y^+}{\eta}}\right)} \quad \ldots\ldots\ldots\ldots (4.18)$$

Hewitt put the constant = 1 which gives

$$\frac{du_L^+}{dy^+} = \frac{1 + \sqrt{1 - \left(s^3/\eta\right) y^+}}{2 K y^+} \quad \ldots\ldots\ldots\ldots\ldots (4.19)$$

This gives $\frac{du_L^+}{dy^+} = \frac{1}{K y^+}$ near the solid wall. This is the same as obtained by differentiation of equation (4.10). However, at the interface equation (4.19) fails.

It gives $\frac{du_L^+}{dy^+} = \frac{1}{2\kappa y^+}$ at the interface for a free falling film ($s^3=1$), whereas $\frac{du_L^+}{dy^+}$ should be 0 as the shear stress is zero. Examination of equation (4.19) suggests that a reasonable alternative which satisfies the boundary conditions, but is unable to satisfy the von Kármán relationship, is:-

$$\frac{du_L^+}{dy^+} = \frac{\sqrt{1-(s^3/\eta)y^+}}{\kappa y^+} \qquad \ldots\ldots\ldots\ldots(4.20)$$

This integrates to:-

$$u_L^+ = A^1 + \frac{1}{\kappa}\left[2\sqrt{1-\frac{s^3}{\eta}y^+} + 2\ln\left(1-\sqrt{1-\frac{s^3}{\eta}y^+}\right) - \ln\frac{s^3}{\eta}y^+ \right]$$

$$\ldots\ldots\ldots\ldots(4.21)$$

Substitution of equation (4.21) into equation (4.11) and integration gives:-

$$N_{Re_L} = \left[A^1\left(y^+ - \frac{1-\sqrt{\alpha}}{2\eta}y^{+2}\right) + \frac{1}{\kappa}\left\{ -\frac{4}{3s^3}\left(1-\frac{s^3}{\eta}y^+\right)^{3/2} \right.\right.$$

$$+ 2y^+\ln\left(1-\sqrt{1-\frac{s^3}{\eta}y^+}\right) - y^+\ln\frac{s^3}{\eta}y^+ + \frac{2\eta}{s^3}\sqrt{1-\frac{s^3}{\eta}y^+}$$

$$- \frac{1-\sqrt{\alpha}}{\eta}\left\{ \frac{2\left(2+3\frac{s^3}{\eta}y^+\right)}{15(s^3/\eta)^2}\left(1-\frac{s^3}{\eta}y^+\right)^{3/2} + y^{+2}\ln\left(1-\sqrt{1-\frac{s^3}{\eta}y^+}\right)\right.$$

$$\left.\left.\left. - \frac{1}{2}y^{+2}\ln\frac{s^3}{\eta}y^+ + \frac{2+(s^3/\eta)y^+}{3(s^3/\eta)^2}\sqrt{1-\frac{s^3}{\eta}y^+} \right\}\right\} \qquad \ldots\ldots\ldots\ldots(4.22)$$

For $s^3 = 1$ this is:-

$$N_{Re_L} = -\frac{1}{K}\left[\frac{2}{3} - \frac{2}{5}(1-\sqrt{\alpha})\right]\eta + A^1\left[1 - \frac{1}{2}(1-\sqrt{\alpha})\right]\eta \quad \ldots\ldots\ldots(4.23)$$

Equation (4.23) suggests that N_{Re_L} is a linear function of η. However, an examination of the data shows that they cannot be fitted by a linear equation. Indeed the logarithmic equation, equation (4.15), is able to fit the data well and can follow the slight upward curve on a log-log plot of $(1-\alpha)$ versus N_{Re_L}. A power relationship is unable to do this.

Integration of equation (4.19) gives an expression for N_{Re_L} half way between equations (4.15) and (4.23). As it contains a logarithmic part it can be made to fit the data by choosing $K = 0.107$ which is about half that required by equation (4.15).

The failing of equation (4.15) is that it does not allow for the disturbance waves. The non-dimensional film thickness, η, is not constant at a particular level in the tube but varies about a mean value. Near the porous wall injector the amplitude of this variation is small. Far downstream from the injector, where the waves are fully developed, the amplitude is larger. The presence of disturbance waves probably means that the average value of the liquid volume fraction is less than if no waves were present.

4.5.3 The liquid volume fraction with co-current gas flow.

In this case equation (4.12) becomes:-

$$\tau_w = \tau_i + \rho_L g h \quad \ldots\ldots\ldots\ldots\ldots\ldots\ldots\ldots\ldots\ldots (4.24)$$

and $$\tau_i = \frac{R-h}{2\rho_L g} \left(-\frac{dp}{dx}\right)^* \quad \ldots\ldots\ldots\ldots\ldots\ldots\ldots\ldots (4.25)$$

where $\left(-\frac{dp}{dx}\right)^*$ is the frictional pressure gradient in feet of water per foot of tube. Substitution of equation (4.25) into equation (4.24) and equation (4.24) into equation (4.13) gives:-

$$\eta = \frac{\rho_L}{\mu_L} h^{3/2} g^{\frac{1}{2}} \sqrt{1 + \frac{R-h}{2h} \left(-\frac{dp}{dx}\right)^*} \quad \ldots\ldots\ldots (4.26)$$

In the general case of combined gas-liquid flow droplet entrainment is present. Hence equation (4.14) does not hold since α depends upon both the liquid film thickness and the droplet concentration in the core. This is discussed further in Section 5 where the interaction between all the results is examined.

4.6. Wave velocity measurements.

The wave velocity results are tabulated in Appendix 1. The velocity of each wave measured is reported as well as the mean velocity and the standard

deviation of the velocities for each run. The experimentally measured mean wave velocities obtained from the medium pressure series of runs at the bottom measurement level, 235 inches below the injector, are graphed in Figure 4.3. The wave velocities in ft/sec are plotted against the liquid Reynolds number. Logarithmic co-ordinates have been used for the x-axis because of the wide range of liquid Reynolds numbers. Linear co-ordinates were used for the y-axis because of the small range of the measured wave velocities. If linear co-ordinates had been used for the x-axis this would have given too much weight to the measurements at high Reynolds numbers.

The graphs for the low and high pressure runs and the points at the top and centre measurement levels are given in Appendix 3. The results obtained at 30 lb/hr liquid rate are not graphed, although they have been tabulated in Appendix 1. The ciné film from which these measurements were made was taken with the test-section illuminated from the front, and it was almost impossible to detect the waves. Consequently, it is likely that some of the disturbance waves in these ciné film sequences were not seen properly.

It should be noted that a more satisfying method

LEGEND

MEAN SUPERFICIAL AIR VELOCITY AT 235 IN. LEVEL (FT/SEC)	MEAN AIR DENSITY AT 235 IN. LEVEL (LB/FT^3)	INJECTOR TYPE	WAVE VELOCITY SYMBOL	WAVE VELOCITY LINE DESIGNATED BY
0	0.0703	Porous Wall	■	M00
10.6	0.0705	Porous Wall	■	M11
20.8	0.0706	Porous Wall	■	M21
50.7	0.0709	Porous Wall	■	M51
51.3	0.0718	Spray	◆	MS51
98.3	0.0715	Porous Wall	■	M98
98.7	0.0719	Spray	◆	MS99
154.4	0.0701	Porous Wall	■	M154
204.8	0.0718	Porous Wall	■	M205
204.1	0.0711	Spray	◆	MS204
335.9	0.0726	Porous Wall	■	M336

(Point (6244, 22.97) is for 277 ft/sec, 0.0730 lb/ft^3)

Figure 4.3 MEAN WAVE VELOCITY VERSUS DIMENSIONLESS LIQUID FLOW RATE, $N_{Re_L} = \frac{W_L}{\pi D \mu_L}$.
MEDIUM PRESSURE SERIES AND 235 INCH LEVEL.

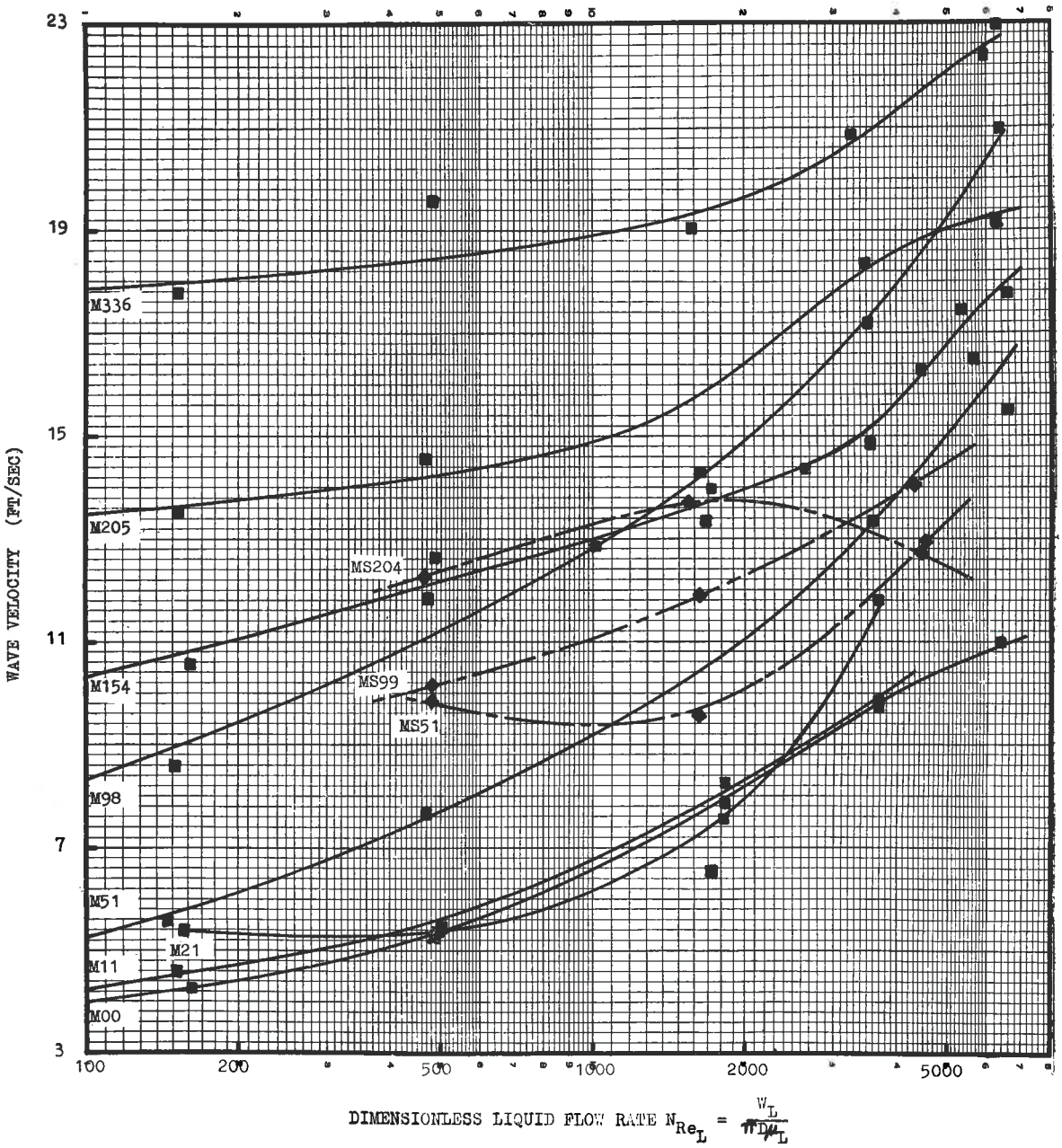
WAVE VELOCITY (FT/SEC)
23
19
15
11
7
3
M336
M205
MS204
M154
MS99
MS51
M98
M51
M21
M11
M00
100
200
500
1000
2000
5000
DIMENSIONLESS LIQUID FLOW RATE $N_{Re_L} = \frac{W_L}{\pi D \mu_L}$

of presentation of the data is to plot the mean wave velocity against the liquid film Reynolds number. This requires that the net flow rate of the liquid film is known. This is done in Section 5. Also, because the temperature was not deliberately varied and water was the only liquid used the Reynolds number is only equivalent to a dimensionless water flow rate.

An analysis of disturbance wave velocities can be made by using the approach of Lighthill and Whitham (1955). This has already been used in Section 2.1.2. to determine the velocity of an infinitesimal disturbance on a laminar liquid film. The analysis predicted that

$$c/\bar{u}_L = \frac{6}{3-s^3} \qquad \text{.....(4.27)}$$

where c is the disturbance velocity, $\bar{u}_L$ is the average film velocity and $s^3 = \frac{1}{I} = \frac{(\rho_L - \rho_c)gh}{\tau_w}$. The method of Lighthill and Whitham applies to situations in which the restoring forces, such as gravity or surface tension, on the wave are negligible and the wave motion is determined by continuity considerations only. Such situations can occur for finite as well as infinitesimal disturbances.

Lighthill and Whitham used their analysis to describe the motion of flood waves in river systems.

In the case of annular flow in a vertical tube gravity does not either stabilize or unstabilize the gas-liquid interface. Surface tension exerts a stabilizing force. This force is powerful for waves of short wave length but weak for waves of longer wave length such as disturbance waves. The analysis of a laminar free falling film by Massot, Irani and Lightfoot (1966) has been reviewed in Section 2.1.2.

If the motion of a disturbance wave is determined by continuity considerations only, then from equation (2.14)

$$c = \frac{dQ_L}{dh} = u^* \frac{dN_{Re_L}}{d\eta} \qquad \text{.....(4.28)}$$

If N_{Re_L} is given by a logarithmic form of equation, such as equation (4.15), then, ignoring curvature,

$$\frac{dN_{Re_L}}{d\eta} = A + \frac{1}{\chi} \ln \eta \qquad \text{.....(4.29)}$$

$$\text{But} \quad \overline{u}_L^+ = \frac{N_{Re_L}}{\eta} = A + \frac{1}{\chi}(\ln \eta - 1) \qquad \text{.....(4.30)}$$

$$\therefore \quad \frac{dN_{Re_L}}{d\eta} = \overline{u}_L^+ + \frac{1}{\chi} \qquad \text{.....(4.31)}$$

$$\therefore \quad c = \bar{u}_L + \frac{u^*}{K} \qquad \ldots\ldots\ldots\ldots\ldots\ldots\ldots\ldots\ldots\ldots (4.32)$$

Equation (4.32) suggests that $(c-\bar{u}_L)$ should be equal to $\frac{u^*}{K} = \frac{1}{K_N}\sqrt{\frac{\tau_w}{\rho_L}}$. Equation (4.32) was compared with the experimental results for zero and low gas velocities, that is under conditions for which there was zero entrainment and $\bar{u}_L$ could be calculated from the liquid flow rate and the liquid volume fraction.

This comparison showed that equation (4.32) was incorrect at low liquid rates. Under these conditions the difference $(c-\bar{u}_L)$ was considerably greater than given by $\frac{u^*}{K}$ with $K = 0.22$. This suggests that the use of an average film velocity for low liquid flow rates is inadequate.

The reason could be that the waves are too few and too widely spaced.

At higher liquid flow rates much better agreement was obtained. This is possibly because at higher liquid flow rates the disturbance waves are more closely spaced and hence the use of an average film velocity more nearly represents the true situation. A further discussion is given in Section 5 where the use of core and film flow data permits the calculation of $\bar{u}_L$ even when droplet entrainment is present.

LEGEND

PRESSURE	INJECTOR TYPE	CAMERA LEVEL (INCH)	SYMBOL
Low	Porous Wall	235	●
Medium	Porous Wall	235	■
High	Porous Wall	235	▲

Figure 4.4 WAVE VELOCITY STANDARD DEVIATION VERSUS MEAN WAVE VELOCITY. LIQUID RATE 600 LB/HR.

Low	Porous Wall	235	●
Medium	Porous Wall	11	□
Medium	Spray	11	◇
Medium	Porous Wall	56	◧
Medium	Spray	56	◈
Medium	Porous Wall	235	■
Medium	Spray	235	◆
High	Porous Wall	11	△
High	Spray	11	▽
High	Porous Wall	56	◭
High	Spray	56	▼
High	Porous Wall	235	▲
High	Spray	235	▼

--- Line of best fit for points at 235 inch level.

— Line of best fit for all points.

Figure 4.5 WAVE VELOCITY STANDARD DEVIATION VERSUS MEAN WAVE VELOCITY. LIQUID RATE 1000LB/HR.

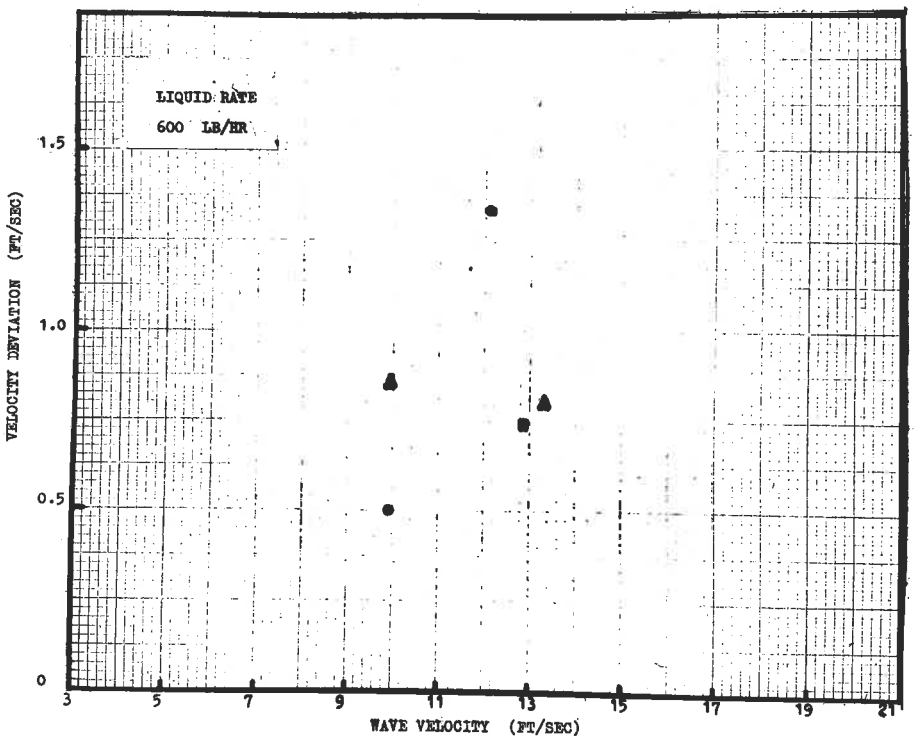
LIQUID RATE
600 LB/HR
VELOCITY DEVIATION (FT/SEC)
0
0.5
1.0
1.5
3
5
7
9
11
13
15
17
19
21
WAVE VELOCITY (FT/SEC)

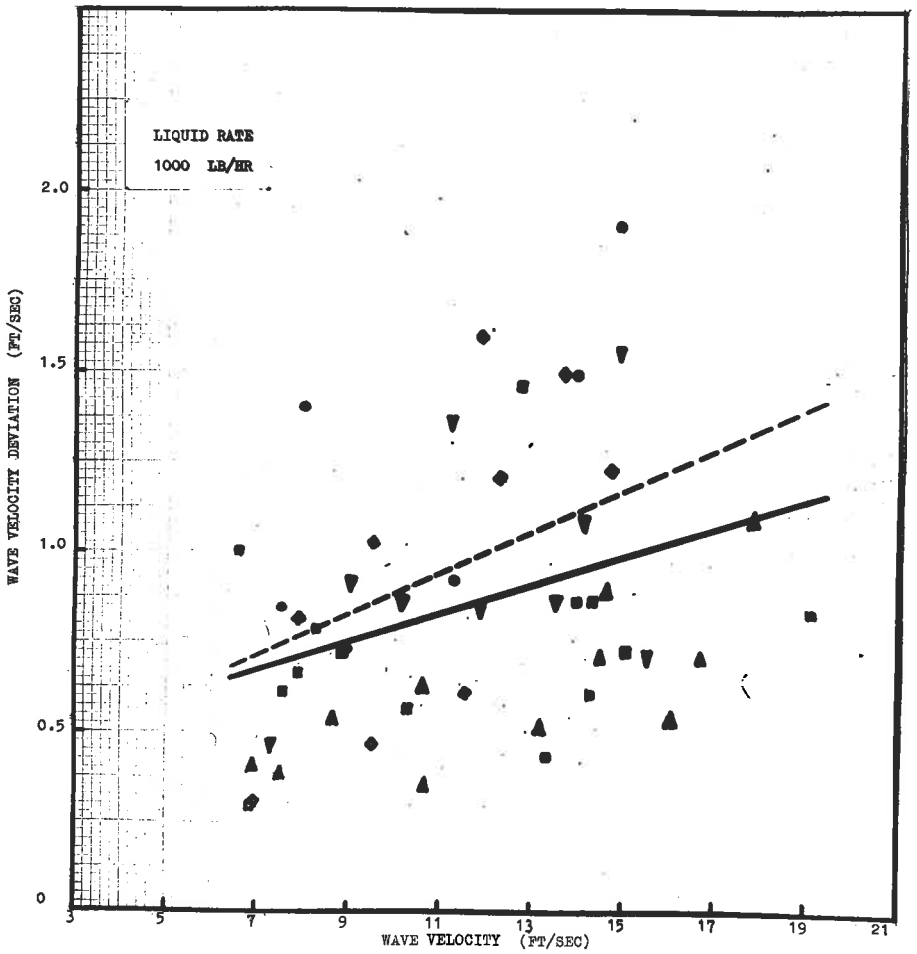
LIQUID RATE
1000 LB/HR
WAVE VELOCITY DEVIATION (FT/SEC)
0
0.5
1.0
1.5
2.0
3
5
7
9
11
13
15
17
19
21
WAVE VELOCITY (FT/SEC)

4.6.1. Wave velocity standard deviations.

The measured wave velocity standard deviations are plotted against the measured mean wave velocities for all of the experimental data obtained at water flow rates of 600 and 1000 lb/hr in Figures 4.4 and 4.5 respectively. The remainder of the experimental data is graphed in Appendix 3.

Hall Taylor and Hedderman (1968) had found that the standard deviations of their wave velocity data were independent of the mean wave velocities. These present results show a very wide spread and it is difficult to draw definite conclusions from them. They were grouped into 8 sets corresponding to the 8 different water flow rates. The data at 100, 300, 1000, 2000, 2700 and 3500 lb/hr water flow rates were fitted with a straight line relationship of the form:-

Velocity deviation = C_4 x (Mean Velocity) + C_5.....(4.33)

A least squares analysis was used to obtain the line of best fit. For the sets of runs at 300, 1000, 2000, and 2700 lb/hr the line of best fit for the bottom points only was also calculated. The values of C_4 and C_5 are given in Table 4.1 below.

Water Rate (lb/hr)	No. of points	C_4	C_5	Standard deviation of the velocity standard deviations
100	18	0.0250	0.296	0.193
300 (bottom)	24	0.0497	0.183	0.309
300 (all)	48	0.0471	0.210	0.247
1000 (bottom)	24	0.0301	0.577	0.400
1000 (all)	49	0.0404	0.378	0.347
2000 (bottom)	21	0.0549	0.266	0.608
2000 (all)	33	0.0541	0.274	0.460
2700*(bottom)	8	0.0562	0.419	0.222
2700*(all)	21	0.0845	0.016	0.134
3500	16	0.0692	0.242	0.443

* omitting two points

Table: 4.1. VALUES OF THE CONSTANTS C_4 AND C_5 AND THE STANDARD DEVIATION FOR THE LINES OF BEST FIT IN THE WAVE STANDARD DEVIATION VERSUS WAVE VELOCITY DATA.

It can be seen from the values of C_4 in the table that, in contrast to the results of Hall Taylor and Nedderman (1968), these results indicate that the velocity standard deviation increases as the wave velocity increases. The rate of increase is greater at the higher liquid flow rates. The column listing the standard deviation of the velocity standard deviation shows the large scatter in these present results. There is not much difference between the slopes of the lines for the bottom points only and the slopes of the lines which are based on all

LEGEND.

MEAN SUPERFICIAL AIR VELOCITY AT 235 IN. LEVEL (FT/SEC)	MEAN AIR DENSITY AT 235 IN. LEVEL (LB/FT^3)	INJECTOR TYPE	TIME BETWEEN WAVES SYMBOL	LINE DESIGNATED BY
0	0.0703	Porous Wall	■	M00
10.6	0.0705	Porous Wall	■	M11
20.8	0.0706	Porous Wall	■	M21
50.7	0.0709	Porous Wall	■	M51
51.3	0.0718	Spray	◆	MS51
98.3	0.0715	Porous Wall	■	M98
98.7	0.0719	Spray	◆	MS99
154.4	0.0701	Porous Wall	■	M154
204.8	0.0718	Porous Wall	■	M205
204.1	0.0711	Spray	◆	MS204
335.9	0.0726	Porous Wall	■	M336

(Point (6277, 0.038) is for 277 ft/sec, 0.0730 lb/ft^3)

Figure 4.6 MEAN TIME BETWEEN WAVES VERSUS DIMENSIONLESS LIQUID FLOW RATE, $N_{Re_L} = \frac{W_L}{\pi D \mu_L}$. MEDIUM PRESSURE SERIES AND 235 INCH LEVEL.

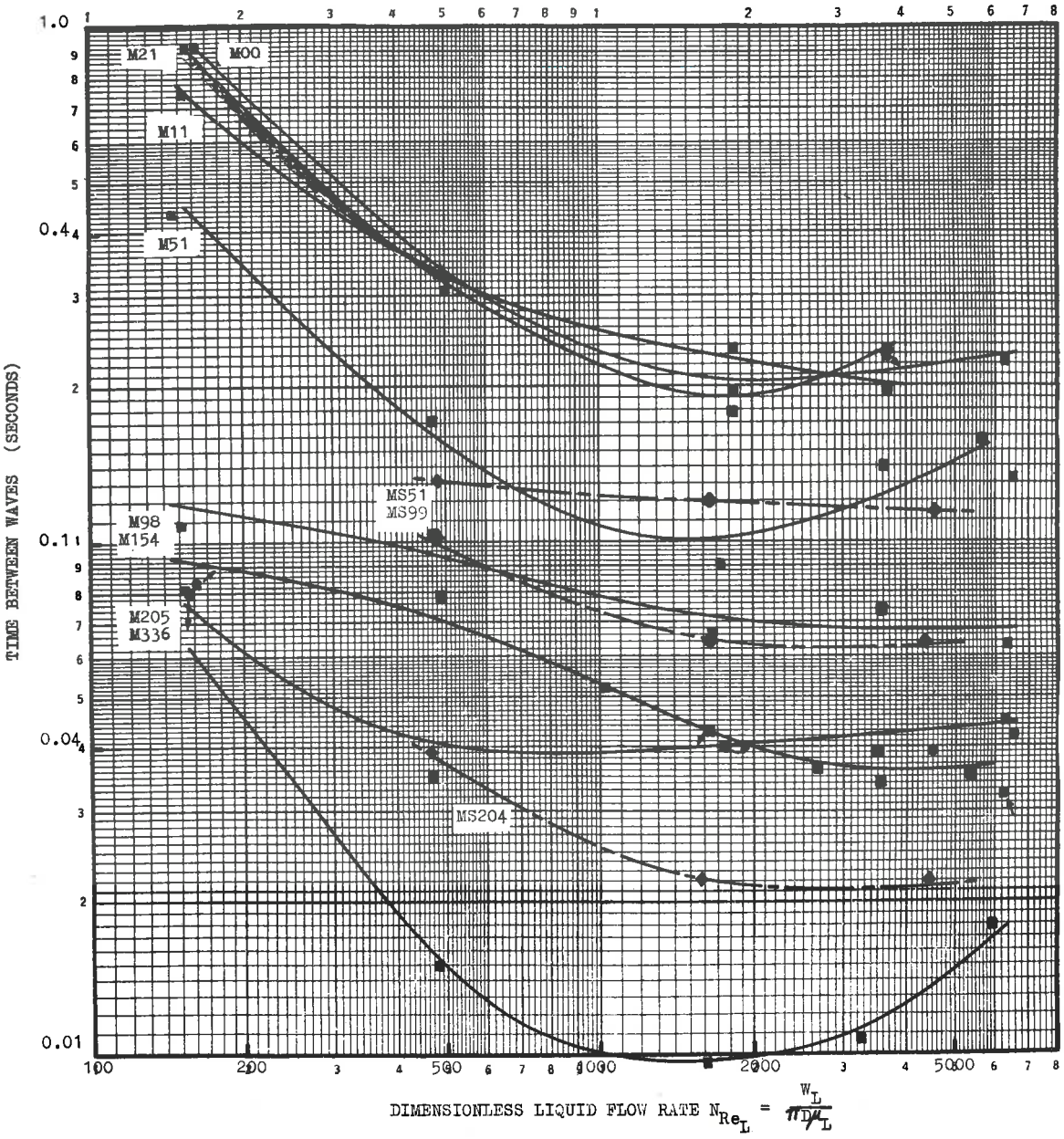
TIME BETWEEN WAVES (SECONDS)
1.0
0.4
0.1
0.04
0.01
M21
M00
M11
M51
MS51
MS99
M98
M154
M205
M336
MS204
100
200
500
1000
2000
5000
DIMENSIONLESS LIQUID FLOW RATE $N_{Re_L} = \frac{W_L}{\pi D \mu_L}$

points and thus it seems likely that the relationship between velocity deviation and mean velocity is unaffected by the distance along the test-section.

4.7. Wave frequency measurements.

The wave frequency measurements are tabulated in Appendix 1. The time interval between successive waves is recorded, together with the mean time interval and the standard deviation of the time intervals for each run. Because the time interval between waves was inherently irregular it was considered much more satisfactory to record and interpret the results on the basis of time intervals rather than wave frequencies.

In Figure 4.6 the experimentally measured mean time intervals for the medium pressure series of runs at the bottom measurement level are graphed against the liquid Reynolds number. They are for the same set of runs as the mean wave velocity data graphed in Figure 4.3. In Figure 4.6 logarithmic co-ordinates are used for the y-axis as well as the x-axis because of the wide range of the measured time intervals.

The graphs for the low and high pressure runs and the points at the top and centre measurement levels are given in Appendix 3. These are for the same sets of data as graphed in the plots of mean wave velocity versus

liquid Reynolds number. Examination of these graphs shows that for a fixed gas flow rate as the liquid flow rate was increased the time interval between waves at the bottom of the test-section initially decreased, then levelled out to an almost constant value and at high liquid rates appeared to increase somewhat. There was not much difference between the spray and porous wall injectors. At the top and centre measuring stations the time intervals between waves was less. Comparisons between all three stations showed that most of the wave merging had occurred by the centre station. In the discussion section the theory of Hall Taylor and Nedderman (1968) on wave merging is discussed and applied to these data.

4.8. Core flow measurements.

Because of the large amount of work required the sampling probe measurements of droplet mass velocities in the core were limited to the 15 psia and 45 psia pressure levels. The experimental results are tabulated in Appendix 1. They have been left in the form in which they were obtained, that is in lb/hr of water through the probe mouth. To obtain a mass velocity it is necessary to divide the measurements by the area of the probe mouth. The data for the runs at 100 ft/sec superficial air velocity and 1000 lb/hr water flow rate are shown in

LEGEND; DROPLET ENTRAINMENT PROFILES

RUN NO.	WATER FLOW RATE (LB/HR)	SUPERFICIAL AIR VELOCITY AT 235 IN.LEVEL (FT/SEC)	AIR DENSITY AT 235 IN. LEVEL (LB/FT^3)	INJECTOR TYPE	DROPLET FLOW THROUGH PROBE POSITION, IN.BELOW INJECTOR	SYMBOL	LINE
86	991	100.6	0.0730	Porous Wall	15.9	□	.....
83	1000	108	0.0714	Porous Wall	60.8	◧	- - - -
84	1000	100.4	0.0714	Porous Wall	244.8	■	———
88	1000	107.3	0.0706	Spray	15.9	◇	------
89	1002	105.4	0.0702	Spray	60.8	◈	- - - -
90	995	92.5	0.0713	Spray	244.8	◆	——— -
91	1002	102.7	0.0709	Spray	244.8	◆	——— - -

Figure 4.7 MEDIUM PRESSURE SERIES MEAN AIR RATE 101.3 FT/SEC MEAN WATER RATE 999 LB/HR

187	1003	98.6	0.2204	Porous Wall	15.9	△	.....
184	994	101.5	0.2182	Porous Wall	60.8	◭	- - - - -
185	998	104.1	0.2207	Porous Wall	244.8	▲	———
188	997	107.6	0.2109	Spray	15.9	▽	------
189	997	103.8	0.2177	Spray	60.8	◸	- - - -
190	1000	101.2	0.2190	Spray	244.8	▼	——— -
191	1004	104.2	0.2180	Spray	244.8	▼	——— - -

Figure 4.8 HIGH PRESSURE SERIES MEAN AIR RATE 103.1 FT/SEC MEAN WATER RATE 999 LB/HR

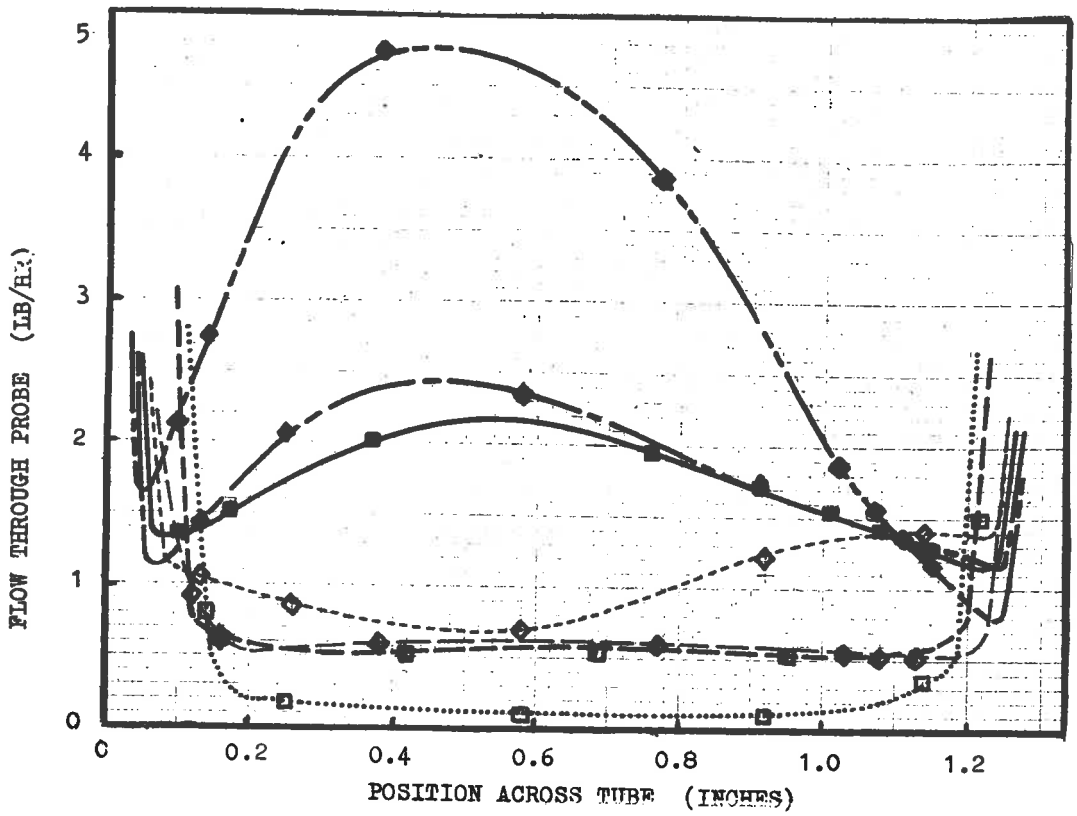
FLOW THROUGH PROBE (LB/HR)
0
1
2
3
4
5
0
0.2
0.4
0.6
0.8
1.0
1.2
POSITION ACROSS TUBE (INCHES)

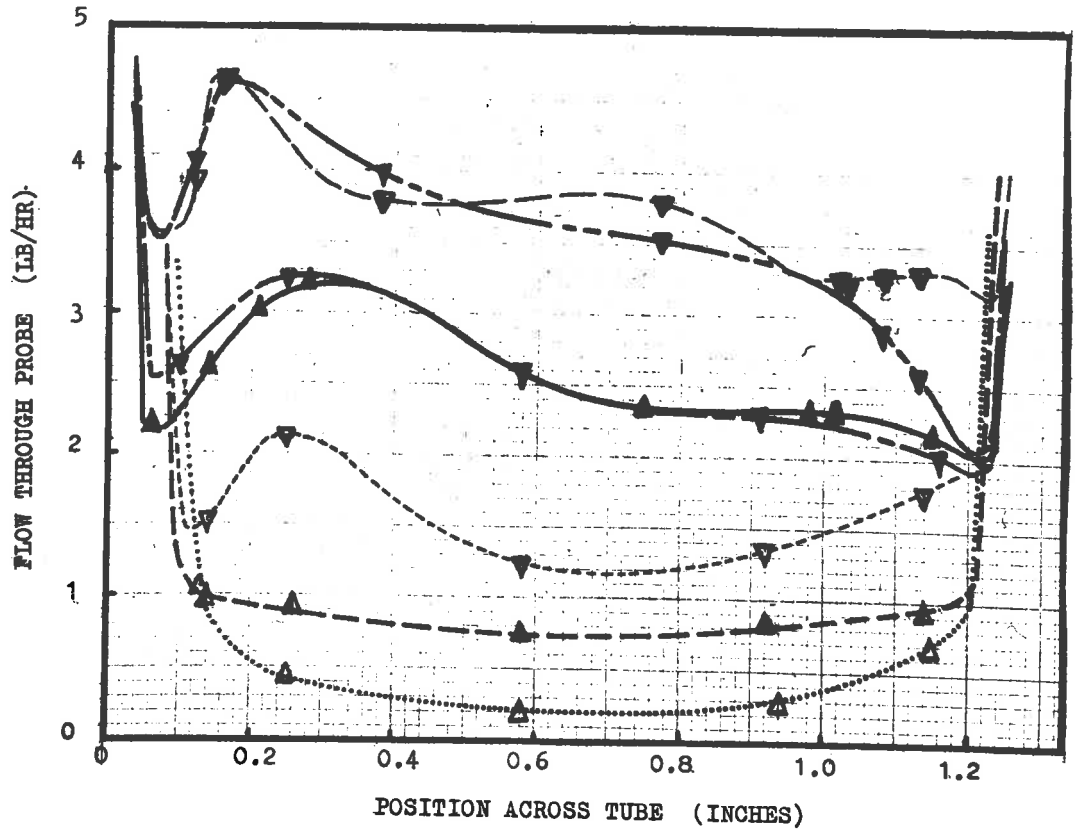
FLOW THROUGH PROBE (LB/HR)
0
1
2
3
4
5
0
0.2
0.4
0.6
0.8
1.0
1.2
POSITION ACROSS TUBE (INCHES)

Figures 4.7 (medium pressure runs) and 4.8 (high pressure runs).

At each pressure a 3 x 3 matrix of sets of runs was done, viz:-

300, 1000 and 2700 lb/hr of water x 50, 100 and 200 ft/sec superficial air velocity for the medium pressure sets of runs.

300, 1000 and 2000 lb/hr of water x 50, 100 and 160 ft/sec superficial air velocity for the high pressure sets of runs.

The results from the 16 of the 18 sets not shown in this section are included in Appendix 3.

From the mass velocity profiles it can be seen that:-

(1) At a gas velocity of 50 ft/sec the droplet mass velocity profiles for liquid injection with the spray and the porous wall injector are nearly the same at the bottom of the tube, with the velocity profiles due to the spray injector being slightly higher. The velocity profiles are almost symmetrical about the tube axis. They show a slight maximum at the axis and a minimum about 0.180 to 0.250 inches from the wall.

(2) When the porous wall injector was used the droplet velocity profile at the top measurement level

(15.9 inches below the injector) was very small or negligible. There was a minimum at the tube axis. At the centre measurement level the droplet flow rate was about 10-25% of the droplet flow rate at the bottom. There was still a minimum at the tube axis. This indicated that the cross flow velocity of the droplets was low.

(3) The spray injector gave irregular results at the top and centre stations. The droplet velocity profile was usually asymmetrical. In some cases the droplet velocity profile at the top measurement level was greater than that at the centre level, in other cases the reverse occurred. The droplet flow rates at the centre level were in some cases greater than and in other cases less than the droplet flow rates at the bottom measurement level.

It is considered that this behaviour was due to two principal causes. Firstly, the droplet velocity profile measurements at the different levels were not made consecutively. Rather, a group of runs was carried out at one measurement level, then the sampling probe assembly and the camera assembly were moved to another level and another group of runs carried out. This meant that the spray injector head setting was

altered when the liquid flow rate was changed as the group of runs was carried out. When the identical run was repeated with the probe at another measurement level it was practically impossible to return the spray injector head to exactly the same setting as previously used. It is considered that the droplet size distribution could have been significantly altered even though the mean liquid velocity at the spray injector head remained close to the design value of 15 ft/sec.

Secondly, the data suggest that the droplet distributions produced by the spray injector were, on the whole, larger in size than the equilibrium core droplet distributions in the two phase flow. A large proportion of these droplets could have reached the wall before the top measuring level under some flow conditions. Under other flow conditions they may have remained in the core until well after the top measuring level. This means that the droplet flow rate at the top level could be greater or less than the droplet flow rate at the centre level.

(4) The entrainment flow rates for a given liquid rate were considerably higher for the runs at 45 psia than the runs at 15 psia.

(5) There was much more entrainment formed in the

runs at 100 ft/sec air velocity. There was a certain amount of asymmetry in the velocity profiles at the bottom of the test-section. However, the velocity profiles due to the porous wall injector at the top and centre measurement levels remained symmetrical.

(6) Repeat runs using the spray injector for the 100 ft/sec 1000 lb/hr, 2000 lb/hr and 2700 lb/hr runs showed considerable disagreement. This reinforces the comments made under point 3.

(7) As had happened in the 50 ft/sec runs the spray injector gave unpredictable velocity profiles at the top and centre measurement levels.

(8) At the highest gas velocities, 200 ft/sec at 15 psia and 160 ft/sec at 45 psia, the porous wall injector still gave symmetrical velocity profiles at the top and centre measurement levels. These profiles had minima at the tube axis. At the bottom of the test-section the profiles were asymmetrical with the maximum points displaced towards the far wall.

4.8.1. Integration of the droplet mass velocity profiles

If the droplet mass velocity profile is assumed to be symmetrical about the tube axis, then the total mass flow through an annulus of radii r and $(r + \delta r)$ feet is

$$W_{LE} = 2\pi G_d r \, \delta r \quad \text{.....(4.34)}$$

where G_d is the local droplet mass velocity (lb/ft^2hr). The total droplet flow rate in the core can be found by integrating rG_d by means of Simpson's rule. A seven point method was used. Hence

$$W_{LE} = 2\pi \int_0^R rG_d \, dr \qquad \text{.....(4.35)}$$

$$= 2\pi \frac{\Delta R}{3} \left[R_0 G_{d_0} + 4R_1 G_{d_1} + 2R_2 G_{d_2} + 4R_3 G_{d_3} + 2R_4 G_{d_4} + 4R_5 G_{d_5} + R_6 G_{d_6} \right] \qquad \text{.....(4.36)}$$

Now $\Delta R = \frac{R}{6}$ and $R_0 = 0$, $R_1 = \Delta R$, $R_2 = 2\Delta R$, $R_3 = 3\Delta R$, $R_4 = 4\Delta R$, $R_5 = 5\Delta R$ and $R_6 = 6\Delta R$.

$$\therefore W_{LE} = 2\pi \frac{(\Delta R)^2}{3} \left[4G_{d_1} + 4G_{d_2} + 12G_{d_3} + 8G_{d_4} + 20G_{d_4} + 6G_{d_6} \right]$$

$$\text{.....(4.37)}$$

$$\text{Also, } G_d = \frac{W_p \times 576}{\pi \times (0.075)^2} \qquad \text{.....(4.38)}$$

where W_p is the mass flow rate through the probe of diameter 0.075 inch.

$$W_{LE} = \frac{8\,(\Delta R)^2}{3\,(0.075)^2} \left[4W_{P_1} + 4W_{P_2} + 12W_{P_3} + 8W_{P_4} + 20W_{P_5} + 6W_{P_6} \right]$$

$$\text{.....(4.39)}$$

where W_{p_1}, W_{p_2}, ... to W_{p_6} are measured at distances

ΔR, $2\Delta R$, ... to $6\Delta R$ from the tube axis

$$\text{or} \quad W_{LE} = \frac{16\ (\Delta R)^2}{3\ (0.075)^2} \left(W_{p_1} + W_{p_1}^{1} + W_{p_2} + W_{p_2}^{1} + 3W_{p_3} + 3W_{p_3}^{1} \right.$$

$$\left. 2\ W_{p_4} + 2W_{p_4}^{1} + 5W_{p_5} + 5W_{p_5}^{1} + 1.5W_{p_6} + 1.5W_{p_6}^{1} \right) \quad \ldots\ldots(4.40)$$

where W_p^{1} is the liquid flow rate through the probe on the opposite side of the tube from and the same distance from the axis as W_p. Equation (4.40) which is equation (4.39) adjusted to allow for asymmetric mass velocity profiles, was the final form of the equation for graphical integration of the droplet mass velocity profiles. As it had constants which were simply related to one another it could be fitted on to the programmable desk calculator in one program.

In order to perform the integration it is necessary to decide on the position of the boundary of the core. This choice determines R, Δ R and the positions of the ordinates. This choice is difficult because:-

(1) The sampling probe is of finite size. The 0.075 inch bore of the probe mouth means that a true local mass velocity will not be obtained where the liquid mass velocity varies with the position of the probe. This is the case near the core-film interface.

(2) Some of the droplet entrainment apparently falls back into the film as soon as it has left the disturbance wave. This has been commented on in the literature review in Section 2.2 which discusses disturbance waves. Associated with and immediately preceding each disturbance wave is a zone of high droplet impingement on the surface of the liquid film. These droplets may be closer to the solid wall than the crest of the disturbance wave and hence almost impossible to collect without collecting some of the disturbance wave itself.

The boundary of the core was chosen somewhat arbitrarily a little closer to the wall than the minimum points of the fully developed droplet mass velocity profiles at the bottom of tube. The boundaries were chosen to be consistent with the liquid film flow rate, the gas velocity and density and the state of development of the disturbance waves.

The integrated droplet flow rates and the chosen boundary positions are reported in Appendix 1.

In Figures 4.9 and 4.10 the integrated droplet flow rates at the bottom measurement level are plotted against the total liquid flow rate. Different curves were obtained for each gas velocity and system

LEGEND

MEAN SUPERFICIAL AIR VELOCITY AT 235 IN.LEVEL (FT/SEC)	MEAN AIR DENSITY AT 235 IN. LEVEL (LB/FT^3)	INJECTOR TYPE	SYMBOL	LINE
(In the order of the curves on figure from the top down)				
207.5	0.0711	Spray	◆	——— -
206.6	0.0700	Porous Wall	■	———
101.0	0.0713	Spray	◆	——— -
105.8	0.0706	Porous Wall	■	———
51.1	0.0718	Spray	◆	——— -
52.7	0.0708	Porous Wall	■	———

Figure 4.9 MEDIUM PRESSURE SERIES. 244.8 INCH LEVEL. TOTAL LIQUID FLOW RATE IN THE CORE VERSUS TOTAL LIQUID FLOW RATE.

(In the order of the curves on the figure from the top down)				
162.2	0.2180	Spray	▼	——— -
159.2	0.2200	Porous Wall	▲	———
103.9	0.2180	Spray	▼	——— -
103.5	0.2201	Porous Wall	▲	———
51.1	0.2193	Spray	▼	——— -
52.0	0.2201	Porous Wall	▲	———

Figure 4.10 HIGH PRESSURE SERIES. 244.8 INCH LEVEL. TOTAL LIQUID FLOW RATE IN THE CORE VERSUS TOTAL LIQUID FLOW RATE.

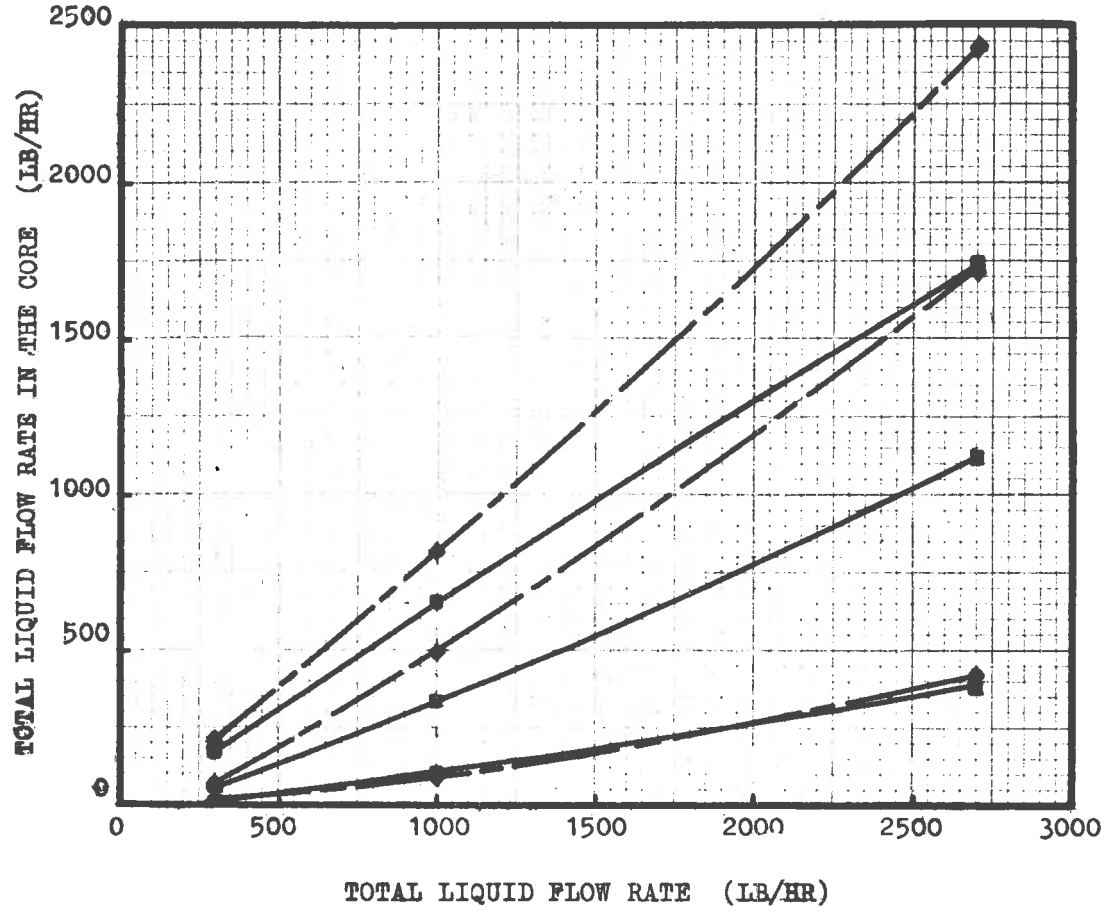
TOTAL LIQUID FLOW RATE IN THE CORE (LB/HR)
2500
2000
1500
1000
500
0
0
500
1000
1500
2000
2500
3000
TOTAL LIQUID FLOW RATE (LB/HR)

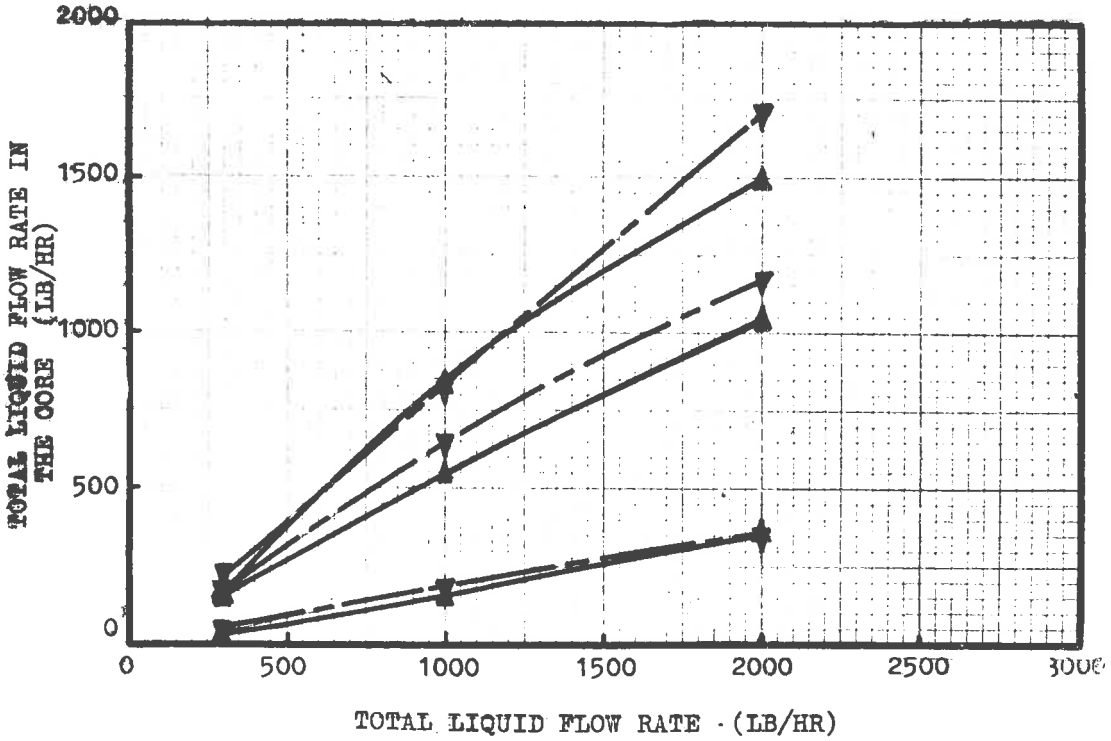
TOTAL LIQUID FLOW RATE IN THE CORE (LB/HR)
2000
1500
1000
500
0
0
500
1000
1500
2000
2500
TOTAL LIQUID FLOW RATE (LB/HR)

pressure. Only the points from the bottom measurement level have been plotted. Because the core flow was not close to equilibrium the points from the top and centre levels were not plotted. Where more than one run was done under the same conditions the average has been used. The two main points which these plots show are:-

(1) The porous wall and spray injectors give almost coincident curves at 50 ft/sec air velocity but not at the higher velocities in which cases the spray injector gives more entrainment. This would suggest that at the higher velocities, at least for the runs with the porous wall injector, a true equilibrium has not been reached even 245 inches downstream from the injector.

(2) These curves are, to a reasonable degree of accuracy, straight lines. If straight lines of best fit are drawn through each set of three points they intersect the x-axis at points slightly to the right of the origin. This result indicates that there is a minimum flow rate before any entrainment occurs at a particular gas flow rate. This is in agreement with the findings of Cousins, Denton and Hewitt (1965) for two phase upward flow reported in Section 2.3.3.

4.8.2. Comparison between the actual total liquid flow rate and the sum of the integrated core flow rate and the film flow rate.

Direct comparison was possible when the film flow rate and the liquid flow rate in the core had both been measured at adjacent points in the same run, that is when the film flow rate at the top extractor and the core flow rate at the centre level had been measured or the film flow rate at the bottom extractor and the core flow rate at the bottom level had been measured.

The comparison was made in 18 runs at 300 lb/hr of water. The average value of the sum of the core and film flow rates was 1.6% low and the root mean square error was 6.3%. 21 runs were examinable at 1000 lb/hr. The sum was 2.3% low and the root mean square error was 6.7%. 20 runs were examinable at 2700 and 2000 lb/hr. The sum was 5.2% low and the root mean square error was 10.7%. In the majority of the runs the sum of the core flow rate and the film flow rate was below the actual liquid flow rate. This was particularly so at the higher liquid flow rates. These results and also visual observation indicate that the porous wall extractors may have been unable completely to remove the liquid film at the higher film flow rates.

5. DISCUSSION

5.1. Introduction

The most important object of this Thesis is to reach an understanding of the factors which determine the amount of droplet entrainment in the gas core in two phase annular flow with droplet entrainment. Once expressions are available which can predict the amount of droplet entrainment in terms of the flow variables and the system geometry, then the film flow rate can be calculated. Due allowance must be made for the mutual interdependence of the film and the core. Droplets are being both entrained from and deposited on the film at the same time.

For a given gas pressure and flow rate the liquid film thickness can be calculated from the liquid film flow rate by using the Dukler analysis or a similar analysis based on the integration of the liquid film velocity profile. From the film thickness and the droplet concentration in the gas core the liquid volume fraction can be calculated. Also, the disturbance wave characteristics are related to the liquid film flow rate rather than the total liquid flow rate.

5.2. Prediction of the equilibrium entrainment flow rate

5.2.1. Experimental observations which need to be considered in analysing the mechanisms of droplet formation

It has been pointed out in the literature review, Sections 2.3.3 and 2.5, that droplet formation is associated with the break-up of the crests of the disturbance waves.

The disturbance wave velocity and frequency measurements have been discussed to some extent in Sections 4.6 and 4.7. It was found that the disturbance wave frequency was a strong function of the air velocity and the water flow rate. In addition the visual appearance of the disturbance waves depended on both the air velocity and the water flow rate.

At low water flow rates and at air velocities up to about 50 ft/sec at 15 psia system pressure the disturbance waves were widely spaced. In between each disturbance wave there was a long region of almost ripple free liquid film. The disturbance waves, although having the characteristic features of a steep highly disturbed leading face and a longer gently sloping moderately disturbed trailing face, were relatively short in comparison with the distance between each wave.

At higher water flow rates and at moderate air velocities the disturbance wave spacing was less, however, more liquid was associated with each wave. The length of the quiescent liquid film between each wave was much shorter

and the trailing surface of each disturbance wave was covered with closely spaced ripples of wavelengths 0.1 to 0.4 inch approximately. If the disturbance waves do have a type of rolling motion then it is possible that these ripples are carried up the trailing surface of the disturbance waves and then break-up or collapse as they pass over the wave crest.

At very high water flow rates and moderate air velocities the disturbance waves were almost head-to-tail. Many of the waves appeared to be double or even triple waves a few inches apart and moving as a single entity.

At high air velocities the whole of the liquid surface was covered with waves. Indeed there was a whole spectrum of waves of various sizes and in some cases it was difficult to decide if the waves were grouped into disturbance waves or behaved as separate entities.

The photographic evidence (Wallis, 1966; Cooper, Hewitt and Pinchin, 1963) indicates that the droplets form at or near the crests of the disturbance waves. The fact that the droplets form so close to the disturbance waves eliminates the possibility that they originate from large lumps of liquid which are thrown into the gas core and are subsequently broken down into droplets by gas shear forces. Also, as Wicks (1967) has pointed out, the maximum gas shear forces occur near the gas-liquid interface.

The experimentally measured volume mean droplet sizes (Cousins and Hewitt, 1968b) ranged from about 80 microns at an air velocity of 93.5 ft/sec at atmospheric pressure to 50 microns at an air velocity of 163 ft/sec. Surface tension forces must be of major importance in the formation of droplets of these sizes.

Conditions for the Onset of Droplet Entrainment

Relatively low equilibrium entrainment flow rates were found in the experimental runs at 50 ft/sec air velocity and 15 psia test-section pressure. These results are reported in Section 4.8 and plotted in Appendix 3 Figures A3.22, A3.24 and A3.26. The equilibrium droplet flow rate ranged from 5.5% of the total water flow rate at a total water flow rate of 300 lb/hr to 10.3% at 1000 lb/hr to 14.8% at 2700 lb/hr. These results show that the critical air velocity for the onset of water droplet entrainment was about 40 ft/sec.

The literature dealing with the critical gas velocity, $\bar{u}_{G_{crit}}$, for droplet entrainment has been reviewed in Section 2.3.3. van Rossum's (1959) criterion, $\bar{u}_{G_{crit}}$ (metres/sec) $\simeq \frac{1}{4}\sigma$(dyne/cm) for air at atmospheric pressure and density, predicts $\bar{u}_{G_{crit}} = 57$ ft/sec. This is using $\sigma = 70$ dyne/cm at 38°C (Weast, Handbook of Chemistry and Physics, 1966). van Rossum's criterion was based on

horizontal flow, so the prediction is quite reasonable. He found that the critical gas velocity decreased as the film thickness increased. These present results substantiate this finding.

Wallis' equation (equation 2.53) was also tested against the present experimental results. His equation is:-

$$\bar{u}_{G_{crit}} = 2.46 \times 10^{-4} \frac{\sigma}{\mu_G} \sqrt{\frac{\rho_L}{\rho_G}} \qquad \text{.....(5.1)}$$

It predicts $\bar{u}_{G_{crit}}$ = 93 ft/sec for air-water at 38°C (= 70 dyne/cm: Weast, "Handbook of Chemistry and Physics, 47th Ed., 1966) and an air density of 0.0712 lb/ft^3. Clearly, this is far too high. However, Wallis' criterion was derived primarily from observations of the flow of air over silicone oils. For these systems σ = 21 dyne/cm. It is the opinion of this writer that semi-theoretical considerations, to be derived later in this section show that $\bar{u}_{G_{crit}}$ should depend on $\sigma^{\frac{1}{2}}$ approximately rather than σ. If this is so then $\bar{u}_{G_{crit}}$ would increase only 1.8 times rather than 3.3 times in changing from σ = 21 dyne/cm to σ = 70 dyne/cm. This would bring Wallis' results and these present results into much closer agreement.

5.2.2. A ripple break-down theory for droplet formation.

We propose that droplets are generated from the break-down of the rippled surface of disturbance waves

near the crest of these disturbance waves. It is postulated that these ripples take up energy from the gas stream and grow to such a size that they become sharp crested and droplets are formed by being torn off their crests.

In applying a stability analysis to ripple growth the most difficult problem is to decide on the relationship to express the relative motion between the gas core and the liquid surface of the disturbance waves. A second problem is to include the effect of liquid viscosity which is neglected in simple stability analyses. These two problems are examined in Section 5.2.3. and 5.2.5. below.

In order to understand how the kinetic energy of the linear motion of two fluids may generate interfacial waves the stability analyses of Miles (1957, 1959a, 1959b) and of Benjamin (1959) have been examined. They are stability analyses of the horizontal flow of two fluids. Miles showed how interfacial waves can be generated at velocities well below the critical Kelvin-Helmholtz velocity in air-water flow. Benjamin extended this analysis to determine the normal and tangential stresses at a wavy interface.

This discussion is limited to an analysis of wave generation by a Kelvin-Helmholtz type of mechanism

using as a basis an analysis originally developed for wave growth on thin liquid films. The relative velocities between the gas and the liquid are well in excess of the critical Kelvin-Helmholtz velocity for wave formation. The possibility that the Miles mechanism could lead to faster rates of wave growth at these relative velocities is not examined.

For horizontal flows the Kelvin-Helmholtz relationship predicts that wave growth can occur if:

$$c_o^2 = \frac{g}{N} + \frac{\sigma N}{\rho_L} < \frac{\rho_G}{\rho_L} u^2 \qquad \text{.....(5.2)}$$

where u is the relative velocity between the two fluids, N is the wave number and c_o is the wave velocity. Differentiation of equation (5.2) shows that the minimum value of c_o^2, that is c_{crit}^2, occurs when the gravity component $\frac{g}{N}$ equals the surface tension component $\frac{\sigma N}{\rho_L}$. This gives the minimum value of $\frac{\rho_G}{\rho_L} u^2$ which can generate waves by the Kelvin-Helmholtz mechanism. At higher values of $\frac{\rho_G}{\rho_L} u^2$ there is a range of waves which are able to grow. They have wave numbers in the range:-

$$\frac{\rho_G u^2}{2\sigma} - \sqrt{\left(\frac{\rho_G u^2}{2\sigma}\right)^2 - \frac{\rho_L g}{\sigma}} < N < \frac{\rho_G u^2}{2\sigma} + \sqrt{\left(\frac{\rho_G u^2}{2\sigma}\right)^2 - \frac{\rho_L g}{\sigma}}$$

.....(5.3)

If equation (5.2) is applied to vertical systems then $\frac{g}{N} = 0$ and wave growth is possible for all $u > 0$.

Also, if $\frac{\rho_G}{\rho_L} u^2 \gg c^2_{crit}$, then the value of the larger solution of the equation (5.3) for horizontal flow is almost the same as the vertical flow solution. Under these conditions the effect of gravity is small. Wave growth is possible for those waves which have

$$N < \frac{\rho_G u^2}{\sigma} \qquad \text{.....(5.4)}$$

It should be noted that equation (5.2) assumes that both fluids are infinite in extent. If the heavier fluid is bounded the equation becomes $c_o^2 = (\frac{g}{N} + \frac{\sigma N}{\rho_L}$ tanh Nh, where h is the fluid depth. For deep fluid tanh Nh ≈ 1. For shallow fluid, Nh< 0.25, tanh Nh $\approx$ Nh.

Equation (5.2) can be written in terms of forces. It becomes a force balance in which the stabilizing forces due to surface tension and/or gravity (when the lighter fluid is on the top of the heavier fluid) are opposed by destabilizing "aerodynamic" forces.

Some of the theoretical and experimental work on the break-down of thin liquid sheets moving through a stationary gas has been reviewed in Section 2.3.1. Both the equations of Squire (1953) equation (2.38) and York, Stubbs and Tek (1953) indicate that:-

$$B = f(N) \left[\rho_G \bar{u}^2 - N\sigma\right]^{\frac{1}{2}} \qquad \text{.....(5.5)}$$

where B is the growth rate of the disturbance, that is the relative increase in amplitude per unit time. Equation (5.5) predicts that there is a maximum wave number which can be generated, $N_{max} = \frac{\rho_G \bar{u}_L^2}{\sigma}$, in the same manner as does equation (5.4).

5.2.3. The effect of relative velocity

If both fluids are of constant densities ρ_G and ρ_L respectively and each fluid is moving at uniform velocities $\bar{u}_G$ and $\bar{u}_L$ respectively then the simple Kelvin-Helmholtz equations become (Lamb, 1945 articles 232, 268; Miles, 1959b)

$$c = \tilde{u} \pm \left[c_o^2 - (\tilde{u^2} - \tilde{u}^2) \right]^{\frac{1}{2}} \quad \ldots\ldots\ldots\ldots\ldots(5.6)$$

where $\tilde{u^m} = \frac{\rho_G \bar{u}_G^m + \rho_L \bar{u}_L^m}{\rho_G + \rho_L}$; m = 1,2 $\ldots\ldots\ldots\ldots\ldots(5.7)$

$$N_{max} = \frac{\rho_G \cdot \rho_L}{\rho_G + \rho_L} \frac{(\bar{u}_G - \bar{u}_L)^2}{\sigma} \quad \ldots\ldots\ldots\ldots\ldots(5.8)$$

c_o is the wave velocity in the absence of liquid flow

$$c_o^2 = \frac{\sigma N}{\rho_G + \rho_L} \quad \ldots\ldots\ldots\ldots\ldots(5.9)$$

Hence if both fluids are moving at uniform velocities the effective relative velocity for determining N_{max} is simply $(\bar{u}_G - \bar{u}_L)$.

However, the gas core is in turbulent flow. The work of Gill, Hewitt, Hitchon and Lacey (1963)

reviewed in Section 2.4.3, indicates that the velocity profile of the core region of the gas core is logarithmic, viz:-

$$u_G^+ = \frac{u_G}{u_G^*} = A + \frac{1}{K} \ln y^+ \quad \text{.....(5.10)}$$

Where $y^+ = \frac{y u_G^* \rho_G}{\mu_G}$ and $u_G^* = \sqrt{\frac{\tau_i}{\rho_G}}$

K was not invariant as it is in single phase flow, but decreased from the single phase value (0.4) at 200 lb/hr of water to about 0.14 at 1250 lb/hr of water (based on the mean core density, gas + entrained droplets).

If we assume that the liquid film is stationary and that the ripple velocity is small in comparison with the gas velocity and also that $\rho_G \ll \rho_L$ then we can write (Miles, 1959b) in place of equation (5.2)

$$c_o^2 = \frac{\rho_G}{\rho_L N} \int_{o^+}^{\infty} u_G^2 \left(f^1(y)^2 + N^2 f(y)^2 \right) dy \text{.....(5.11)}$$

Where f(y) must satisfy:-

$$\left[u_G^2 f^1(y) \right]^1 - N^2 u_G^2 f(y) = 0 \quad \text{.....(5.12)}$$

Equation (5.11) is satisfied approximately by

$$f(y) = e^{-Ny} \quad \text{.....(5.13)}$$

The error is $\left[u_G^2 \right]^1 f^1(y)$

Substitution from equations (5.9) and (5.12) into equation (5.10) and integration by the method of Miles

(1959b) gives:-

$$c_o^2 = \frac{\rho_G}{\rho_L}(u_G^*)^2\left[\frac{\pi^2}{6K^2} + \left(A + \frac{1}{K}\ln\frac{u_G^*\rho_G}{3.56\,N\,\mu_G}\right)^2\right] \qquad \text{.....(5.14)}$$

We note that the integration is to infinity and neglects the fact that the gas is flowing in a tube and is therefore bounded.

If we combine equations (5.8) and (5.9) we obtain

$$c_o^2 = \frac{\sigma N_{max}}{\rho_G + \rho_L} \approx \frac{\rho_G}{\rho_L}(\bar{u}_G - \bar{u}_L)^2 \qquad \text{.....(5.15)}$$

Comparison of equations (5.14) and (5.15) shows that

$$u_G^*\left[\frac{\pi^2}{6K^2} + \left(A + \frac{1}{K}\ln\frac{u_G^*\rho_G}{3.56\,N\,\mu_G}\right)^2\right]^{\frac{1}{2}}$$

is an improved expression for the effective gas velocity in place of the mean gas velocity $\bar{u}_G$.

The total gas flow is $\int_o^R 2\pi u_G r\,dr$. Substitution for u_G from equation (5.10) and integration gives the total gas flow and hence the mean gas velocity $\bar{u}_G$.

$$\bar{u}_G = u_G^*\left[A + \frac{1}{K}\ln R^+ - \frac{3}{2K}\right] \qquad \text{.....(5.16)}$$

where R^+ is the value of y^+ at the tube axis. This integration neglects the reduction of the core radius caused by the liquid film on the wall and also assumes

that the logarithmic core profile extends right to the gas-liquid interface. Now $\frac{u_G^* \rho_G}{\mu_G} = \frac{R^+}{R}$. Hence the expression for the effective gas velocity becomes :-

$$\text{Effective Gas Velocity} = \bar{u}_G \frac{\left[\frac{\pi^2}{6K^2} + \left(A + \frac{1}{K} \ln \frac{R^+}{3.56\, N\, R}\right)^2\right]^{\frac{1}{2}}}{A + \frac{1}{K} \ln R^+ - \frac{3}{2K}} \qquad \ldots\ldots\ldots(5.17)$$

This method of calculating the effective relative velocity assumes that the liquid film is stationary. A complete expression would have to allow for this liquid film motion as well. However, as $\bar{u}_G$ is considerably greater than $\bar{u}_L$, 5 times or more in air-water flows in which the air velocity is sufficient to cause droplet entrainment, the effective gas velocity can be taken as equal to the effective relative velocity.

5.2.4. A sample calculation

Assume $\left(-\frac{dp}{dx}\right)_{tot}$ = 0.1 ft water/ft tube, ρ_G = 0.0712 lb/ft^3 and μ_G = 0.0185 centipoise. Then $R^+ = \frac{R\sqrt{\tau_i \rho_G}}{\mu_G}$ = 2800. This is the situation for a water flow rate of 2000 lb/hr and an air velocity of 50 ft/sec. We take K = 0.2 and A = 3.8. This is the single phase flow value of A. This value has been used because the true value in this two phase flow is not known. Then for waves of wavelength λ = 0.2 inch, $N = \frac{2\pi}{\lambda}$ = 31.4 in^{-1}. Substitution in equation (5.17) gives

the effective gas velocity as 0.635 $\bar{u}_G$. If λ= 0.4 inch then the effective gas velocity is 0.73 $\bar{u}_G$. The higher effective gas velocity associated with the longer waves is as one would expect, for these waves can, potentially at least, have larger amplitudes and therefore penetrate further into the gas core where the gas velocity is higher.

Substitution into equation (5.15) with σ= 70 dyne/cm gives $\bar{u}_{G_{min}}$ = 45 ft/sec as the minimum air velocity to generate waves of wavelength λ= 0.2 inch and $\bar{u}_{G_{min}}$ = 28 ft/sec to generate waves of wavelength λ= 0.4 inch.

These are the shortest waves which can be generated at these respective air velocities. The waves of most interest are those with the fastest rate of growth. The theory of Squire (1953) indicates that the waves with the fastest rate of growth have wave numbers.

$$N_{opt} = \tfrac{1}{2} N_{max} \text{ (see equation 2.40)} \quad \ldots\ldots\ldots (5.18)$$

The theory of York, Stubbs and Tek (1953) (equation 2.41) indicates that

$$N_{opt} = \tfrac{3}{4} N_{max} \quad \ldots\ldots\ldots\ldots\ldots\ldots (5.19)$$

These theories have been derived for thin sheets of liquid moving in a stationary gas. However, because the neutral stability criteria for break-down of a liquid sheet and for wave formation on a liquid film are similar it is likely that the maximum growth rate wave number is about the same proportion of the maximum wave number.

These theories neglect liquid viscosity. It is shown in Section 5.2.5 below that liquid viscosity can retard wave growth only in very thin films such as could occur between disturbance waves. The region of a disturbance wave which is covered by ripples is likely to be too thick to be much affected by viscosity.

Hence it seems likely that the wavelengths with the maximum rate of growth are about 50% longer than the shortest possible wavelengths λ_{min}. Thus for $\bar{u}_g = 45$ ft/sec the dominant waves should be around 0.3 inch wavelength. In fact $\lambda = 0.3$ inch is in the range of ripple wavelengths observed at gas velocities of 50 ft/sec and therefore it is concluded that this method of analysis does give realistic results.

5.2.5. The effect of liquid viscosity

Viscosity can be ignored when the two fluids are unbounded or the boundary is a long way away compared with the wavelength of the interfacial waves. The waves decay because of the effect of liquid viscosity at the gas-liquid interface. However, as is shown later in this section, the rate of wave decay due to this effect is negligible in comparison with the rate of wave growth due to aerodynamic forces. When the liquid film is thin, liquid viscosity must be considered.

For example, the theory of Massot, Irani and Lightfoot (1966) for free falling wavy laminar films,

reviewed in Section 2.1.2, predicts that the controlling factor in the wave motion is the liquid film Weber number $N_{We_L} = \frac{\bar{u}_L^2 \rho_L h}{\sigma}$. In view of the discussion on stability earlier in this section this is not surprising as the Weber number is a measure of the ratio of inertia forces or "liquid aerodynamic forces" to surface tension forces.

However, this Weber number does include a liquid viscosity effect. From equation (2.11), neglecting ρ_G in comparison with ρ_L,

$$\bar{u}_L = \frac{\rho_L g h^2}{3 \mu_L} \qquad \text{.....(5.20)}$$

If equation (5.20) for a smooth liquid film also holds approximately for a wavy liquid film then,

$$N_{We_L} \propto Q_L^{5/3} \left(\frac{\rho_L}{\sigma}\right)^{4/3} \left(\frac{g}{3\mu_L}\right)^{1/3} \qquad \text{.....(5.21)}$$

where $Q_L = \bar{u}_L h$ is the liquid flow rate per unit width of wall. From equation (5.21) it can be seen that at a given liquid flow rate N_{We_L} is inversely proportional to $\mu_L^{1/3}$. That is, at a given liquid flow rate, increasing μ_L decreases N_{We_L} and makes the flow more stable. Also, it can be seen that an increase in surface tension has a much greater stabilizing effect than the same relative increase in viscosity.

In Section 2.1.2. of the literature review it

was pointed out that various workers had suggested values of N_{Re_L} from 0 to 7 for the transition from smooth laminar to wavy laminar flow for a free falling water film on a vertical surface. The theory of Massot, Irani and Lightfoot predicts wavy laminar flow on a vertical surface for $N_{We_L} > 0$ and hence $N_{Re_L} > 0$.

However, at low flow rates the waves are almost unnoticeable. A practical but arbitary transition point for water is $N_{Re_L} = 10$. From equation (5.21) the appropriate Reynolds number, $N_{Re_L} = \frac{Q_L \rho_L}{\mu_L}$, is related to the Weber number by:-

$$N_{We_L} = \left(N_{Re_L}\right)^{5/3} \frac{\mu_L}{\sigma}^{4/3} \left(\frac{g}{3\rho_L}\right)^{1/3} \quad \ldots\ldots\ldots\ldots(5.22)$$

Substitution in equation (5.22) gives $N_{We_L} = 5.8 \times 10^{-3}$ at the transition point.

When there is co-current gas flow it is necessary to include the effect of the interfacial shear stress. Equation (2.11) can be put in the form:-

$$\bar{u}_L = \frac{\tau_w h}{2\mu_L} - \frac{\rho_L g h^2}{6\mu_L} = \frac{\rho_L g h^2}{6\mu_L}(3T-1) \quad \ldots\ldots\ldots\ldots(5.23)$$

where $T = \frac{\tau_w}{\rho_L g h} = \frac{\tau_i}{\rho_L g h} + 1$ and ρ_c is neglected as it is assumed that $\rho_c << \rho_L$. Equation (2.6) can be put in the form:-

$$u_L = \frac{\tau_w}{\mu_L} y - \frac{\rho_L g y^2}{2\mu_L} = \frac{\rho_L g h y}{2\mu_L}\left(2T - \frac{y}{h}\right)$$

$$\ldots\ldots\ldots\ldots(5.24)$$

$$\therefore \quad u_L = \frac{3\,\bar{u}_L\, y}{h} \times \frac{2T - \frac{y}{h}}{3T - 1} \qquad \text{.....(5.25)}$$

Equation (5.25) can be applied to wavy laminar flow. In this case $\bar{u}_L$, h and T are functions of x and t. Equation (5.25) is differentiated to obtain expressions for $\frac{\partial u_L}{\partial x}$, $\frac{\partial u_L}{\partial y}$, $\frac{\partial u_L}{\partial t}$, $\frac{\partial^2 u_L}{\partial x^2}$ and $\frac{\partial^2 u_L}{\partial y^2}$ respectively. By continuity $\frac{\partial v_L}{\partial y} + \frac{\partial u_L}{\partial x} = 0$ and hence $v_L = \int (-\frac{\partial u_L}{\partial x})\, dy$. These expressions can be substituted into the Navier-Stokes equations.
By linearizing the resultant equation in the same manner as did Massot, Irani and Lightfoot (1966) a similar equation to theirs can be derived, viz:-

$$N_{We_L}\left(\tfrac{3}{2}T - \tfrac{1}{8}\right) = \frac{3}{\left(\frac{c}{\bar{u}_L} - \frac{3}{2}\,,\ \frac{2T-1}{\frac{3}{2}T - \frac{1}{8}}\right)} \times$$

$$\frac{3 - \frac{c}{\bar{u}_L}}{\left(\frac{c}{\bar{u}_L}\right)^2 - 3\left(\frac{\frac{3}{10} - \frac{3}{2}T + 2T^2}{\left(\frac{3}{2}T - \frac{1}{8}\right)^2}\right)\left(\frac{c}{\bar{u}_L}\right) + \frac{3T\left(\frac{2}{5} - \frac{3}{2}T + \frac{3}{2}T^2\right)}{\left(\frac{3}{2}T - \frac{1}{8}\right)^3}}$$

.....(5.26)

Equation (5.26) reduces to the equation of Massot, Irani and Lightfoot if T = 1. For large T equation (5.26) becomes:-

$$N_{We_L}\left(\tfrac{3}{2}T - \tfrac{1}{8}\right) = \frac{3\left[3 - \frac{c}{\bar{u}_L}\right]}{\left[\frac{c}{\bar{u}_L} - 2\right]^2\left[\frac{c}{\bar{u}_L} - \frac{2}{3}\right]} \qquad \text{.....(5.27)}$$

For very small values of the left hand side of equation (5.26) $\frac{c}{\bar{u}_L} = 3$ and is unaffected by changes in T so long as $N_{We_L}(\frac{3}{2}T - \frac{1}{2})$ remains constant. For very large values of the left hand side $\frac{c}{\bar{u}_L}$ is determined by the larger root of the quadratic portion of the denominator of the right hand side. This ranges from $\frac{1}{5}(6+\sqrt{6}) = 1.689$ at T = 1 to 2 at $T = \infty$.

These results verify the results obtained by the simple analysis in Section 2.1.2. There the method of Lighthill and Whitham (1955) was used to show that $\frac{c}{\bar{u}_L}$ ranges from 3 at T = 1 (equivalent to the left hand side of equation (5.26) = 0) to 2 at $T = \infty$ (equivalent to the left hand side = ∞).

In the flow of very thin laminar liquid films with co-current gas flow it seems reasonable to assume that the transition to wavy laminar flow depends on the value of the left hand side of equation (5.26) $N_{We_L}(\frac{3}{2}T - \frac{1}{2})$.
We take $N_{We_L}(\frac{3}{2}T - \frac{1}{2}) = 5.8 \times 10^{-3}$ to be the criterion for the onset of wavy laminar film flow when there is co-current gas flow.

When $\bar{u}_L$, from equation (5.23), is substituted in $N_{We_L} = \frac{h\bar{u}_L^2 \rho_L}{\sigma}$, the criterion becomes:-

$$5.8 \times 10^{-3} = \frac{\rho_L^3 g^2 h^5}{9 \mu_L^2 \sigma} \left(\frac{3}{2}T - \frac{1}{2}\right)^3 \approx \frac{3h^2 \tau_w^3}{8g \mu_L^2 \sigma} \quad \ldots\ldots\ldots(5.28)$$

The approximate part of the equation (5.28) applies when T is large, that is $\tau_w \gg \rho_L g h$.

If the pressure gradient is 0.010 ft water/ft tube then the interfacial shear stress $\tau_i = 0.555$ lb/ft sec^2. Substitution of the appropriate values in equation (5.28) shows that the transition occurs at h = 0.0021 inch at a temperature of 38°C. The pressure gradient used is the value for air flowing alone at a velocity of 50 ft/sec and a density of 0.0712 lb/ft^3 in a 1.330 inch diameter tube. For the flow of a gas over smooth very thin laminar liquid films it seems reasonable to assume that the friction factor and therefore the pressure gradient is unchanged. This is possibly the situation where there is a thin smooth liquid film between disturbance waves. An examination of equation (5.28) shows that, for a constant pressure gradient, $N_{Re_L} \left(\frac{3}{2}T - \frac{1}{2}\right)$ varies as h^5 when T is close to one and varies as h^2 when T is large.

The relative importance of liquid viscosity in the liquid film depends on the ratio of the viscous forces to the inertia forces, that is on the liquid film Reynolds number $N_{Re_L} = \frac{h\bar{u}_L \rho_L}{\mu_L}$. Substitution for $\bar{u}_L$ from

equation (5.23) shows that N_{Re_L} varies as h^3 when T is close to one and as h^2 when T is large. This suggests that for film thicknesses greater than about 0.005-0.006 inch wave motion could take place with little viscous damping. In the case of the trailing surface of a disturbance wave there is a variable film thickness. This analysis indicates that viscous effects on wave motion should be small in all parts of the wave greater than 0.005-0.006 inch deep.

We now examine wave growth and decay to see if the same influence of film thickness can be predicted. The decay rate, that is the relative decrease in amplitude per unit time, of deep liquid waves caused by viscous effects (Lamb, 1945; Article 348) is $\frac{2\mu_L N^2}{\rho_L}$. In shallow liquid the wave velocity is reduced in proportion to $(\tanh Nh)^{\frac{1}{2}}$. The total wave energy also is reduced in this proportion and therefore the decay rate due to surface effects remains constant.

In shallow liquid we also must consider the viscous dissipation caused by the presence of the solid wall. This case has been considered by Miles (1962). He found that the decay rate due to the presence of the solid wall was $N\left[\frac{N\mu_L c}{2\rho_L}\right]^{\frac{1}{2}} (\tanh Nh)^{\frac{1}{4}} \operatorname{csch} 2Nh$. c is given by equation (5.2). Where the gravity component can be neglected, such as for short waves, $c^2 = \frac{\sigma N}{\rho_L}$. Miles' expression is not strictly correct for very thin films, such as those being studied in this Thesis.

Miles (1962) also gives a theoretical analysis of how short wavelength waves can be generated by means of viscous stresses acting in the immediate neighbourhood of the gas-liquid interface. He points out that his analysis does not apply to high gas velocities such as are typical in this Thesis. He suggests that under such conditions the Kelvin-Helmholtz mechanism would be the relevant mechanism for wave generation.

Miles' graphs of gross growth rate versus wave length are plotted with friction velocity, $u_G^* = \sqrt{\tau_i / \rho_G}$, as parameter up to a maximum value $u_G^* = 30$ cm/sec. Even most of the lower values of the pressure gradients measured in this Thesis correspond to values of u_G^* in excess of 30 cm/sec. For instance a pressure gradient of 0.010 ft water/ft tube, which occurs for air flowing at a velocity of 50 ft/sec and a density of 0.0712 lb/ft^3, corresponds to $u_G^* = 2.56$ ft/sec = 84 cm/sec. The shape of Miles' graphs suggest that at $u_G^* = 30$ cm/sec and $\lambda = 3$ cm (the upper limit of the graphs) the gross growth rate is proportional to $u_G^{*2} / \lambda^{3/2}$. This would lead to higher growth rates than the Kelvin-Helmholtz type of mechanism proposed below.

The following analysis is based on the postulate that the growth rate of small ripple waves is given by the

equation of York, Stubbs and Tek (1953). This is equation (2.36) with $\coth\frac{Nh}{2}$ replaced by $\tanh Nh$. It was derived for wave growth on one side of a liquid sheet. It indicates that for small Nh the growth rate is proportional to $h^{\frac{1}{2}}$ and for large Nh it is independent of h. This would seem to be of the right form. The equation of Squire (1953) was also examined. As it contained a $\coth\frac{Nh}{2}$ term it implied that decreasing h increased the growth rate for small Nh. This did not seem to be correct.

Because the velocity enters into the expression in the same manner as it does in the Kelvin-Helmholtz equation it can be replaced by an effective relative velocity u_{rel}. For $\rho_G << \rho_L$ equation (2.36) becomes:-

$$B = \left[\frac{N^2}{\rho_L}\tanh Nh\right]^{\frac{1}{2}}\left[\rho_G u_{rel}^2 - N\sigma\right]^{\frac{1}{2}} \quad \ldots\ldots\ldots(5.29)$$

Therefore we have:-

Net growth rate = Gross growth rate - decay rate

i.e. $$B_{net} = \left[\frac{N^2}{\rho_L}\tanh Nh\right]^{\frac{1}{2}}\left[\rho_G u_{rel}^2 - N\sigma\right]^{\frac{1}{2}} - \frac{2\mu_L N^2}{\rho_L}$$

$$- N\left[\frac{N\mu_L}{2\rho_L}\right]^{\frac{1}{2}}\left[\frac{\sigma N}{\rho_L}\tanh Nh\right]^{\frac{1}{4}}\operatorname{csch} 2Nh \quad \ldots\ldots\ldots\ldots(5.30)$$

In effect, equation (5.30) states that the net ripple growth rate is equal to the gross growth rate due to the transfer of energy from the gas phase into the ripples by means

of a Kelvin-Helmholtz type of mechanism minus the decay rate due to viscous energy losses in the liquid film, both at the gas-liquid interface and due to the presence of the solid wall. We note that, for a given relative velocity and film thickness, there is a particular value of N, N_{opt}, at which B_{net} is a maximum.

We wish to find the maximum film thickness, h_{vis}, for which ripple growth is prevented by viscous decay.

For these conditions $B_{net,\,max} = 0$ and $\left(\frac{\partial B_{net}}{\partial N}\right)_h = 0$.

The film will be very thin and therefore Nh will be less than 0.25. Hence tanh Nh = Nh and csch $2Nh = \frac{1}{2Nh}$.

Differentiation of equation (5.30) gives:-

$$\left[\frac{\partial B_{net}}{\partial N}\right]_h = \frac{\frac{3}{2}\rho_G u_{rel}^2 - 2N\sigma}{\left[\rho_G u_{rel}^2 - N\sigma\right]^{\frac{1}{2}}}\left[\frac{Nh}{\rho_L}\right]^{\frac{1}{2}} - \frac{4\mu_L N}{\rho_L} - \left[\frac{\mu_L}{2\rho_L}\right]^{\frac{1}{2}}\left[\frac{\sigma h}{\rho_L}\right]^{\frac{1}{4}}\frac{1}{2h} \quad \ldots\ldots\ldots\ldots\ldots\ldots(5.31)$$

At $N = N_{opt}$ $\left(\frac{\partial B_{net}}{\partial N}\right)_h = 0$.

Dividing equation (5.30) through by N gives:-

$$0 = \left[\rho_G u_{rel}^2 - N_{opt}\sigma\right]^{\frac{1}{2}}\left[\frac{N_{opt} h_{vis}}{\rho_L}\right]^{\frac{1}{2}} - \frac{2\mu_L N_{opt}}{\rho_L} - \left[\frac{\mu_L}{2\rho_L}\right]^{\frac{1}{2}}\left[\frac{\sigma h_{vis}}{\rho_L}\right]^{\frac{1}{4}}\frac{1}{2h_{vis}} \quad \ldots\ldots\ldots\ldots\ldots(5.32)$$

for the conditions $N = N_{opt}$, $h = h_{vis}$ and $N_{opt} h_{vis} < 0.25$.

Twice equation (5.32) - equation (5.31) gives:-

$$\frac{\frac{1}{2}\rho_G u_{rel}^2}{\left[\rho_G u_{rel}^2 - N_{opt}\sigma\right]^{\frac{1}{2}}}\left[\frac{N_{opt}\, h_{vis}}{\rho_L}\right]^{\frac{1}{2}} =$$

$$\left[\frac{\mu_L}{2\rho_L}\right]^{\frac{1}{2}}\left[\frac{\sigma h_{vis}}{\rho_L}\right]^{\frac{1}{2}}\frac{1}{2h_{vis}} \qquad \text{.....(5.33)}$$

Equation (5.31) - equation (5.32) gives:-

$$\frac{\frac{1}{2}\rho_G u_{rel}^2 - N_{opt}\sigma}{\left[\rho_G u_{rel}^2 - N_{opt}\sigma\right]^{\frac{1}{2}}}\left[\frac{N_{opt}\, h_{vis}}{\rho_L}\right]^{\frac{1}{2}} = \frac{2\mu_L N_{opt}}{\rho_L} \qquad \text{...(5.34)}$$

Dividing equation (5.34) by equation (5.33) and rearranging gives:-

$$N_{opt}\sigma = \tfrac{1}{2}\rho_G u_{rel}^2\left[1 - 4N_{opt}\, h_{vis}\left(\frac{4\mu_L^2}{\rho_L \sigma h_{vis}}\right)^{\frac{1}{4}}\right] \qquad \text{...(5.35)}$$

In this case $h_{vis} \approx 0.002$ inch and $N_{opt} = 20.9$ in^{-1}. This gives $4N_{opt}\, h_{vis}\left[\frac{4\mu_L^2}{\rho_L \sigma h_{vis}}\right]^{\frac{1}{4}} \approx 0.02$ and therefore it can be neglected. This is equivalent to saying that the decay rate due to interfacial viscous losses is much less than the decay rate caused by viscous losses due to the presence of the solid wall.

Substituting from equation (5.35) in equation (5.33) and rearranging gives:-

$$h_{vis}^{5/2} = \frac{\mu_L \sigma^{3/2}}{8(\frac{1}{2}\rho_G u_{rel}^2)^2 \rho_L^{\frac{1}{2}}} = \frac{\mu_L}{8 N_{opt}^2 (\sigma \rho_L)^{\frac{1}{2}}} \quad \ldots\ldots(5.36)$$

If λ_{opt} = 0.3 inch, then N_{opt} = 20.9 in^{-1} and u_{rel} = 33 ft/sec by equation (5.35). This corresponds to an air velocity of about 50 ft/sec at a density of 0.0712 lb/ft^3. Then, from equation (5.36), h_{vis} = 0.0018 inch. This result is in reasonable agreement with the result based on the onset of ripple flow earlier in this section. There it was found that h = 0.0021 inch for the same flow conditions.

It can be seen from equation (5.31) that if the viscous terms are negligible then the maximum value of B, B_{max}, occurs when $N_{opt}\sigma = \frac{3}{4}\rho_G u_{rel}^2$. For small Nh the gross growth rate varies as $h^{\frac{1}{2}}$ and the decay rate due to the solid wall varies as $h^{-\frac{3}{2}}$. The decay rate due to the gas-liquid interface is very small. Hence the ratio of the decay rate to the gross growth rate varies as $h^{-5/4}$ for small Nh. This is ignoring the slight effect due to the variation in N_{opt} with the variation in h. This is a much slower rate of decrease than the h^{-2} to h^{-3} predicted by the wavy laminar film analysis. Nevertheless, this analysis shows that for films thicker than about 0.010 inch the decay rate is small compared with the gross growth rate.

It should be noted that this section has been concerned with the effect of viscosity on the short wavelength ripples. These ripples move slowly. For example if $N = 31.4\ in^{-1}$, $c_o = \left[\frac{\sigma N}{\rho_L}\right]^{\frac{1}{2}} = 2.44$ ft/sec. The disturbance wave velocities are mostly in the range 4–20 ft/sec. The viscous energy dissipated by the ripple motion is negligible compared with that dissipated by the bulk motion of the liquid.

5.2.6 Wave growth.

We limit ourselves to liquid films thick enough for viscosity to be neglected. Hence the viscosity terms in the growth rate equation (equation 5.30) can be neglected. The result of differentiating equation (5.30) for shallow liquid films ($Nh < 0.25$) with respect to N has been given in equation (5.31). The maximum growth rate of the ripples, B_{max} is

$$B_{max} = \frac{3\sqrt{3}}{16}(\rho_G u_{rel}^2)^2\left[\frac{h}{\rho_L \sigma^3}\right]^{\frac{1}{2}} = \frac{1}{N\sqrt{3}} N_{opt}^2 \left[\frac{h\sigma}{\rho_L}\right]^{\frac{1}{2}} \qquad \text{.....(5.37)}$$

$$\text{at } N_{opt} = \frac{1}{4}\frac{\rho_G u_{rel}^2}{\sigma}$$

For waves in deep liquid such that $\tanh Nh \approx 1$ differentiation of equation (5.30) gives:-

$$\left(\frac{\partial B}{\partial N}\right)_h = \frac{1}{\rho_L^{\frac{1}{2}}} \frac{\rho_G u_{rel}^2 - \frac{3}{2} N\sigma}{\left[\rho_G u_{rel}^2 - N\sigma\right]^{\frac{1}{2}}} \qquad \text{.....(5.38)}$$

Therefore the maximum growth rate is

$$B_{max} = \frac{2}{3\sqrt{3}} (\rho_G u_{rel}^2)^{3/2} \left[\frac{1}{\rho_L \sigma^2}\right]^{\frac{1}{2}} = \frac{1}{\sqrt{2}} N_{opt}^{3/2} \left[\frac{\sigma}{\rho_L}\right]^{\frac{1}{2}} \quad \text{.....(5.39)}$$

$$\text{at } N_{opt} = \frac{2}{3} \frac{\rho_G u_{rel}}{\sigma}$$

As might be expected equation (5.39) shows that in deep liquid B_{max} is independent of the film thickness.

Equations (5.37) and (5.39) fail to predict a critical gas velocity below which ripple growth will not occur. They merely imply that at low gas velocities the ripple wavelength is longer and the growth rate slower. The experimental evidence is in agreement with this for ripples are still present on disturbance waves even when the gas velocity is too low to cause droplet entrainment.

However, the lifetime of a ripple is limited by the finite length of each disturbance wave. We postulate that a surface disturbance is able to grow only when it is on part of the "active length" of a disturbance wave. The active length extends from the disturbance wave crest back to where the film is so thin that viscous decay due to the presence of the solid wall retards wave growth. As has already been shown in Section 5.2.5 the retarding effect of liquid viscosity on the growth rate is very small in films of water thicker than about 0.010 inch.

An examination of the cine film photographs showed that this active length was up to 2 inches long for single waves. At high liquid flow rates the double waves appeared to consist of two separate ripple regions. At low liquid flow rates the active length could be under an inch long. The active length was taken as that length of a disturbance wave which could be seen covered with ripples in the visual examination of the ciné photographs. However, the actual active length could be perhaps twice as long as this in some cases because the ripples would be too small to be visible.

The surface of a disturbance wave moves more rapidly than its mean velocity if its motion is determined by continuity considerations as was suggested in Section 4.6. From equation (4.32)

$$c - \bar{u}_L = \frac{u_L^*}{K} \qquad \text{.....(5.40)}$$

where c is the disturbance wave velocity and $\bar{u}_L$ is the average velocity of the liquid in the disturbance wave. It was shown in Section 4.6 that putting $\bar{u}_L$ equal to the average velocity of the whole liquid film was unsatisfactory. As the surface velocity of a disturbance wave exceeds its mean velocity in effect it "rolls" along.

Combination of equations (4.28) and (4.29) in the application of the analysis of Lighthill and Whitham (1955)

in Section 4.6 gives:

$$c = u_L^* \frac{d^N Re_L}{d\eta} = u_L^* \left(A + \frac{1}{K} \ln \eta\right) = u_{L_{surf}} \quad \ldots\ldots(5.41)$$

where $u_{L_{surf}}$ is the surface liquid velocity at the gas-liquid interface. If restoring forces were present at the interface then the wave velocity would be greater than the surface velocity. Hence the velocity of a point of the disturbance wave surface relative to the average velocity of the liquid in the wave is $c - \bar{u}_L$.

As the earliest a ripple can begin to grow is near the start of the active length then the maximum time it has for growth, t_{gr}, is

$$t_{gr} = \frac{l}{c - \bar{u}_L} = \frac{Kl}{u_L^*} \quad \ldots\ldots\ldots\ldots\ldots(5.42)$$

where l is the active length. Equation (5.42) assumes that the ripple velocity can be neglected.

Hence the maximum amount of growth possible is $\int_0^{t_{gr}} B_{max} dt$. For deep liquid waves B_{max} is independent of h and for shallow liquid waves it varies as $h^{\frac{1}{2}}$ provided that the liquid film is thick enough for viscous effects to be negligible. Most ripples will have shorter lives than t_{gr} because they will form closer to the disturbance wave crest than the start of the active length.

5.2.7. Droplet formation.

The break-down mechanism proposed by Fraser, Eisenklam, Dombrowski and Hasson (1962) for liquid sheets from spray nozzles was examined to see if it could be applied to the formation of droplets from disturbance waves. Their theory is discussed in Section 2.3.1. They proposed that the sheet breaks up into ligaments of wavelength λ_{opt} and thickness h_{br}. λ_{opt} is given by Squire's theory (1953) and h_{br} is the thickness of the liquid sheet at break-up. These ligaments then break into droplets by the Rayleigh mechanism giving droplets of diameter proportional to $\sqrt{\lambda_{opt} h_{br}}$. The constant can be readily calculated.

When applied to the break-up of ripples on disturbance waves this theory requires that the ripples elongate into very, very thin sheets, say 0.00001 inch thick, to give droplets of the correct size range [about 80 microns for an air velocity of 93.5 ft/sec as measured by Cousins and Hewitt (1968b)]. This is highly improbable.

Instead, we postulate that the ripples, which are initially sinusoidal, grow into ragged sharp crested waves. It is postulated that spray is formed by disintegration of these crests. This mechanism is akin to the way spray forms from patches of "white water" on ocean waves. However, it should be noted that in the ocean wave

case white water is probably caused by small, in comparison with the wave scale, turbulent wind eddies. In the entrainment of droplets from disturbance waves the gas flow behaves like a steady wind.

Now the great difficulty with the growth equations, equations (5.37) and (5.39), is that they give a relative rate of growth. When they are multiplied by a time they give a growth ratio, that is they merely predict the ratio of the final ripple amplitude to the initial ripple amplitude. However, if the initial disturbances which grow into ripples and thence into sharp crested waves are all about the same size it seems reasonable to expect that there is a minimum value of $(B_{max} t_{gr})$ before droplet entrainment can begin. It should be noted that the exponential growth equations only apply to ripples of sinusoidal form. Once the ripples have begun to change the growth equations no longer strictly apply.

The minimum value of $(B_{max} t_{gr})$ for entrainment is not a sharp cut off because there will be a variation in the initial disturbances which are amplified. However the form of the expressions for $(B_{max} t_{gr})$ should indicate the factors which control the onset of droplet entrainment. Combining equation (5.42) with equations (5.37) and (5.39) respectively and putting $u_L^* = \sqrt{\tau_w / \rho_L}$ gives:-

Shallow water:-

$$(B_{max}t_{gr}) = \frac{3\sqrt{3}}{16}\left(\rho_G u_{rel}^2\right)^2 \left[\frac{h}{\sigma^3}\right]^{\frac{1}{2}} \frac{K1}{\sqrt{\tau_w}} \quad \ldots\ldots(5.43)$$

Deep water:-

$$(B_{max}t_{gr}) = \frac{2}{3\sqrt{3}}\left(\rho_G u_{rel}^2\right)^{3/2} \frac{1}{\sigma} \frac{K1}{\sqrt{\tau_w}} \quad \ldots\ldots(5.44)$$

5.2.8 The variables affecting the onset of droplet entrainment

The relationships between variables which affect the onset of droplet entrainment can be deduced from equations (5.43) and (5.44). These equations can indicate the likely effect of variations in the values of the controlling variables on $\bar{u}_{G_{crit}}$, the gas velocity necessary for droplet formation, but they are unable to predict absolute values of $\bar{u}_{G_{crit}}$.

(1) Gas density

An examination of equation (5.17) shows that the ratio $\frac{u_{rel}}{\bar{u}_G}$ is almost unaffected by changes in ρ_G and $\bar{u}_G$ provided that $\rho_G \bar{u}_G^2$ remains constant. In equations (5.43) and (5.44) the effect of ρ_G and $\bar{u}_G$ on τ_w depends on $\rho_G \bar{u}_G^2$. Hence, the combined effect of gas velocity and density on $(B_{max}t_{gr})$ depends on $\rho_G \bar{u}_G^2$. $(B_{max}t_{gr})$ is a constant for the onset of droplet entrainment and

therefore $\bar{u}_{G_{crit}}$ is proportional to $\rho_G^{-\frac{1}{2}}$.

(2) Surface tension

If we assume that u_{rel} is proportional to $\bar{u}_G$

then for constant ρ_G, h, K and l we have:-

Shallow water: $$\frac{\bar{u}_{G_{crit}}^4}{\sigma^{3/2}\tau_w^{\frac{1}{2}}} = \text{constant} \quad .....(5.45)$$

Deep water: $$\frac{\bar{u}_{G_{crit}}^3}{\sigma\tau_w^{\frac{1}{2}}} = \text{constant} \quad .....(5.46)$$

An examination of the graphs of pressure gradient versus reduced velocity indicates that there is a steep increase in pressure gradient in the region of the onset of droplet entrainment. Even after allowing for the inadequacies of a reduced velocity in this region [c.f. Section 4.4.2, comment (3)] the graphs show that the pressure gradient and hence τ_w, as the effect of the weight of the liquid film is generally small, increases as $\bar{u}_G^2$ to $\bar{u}_G^{2.5}$. This is because of the increasing intensity of the film-core interaction as the gas velocity is increased over this range.

Hence, from equation (5.45):-

$\bar{u}_{G_{crit}}$ is proportional to $\sigma^{\frac{1}{2}}$ to $\sigma^{6/11}$

and from equation (5.46)

$\bar{u}_{G_{crit}}$ is proportional to $\sigma^{\frac{1}{2}}$ to $\sigma^{4/7}$

Thus overall $\bar{u}_{G_{crit}}$ should vary approximately as $\sigma^{\frac{1}{2}}$.

(3) Liquid viscosity

Liquid viscosity does not enter into equations (5.37) and (5.39) and hence moderate variations in liquid viscosity should not affect $\bar{u}_{G_{crit}}$. However, the analysis of this section assumes that the liquid film is flowing as disturbance waves. If the liquid viscosity was large enough to suppress disturbance waves then entrainment would not occur by the mechanism postulated in this section.

(4) Liquid flow rate

An examination of the tabulated results shows that at a gas velocity of 50 ft/sec the total pressure gradient and hence τ_w varies as $Q_L^{2/3}$ approximately. An examination of the graphs of the disturbance wave time intervals versus the water flow rate shows that at an air velocity of 50 ft/sec and an air density of 0.0712 lb/ft^3 the frequency of disturbance waves varies as $Q_L^{\frac{1}{2}}$ at low liquid flow rates but is approximately constant at high liquid flow rates.

As the liquid volume fraction varies as $Q_L^{\frac{1}{2}}$ approximately at the same air conditions this indicates that the average disturbance wave size is approximately constant at low water rates but increases as $Q_L^{\frac{1}{2}}$ at high water rates. This suggests that $l\sqrt{h}$ varies as Q_L^0 to $Q_L^{0.4}$ and l varies as Q_L^0 to $Q_L^{\frac{1}{2}}$ with increasing water flow rate.

Overall it would seem that $(B_{max} t_{gr})$ which is proportional to $l\sqrt{\frac{h}{\tau_w}}$ for shallow liquid conditions and $\frac{1}{\sqrt{\tau_w}}$ for deep liquid conditions is almost unaltered by changes in the water flow rate. This would suggest that $\bar{u}_{G_{crit}}$ is unaltered by changes in the liquid flow rate. Also it should be noted that this analysis has assumed that K, which is a measure of the shape of the disturbance wave velocity profile, is independent of Q_L.

However the experimental evidence discussed in Part 2.1 of this section shows that $\bar{u}_{G_{crit}}$ decreases as the liquid flow rate is increased. This failing of equations (5.43) and (5.44) probably arises because the expression for the maximum growth time for a ripple is inadequate (equation 5.42) and also because the increase in liquid flow rate may result in larger initial disturbances before amplification and growth into ripples.

The motion of a disturbance wave is much more complex than has been assumed in the simple model based on continuity which has been used in this analysis.

Although "roll" wave motion is possible near the disturbance wave crest, in the thin film near the tail the motion must be more like that of a draining viscous liquid film (Bird, Stewart and Lightfoot, 1960, p. 69).

The possibility of variations in the initial disturbances with liquid flow rate is very likely. However, as there is no theory available to predict independently how initial disturbances arise, this possibility cannot be checked.

The experimental results indicate that $\bar{u}_{G_{crit}}$ may vary as $Q_L^{-\frac{1}{8}}$ to $Q_L^{-1/6}$ over the range 300 to 2700 lb/hr in a 1.330 inch tube at an air density of 0.0712 lb/ft^3.

5.2.9 The droplet formation rate.

If the test section is sufficiently long then irrespective of how the liquid and gas are introduced the flow will eventually come to an equilibrium condition in which entrainment of droplets from the liquid film into the gas core is balanced by an equal deposition of droplets from the gas core on to the liquid film. This is only approximately true because the decrease in pressure and hence the increase in gas velocity along the tube causes an increase in the equilibrium droplet flow rate along the tube.

In the 245 inch test section used in this work

equilibrium was definitely attained in the flows at an air velocity of 50 ft/sec but not, at least when the porous wall injector was used, at the higher air velocities. This is shown by the graphs in Figures 4.9 and 4.10, for at an equilibrium position the amount of droplet entrainment does not depend on the type of liquid injector.

We postulate that when a ripple has grown into a sharp crested wave which is emitting droplets then for the rest of its life it remains the same size and the growth is channelled into droplet formation. The following analysis is based on sinusoidal waves. Because the ripples in fact are sharp crested and not sinusoidal the analysis can be only approximately correct.

The cross sectional area of the crest half of a sinusoidal wave of length λ and amplitude a is $\frac{a\lambda}{\pi}$, that is $\frac{2a}{N}$ where N is the wave number. For exponential growth of a wave of optimum wave number:

$$a = a_o \exp (B_{max} t) \qquad \ldots\ldots\ldots\ldots\ldots (5.47)$$

where a_o is the initial amplitude of the wave.

$$\text{i.e. } \frac{da}{dt} = a B_{max} \qquad \ldots\ldots\ldots\ldots\ldots (5.48)$$

$$\text{Hence } \frac{d\,(\text{wave crest area})}{dt} = \frac{2a B_{max}}{N} \qquad \ldots\ldots\ldots (5.49)$$

But there are N ripples in a length 2π. Hence the rate of change of crest cross-sectional area per unit length of

ripples is $\frac{a\, B_{max}}{\pi}$. When a ripple is emitting droplets this change of area becomes droplets and the ripple amplitude remains constant.

It is now necessary to estimate the amplitude of a wave at which it emits droplets. Michell (1893) showed theoretically that the maximum possible height of an ocean wave is $0.142\,\lambda$. The wave form of such a wave is approximately trochoidal. We assume that this same limit can be applied to the sharp crested ripples being considered in this analysis. Hence,

$$a = 0.071\lambda = \frac{0.446}{N} \qquad \ldots\ldots\ldots\ldots(5.50)$$

Therefore, assuming that the ripples all have the optimum wave number N_{opt},

$$\text{Rate of formation of droplets per unit width per unit length of fully developed rippled film} = \frac{0.142\, B_{max}}{N_{opt}} \qquad \ldots(5.51)$$

The ripples have grown to the size at which they start to emit droplets at time t given by:-

$$B_{max,actual} \cdot t = B_{max,crit} \cdot t_{gr} \qquad \ldots\ldots\ldots(5.52)$$

From time t to time t_{gr} the ripples emit droplets. If the ripples are carried up the surface of the disturbance wave at a constant velocity then the fraction of the active length over which they emit

droplets is:-

$$\text{Fraction of active length which is an emitting surface} = 1 - \frac{t}{t_{gr}} = 1 - \frac{B_{max,crit}}{B_{max,actual}}. \qquad \ldots\ldots\ldots\ldots(5.53)$$

Hence the mean mass rate of film atomization or droplet formation per unit surface area of film, M_a, is:-

$$M_a = \frac{0.142 B_{max}}{N_{opt}} \rho_L \left[1 - \frac{B_{max,crit}}{B_{max,actual}}\right] \times \frac{\text{active length}}{\text{distance between disturbance waves}} \qquad \ldots\ldots\ldots\ldots(5.54)$$

where $\left[1 - \frac{B_{max,crit}}{B_{max,actual}}\right] \times \frac{\text{active length}}{\text{distance between disturbance waves}}$ is the ratio of the area of the film surface covered by droplet emitting ripples to the total film surface area. To evaluate M_a from equation (5.54) it is necessary to express this ratio in terms of measurable quantities.

Substitution in equations (5.37) and (5.39) shows that:-

<u>Shallow liquid</u>: $$\frac{0.142 B_{max} \rho_L}{N_{opt}} = 0.142 \frac{\sqrt{3}}{4} \rho_G u_{rel}^2 \left[\frac{h \rho_L}{\sigma}\right]^{\frac{1}{2}} \qquad \ldots\ldots\ldots\ldots(5.55)$$

<u>Deep liquid</u>: $$\frac{0.142 B_{max} \rho_L}{N_{opt}} = \frac{0.142}{\sqrt{3}} \left[\rho_G \rho_L\right]^{\frac{1}{2}} u_{rel} \qquad \ldots\ldots\ldots\ldots(5.56)$$

5.2.10 The droplet deposition rate.

The literature pertaining to core-film equilibrium has been reviewed in Section 2.4.6. Cousins and Hewitt (1968b) thought of droplet deposition in terms of mass transfer. Accordingly they put the droplet deposition rate per unit film surface area, N_d, equal to a deposition coefficient multiplied by the droplet concentration in the gas core (equation 2.68). Hoogendoorn and Welling (1965) thought of the droplet deposition rate per unit length of tube as being proportional to the droplet flow rate and inversely proportional to the tube diameter (equation 2.72). This is equivalent to putting the droplet deposition rate proportional to the concentration multiplied by the superficial gas velocity (equation 2.73). Cousins and Hewitt (1968b) showed experimentally that the droplets have axial velocities close to the local linear gas velocity.

The effect of gas velocity on the droplet deposition rate.

The apparently contradictory results of Cousins and Hewitt and of Hoogendoorn and Welling on the effect of gas velocity on deposition rate have been commented on in the literature review. Cousins and Hewitt found that the radial velocities of the larger droplets were larger than the radial velocities of the smaller droplets.

They found that the droplet deposition rate was independent of the gas velocity. In contrast Hoogendoorn and Welling found that the droplet deposition rate was proportional to the gas velocity.

An approximate analysis of the likely droplet radial stopping distance is possible if the drag forces on the droplet are assumed to follow Stokes' equation. The basic assumption, admittedly a very doubtful one, is that the axial and radial forces on the droplet act independently.

The drag force on a droplet of diameter d moving at a radial velocity u_d is $3\pi\mu_G d u_d$ and the mass of the droplet is $\frac{\pi}{6} d^3 \rho_L$. Hence the rate of deceleration is:-

$$\frac{d u_d}{dt} = - \frac{18 \mu_G u_d}{\rho_L d^2} \qquad \text{.....(5.57)}$$

$$\therefore \quad u_d = u_{d_o} \exp\left[- \frac{18 \mu_G t}{\rho_L d^2} \right] \qquad \text{.....(5.58)}$$

$$\therefore \quad \mathcal{D} = \int_o^\infty u_d \, dt = u_{d_o} \frac{\rho_L d^2}{18 \mu_G} \qquad \text{.....(5.59)}$$

The radial stopping distance $\mathcal{D}$ is obtained by integrating equation (5.57) twice as is indicated by equations (5.58) and (5.59).

The radial velocity of injection $(u_d)_{rad,o}$ is assumed to be the potential rate of change of amplitude of the crest of a ripple as it emits droplets. This neglects any retarding effect on the droplets due to surface tension forces as they break free from the ripple surface. Combining equations (5.48) and (5.50) gives:-

$$u_{d_o} = \frac{da}{dt} = \frac{0.446B_{max}}{N_{opt}} \qquad \text{.....(5.60)}$$

Substitution into equation (5.39) gives:-

$$u_{d_o} = \frac{0.446}{\sqrt{3}} \left[\frac{\rho_G}{\rho_L}\right]^{\frac{1}{2}} u_{rel} \qquad \text{.....(5.61)}$$

The deep liquid growth rate equation has been used because it is simpler to handle than the shallow liquid growth rate equation and because the degree of approximation inherent in the drag assumption means that greater accuracy is unnecessary.

$$\therefore \mathcal{D} = \frac{0.446}{18\sqrt{3}} \left[\rho_G \rho_L\right]^{\frac{1}{2}} \frac{d^2}{\mu_G} u_{rel} \qquad \text{.....(5.62)}$$

For a water droplet of diameter 100 microns being atomized into an air stream of density 0.0712 lb/ft^3 and velocity 93.5 ft/sec equation (5.62) gives $\mathcal{D}$= 0.16 inch. This is assuming that u_{rel} = 50 ft/sec = 0.54 $\bar{u}_G$.

This analysis shows that only very large droplets, greater than about 200 microns, could retain a portion of

their initial velocity for a significant proportion of the diameter of a 1.330 inch diameter tube. The results of Cousins and Hewitt (1968b) were obtained from a $\frac{5}{8}$ inch tube. In a tube of this size droplets as small as 110 microns would retain a portion of their initial velocity for half of the tube diameter. This is a possible reason for the higher deposition rates of the larger droplets observed by Cousins and Hewitt.

As most of the droplets are too small to retain a portion of their initial velocity for a significant part of their travel across the gas core it seems necessary to assume that they move to the wall by a type of diffusion mechanism. However, most of the droplets are too large to follow the gas turbulent eddies significantly as the analysis of Longwell and Weiss (1953), reviewed in Section 2.4.6, has shown. They probably pick up small radial motions from the gas turbulent eddies and move with a slow random motion. If such is the case then the droplets should behave in a similar manner to the diffusion of a gas molecule due to turbulent motion. In this case the radial velocity is proportional to $(\bar{u}_G)^{0.8}$. It seems reasonable to assume that the small and medium sized droplets show much the same dependence on the gas velocity.

The effect of droplet concentration on the droplet deposition rate

At low droplet concentrations such as were used by Cousins and Hewitt (1968b) the interference between

droplets would have been minimal. However, this is no longer true at the much higher droplet concentrations studied in this Thesis.

If we consider an infinitesimal area parallel to and close to the tube wall, then the droplet volume flux per unit area through this area towards the wall is $\frac{1}{2}\gamma(\bar{u}_d)_{rad}$, where γ is the droplet volume fraction and $(\bar{u}_d)_{rad}$ is the mean droplet radial velocity. The $\frac{1}{2}$ is necessary because half of the droplets crossing the area are moving towards the wall and half are moving away from it. As the area can be chosen as close to the tube wall as we like it follows that $\frac{1}{2}\gamma(\bar{u}_d)_{rad}$ is the droplet volume flux per unit area on the wall itself. In this analysis the gas axial velocity is assumed to be uniform across the tube and the droplets are assumed to have random velocities with reference to a co-ordinate system moving with the gas stream. Hence,

$$(\bar{u}_d)_{rad} = (\bar{u}_d)_{tang} = (\bar{u}_d)_{ax} = \frac{1}{\sqrt{3}}\,\bar{u}_d \quad \ldots\ldots(5.63)$$

where $(\bar{u}_d)_{tang}$ and $(\bar{u}_d)_{ax}$ are the mean tangential and axial droplet velocities and $\bar{u}_d$ is the mean droplet velocity.

$$\therefore \text{ average droplet lifetime} = \frac{\text{volume occupied by droplets per unit length of tube}}{\text{volume flux at tube wall per unit length of tube}}$$

$$= \frac{\pi R^2 \gamma}{\frac{1}{2}\gamma(\bar{u}_d)_{rad} \cdot 2\pi R} = \frac{R}{(\bar{u}_d)_{rad}} \quad \ldots\ldots\ldots\ldots\ldots(5.64)$$

$$\text{average pathlength of droplets} = \frac{R}{(\bar{u}_d)_{rad}} \cdot \bar{u}_d = \sqrt{3}\,R \quad \ldots\ldots\ldots(5.65)$$

It is shown in Appendix 5 that the droplet mean free path, that is the mean distance that a droplet travels between collisions with other droplets, is $\frac{d}{8\gamma}$ if all droplets are assumed to have the same diameters, d, and travel at the same speed.

In the most concentrated core conditions studied in this Thesis the mean free path was much smaller than the average path length. For example in one case the air volumetric flow rate was 3660 ft^3/hr and the droplet volumetric flow rate was 27 ft^3/hr corresponding to $\gamma = 0.0074$. At this air velocity (100 ft/sec) and density (0.2190 lb/ft^3) the work of Cousins and Hewitt (1968b) indicates that the mean droplet diameter would be about 70 microns = 0.0028 inch. Hence the mean free path = 0.047 inch, and the droplets would have an average of 24.4 collisions.

Because, at least in the centre part of the core, the droplet speeds relative to each other are small, collisions are likely to lead to coalescence. The coalescing of droplets reduces their average speed for two reasons:-

(i) On the average the velocity of the centre of mass of a group of droplets is less than the mean velocity of the individual droplets. If the individual droplets all have the same speed, then, on average, two droplets combined have 2/3

of the individual droplet speed, three droplets combined have 13/24 and four droplets combined have 7/15. For m droplets the factor is approximately $m^{-\frac{1}{2}}$. This is discussed in Appendix 5.

(ii) The heavier droplets thus formed respond to a lesser degree to the turbulent gas eddies and therefore would be expected to have lower drift velocities. The equation of Longwell and Weiss (1953) indicates that the ability of the droplet to follow the eddies is inversely proportional to the 4/3 power of its mass.

The net effect of coalescence is that at high droplet concentrations the droplet deposition rate is no longer proportional to the droplet concentration. Under these conditions the deposition rate may vary as $\gamma^{\frac{1}{2}}$ approximately.

5.2.11 The equilibrium entrainment flow rate.

Equating equations (5.54) and (5.56) with the factors affecting droplet deposition gives, for the deep liquid case:-

$$\frac{0.071}{\sqrt{3}} \left[\rho_G \rho_L\right]^{\frac{1}{2}} u_{rel} \left[1 - \frac{B_{max,crit}}{B_{max,actual}}\right] \times \frac{\text{active length}}{\text{distance between disturbance waves}}$$

$$= b\, f(\gamma)\, \rho_L \bar{u}_G \qquad \ldots\ldots\ldots \ldots(5.66)$$

In this equation it is assumed that the droplet deposition rate is proportional to the gas velocity. b is the deposition coefficient (dimensionless) defined in the same

way as was done by Hoogendoorn and Welling (1965) (c.f. Section 2.4.6, equation (2.72)). In the case of a shallow liquid film $\frac{0.071}{\sqrt{3}} (\rho_G \rho_L)^{\frac{1}{2}} u_{rel}$ is replaced by $\frac{0.071}{4} \sqrt{3} \rho_G u_{rel}^2 (\frac{h \rho_L}{\sigma})^{\frac{1}{2}}$. $f(\gamma)$ is equal to γ at low concentrations but is less than γ at high concentrations due to droplet coalescence.

In order to calculate $f(\gamma)$ all the other quantities in equation (5.66) must be known. u_{rel} can be expressed in terms of $\bar{u}_G$ and the pressure gradient by means of equation (5.17). The ratio $\frac{u_{rel}}{\bar{u}_G}$ changes slowly with variations in flow conditions.

The deposition coefficient b is expected to be a complex function of the droplet size distribution and the gas flow rate. Some of the factors which affect b have been touched on in Part 2.10 of this section. Hoogendoorn and Welling (1965) found that $b = 0.02 \pm 0.005$ for their range of experiments.

In the formation of droplets the problem parameter is the proportion of the film surface area which is covered with ripples which are emitting droplets. This area ratio is expressed as the product of two separate factors in equation (5.66)

They are considered below.

(i) $\left(1 - \frac{B_{max,crit}}{B_{max,actual}} \right)$

This factor represents the fraction of the active length of a disturbance wave which is emitting droplets. $B_{max,crit}$ is the value of B_{max} at the minimum value of the gas relative velocity, u_{rel}, which can initiate entrainment from the disturbance wave assuming no change in disturbance wave size and length. From equations (5.37) and (5.39) this ratio is $\left[1 - \left(\frac{u_{rel,crit}}{u_{rel}}\right)^3\right]$ for a deep liquid film and $\left[1 - \left(\frac{u_{rel,crit}}{u_{rel}}\right)^4\right]$ for a shallow liquid film.

$\left(1 - \frac{B_{max,crit}}{B_{max,actual}}\right)$ must be calculated for the actual size and length of the disturbance waves in the flow. However it has been shown in Section 5.28 that $\bar{u}_{G_{crit}}$ and hence $u_{rel,crit}$ depends on the gas density, the surface tension and on the liquid flow rate. Thus the evaluation of $u_{rel,crit}$ is extremely difficult.

Fortunately, for gas velocities such that u_{rel} is twice or more times $u_{rel,crit}$, $\left[1 - \frac{B_{max,crit}}{B_{max,actual}}\right]$ is approximately equal to 1. This would be the case for air velocities in excess of 90 ft/sec at a density of 0.0712 lb/ft^3.

(ii) The ratio $\frac{\text{active length}}{\text{distance between disturbance waves}}$

This ratio is a function of both the liquid flow rate and the gas velocity. At a constant gas velocity the frequency of the disturbance waves varies as $Q_L^{\frac{1}{2}}$ at low liquid flow rates but is approximately constant at high liquid flow rates. At a constant gas velocity the velocity of the disturbance waves increases as $Q_L^{1/5}$ or $Q_L^{\frac{1}{4}}$ approximately.

The exponent was lower at low liquid rates and higher at high liquid rates. This applies only to moderate gas velocities. Hence the wave frequency variation is the major factor affecting the variation in the distance between disturbance waves at a constant gas velocity and a varying liquid flow rate.

At a given gas velocity the active length of a disturbance wave depends on the disturbance wave size. The wave size is approximately constant at low water rates but varies as $Q_L^{\frac{1}{2}}$ at high water rates. Overall, the ratio $\frac{\text{active length}}{\text{distance between disturbance waves}}$ varies as $Q_L^{\frac{1}{2}}$ at constant moderate gas velocities. At high liquid rates where the liquid film is everywhere greater than about 0.010 inch thick, the actual value depending on the pressure gradient, the ratio is constant at 1.

At high gas velocities much or most of the liquid flows as droplets in the core. For this reason and because of the high pressure gradient the liquid film is very thin. Because of the high interfacial shear stress ripple growth can occur on very thin films. Equation (5.28) shows that the minimum thickness for ripple growth varies as $\tau_w^{3/2} = \left(-\frac{dp}{dx}\right)^{3/2}$. The ratio $\frac{\text{active length}}{\text{distance between disturbance waves}}$ approaches 1 unless the total liquid flow rate is very low.

In this case disturbance waves might not form and therefore there would be no droplet entrainment even at high gas velocities.

The effects of the flow parameters on $f(\gamma)$ can be summarised as follows:-

(1) Gas density

The left-hand side of equation (5.66) is directly proportional to ρ_G (shallow film) or $\rho_G^{\frac{1}{2}}$ (deep film). The gas density also affects the ratio $\frac{u_{rel}}{\bar{u}_G}$ and the ratio $\frac{\text{active length}}{\text{distance between disturbance waves}}$.

Increasing the gas density decreases $u_{rel,crit}$ and hence decreases $\frac{u_{rel,crit}}{u_{rel}}$. Increasing the gas density increases the pressure gradient and decreases the film thickness.

Overall, it is expected that $f(\gamma)$ will vary as ρ_G approximately at gas velocities slightly in excess of the critical gas velocity. At high gas velocities the liquid film is thin because of the high interfacial shear stress and because much of the liquid is flowing as droplets in the core. Therefore increases in gas density can cause only small relative increases in $f(\gamma)$.

These comments are substantiated by the experimental results. At an air velocity of 50 ft/sec and a water rate of 300 lb/hr increasing the air density from 0.0712 lb/ft^3 to 0.2192 lb/ft^3 increases the equilibrium fractional

entrainment from 0.055 to 0.125.

When the air velocity is 200 ft/sec and the density is 0.0712 lb/ft^3 the fractional entrainment is 0.65. Clearly there is no possibility of a further large relative increase in the fractional entrainment if the air density is increased to 0.2192 lb/ft^3.

At high liquid rates and moderate gas velocities the fractional entrainment varies as $\rho_G^{\frac{1}{2}}$ approximately as would be expected in a deep liquid film. At high gas velocities and high liquid rates most of the liquid flows in the core and changes in ρ_G have little effect on the fractional entrainment.

(ii) Gas velocity

At gas velocities slightly in excess of the critical velocity for the onset of entrainment small variations in velocity will cause large variations in the amount of surface emitting droplet entrainment and hence large relative variations in the fractional entrainment.

At high gas velocities most of the surface is generating droplet entrainment. The effects of increases in gas velocity are counterbalanced by decreases in film thickness and hence the fractional entrainment, already close to 1, does not alter very much. $f(\gamma)$ decreases because of the increased gas volume.

(iii) Liquid flow rate

This is perhaps the most interesting case for the experimental results show that the droplet flow rate is almost a linear function of the total liquid flow rate for a constant gas velocity and density. This is shown in Figures 4.9 and 4.10.

It has already been shown that the ratio $\frac{\text{active length}}{\text{distance between disturbance waves}}$ varies as $Q_L^{\frac{1}{2}}$ at moderate gas velocities. An increase in Q_L causes an increase in h and hence B_{max} for the shallow liquid case. It has been pointed out in Part 8 of this section that an increase in Q_L reduces the gas velocity for the onset of droplet entrainment. This means that an increase in Q_L reduces $B_{max,crit}$. Overall it is quite possible that $f(\chi)$ varies as Q_L approximately at moderate gas velocities. At high gas velocities the exponent on Q_L would be less than 1.

5.2.12. Summary and criticism of the theory

(1) The basis of this analysis of droplet entrainment has been the postulate that droplet entrainment is formed from the tips of ripples on and near the crests of entrainment waves.

(2) It is shown that the wavelength of the ripples can be approximately predicted by a stability analysis based on

the interaction of aerodynamic and surface tension forces.

(3) It is shown that the smooth film between the disturbance waves is caused by the retarding effect of liquid viscosity on the ripple growth.

(4) The theory is able to indicate that there is a critical gas velocity for the onset of droplet entrainment but is unable to predict its magnitude.

(5) It fails to predict that the critical gas velocity for the onset of the droplet entrainment decreases as the liquid flow rate increases.

(6) The theory predicts droplet injection velocities and stopping distances which can explain some of the results of Cousins and Hewitt (1968b). They found that the very large droplets have higher radial velocities than the rest of the droplets.

(7) Although the theory may well predict the correct rate of droplet formation from an emitting surface, it does not analyse the factors which affect the ratio of the area of the emitting surface to the total liquid film surface.

5.3 Discussion of Points Not Fully Discussed in the Experimental Section

5.3.1. The total pressure gradient equation

In Section 4.4, in which the experimental pressure gradient results were presented, the frictional pressure gradient was assumed to be the dominant part of the total pressure gradient. In the derivation of equations for the

calculation of the pressure gradient at a point from the pressure difference between two points the total pressure gradient was assumed to be proportional to the fractional pressure gradient. On the graph the experimentally measured total pressure gradient was plotted against the reduced velocity. The single phase flow lines used for comparison were frictional pressure gradients not total pressure gradients.

5.3.1.1 The accelerational pressure gradient

This is that component of the pressure gradient which is used in accelerating the two phase mixture as the velocity increases due to the decrease in the total pressure and the gas density along the test section. The basic equation is:-

$$\text{Force} = \text{mass} \times u\frac{du}{dx} \qquad \ldots\ldots\ldots\ldots\ldots\ldots(5.67)$$

The accelerational pressure gradient:- $\left(-\frac{dp}{dx}\right)_{acc}$ is

$\frac{\text{force}}{\text{area} \times \text{distance}} = \frac{\text{force}}{\text{volume}}$. Hence

$$\left(-\frac{dp}{dx}\right)_{acc} = \rho u\frac{du}{dx} \qquad \ldots\ldots\ldots\ldots\ldots\ldots(5.68)$$

We confine our attention to the gas-droplet core. ρu is the mass velocity $\frac{1}{\mathcal{A}}(W_G + W_{LE})$ where $\mathcal{A}$ is the core cross-sectional area. We assume that the droplets are moving at the gas velocity. Hence $u = \frac{1}{\mathcal{A}}\left[\frac{W_G}{\rho_G} + \frac{W_{LE}}{\rho_L}\right]$

$$\therefore \quad \frac{du}{dx} = -\frac{W_G}{A\rho_G^2}\frac{\rho_G}{dx} = \frac{W_G}{A\rho_G p}\left(-\frac{dp}{dx}\right)_{tot} \qquad \ldots\ldots\ldots(5.69)$$

Equation (5.69) assumes that the gas obeys the perfect gas law, in particular that its density is proportional to the total pressure.

$$\therefore \left(-\frac{dp}{dx}\right)_{acc} = \frac{W_G\left[W_G + W_{LE}\right]}{A^2 \rho_G p}\left[-\frac{dp}{dx}\right]_{tot} \qquad \ldots\ldots\ldots(5.70)$$

The relative importance of the accelerational pressure gradient depends upon the value of $\frac{W_G\left(W_G + W_{LE}\right)}{A^2 \rho_G p}$.

Equation (5.70) neglects the component of the pressure gradient required to accelerate the liquid film. This is small because the liquid film velocity is low. A more serious error may arise at high gas velocities and when the droplet flow rate is large. The results of Cousins and Hewitt (1968b) indicate that the mean droplet velocity may be a little less than the mean gas velocity. If the droplet velocity were 10% less then the value of $\left(-\frac{dp}{dx}\right)_{acc}$ calculated from equation (5.70) could be up to 20% high depending on the ratio W_{LE}/W_G.

$\frac{W_G\left(W_G + W_{LE}\right)}{A^2 \rho_G p}$ can be put in the form $\bar{u}_{G_{actual}}^2 \left[1 + \frac{W_{LE}}{W_G}\right] \frac{\rho_G}{p}$, where $\bar{u}_{G_{actual}}$ is the mean gas

velocity based on the gas flow cross sectional area. $\frac{\rho_G}{p}$ is constant for air near atmospheric pressure and temperature apart from small effects caused by the water vapour present. $\frac{W_{LE}}{W_G}$ increases with increases in gas velocity except at high gas velocities when nearly all the liquid is entrained and further increases in W_{LE} are not possible. Therefore when $\frac{W_{LE}}{W_G}$ is increasing $(-\frac{dp}{dx})_{acc}$ increases more rapidly than the square of $\bar{u}_{G_{actual}}$. In run 141, assuming a fractional entrainment of 0.8, the ratio $(-\frac{dp}{dx})_{acc} : (-\frac{dp}{dx})_{tot} = 0.503$.

In this run $\bar{u}_{G_{actual}} = 338$ ft/sec and $\left[1 + \frac{W_{LE}}{W_G}\right] \simeq 4.3$

The accelerational factors were calculated for runs at velocities in excess of 150 ft/sec. When the total pressure gradient minus the accelerational pressure gradient was plotted against the reduced velocity it could be seen that all the graphs approached the single phase reference lines at high gas velocities. In runs at gas velocities less than 150 ft/sec the accelerational factors were less than 0.1.

5.3.1.2 The gravitational pressure gradient

The gravitational pressure gradient is:-

$$(-\frac{dp}{dx})_{grav} = -\left[1 - \alpha + \frac{\rho_G}{\rho_L}\alpha\right] \sin\theta \quad \ldots\ldots\ldots\ldots (5.71)$$

where θ is the angle of inclination of the test-section

below the horizontal in the flow direction. The units of equation (5.71) are ft of liquid/ft of tube.

For most of the flows studied in this Thesis the void fraction was in the range 0.90 to 0.99, and hence $(-\frac{dp}{dx})_{grav}$ was in the range -0.10 to -0.010 ft water/ft tube. Thus $(-\frac{dp}{dx})_{grav}$ could be important at low gas velocities and high liquid flow rates.

5.3.1.3 The pressure gradient caused by droplet exchange between the gas core and the liquid film

Another pressure gradient which may either be thought of as an accelerational pressure gradient or a frictional pressure gradient is that which arises because of the dynamic exchange of droplets between the film and the core. The mass deposition rate of droplets per unit surface area is $k_d \gamma \rho_L$ where k_d is the droplet deposition coefficient and γ is the droplet volume fraction in the core. Hence the momentum transferred to the film per unit length of tube is $k_d \gamma \rho_L \pi D \bar{u}_{G_{actual}}$.

This assumes that the droplets are moving at the mean gas axial velocity when they impact on the liquid film. Dividing by the cross sectional area of the flow and $\rho_L g$ gives the pressure gradient in ft liquid/ft tube:-

$$(-\frac{dp}{dx})_{\substack{dynamic \\ exchange}} = \frac{4\, k_d \gamma \bar{u}_{G_{actual}}}{g\, D} \qquad \text{.....(5.72)}$$

To be strictly correct the D term should be multiplied by $(1 - \sqrt{1 - \alpha_c})$, where α_c is the core volume fraction, to allow for the thickness of the liquid film on the wall.

Equation (5.72) predicts values of $\left(-\frac{dp}{dx}\right)_{\substack{\text{dynamic} \\ \text{exchange}}}$ which can be appreciable at high droplet concentrations and high gas velocities. For example, in run 132S the droplet volume fraction was 0.0053 and the gas actual mean velocity was 212.7 ft/sec. We put $k_d = 1.0$ ft^3/ft^2, sec. This figure is a very approximate one based on the results of Cousins and Hewitt (1968a). Substitution of these values into equation (5.72) gives:-

$$\left(-\frac{dp}{dx}\right)_{\substack{\text{dynamic} \\ \text{exchange}}} = 0.127 \text{ ft water/ft tube.}$$

However, equation (5.72) is not very satisfactory and it probably overestimates the importance of droplet exchange as a means of transferring momentum from the core to the film. Only the very large droplets have sufficient radial velocity and sufficient mass to penetrate through the low velocity gas near the liquid film and reach the film with most of their original axial momentum. The major part of the droplet mass flow is composed of droplets which are so small that their velocities are close to the local gas axial velocity at all points in the gas stream.

If droplet exchange is an important mechanism for transferring momentum it should cause a distinct flattening of the core velocity profile. In fact Gill, Hewitt, Hitchon and Lacey (1963) have shown that the gas core velocity profile is very much steeper in a two phase annular flow than in a single phase gas flow with the same mean gas velocity. This shows that the influence of the liquid film on the gas core velocity profile is much greater than the influence of droplet exchange on the gas core velocity profile. This suggests that droplet exchange is not an important mechanism for transferring momentum from the central part of the core to the part of the core near the wall. From the pressure gradient point of view it is more satisfactory to consider the gas core or at least the central part of it, to be a homogeneous mixture of gas and droplets.

5.3.2 The distribution of the liquid volume fraction between the film and the core

The gas volume fraction in the core is $1 - \gamma$

where $\gamma = \dfrac{W_{LE}/\rho_L}{W_G/\rho_G + W_{LE}/\rho_L} \approx \dfrac{W_{LE}\rho_G}{W_G\rho_L}$. γ is the liquid volume fraction in the core. This assumes that the liquid droplets move at the local gas axial velocity. Hence the gas volume fraction of the whole flow (film + core), α, is given by:-

$$\alpha = \alpha_c (1-\gamma) \qquad \text{.....(5.73)}$$

where α_c is the core volume fraction, that is the ratio of the core cross sectional area to the total flow area. Therefore the liquid film volume fraction is:-

$$1 - \alpha_c = 1 - \frac{\alpha}{1-\gamma} \qquad \text{.....(5.74)}$$

The ratio of the liquid film volume fraction to the total liquid volume fraction is:-

$$\frac{1-\alpha_c}{1-\alpha} = 1 - \frac{\alpha}{1-\alpha} \therefore \frac{\gamma}{1-\gamma} \qquad \text{.....(5.75)}$$

Values of $\frac{1-\alpha_c}{1-\alpha}$ calculated for some of the experimental runs with large values of γ are tabulated below:-

RUN	WATER FLOW RATE (LB/HR)	AIR FLOW RATE (LB/HR)	AIR DENSITY (LB/FT^3)	γ	$\frac{1-\alpha_c}{1-\alpha}$
69S	300	493	0.0704	0.00053	0.86
100S	999	506	0.0721	0.0018	0.77
119S	2702	126	0.0716	0.0038	0.97
125S	2700	260	0.0723	0.0072	0.92
132S	2700	514	0.0709	0.0056	0.70
172S	301	1215	0.2183	0.00065	0.84
199S	990	1238	0.2198	0.0022	0.57
210S	2002	385	0.2181	0.0042	0.95
217S	2000	774	0.2178	0.0047	0.90
226S	2001	1234	0.2172	0.0048	0.67

Table 5.1 VALUES OF THE RATIO OF THE FILM VOLUME FRACTION TO THE TOTAL LIQUID VOLUME FRACTION, $\frac{1-\alpha_c}{1-\alpha}$, IN FLOWS WITH A LARGE AMOUNT OF DROPLET ENTRAINMENT.

The values of $\frac{1-\alpha_c}{1-\alpha}$ in Table 5.1 show that at high gas velocities and high liquid flow rates the core liquid volume fraction is an important part of the total liquid volume fraction. Equation (4.14) now becomes

$$h = R\left(1 - \sqrt{\alpha_c}\right) \qquad \ldots\ldots\ldots\ldots (5.76)$$

Equations (4.24) to (4.26) remain the same but with h calculated from equation (5.76).

5.3.3 Disturbance wave velocity measurements

In Figure 5.1 p.211 the mean wave velocities for the medium pressure series of runs at the bottom measurement level are plotted against the liquid film Reynolds number for those runs in which the droplet flow rate was measured. These are some of the runs in which the mean wave velocities were plotted against the total liquid Reynolds number in Figure 4.3 (p.129). The graph lines have been so drawn in Figure 5.1 that they are equivalent to their parent lines in Figure 4.3.

With the exception of the anomalous line MS 204 the graph lines in Figure 5.1 were replotted using logarithmic co-ordinates on both axes to check if there was a power form of relationship between the mean wave velocity and the liquid film Reynolds number. However the exponent on the liquid film Reynolds number was not constant but increased from about 0.12 - 0.2 at low liquid film

LEGEND

MEAN SUPERFICIAL AIR VELOCITY AT 235 IN.LEVEL (FT/SEC)	MEAN AIR DENSITY AT 235 IN.LEVEL (LB/FT^3)	INJECTOR TYPE	WAVE VELOCITY SYMBOL	WAVE VELOCITY LINE DESIGNATED BY
50.7	0.0709	Porous Wall	■	M51
51.3	0.0718	Spray	◆	MS51
98.3	0.0715	Porous Wall	■	M98
98.7	0.0719	Spray	◆	MS99
204.8	0.0718	Porous Wall	■	M205
204.1	0.0711	Spray	◆	MS204

Figure 5.1 MEAN WAVE VELOCITY VERSUS DIMENSIONLESS LIQUID FILM FLOW RATE, $N_{Re_{L,f}} = \frac{W_f}{\pi D \mu_L}$ MEDIUM PRESSURE SERIES AND 235 INCH LEVEL.

These curves are equivalent to those of figure 4.3 (p.129) for which film and core flow data were obtained.

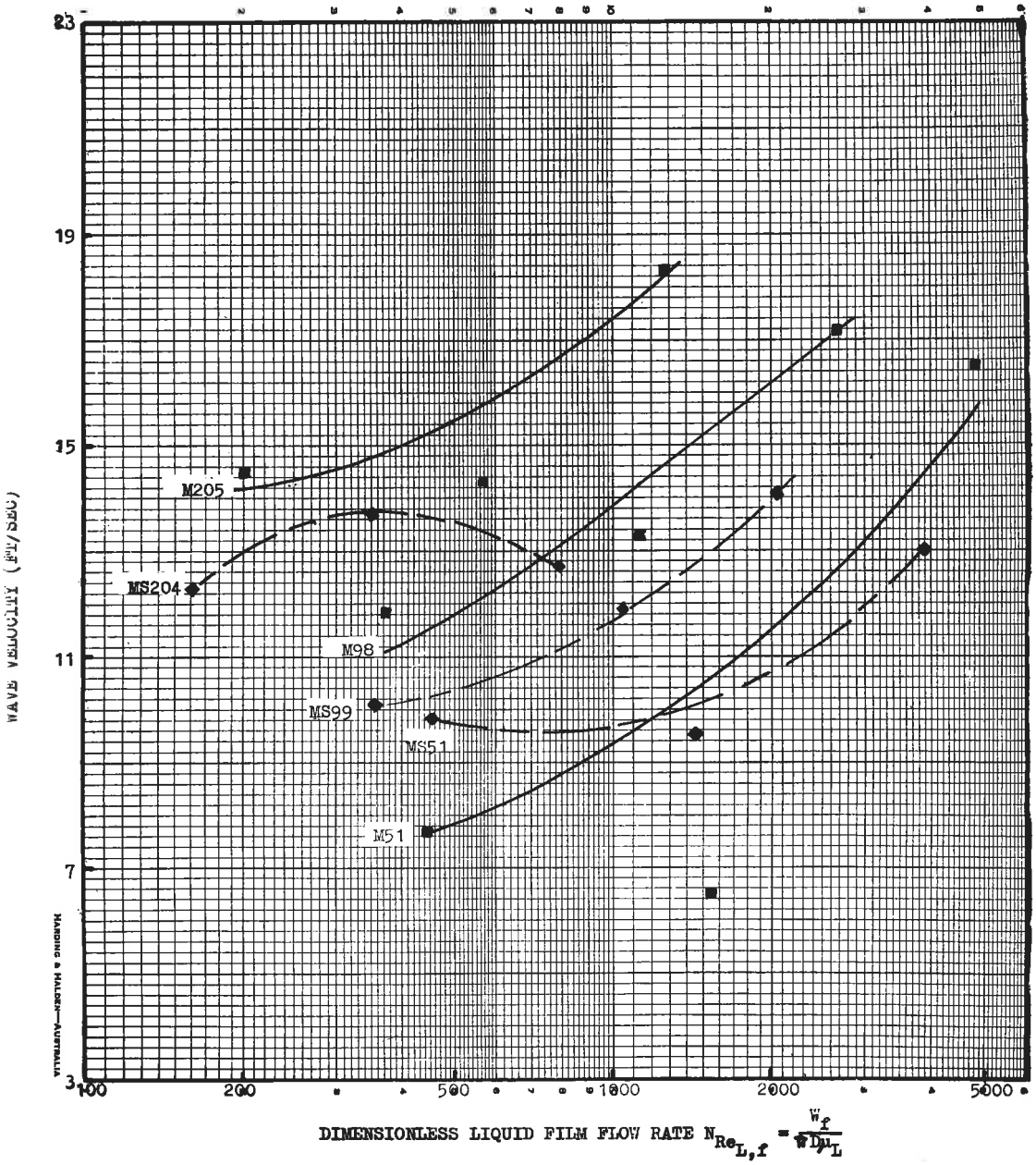
23
19
15
11
7
3
WAVE VELOCITY (FT/SEC)
M205
MS204
M98
MS99
MS51
M51
100
200
500
1000
2000
5000
DIMENSIONLESS LIQUID FILM FLOW RATE $N_{Re_{L,f}} = \frac{W_f}{\pi D \mu_L}$
HARDING & HALDEX—AUSTRALIA

Reynolds numbers to 0.25 - 0.35 at high liquid film Reynolds numbers.

5.3.4 A further examination of the relationship between the disturbance wave velocity and the average film velocity

In Section 4.6 it was shown that if the motion of a disturbance wave in a vertical tube was governed by continuity considerations only then:-

$$c - \bar{u}_L = \frac{u_L^*}{K} = \frac{1}{K}\sqrt{\frac{\tau_w}{\rho_L}} \quad \text{.....(4.32)}$$

$\bar{u}_L$ is the mean velocity of the liquid in the disturbance wave. If it is assumed that the whole of the film flow is associated with the disturbance waves then

$$\bar{u}_L = \frac{W_f}{\mathcal{A}\rho_L} \quad \text{.....(5.77)}$$

where W_f is the film flow rate and $\mathcal{A}$ is the gas core cross sectional area. Equations (4.24) and (4.25) can be rearranged to show that:-

$$u_L^* = \sqrt{\frac{\tau_w}{\rho_L}} = \sqrt{g\,R}\cdot\sqrt{\frac{h}{R} + \frac{R-h}{2R}\left(-\frac{dp}{dx}\right)_{fric}} \quad \text{.....(5.78)}$$

where $\left(-\frac{dp}{dx}\right)_{fric}$ is the frictional pressure gradient in feet of water per foot of tube.

Values of c, $\bar{u}_L$ and $\sqrt{\frac{\tau_w}{\rho_L}}$ are tabulated below for a number of the experimental runs. In the final column of the table the values of K, calculated by means of equation (4.32), are listed.

RUN	WATER FLOW RATE lb/hr	AIR SUPER-FICIAL VELO-CITY ft/sec	AIR DENSITY lb/ft^3	$\bar{u}_L$ ft./sec.	c ft/sec	$\sqrt{\frac{\tau_w}{\rho_L}}$ ft/sec	K
38	102	0	0.0718	1.86	4.25	0.15	0.06
6	301	0	0.0266	3.04	5.11	0.20	0.10
46	300	0	0.0724	3.16	5.26	0.20	0.09
148	299	0	0.2273	2.84	4.87	0.21	0.10
73	997	0	0.0693	5.26	7.87	0.28	0.11
20	1993	0	0.0266	7.40	9.89	0.33	0.13
104	2011	0	0.0691	6.96	9.77	0.35	0.13
136	3362	0	0.0689	8.53	11.00	0.41	0.17
149	300	20.1	0.2230	3.56	5.60	0.20	0.10
203	2002	20.5	0.2199	7.74	9.93	0.36	0.17
230	3516	20.6	0.2182	9.07	11.20	0.46	0.22
7	300	49.8	0.0281	3.39	5.82	0.20	0.08
21	2002	52.1	0.0262	8.15	10.65	0.31	0.12
119S	2702	50.7	0.0716	8.46	12.98	0.46	0.10
28	3496	52.2	0.0259	9.84	12.68	0.48	0.17
90S	995	92.5	0.0713	7.26	11.90	0.47	0.10
190S	1000	101.2	0.2190	8.79	14.17	0.59	0.11
217S	2000	102.4	0.2178	10.80	15.47	0.73	0.15
125S	2700	103.5	0.0723	7.20	14.07	0.54	0.08
226S	2001	163.6	0.2172	7.14	15.42	0.80	0.10

Table 5.2 REPRESENTATIVE VALUES OF c, $\bar{u}_L$, $u_L^* = \sqrt{\frac{\tau_w}{\rho_L}}$, and K.

An examination of Table 5.2 shows that K increases with increases in the liquid flow rate. K is apparently independent of changes in the gas velocity and density for a constant total liquid flow rate. K has a low order of accuracy because it is calculated from the difference between c and $\bar{u}_L$ both of which are subject to almost independent errors.

These results fail to verify equation (4.32). On the other hand they do not disprove it. $\bar{u}_L$ underestimates the mean velocity of the liquid in the disturbance wave as it includes the effect of the slower moving liquid film between the waves. This means that $c - \bar{u}_L$ is overestimated and K underestimated. This effect would be greatest at low liquid rates where there are few disturbance waves. It is at these low liquid rates that the smallest values of K were obtained.

5.3.5 Wave frequency measurements

In Figure 5.2 p.215 the mean time intervals between waves for the medium pressure series of runs at the bottom measurement level are plotted against the liquid film Reynolds number for those runs in which the droplet flow rate was measured. These are some of the runs in which the mean time intervals were plotted against the total liquid Reynolds number in Figure 4.6 (p.136). The curves are drawn so that they are equivalent to their parent curves in Figure 4.6.

LEGEND

MEAN SUPERFICIAL AIR VELOCITY AT 235 IN. LEVEL (FT/SEC)	MEAN AIR DENSITY AT 235 IN. LEVEL (LB/FT^3)	INJECTOR TYPE	TIME BETWEEN WAVES SYMBOL	TIME BETWEEN WAVES LINE DESIGNATED BY
50.7	0.0709	Porous Wall	■	M51
51.3	0.0718	Spray	◆	MS51
98.3	0.0715	Porous Wall	■	M98
98.7	0.0719	Spray	◆	MS99
204.8	0.0718	Porous Wall	■	M205
204.1	0.0711	Spray	◆	MS204

Figure 5.2 MEAN TIME BETWEEN WAVES VERSUS DIMENSIONLESS LIQUID FILM FLOW RATE, $N_{Re_{L,f}} = \frac{W_f}{\pi D \mu_L}$ MEDIUM PRESSURE SERIES AND 235 INCH LEVEL.

These curves are equivalent to those of figure 4.6 (p.136) for which film and core flow data were obtained.

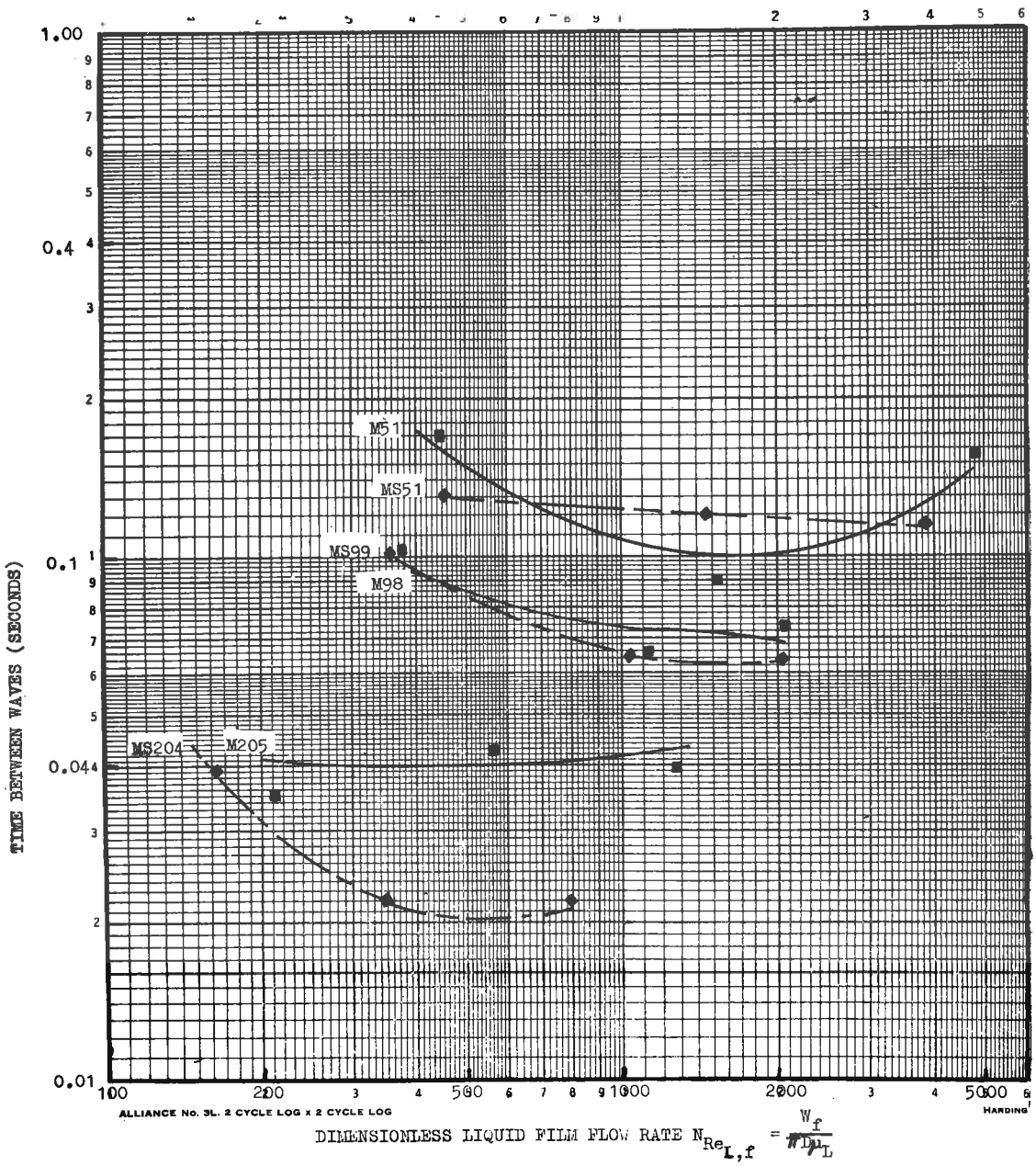
TIME BETWEEN WAVES (SECONDS)
1.00
0.4
0.1
0.044
0.01
M51
MS51
MS99
M98
MS204
M205
100
200
500
1000
2000
5000
ALLIANCE No. 3L. 2 CYCLE LOG x 2 CYCLE LOG
HARDING
DIMENSIONLESS LIQUID FILM FLOW RATE $N_{Re_{L,f}} = \frac{W_f}{\pi D \mu_L}$

The curves in Figure 5.2 are relatively flat with the exception of MS204. This is not surprising as they relate to the relatively flat central portion of the curves in Figure 4.6.

The change in the time interval between disturbance waves in going from the top to the centre measurement level was compared with the change predicted by the equation of Hall Taylor and Nedderman (1968). Their equation can be written in the form:-

$$\Delta t_C - \Delta t_T = \sqrt{\frac{8}{\pi}} \frac{\Sigma 1}{\bar{U}^2} \simeq \sqrt{\frac{8}{\pi}} \frac{\Sigma 1}{\bar{U}_T \bar{U}_C} \quad \ldots\ldots\ldots\ldots (5.79)$$

This equation was derived with the assumption that the disturbance wave mean velocity did not change in going from one measurement level to the other. In these experiments it changed, so it was necessary to use $\bar{U}_T\ \bar{U}_C$ instead of $\bar{U}^2$. In equation (5.79) Δt is the time interval between waves, Σ is the standard deviation of the disturbance wave velocities and 1 is the distance between measurement levels. T and C refer to the top and centre measurement levels respectively.

$\bar{U}_T$, $\bar{U}_C$, Δt_T, Δt_C and Σ were obtained from measurements on the ciné films. The use of measurements from two levels meant that the results from a pair of similar runs had to be used. As the individual measurements of Σ showed a wide scatter the value used in the calculation

was taken from the graph of wave velocity standard deviation versus mean wave velocity for a particular water flow rate. These graphs are Figures 4.4, 4.5 and A3.12 to A3.17 inclusive. A geometric mean of the values corresponding to $\bar{U}_T$ and $\bar{U}_C$ was used.

The predicted increases in the time interval are compared with the actual increases in Table 5.3. It can be seen that in all cases the prediction considerably overestimates the increase in the time interval. Hall Taylor and Nedderman (1968) had found that their results could be fitted by an artificial constant value, Σ = 0.67 ft/sec. The predicted increases in Table 5.3 were recalculated using Σ = 0.67 ft/sec. The values of Σ which had been obtained from the wave velocity standard deviation versus mean wave velocity graphs were mostly greater than 0.67 ft/sec. These new predictions still overestimated the change in time interval but the error was much smaller.

The evidence suggests that the wave velocity standard deviations obtained in this present work were too large. The values obtained were the combined effect of the inherent disturbance wave standard deviation and a fairly large measurement standard deviation.

At high gas velocities the disturbance waves stabilize rapidly. They quickly settle into a preferred

TYPE OF RUNS	RUNS	VELOCITY ft/sec		TIME INTERVAL milliseconds			
				PRED.	MEASURED VAL.		ACT.
		TOP	CENTRE	INCR.	TOP	CENTRE	INCR.
300 lb/hr	55,56	6.63	9.09	57	34	78	44
Water	59S,60S	6.28	8.36	63	38	87	49
Medium	63,64	10.93	12.65	33	15	39	24
Pressure	67S,68S	8.14	11.31	44	15	39	24
300 lb/hr	150,151	6.37	8.02	65	33	69	36
Water	154S,155S	6.13	6.54	76	43	94	51
High	157,158	10.66	11.73	36	19	37	18
Pressure	161S,162S	8.34	9.12	49	24	46	22
	164,165	14.45	15.45	24	10.9	23	12.1
	168S,170S	12.54	10.96	33	13.6	17	3.4
1000 lb/hr	76,77	6.84	8.84	69	43	86	43
Water	80S,81S	6.94	7.87	74	37	92	55
Medium	83,84	10.21	12.73	39	26	55	29
Pressure	88S,89S	9.50	12.29	42	26	45	19
	93,94	14.33	15.01	31	12.6	32	18.4
	98S,99S	11.52	14.74	32	18	26	8
1000 lb/hr	177,178	8.62	10.61	50	30	53	23
Water	181S,182S	7.28	9.00	65	28	50	22
High	184,185	13.20	14.66	29	18	31	13
Pressure	188S,189S	11.86	10.14	41	16	32	16
	192,193	16.74	17.83	22	11.4	12.7	0.7
	196S,197S	14.87	13.50	28	9.2	13.3	4.1
2700 lb/hr	113,114	9.82	12.02	47	64	82	18
Water	120,121	13.79	16.20	34	37	56	19
Medium	127,128	17.55	21.28	26	20	37	17
Pressure	130S,131S	15.14	16.13	32	15.6	27	11.4
2000 lb/hr	204,205	11.47	13.33	41	22	57	35
Water	208S,209S	13.12	12.06	36	15.7	49	33.3
High	211,212	15.28	17.72	26	19	35	16
Pressure	215S,216S	13.66	13.83	32	13.7	26	12.3
	219,220	20.68	20.23	20	12.6	13.1	0.5
	223S,224S	15.77	15.02	28	8.7	12.5	3.8

Table 5.3. COMPARISON OF THE ACTUAL INCREASE IN THE TIME INTERVAL BETWEEN WAVES IN GOING FROM THE 11 INCH TO THE 56 INCH LEVEL WITH THE INCREASE PREDICTED BY THE EQUATION OF HALL TAYLOR AND NEDDERMAN.

spacing and there is reduced coalescence. The analysis of Hall Taylor and Nedderman assumes that there is no preferred spacing and therefore is not applicable to these cases. Also at these high gas velocites the waves lose mass by droplet entrainment. This could lead to the formation of new waves from the deposited droplets.

These results suggest that the approach of Hall Taylor and Nedderman is a useful analysis of disturbance wave coalescence in the region near the injector. The main weakness of the analysis is the assumption that each wave has a constant velocity as it moves along the tube. The evidence shows that large waves move faster. Waves grow by coalescing and by gathering liquid from the film between the waves. They lose liquid by entrainment of droplets. The results tabulated in Table 5.3 show that most waves, particularly those in the runs at low gas velocity, increased in velocity between the top and centre measurement levels.

5.4 Accuracy of the Experimental Data

Because of its height the experimental apparatus had to be housed on the outside wall of the Chemical Engineering Department. The ambient temperature could not be controlled. Most of the runs were carried out with the test-section temperature in the range 30° C to 40° C (86° F -104° F). However, at low liquid rates on cool days

the test-section temperature was often below 30°C.

5.4.1 The controlled variables

The major problem with the controlled variables, that is the pressure, temperature and the air and water flow rates was to keep them constant over the hour or so needed to measure or record the experimental results.

(1) Air flow rate

Almost constant air flow rates could be maintained with very little difficulty for nearly all the air-water flow rates and air pressure combinations. The drift could be held to better than ± 3% at high gas rates and ± 5% at low gas rates.

In addition a systematic error was possible because the gas flow meters were uncalibrated. This was about ± 2% at high gas flow rates and ± 4% at low gas flow rates. The gas mass flow rate depends on the square root of the gas density for a constant rotameter reading. The errors due to inaccuracies in pressure measurements at the rotameters could have made an additional error in the flow rate of ½%, 1% and 2% at 45 psia, 15 psia and 5½ psia respectively.

(2) Water flow rate

At medium flow rates (1000 lb/hr) the flow could be kept steady with little difficulty. At low flow rates the flow rate tended to drift lower. This was

because the liquid feed pump output had to be throttled even while it was being operated at its minimum speed. At very high flow rates the flow rates tended to drift lower also. At very high flow rates there was a high pressure drop across the porous wall injector. The injector tended to clog with rust and increse the pressure drop still further. The likely drift errors were ± 3% at medium flow rates and -9% to + 3% at high and low flow rates.

As the rotameters were calibrated there were no systematic errors. An air chamber together with the filter press (c.f. Figure 3.1, p. 81) practically eliminated any flow fluctuations caused by the gear pump.

(3) Temperature

Temperature variations were minimized by waiting for stable temperature conditions before starting a run.

(4) Pressure

The pressure control method maintained stable pressures under almost all operating conditions (c.f. p. 95 and 96). Fluctuations in density due to the pressure control method probably did not exceed ± 2%, ± 1% or ± ½% at 5½, 15 and 45 psia test-section pressure respectively.

5.4.2 The measured variables

(1) Pressure gradient

An estimate of the errors can be made from the data obtained. These data show that at pressure gradients

up to about 0.100 ft water/ft tube large errors (± 25% or more) were possible. These errors were caused by the presence of air bubbles in the manometer lines. The errors were independent of the pressure gradient. At high pressure gradients, such as 1.0 ft water/ft tube, the likely error was about ± 5%.

(2) Liquid volume fraction

The hold-up cocks could be shut simultaneously in the same direction of rotation in about one quarter of a second. The distance between the cocks was 9 feet. At a liquid velocity of 10 ft/sec, 2½ feet of liquid could move into and out of the test-section as the hold-up cocks were shut. It was hoped that the cocks were still able to take a representative sample of the flowing liquid.

The scatter of repeated measurements of the liquid hold-up at the same flow conditions was about ± 0.1 inch for liquid volume fractions up to 0.05 and ± 0.2 inch for liquid volume fractions greater than 0.05. This means that the likely relative measurement errors of the samples taken ranged from ± 50% at a liquid volume fraction of 0.002 to ± 2% at a liquid volume fraction of 0.10.

(3) Core flow measurements and liquid film flow rate measurements

The core flow measurements were most accurate at moderate droplet flow rates. At low droplet flow

rates only a very small sample could be obtained in a reasonable time. At high droplet flow rates the sample receiver was filled in about 30 seconds. This meant that the timing errors were appreciable. Overall the errors in droplet flow rate measurements were probably about ± 5% at moderate droplet flow rates and ± 10% at high or low droplet flow rates.

The probe could be accurately traversed across the tube but it was difficult to ensure it was pointing straight up the tube. The effect of any small angle of tilt of the probe on the effective sampling area is negligible as this area varies as the cosine of the angle of tilt. The effect of tilt on the difference between the true and the apparent distances of the probe from the tube axis is largest when the probe is near the tube axis. Fortunately, in this region the droplet mass velocity profile is fairly flat. Therefore, small angles of tilt should not significantly affect the accuracy of the droplet mass velocity profile.

A comparison of the sum of the integrated core flow rate and the film flow rate with the total liquid flow rate has already been made in Section 4.8.2 (p.149)

(4) Variables obtained from measurements on the ciné films

The Vinten camera used was powered by a D.C. motor. The D.C. was rectified from the A.C. mains supply.

The camera speed depended on the amounts of film on the feed and take up spools and on the actual short term A.C. voltage. The framing rate was calculated by counting the timing marks on the film edge. These marks were at $\frac{1}{100}$ second time intervals. The mean framing rates of all the high speed runs ranged from about 0.0036 second to 0.0044 second.

After deducting the portions of the film exposed while the camera drive was accelerating or decelerating about 6-12 feet (240-480 frames) of usable film was obtained for most runs. This length of film would have about 100-200 timing marks. These marks were sometimes difficult to see and could be inadvertently omitted when they were being counted. Even so the likely accuracy of the framing rate is better than $\pm$ 1%.

The camera field of view covered a 9 inch length of the test-section. The waves were photographed against a strongly illuminated white card. Because their disturbed surface scattered some of the incident light the waves appeared as dark bands against a light background. In the ciné films any particular wave could be seen in about 8-20 successive frames depending on the wave velocity and the camera framing rate. The distance a wave moved in a particular number of frames was obtained from the scale photographed with the waves. Each wave position was measured to the nearest $\frac{1}{8}$ inch in frames in which

it appeared near the top and near the bottom of the ciné photographs respectively. Thus the likely error in distance was ± ½ inch in about 8 inches, or ± 6%.

Combining this distance error with the time error gave a likely error in velocity of ± 7%. However, this was for optimum conditions. It required that the visible appearance of the wave did not alter. It required that the disturbed part of the wave should be relatively short so that it could be accurately located. Such conditions were satisfied at low to moderate water rates and air velocities up to 50 ft/sec. The disturbed parts of the waves were fairly short and each wave was separated from the next by a section of smooth liquid film.

If the disturbance waves all moved at the same velocity then the mean velocity could be obtained with a quite high degree of accuracy by averaging the measured velocities of a large number of waves. However, the wave velocities were intrinsically variable. The waves which appeared longer and more disturbed and which apparently were larger had higher velocities than the smaller looking waves. Another difficulty was to decide if two waves which were close together should be considered to be one or two waves. Overall, the mean wave velocity could probably be determined to an accuracy about ± 10% under optimum conditions.

At the top photographic level the waves were not properly developed and were difficult to see. At high liquid flow rates and or high gas velocities nearly the whole surface appeared to be covered with waves. It was very difficult to separate one wave from the next. The errors in velocity measurements may have been ± 25% under any of these conditions.

In wave frequency measurements the key problem was to set a consistent criterion for separating a given disturbance wave from smaller waves which could be subsidiary parts of the main disturbance wave. The mean wave frequency is probably only accurate to ± 15% under optimum conditions. Under poor conditions, such as when there are high liquid flow rates and at the top measurement level the error could be as high as ± 50%.

5.5. Suggestions for future work

In the region of gas velocities which are of most interest the mechanisms of the formation of droplet entrainment apparently depend on the nature of disturbance waves.

In order to understand such mechanisms a detailed knowledge of the velocity profiles of the liquid in a disturbance wave and the gas immediately adjacent to it is required. These profiles determine and are determined by the way energy is transferred from the gas to the liquid

film. Although the gas velocity profile is logarithmic it is very much steeper than the equivalent single phase flow profile. Therefore it would be reasonable to expect unusual behaviour near the gas-liquid interface.

A careful examination of disturbance wave crests is needed to determine how droplets are formed. A single mechanism could well be inadequate to explain how such a wide range, 25 microns to over 300 microns in some cases, of droplets could be formed.

It is likely that the major gas physical property variable is its density. If this is so there is little point in using gases other than air except to attain high densities at moderate pressures. For the liquid phase the major physical property variables are probably the density, the surface tension (actually a liquid-gas physical property variable) and the viscosity.

Suitable equipment is needed to measure gas and liquid velocity profiles. These measurements are needed in flows which are generating droplet entrainment if possible.

6. CONCLUSIONS

1. The droplet mass velocity profile in the gas core of a two phase downwards flow with droplet entrainment is similar to that of a two phase upwards flow with droplet entrainment. Far from the injector the profile has a maximum at the tube axis.

2. The equilibrium droplet flow rate is approached slowly. At the sampling level 245 inches (184 diameters) downstream from the injector equilibrium was attained in runs at 50 ft/sec air velocity but not at higher air velocities when the water was injected with a porous wall injector. When a spray injector was used equilibrium entrainment may have been attained at the higher air velocities as well as at an air velocity of 50 ft/sec.

3. The spray injector was more prone to produce asymmetrical droplet mass velocity profiles than the porous wall injector. Both injectors produced asymmetrical profiles at high gas velocities. This indicated the need for careful alignment of a test-section to obtain symmetrical profiles.

4. The plotting of the experimental pressure gradients against a "reduced" velocity proved useful. The "reduced" velocity was based on the mean velocity of a hypothetical homogeneous two phase flow with a gas density of 0.0712 lb/ft^3 which flowed at the same gas and liquid mass flow rates as the actual two phase flow. At very high air velocities, in excess of 300 ft/sec at

an air density of 0.0712 lb/ft^3, the frictional pressure gradient approaches the homogeneous value. Due allowance had to be made for accelerational effects at these velocites. This approach to the homogeneous value probably occurred because the liquid film on the wall was negligible.

5. At moderate gas velocities, 50-200 ft/sec at a density of 0.0712 lb/ft^3, the pressure gradient of the two phase flow was up to twice the value it would have been if it was a fully homogeneous flow.

6. The use of reduced velocity permitted pressure gradients from flows at different gas densities to be compared.

7. Injection of the water with a spray injector resulted in slightly lower pressure gradients than if a porous wall injector had been used in most cases. This was in agreement with the results of other workers for upwards flow. It was caused by the lower liquid film flow rates because of the increased droplet flow rates.

8. The liquid film thicknesses at low gas velocities where there was no entrainment were 10-15% less than predicted by Dukler's analysis. These measurements were made at a mean distance of 15 feet downstream from the liquid injector. This difference probably arose because Dukler's analysis was based on a smooth film whereas the flow actually consisted of fully developed disturbance waves.

The flow rate versus mean film thickness relationship could be described by an integrated logarithmic velocity profile.

9. The disturbance wave velocity increased with increases in the water flow rate, the air velocity or the air density. It ranged from 4 ft/sec at a water flow rate of 100 lb/hr in the 1.330 inch diameter test-section with no air flow to 23 ft/sec at a water rate of 3500 lb/hr, at an air velocity of 300 ft/sec and an air density of 0.072 lb/ft^3.

10. At a fixed air flow rate the time intervals between disturbance waves decreased with increasing water flow rate at low water flow rates, but were almost independent of changes in the water flow rate at high water flow rates. The actual changes in the mean time intervals between disturbance waves at the 11 inch and the 56 inch photographic levels were compared with the changes predicted by the theory of Hall Taylor and Nedderman (1968). To apply the theory it was necessary to use experimental values of the wave velocity standard deviations. There was general agreement with the trend of their theory, but the predicted changes always exceeded the actual changes. It is considered that the velocity standard deviations obtained in this work were too large, for if the velocity standard deviation used by Hall Taylor and Nedderman (1968) was used reasonable

agreement was obtained.

11. A theory for the formation of droplets from the break up of ripples on the crests of disturbance waves was developed. This theory was able to predict the observed range of wavelengths of the ripples. The theory was able to indicate that the very large droplets have higher radial velocites than the smaller droplets which comprise the major part of the droplet mass.

7. NOMENCLATURE

a	amplitude
A	constant in logarithmic velocity profile, equations (2.56) and (4.10), ft/sec
A'	constant in modified logarithmic velocity profile, equation (4.21), ft/sec
A_1	constant in equation (2.74), ft^{-2}, in^{-2} or $micron^{-2}$
$\mathcal{A}$	core area of cross section, ft^2
b	deposition coefficient, dimensionless
B	exponential wave growth factor, sec^{-1}
c	wave or ripple velocity, ft/sec
C	concentration, lb/ft^3
C_1, C_2	constants in equation (2.61), dimensionless
C_4	constant in equation (4.33), dimensionless
C_5	constant in equation (4.33), ft/sec
d	droplet diameter, ft
D	tube diameter, ft
$\mathcal{D}$	stopping distance, ft or in
e	equivalent sand roughness, ft
E	fractional entrainment, that is the fraction of the total liquid flow which is carried as droplets in the gas core, dimensionless
$\mathcal{E}$	$\ln \frac{\text{wave amplitude at break-up point}}{\text{wave amplitude at orifice}}$, dimensionless. This refers to the break-up of the thin liquid sheet coming out of a spray nozzle.
f	friction factor, dimensionless

F	frequency, sec^{-1}
g	acceleration due to gravity, ft/sec^2
G	mass velocity, lb/ft^2, hr
h	film thickness, ft or in
k	mass transfer coefficient, ft^3/ft^2, hr or ft^3/ft^2, sec
K_1	constant in equations (2.21) and (4.16), dimensionless
K_2	constant in equation (2.42), ft^2
l	distance in the flow direction, ft
m	Integer
M	mass transfer rate normal to the flow direction, lb/ft^2, hr
n	constant in Deissler equation, equation (2.22), dimensionless
N	wave number, number of waves in a distance 2π, ft^{-1} or in^{-1}
p	pressure, lb/ft^2 or lb/in^2
PB	pressure at bottom of test-section, lb/ft^2 or lb/in^2
PT	pressure at top of test-section, lb/ft^2 or lb/in^2
ΔPB	pressure gradient at bottom of test-section, lb/ft^2 or lb/in^2
Δ PT	pressure gradient at top of test-section, lb/ft^2 or lb/in^2
Q	volume flow rate per unit width of wall, ft^3/ft, hr
r	radial co-ordinate, ft

R	tube radius, ft
s	Dukler's term, the cube root of the net weight of the liquid film divided by the wall shear stress, i.e. $\left[\frac{(\rho_L-\rho_c)gh}{\tau_w}\right]^{\frac{1}{3}}$, dimensionless
t	time, sec
t_{gr}	the lifetime of a ripple, it is the time it takes to be carried up the "active length" of a disturbance wave, sec
Δt	time interval, sec
T	ratio $\frac{\text{wall shear stress}}{\text{net weight of liquid film}}$, $\left(\frac{\tau_w}{(\rho_L-\rho_c)gh}\right)$, dimensionless
TE	temperature
u	velocity in the flow direction, ft/sec
u'	fluctuating component of the velocity in the flow direction, ft/sec
u^*	friction velocity, $\sqrt{\frac{\tau_w}{\rho_L}}$ (liquid); $\sqrt{\frac{\tau_i}{\rho_c}}$ or $\sqrt{\frac{\tau_i}{\rho_G}}$ (gas), ft/sec
u^+	dimensionless velocity defined as, $\frac{u}{u^*}$
U	disturbance wave velocity, ft/sec
v	velocity normal to both the flow direction and the wall, ft/sec
v'	fluctuating component of the velocity normal to both the flow direction and the wall, ft/sec
V	volumetric flow rate, ft^3/hr
W	mass flow rate, lb/hr

x co-ordinate in the flow direction, ft

X Martinelli - Lockhart parameter, defined by X^2 = pressure gradient of liquid flowing alone at the same flow rate as in the two phase flow / pressure gradient of gas flowing alone at the same flow rate as it had in the two phase flow, dimensionless

y co-ordinate normal to the wall, ft

y^+ dimensionless distance defined as, $\frac{y u^* \rho_L}{\mu_L}$

z ratio of the momentum of two groups of droplets, dimensionless

Z (Appendix 5) an angle such that $Z = 2\arccos \frac{\overline{OR}}{2\overline{UN}}$,

α gas volume fraction, dimensionless

β dimensionless shear stress defined as $\frac{\tau_i}{\left[\rho_L g^2 \mu_L^2\right]^{\frac{1}{3}}}$

γ droplet volume fraction in the core, dimensionless

Γ coefficient defined by equation (2.46), units are reciprocal of pressure gradient, either dimensionless or $ft^2 sec^2/lb$

ϵ eddy diffusivity, ft^2/hr

η value of y^+ at the interface $\eta = \frac{h u^* \rho_L}{\mu_L}$, dimensionless

θ angle of inclination of the flow section in the flow direction below the horizontal, dimensionless

κ constant in von Kármán equation, equation (2.23), and in integrated forms of this equation, dimensionless

λ wavelength, ft or in

μ viscosity, lb/ft, hr

ν kinematic viscosity, ft^2/hr

ρ density, lb/ft^3

Σ standard deviation, used for velocity, time interval or distance

σ liquid-core interfacial (surface) tension, lb/sec^2 or dyne/cm

τ shear stress, lb/ft, sec^2

ϕ Martinelli - Lockhart parameter defined by

$$\phi^2 = \frac{\text{two phase pressure gradient}}{\text{pressure gradient of one of the phases flowing alone at the same flow rate as it had in the two phase flow}}$$

dimensionless

ψ parameter defined by $\psi_G^2 = \frac{\text{Droplet transport rate in two phase flow}}{\text{Mass transfer rate in a single phase flow}}$

Ω dimensionless coefficient in equation (2.74), the ratio of the droplet diameter to the difference between the maximum stable droplet diameter and the droplet diameter

ω also ω', ω'' angle between the directions of motion of two droplets

Dimensionless numbers

N_{Re_G} gas Reynolds number, defined as $\frac{D\,\bar{u}_{Gs}\,\rho_G}{\mu_G}$

N_{Re_L} liquid Reynolds number, defined as $\frac{Q_L\,\rho_L}{\mu_L}$

N_T Dukler's term, Nusselt film thickness

$$h\left[\frac{g\,\rho_L^2}{\mu_L^2}\right]^{\frac{1}{3}}\left[\frac{\rho_L - \rho_c}{\rho_L}\right]^{\frac{1}{3}}$$

N_{Vi} viscosity number, $\frac{\mu_L}{\sqrt{\rho_L \sigma d}}$

N_{We_d} droplet Weber number $\frac{\rho_G u_G^2 d}{\sigma}$

N_{We_L} liquid Weber number $\frac{\rho_L \bar{u}_L^2 h}{\sigma}$

Subscripts

a	atomization
acc	accelerational
actual	actual
ax	axial
br	break-up
C	centre measurement level
c	core
crit	critical
d	droplet; droplet deposition
f	film
form	form
fric	frictional
G	gas
gr	growth
grav	gravitational
H	thermal
i	interface
in	interchange
inj	injector

L	liquid
LT	total liquid
M	mass
m	mean
max	maximum
min	minimum
mw	moving wall
net	net
o	initial condition
opt	optimum
p	probe
rad	radial
ref	reference
rel	relative
s	superficial
T	top measurement level
tang	tangential
tot	total
tr	transfer
vis	viscous
w	wall

Superscript

-	mean value of

APPENDIX 1.

TABULATION OF EXPERIMENTAL RESULTS

Runs 1 to 30 are the low pressure series, runs 31 to 142 the medium pressure series and runs 143 to 233 the high pressure series. The runs are not numbered chronologically.

Meaning of abbreviations

RUN Run. If there is the letter S after the run number then the spray injector was used, if not, the porous wall injector was used.

CAM Camera location. The letter T means that ciné photographs were taken at the 10.9 inch level, C means that they were taken at the 55.8 inch level and B means they were taken at the 235.1 inch level.

SAMP Sampling probe location. The letter T means that samples were taken at the 15.9 inch level, C means that they were taken at the 60.8 inch level and B means that they were taken at the 244.8 inch level.

LIQ Water flow rate (lb/hr).

GAS Air flow rate (lb/hr). The air was assumed to be saturated with water vapour. The mass flow is that of the air-water vapour mixture.

TEMP Temperature (^{o}C) at the bottom of the test section, 256.8 inch below the injector.

PT Absolute pressure at the 2.9 inch level (psia).

PB Absolute pressure at the 245.2 inch level (psia). For runs 31-37 which are marked * PB was measured at the 188.6 inch level.

ΔPT Differential pressure (feet of water / foot of tube) between the 2.9 and 61.4 inch levels.

ΔPB Differential pressure (feet of water / foot of tube) between the 188.6 and 245.2 inch levels.

VOID The average liquid volume fraction in the interval 131.5 inches to 240.9 inches below the injector.

FT The measured film flow rate (lb/hr) at the 66.9 inch level.

FB The measured film flow rate (lb/hr) at the 250.5 inch level.

LIQ to FB inclusive comprise the experimentally measured flow parameters. Under the heading "DRVD" (derived) are listed the derived flow parameters calculated from these. These derived parameters are:-

P11 The value of the top absolute pressure when adjusted to the 11 inch level.

Δ11 The point value of the top differential pressure when adjusted to the 11 inch level.

VRT The calculated homogeneous velocity at the 11 inch level.

P235 The value of the bottom absolute pressure when adjusted to the 235 inch level.

Δ235 The point value of the bottom differential pressure when adjusted to the 235 inch level.

DEN The density (lb/ft^3) at the 235 inch level calculated from P235 and the temperature at the bottom of the test section which was assumed to be the same as the temperature at the 235 inch level.

VS The air superficial velocity (ft/sec) at the 235 inch level calculated from the air flow rate and density at the 235 inch level and the tube cross-sectional area.

VHB The calculated homogeneous velocity at the 235 inch level.

NREL The calculated liquid film Reynolds number, assuming that all the liquid flowed in the film. The equation used was $NREL = \frac{W_L}{\pi D \mu_L}$, the values of the liquid viscosity μ_L were taken from the table given in Appendix 2.

These symbols (RUN to NREL) are listed down the left hand edge of each page. The relevant values are listed in the column under the run number.

In the columns headed "WAVES" are listed the wave velocities, and the time intervals between waves,

obtained from frame-by-frame measurements of the cine film sequence. The figures under "VEL" are the wave velocities in ft/sec, and those under "TIME" are the time intervals between successive waves in milliseconds. The arithmetic mean ("MEAN") and the root mean square deviation ("DEV") of both the wave velocities and the time intervals are listed as well.

In the column "CORE SAMPLE" the sampling probe positions (inches from the far wall) and the water flow rates (lb/hr through the probe mouth), are listed. At the bottom of this column under the headings "CALC TOTAL" and "EDGE" are listed the integrated liquid flow rates in the core (lb/hr) and the corresponding estimated distances from the wall (in.) of the edges of the core regions.

RUN	1	WAVES	2	WAVES	3	WAVES	4	WAVES
CAN	B	VEL	B	VEL	B	VEL	B	VEL
SAMP	-	4.4	-	5.9	-	6.4	-	9.2
		3.5		5.5		6.0		9.7
LIQ	99.3	5.3	99.6	4.7	99.1	6.2	98.7	8.6
		4.2		4.6		6.4		8.6
GAS	0	3.5	47.4		97.3		189	8.7
		4.3		MEAN		MEAN		8.7
TEMP	27.5	5.0	20.9	5.17	18.9	6.25	17.4	7.7
		4.1		DEV		DEV		
PT	5.34	3.8	5.52	0.54	6.31	0.17	6.32	MEAN
		4.3						8.74
PB	5.49		5.44	TIME	6.12	TIME	5.91	DEV
		MEAN						0.57
ΔPT	0	4.24	0.017	418	0.012	418	0.028	
		DEV		995		152		TIME
ΔPB	0.005	0.55	0.024	418	0.009	418	0.067	
				896		620		
VOID	.027	TIME	.026	895	.021		.014	254
						MEAN		91
PT		609		MEAN		402		210
		504		724		DEV		183
PB		441		DEV		166		167
		1407		253				167
DRVD		735						191
		546						60
P11	5.34	441	5.52		6.31		6.31	
		357						MEAN
Δ11	0	504	0.017		0.012		0.028	165
		882						DEV
VRT	1.1	378	53.9		83.8		142.1	59
P235	5.49	MEAN	5.45		6.12		5.93	
		619						
Δ235	0.005	DEV	0.024		0.009		0.067	
		290						
DEN	.0266		.0273		.0310		.0303	
VS	0		50.0		90.4		179.6	
VRB	1.1		54.2		85.1		146.5	
HRML	140.1		120.6		114.3		109.7	

RUN	5	WAVES	6	WAVES	7	WAVES	8	WAVES
GAS	B	VEL	B	VEL	B	VEL	B	VEL
BARP	-	15.4	-	5.1	-	6.4	-	7.9
		15.0		5.0		5.5		8.1
LIQ	98.6	14.5	301	5.5	300	5.6	301	7.6
		15.0		4.8		4.7		8.6
GAS	348	15.0	0	5.6	48.6	6.0	94.5	8.7
		14.2		5.1		5.5		9.0
TEMP	18.9	12.8	31.9	4.7	26.2	5.6	26.0	7.9
				4.8		6.0		
PT	7.92	MEAN	5.91	5.6	5.66	5.8	6.37	MEAN
		14.56		4.8		5.8		8.26
PB	5.77	DEV	5.62	5.3	5.77	6.2	5.71	DEV
		0.80		4.7		6.4		0.47
ΔPT	0.196		0.011		0.001	6.2	0.049	
		TIME		MEAN				TIME
ΔPB	0.235		0	5.11	0.005	MEAN	0.039	
		106		DEV		5.82		113
VOID	.0027	252	.046	0.33	.041	DEV	.035	56
		223				0.45		106
PT		166		TIME				213
		207				TIME		187
PB		138		367				231
		138		194		266		186
DRVD				497		421		156
		MEAN		238		155		
P11	7.86	176	5.91	346	5.66	111	6.36	MEAN
		DEV		389		311		156
Δ11	0.192	49	0.011	216	0.001	311	0.049	DEV
				410		244		56
VRT	215.7		3.3	281	82.0	289	116.3	
				324		422		
P235	5.86		5.62	280	5.77	133	5.72	
						488		
Δ235	0.241		0	MEAN	0.005	178	0.039	
				322				
DEN	.0297		.0266	DEV	.0281	MEAN	.0279	
				87		277		
VS	337.4		0		49.8	DEV	97.5	
						117		
VRB	251.7		3.3		81.2		123.1	
NREL	113.7		467		411		411	

RUN	9	WAVES	10	WAVES		11	WAVES
CAM	B	VEL	B	VEL	TIME	B	VEL
SAMP	-	11.3	-	15.1	42	-	10.0
		11.7		14.6	33		10.0
LIQ	301	10.6	301	15.1	37	594	9.4
		11.0		13.4	33		8.9
GAS	193	11.3	353	14.2	41	99.7	10.0
		10.0		12.6	25		10.4
TEMP	22.9	11.5	19.8	13.1	17	30.0	10.0
		10.6		14.2	54		10.7
PT	6.84	11.3	8.78	14.2	21	6.16	9.7
		12.5		15.1	50		
PB	5.43		5.27	12.6	33	5.42	MEAN
		MEAN		15.1	66		9.90
ΔPT	0.169	11.18	0.255	15.1	33	0.064	DEV
		DEV		14.7	50		0.50
ΔPB	0.199	0.65	0.457	15.1	33	0.089	
				15.5	66		TIME
VOID	.017	TIME	.005	12.6	42	.045	167
		92		13.5	25		71
PT		96		13.8	29		90
		100		14.2	37		84
PB		142			37		103
		29		MEAN	25		129
DRVD		117		14.19	25		45
		96		DEV	MEAN		109
P11	6.79	71	8.71	0.93	37	6.14	174
		125			DEV		90
Δ11	0.166	46	0.249		13	0.063	MEAN
		154					106
VRT	180.1	MEAN	246.2			160.6	DEV
		97					38
P235	5.51	DEV	5.45			5.45	
		36					
Δ235	0.204		0.481			0.089	
DEN	.0273		.0274			.0260	
VS	203.5		370.9			110.4	
VRB	201.8		316.6			171.2	
NREL	382		356			885	

RUN	12	WAVES		13	WAVES	14	WAVES	
CAM	B	VEL	TIME	B	VEL	B	VEL	TIME
SAMP	-	14.6	50	-	6.6	-	6.4	100
		14.0	33		6.0		9.1	94
LIQ	596	12.4	58	998	6.5	996	8.8	200
		13.4	29		7.0		7.8	154
GAS	203	10.7	25	0	7.3	49.0	7.9	181
		12.6	54		8.7		9.6	147
TEMP	26.9	10.3	58	34.0	7.9	31.8	5.0	174
		11.8	50		8.2		5.3	74
PT	7.55	13.8	29	5.75	8.7	5.72	7.6	80
		10.0	25		7.9		8.2	153
PB	5.23	12.0	54	5.77	8.1	5.65	9.1	94
		12.4	79		7.0		9.1	174
ΔPT	0.221	11.8	79	0	8.2	0.007	8.2	228
		12.2	75				6.9	274
ΔPB	0.261	11.0	33	0	MEAN	0.014	8.2	114
		12.2	79		7.5		8.2	167
VOID	.022	10.0	62	.088	DEV	.079	10.6	147
			41		0.84		6.2	261
FT		MEAN	29				8.2	181
		12.07			TIME			127
PB		DEV	MEAN				MEAN	
		1.33	49		143		7.92	MEAN
DRVD			DEV		167		DEV	156
			19		143		1.40	DEV
P11	7.49			5.75	190	5.72		55
					357			
Δ11	0.216			0	286	0.007		
					333			
VRT	223.1			11.1	190	139.6		
					238			
P235	5.33			5.77	143	5.66		
					167			
Δ235	0.269			0	357	0.014		
					95			
DEN	.0259			.0270	190	.0268		
VS	225.7			0	MEAN	52.6		
					214			
VRS	267.2			11.1	DEV	140.4		
					83			
NREL	830			1617		1541		

RUN	15	WAVES		16	WAVES		17	WAVES	
GAS	B	VEL	TIME	B	VEL	TIME	B	VEL	TIME
NAME	-	11.6	116	-	14.7	66	-	18.7	16
		12.6	153		16.0	39		16.9	36
LIQ	1000	11.6	98	999	14.7	55	1000	13.0	32
		11.3	73		12.9	63		14.1	16
GAS	97.3	11.3	110	204	13.9	62	296	16.3	36
		13.7	134		16.0	31		16.9	30
TEMP	29.9	11.3	159	27.2	10.7	31	26.3	12.3	20
		10.0	92		13.3	43		16.9	28
PT	6.59	10.3	85	8.81	13.9	74	10.03	11.4	12
		10.3	86		12.9	55		13.8	32
PB	5.66	10.3	92	5.48	16.0	35	4.92	14.9	40
		11.3	79		13.7	66		14.9	20
ΔP2	0.112	11.8	128	0.360	12.0	82	0.507	14.1	32
		11.6	128		16.9	63		13.0	32
ΔPB	0.138	11.0	116	0.463	12.8	39	0.721	16.8	32
			134		13.1	39		12.8	24
VOID	.059	MEAN		.052	14.7	39	.021	16.3	28
		11.33	MEAN		13.5	39		14.9	20
FT		DEV	111			70		16.3	36
		0.92	DEV		MEAN	55		13.4	36
FB			26		13.96			12.8	16
					DEV	MEAN		14.5	40
DRVD					1.49	52		13.8	40
						DEV		13.2	20
P11	6.56			8.71		15	9.89	17.9	40
								13.4	40
Δ11	0.111			0.348			0.487	17.4	40
VR1	189.9			249.4			292.9	MEAN	MEAN
								14.84	29
P235	5.71			5.66			5.22	DEV	DEV
								1.90	8.8
Δ235	0.140			0.487			0.782		
MEN	.0273			.0275			.0254		
VB	102.6			213.6			335.5		
VRB	204.3			314.5			413.8		
MEAN	1486			1400			1373		

RUN	18	WAVES		19	WAVES		20	WAVES	
C.J.	B	VEL	TIME	B	VEL	TIME	B	VEL	TIME
SAMP	-	9.2	99	-	18.7	32	-	11.3	305
		12.1	37		17.2	63		9.6	304
LIQ	1507	13.4	118	1506	17.4	48	1993	9.6	325
		14.3	124		12.0	47		11.5	305
GAS	98.7	9.1	62	202	17.9	63	0	8.6	203
		13.4	68		16.3	32		10.3	183
TEMP	31.1	13.8	99	29.1	16.8	75	34.0	8.6	122
		13.4	124		15.3	59		9.9	183
PT	6.88	13.0	87	9.10	17.5	40	5.67	8.9	203
		12.7	124		12.5	63		8.6	305
PB	5.44	14.3	99	5.29	17.9	55	5.70	10.6	223
		13.4	161		16.7	32		9.6	345
ΔPT	0.151	11.9	93	0.435	13.8	67	0.005	11.3	183
		13.0	87		16.3	87		9.6	183
ΔPB	0.201	13.4	111	0.589	16.2	28	0	11.3	284
		13.0	93		15.8	28		9.9	223
VOID	.068	14.4	93	.041	13.5	59	.125	10.9	162
					13.8	48		10.9	162
FT		MEAN	MEAN			36		9.2	162
		12.81	99		MEAN	40		9.2	204
FB		DEV	DEV		15.87			8.6	102
		1.49	27		DEV	MEAN		10.6	284
DRVD					1.91	50		8.9	101
						DEV		10.3	304
F11	6.84			8.99		16.6	5.67	8.6	142
								8.9	183
Δ11	0.148			0.419			0.005	11.3	223
								10.3	203
VRT	224.6			289.2			22.1		
								MEAN	MEAN
F235	5.52			5.53			5.70	9.89	220
								DEV	DEV
Δ235	0.206			0.628			0	0.98	69
DEN	.0262			.0266			.0266		
VS	108.5			218.7			0		
VRB	251.8			375.5			22.1		
NREL	2298			2200			3228		

RUN	21	WAVES	22	WAVES		23	WAVES	
CAM	B	VEL	B	VEL	TIME	B	VEL	TIME
LAMP	-	11.4	-	15.9	98	-	16.9	53
		10.3		15.9	122		18.3	15
LIQ	2002	10.7	2002	13.6	61	1998	16.5	38
		10.7		14.6	116		19.2	103
GAS	47.4	9.7	95.8	10.9	98	186	17.5	110
		10.7		14.1	37		14.3	80
TEMP	34.8	10.3	32.6	13.6	92	29.9	15.9	42
		11.4		12.9	80		16.0	23
PT	5.89		6.75	13.2	55	9.25	14.6	76
		MEAN		15.6	98		16.5	19
PB	5.60	10.65	5.28	13.6	110	4.94	15.5	57
		DEV		16.5	165		18.1	61
ΔPT	0.034	0.53	0.187	14.5	86	0.425	12.9	80
				15.6	165		15.1	61
ΔPB	0.071	TIME	0.247	13.6	98	0.691	15.9	68
							16.0	46
VOID	.114	103	.081	MEAN	MEAN	.053	15.5	42
		193		14.27	99		17.5	95
PT		115		DEV	DEV		17.6	99
		115		1.42	34		18.6	65
PB		217						72
		79					MEAN	
DRVD		211					16.42	MEAN
		296					DEV	62
P11	5.88	193	6.70			9.13	1.54	DEV
								26
Δ11	0.034	MEAN	0.183			0.410		
		169						
V.T	188.1	DEV	259.0			309.0		
		67						
P235	5.63		5.37			5.22		
Δ235	0.072		0.254			0.747		
DEN	.0262		.0253			.0249		
Vs	52.1		109.0			215.1		
VAS	192.4		286.5			418.0		
NAEL	3297		3151			2970		

RUN	24	WAVES		25	WAVES		26	WAVES	
CAM	B	VEL	TIME	B	VEL	TIME	B	VEL	TIME
SAMP	-	17.7	44	-	15.3	85	-	12.0	87
		17.2	16		15.8	115		17.8	24
LIQ	1994	16.1	32	2716	14.7	103	2709	19.8	16
		17.7	44		14.7	97		19.3	67
GAS	208	17.2	40	97.2	13.8	79	181	17.8	60
		17.2	20		13.8	97		17.8	52
TEMP	28.5	18.2	48	32.4	15.1	79	29.8	17.8	72
		13.1	16		14.2	85		12.0	79
PT	9.61	16.7	28	7.49	16.8	109	9.64	17.8	36
		17.2	32		13.0	103		19.8	32
PB	4.95	16.7	44	5.30	14.8	109	4.92	12.0	67
		16.7	32		13.8	48		14.1	56
ΔPT	0.479	16.7	24	0.249	18.4	103	0.462	14.0	40
		18.7	36		16.8	103		16.3	20
ΔPB	0.807	18.7	24	0.319	15.1	115	0.776	17.8	24
			20			121		15.3	107
VOID	.049	MEAN	32	.099	MEAN		.073	16.8	48
		17.05	52		15.07	MEAN		17.3	24
FT		DEV	28		DEV	97		17.2	75
		1.28	32		1.36	DEV		17.7	44
FB			28			18		18.7	91
			44					16.8	44
DRVD			28					17.3	40
			48					17.8	40
P11	9.48			7.42			9.51	16.8	44
			MEAN					17.3	60
Δ11	0.460		33	0.243			0.447	13.3	67
			DEV					17.5	28
VRT	321.5		10.3	279.8			340.4		56
								MEAN	
P235	5.28			5.42			5.24	16.64	MEAN
								DEV	52
Δ235	0.882			0.331			0.846	2.20	DEV
									23
DEN	.0255			.0256			.0251		
VS	235.3			109.3			207.7		
VRB	440.1			329.8			468.2		
NREL	2875			4257			4018		

RUN	27	WAVES		28	WAVES	29	WAVES	
CAM	B	VEL	TIME	B	VEL	B	VEL	TIME
SAMP	-	7.9	189	-	12.5	-	14.7	106
		8.4	147		13.7		14.3	35
LIQ	3497	8.9	168	3496	12.9	3490	12.8	113
		9.2	147		15.4		14.7	86
GAS	0	9.2	210	47.0	12.3	93.2	16.5	63
		8.4	210		11.2		13.7	121
TEMP	32.8	9.2	189	35.5	12.9	31.2	17.6	113
		8.9	210		12.2		15.1	133
PT	5.28	9.5	105	6.09	12.3	7.51	16.4	70
		9.1	189		11.4		13.9	78
PB	5.66	8.1	168	5.55		5.10	16.5	102
		8.9	210		MEAN		16.9	63
ΔPT	0.005	8.5	210	0.072	12.68	0.279	17.4	141
		9.6	168		DEV		17.6	70
ΔPB	0	10.5	189	0.103	1.14	0.267		78
		9.8	147				MEAN	
VOID	.191	8.1	147	.165	TIME	.110	15.58	MEAN
		9.2	189				DEV	93
FT		10.5	252		177		1.54	DEV
		9.5	273		116			29
FB		10.2	147		140			
		9.2	147		201			
DRVD		9.8	105		164			
		8.4	126		110			
P11	5.28	9.8	105	6.07	97	7.43		
		9.5	168		110			
Δ11	0.005	10.5	294	0.071	195	0.271		
		10.5	252					
VRT	38.8	8.1	210	239.6	MEAN	306.1		
		9.1	126		145			
P235	5.66	9.8	189	5.59	DEV	5.20		
		9.8	147		37			
Δ235	0	10.2		0.104		0.276		
			MEAN					
DEN	.0266	MEAN	179	.0259		.0247		
		9.28	DEV					
VS	0	DEV	46	52.2		108.6		
		0.75						
VRB	38.8			250.7		368.8		
NREL	5526			5838		5333		

RUN	30	WAVES		31	WAVES	32	WAVES
CAM	B	VEL	TIME	B	VEL	B	VEL
SAMP	-	20.4	58	-	1.3	-	1.4
		13.8	50		1.0		1.4
LIQ	3487	18.9	31	30.0	1.3	29.7	1.3
		18.3	50		1.1		1.5
GAS	183	12.2	46	0	1.4	24.7	1.6
		18.5	43		1.5		1.6
TEMP	34.3	17.3	54	32.5	1.3	30.6	1.8
		15.1	50		1.2		1.4
PT	10.12	13.5	46	15.22	1.3	15.21	1.5
		20.2	46		1.3		1.4
PB	5.13	13.9	70	15.06*	1.4	15.08*	1.5
		15.1	54				
ΔPT	0.382	19.2	85	0	MEAN	0.009	MEAN
		16.5	120		1.28		1.49
ΔPB	0.801	19.2	23	0	DEV	0.001	DEV
		19.2	54		0.13		0.13
VOID	.085	12.9	89	.010		.009	
		18.5	31		TIME		TIME
FT		16.5	104				
					199		391
FB		MEAN	MEAN		344		316
		16.80	58		597		279
DRVD		DEV	DEV		452		428
		2.57	24		561		632
P11	10.01			15.22	308	15.21	484
					670		167
Δ11	0.371			0	724	0.009	539
							335
VRT	376.8			0.3	MEAN	14.0	
					482		MEAN
P235	5.46			15.06	DEV	15.08	397
					175		DEV
Δ235	0.872			0		0.001	134
DEN	.0255			.0727		.0734	
VS	206.9			0		9.7	
VRB	523.4			0.3		14.2	
NREL	5683			47.1		44.8	

RUN	33	WAVES	34	WAVES	35	WAVES
CAM	B	VEL	B	VEL	B	VEL
SAMP	-	1.3 1.4	-	1.8 1.5	-	3.8 3.1
LIQ	29.7	1.2 1.3	30.0	1.6 1.7	29.6	3.7 3.5
GAS	51.4	1.3 1.2	125	1.8 1.7	254	4.0
TEMP	32.7	1.1 1.4	31.5	1.5 1.6	32.1	MEAN 3.62
PT	15.24	1.5	15.27	MEAN	15.46	DEV 0.31
PB	14.99*	MEAN 1.30	15.04*	1.65 DEV	15.03*	TIME
ΔPT	0.019	DEV 0.12	0.037	0.11	0.026	WAVES
ΔPB	0.009	TIME	0.013	TIME	0.051	ALMOST IMPOSSIBLE
VOID	.004	515	.0014	213 230	.0008	TO SEE TIMING
PT		644 221		224 112		NOT DONE
PB		350 331		309		
DRVD		202 423		MEAN 218		
P11	15.23	331	15.26	DEV 63	15.45	
Δ11	0.019	MEAN 377	0.037		0.025	
VRT	25.3	DEV 138	54.6		104.9	
P235	14.97		15.02		14.94	
Δ235	0.009		0.013		0.051	
DEN	.0721		.0728		.0722	
VS	20.5		49.4		101.3	
VRB	25.6		55.3		107.4	
NREL	46.8		46.1		46.1	

RUN	36	WAVES	37	WAVES	38	WAVES
CAM	B	MIST FLOW NO LIQUID FILM COULD BE SEEN	B	MIST FLOW NO LIQUID FILM COULD BE SEEN	B	VEL. 4.6 4.3 4.3 3.8 MEAN 4.25 DEV 0.29
SAMP	-		-		-	
LIQ	30.1		29.7		101.6	
GAS	522		890		0	
TEMP	33.2		32.0		33.3	
PT	16.27		18.18		15.18	
PB	15.02*		14.95*		14.95	TIME 1492 291 983 MEAN 922 DEV 493
ΔPT	0.110		0.362		0.019	
ΔPB	0.131		0.448		0	
VOID	0		0		.025	
FT						
FB						
DRVD						
P11	16.24		18.07		15.17	
Δ11	0.109		0.356		0.019	
VRT	204.6		327.5		1.1	
P235	14.80		14.20		14.95	
Δ235	0.132		0.457		0	
DEN	.0712		.0687		.0718	
VS	211.1		373.1		0	
VRB	216.7		372.6		1.1	
NREL	48.0		46.2		162.2	

RUN	39	WAVES	40	WAVES	41	WAVES	42	WAVES
CAM	B	VEL	B	VEL	B	VEL	B	VEL
SAMP	-	5.7 3.5	-	5.7 4.8	-	5.4 5.5	-	9.1 8.9
LIQ	97.6	4.6	100.2	4.7	102.2	5.2 5.2	100.5	9.2 8.6
GAS	26.4	MEAN 4.60	50.3	MEAN 5.40	125.2	6.8 5.7	256	8.1 8.0
TEMP	32.2	DEV 0.90	32.3	DEV 0.50	28.3	5.5 5.2	30.6	8.0
PT	14.95		14.82		15.22		15.41	MEAN 8.56
PB	14.95	TIME 841	14.91	TIME 1157	15.03	MEAN 5.56	15.00	DEV 0.49
Δ PT	0.016	662 1253	0	1299 303	0.026	DEV 0.50	0.063	TIME
Δ PB	0.006	233	0		0.007	TIME	0.021	110
VOID	.023	MEAN 747	.023	MEAN 920	.021	476 659	.014	104 104
PT		DEV 366		DEV 440		549 238		87 87
PB						385 201		87 145
DRVD						531		87 162
P11	14.95		14.82		15.21	MEAN 434	15.39	MEAN
Δ 11	0.016		0		0.026	DEV 156	0.063	108 DEV
VRT	21.9		33.9		65.3		117.7	26
P235	14.95		14.91		15.03		15.01	
Δ 235	0.006		0		0.007		0.021	
DEN	.0722		.0720		.0738		.0730	
Vs	10.5		20.1		48.8		101.0	
VRB	21.9		33.8		65.7		119.3	
NAEL	152.3		156.7		146.7		151.6	

RUN	43	WAVES	44	WAVES	45	WAVES	46	WAVES
CAM	B	VEL	B	VEL	B	VEL	B	VEL
SAMP	-	10.9	-	14.9	-	19.3	-	5.7
		10.4		14.1		17.7		5.7
LIQ	100.6	9.9	100.6	14.1	101.4	18.5	300	5.7
		10.4		13.7		16.9		5.7
GAS	375	10.7	524	13.2	868	17.7	0	4.7
		10.7		12.8		16.9		4.7
TEMP	33.5	10.9	31.2	12.8	30.9	18.5	33.9	5.3
				12.3		16.9		4.7
PT	15.98	MEAN	16.69	13.7	18.78	17.7	14.96	4.7
		10.56						5.7
PB	14.77	DEV	15.05	MEAN	14.96	MEAN	15.10	
		0.33		13.51		17.79		MEAN
ΔPT	0.105		0.101	DEV	0.202	DEV	0.008	5.26
		TIME		0.77		0.80		DEV
ΔPB	0.115		0.181		0.509		0	0.47
		129		TIME		WAVES		
VOID	.005	80	.003		0	VERY	.044	TIME
		38				DIFF-		
FT		65		103		ICULT		510
		87		46		TO		370
FB		99		87		FOLLOW		370
		80		99				387
DRVD				61		MEAN		211
		MEAN		95		APPROX		158
P11	15.95	83	16.66	95	18.72	80	14.96	194
		DEV		106				299
Δ11	0.104	26	0.101	137	0.200		0.008	458
				57				
VRT	162.9		214.9	38	323.9		3.3	MEAN
				49				329
P235	14.81		15.12		15.15		15.10	DEV
				MEAN				115
Δ235	0.116		0.182	81	0.520		0	
				DEV				
DEN	.0711		.0734	29	.0736		.0724	
VS	151.9		205.5		339.6		0	
VRB	169.7		226.4		363.2		3.3	
NREL	161.3		153.7		154.0		485	

NUM	47	WAVES	48	WAVES	49	WAVES	CORE SAMPLE
CAL	B	VEL	B	VEL	T	VEL	
LAMP	-	5.3 5.3	-	5.2 6.0	C	4.1 3.5	0.419" NIL IN 28 MINS
LIQ	300	5.8 5.6	300	5.0 5.1	297	4.4 4.0	
GAS	25.4	5.8 6.1	51.4	5.2 5.8	128.3	4.0 4.5	
TEMP	35.4	5.1 5.2	34.8	5.6 5.2	30.1	3.8	
PT	14.87	5.4 5.1	14.89	5.4		MEAN 4.04	
PB	14.91	MEAN	15.02	MEAN 5.39	15.05	DEV 0.32	
ΔPT	0.006	5.47 DEV	0.005	DEV 0.32			
ΔPB	0.003	0.32	0			TIME	
VOID	.044	TIME	.043	TIME		TOO CLOSE TO THE INJECT -OR WAVES NOT YET FORMED	
PT		304 322		272 308			
PB		286 233		217 344			
DRVD		430 465		453 380 471			
P11	14.87	215 286	14.89	199			
Δ11	0.006	197	0.005	MEAN 330			
VRT	34.3	MEAN 304	51.4	DEV 94			
P235	14.91	DEV 86	15.02		15.05		
Δ235	0.003		0				
DEN	.0710		.0717		.0734		
VS	10.3		20.6		50.3		
VRB	34.3		51.2				
NREL	500		494		443		

RUN	50	WAVES	CORE SAMPLE	51	WAVES		52S	WAVES	CORE SAMPLE
CAM	C	VEL		B	VEL	TIME	T	VEL	
			0.090"						0.130"
CAMP	B	7.1	0.30	-	6.5	185	T	4.3	0.057
		6.2			7.3	148		4.8	
LIQ	301	6.0	0.170"	300	7.0	148	301	4.4	0.240"
		8.6	0.072		7.6	167		4.8	0.050
GAS	132	8.3		127.2	7.6	222	132	4.1	
		8.6	0.390"		7.3	202		4.8	0.580"
TEMP	31.3	9.2	0.076	32.4	8.2	130	31.1	5.2	0.083
		8.9			7.0	148			
PT		8.3	0.750"	15.15	7.6	111		MEAN	0.910"
		9.2	0.082		8.2	240		4.63	0.091
PB	14.78			15.05	8.2	167	14.91	DEV	
		MEAN	0.970"		7.9	185		0.35	1.210"
ΔPT		8.04	0.072	0.022	8.2	259			0.081"
		DEV			7.6	111		TIME	
ΔPB		1.12	1.120"	0.007	8.0	130			CALC
			0.060		8.2			NOT	TOTAL
VOID		TIME		.037		MEAN		POSS-	14
			CALC		MEAN	170		IBLE	
PT	294	144	TOTAL		7.65	DEV			EDGE
		63	15		DEV	44		VEL	0.131"
PB	297	113			0.51			MEAS-	
		77	EDGE					URE-	
DRVD		68	0.131"					MENTS	
		81						BASED	
P11		41		15.14				ON	
		81						SMALL	
Δ11		76		0.022				BUMPS	
								DEF-	
VRT		68		89.6				INITE	
		63						WAVES	
P235	14.78	90		15.05			14.91	NOT	
								PRESENT	
Δ235		MEAN		0.022					
		77							
DEN	.0717	DEV		.0726			.0724		
		27							
VS	53.0			50.4			52.5		
VRB				89.6					
NREL	461			470			459		

RUN	53S	WAVES		CORE BARREL	54S	WAVES	CORE BARREL
CAN	C	VEL	TIME	0.130"	B	VEL	0.110"
CAMP	C	6.2	150	0.071	B	10.1	0.21
LIQ	301	6.0	137			10.4	
GAS	127	6.0	138	0.180"	301	9.7	0.240"
TEMP	32.0	5.9	156	0.028		10.0	0.074
PT		6.7	187		128	9.0	
PB	15.21	5.6	50	0.360"		10.1	0.580"
ΔPT		5.3	181	0.023	33.5	9.7	0.099
ΔPB		6.2	131			9.7	
VOID		6.2	81	0.780"	15.32		0.910"
PT	271	6.2	100	0.016		MEAN	0.095
PB	282	6.1	56		15.14	9.84	
DRVD		6.7	100	1.090"		DEV	1.160"
P11		6.0	81	0.015	0.024	0.39	0.083
Δ11		5.8	88				
VRT		5.4	112	CALC	0.013	TIME	CALC
P235	15.21		50	TOTAL			TOTAL
Δ235		MEAN	113	7	.033	133	18
DEN	.0736	6.02	112			149	
VS	49.7	DEV	69	EDGE		162	EDGE
VRB		0.38	100	0.131"		62	0.131"
NREL	468		88			199	
			119			125	
						62	
			MEAN			174	
			109		15.31	108	
			DEV			100	
			38		0.024	166	
					89.8	MEAN	
						131	
					15.14	DEV	
						43	
					0.013		
					.0727		
					50.7		
					90.4		
					483		

RUN	55
CAM	T
CAMP	C
LIQ	300
GAS	227
TEMP	31.8
PT	
PB	14.59
ΔPT	
ΔPB	
VOID	
FT	294
FB	
DRVD	
P11	
Δ11	
VRT	
P235	14.61
Δ235	
DEN	.0707
VS	92.4
VRB	
NREL	464

WAVES			CORE SAMPLE
VEL	47	18	
	47	47	0.153"
6.9	53	29	0.067
7.2	18	29	
7.1	29	29	0.419"
6.7	47	41	0.038
5.5	35	35	
6.9	23	17	0.685"
7.2	41	35	0.036
6.9	47	41	
6.4	41	35	0.951"
6.2	47	23	0.038
6.4	23	23	
6.2	29	18	1.217"
	35	41	0.30
MEAN	47	41	
6.63	47	23	CALC
DEV	41	41	TOTAL
0.49	35	41	19
	47	17	
TIME	41	23	EDGE
	18	41	0.107"
29	35	23	
35	41	41	
23	47	23	
23	29	18	
18	41	53	
35	23	29	
41	29	35	
41	29	23	
23	47	29	
29	18	23	
35	41	35	
47	23	17	
29	35	35	
47	35		
	35	MEAN	
	29	34	
	41	DEV	
		9.8	

RUN	56	WAVES		CORE SAMPLE	57	WAVES	58	CORE SAMPLE
CAN	C	VEL	TIME	0.090"	B	VEL	-	0.130"
SAMP	B	10.2	81	0.27	-	13.2	T	0.062
		8.9	74			11.9		
LIQ	301	8.2	102	0.150"	300	11.9	301	0.230"
		7.6	95	0.24		10.9		0.009
GAS	265	10.3	88		207	11.4	248	
		9.0	47	0.380"		11.4		0.580"
TEMP	31.5	8.2	68	0.27	32.5	11.9	29.7	0.003
		8.6	74			11.9		
PT		8.5	115	0.750"	15.53	11.9		0.960"
		10.2	81	0.29				0
PB	14.65	8.0	47		15.00	MEAN	14.91	
		8.2	61	0.950"		11.82		1.170"
ΔPT		8.7	81	0.26	0.067	DEV		0.067
		9.8	68			1.91		
ΔPB		9.6	88	1.020"	0.052			CALC
		9.5	61	0.27		TIME		TOTAL
VOID		8.7	47		.026			3.2
		9.2	47	1.110"		129		
PT	255	9.2	95	0.25		106		EDGE
		8.1	41			78		0.113"
PB	216	7.9	135	CALC		67		
		10.3	34	TOTAL		84		
DRVD		8.2	135	60		123		
		10.9	68			84		
P11		9.6	95	EDGE	15.51	123		
		9.2	74	0.089"		134		
Δ11		11.2	68		0.067			
		9.5	68			MEAN		
VRT		8.7	129		124.2	103		
		8.7				DEV		
P235	14.67	9.0	MEAN		15.02	24	14.93	
			78					
Δ235		MEAN	DEV		0.052			
		9.09	27					
DEN	.0711	DEV			.0725		.0729	
		0.89						
VS	107.3				82.2		97.9	
VRB					126.3			
NREL	463				471		446	

RUN	598
CAM	T
SAMP	T
LIQ	299
GAS	244
TEMP	32.6
PT	
PB	14.95
Δ PT	
ΔPB	
VOID	
FT	
FB	
DRVD	
P11	
Δ11	
VRT	
P235	14.98
Δ235	
DEN	.0722
VS	97.3
VRB	
NREL	470

WAVES		
VEL	54	48
	54	48
6.9	36	36
6.9	36	30
7.0	36	24
5.9	24	36
5.9	48	30
5.6	18	54
6.3	48	42
5.8	30	36
6.5	54	36
6.2	30	48
5.6	36	66
	30	18
MEAN	36	42
6.28	42	24
DEV	30	36
0.53	30	30
	30	
TIME	24	MEAN
48	24	38
36	42	DEV
42	48	11
42	36	
18	54	
36	24	
24	42	
42	48	
42	36	
48	54	
36		

CORE SAMPLE
0.075"
0.83
0.100"
0.45
0.200"
0.44
0.580"
0.38
0.870"
0.23
0.980"
0.19
CALC
TOTAL
72
EDGE
0.095"

RUN	60S	WAVES	CORE SAMPLE	61S	WAVES	CORE SAMPLE	62	WAVES
CAM	C	VEL		B	VEL		B	VEL
			0.120"			0.100"		
SAMP	C	8.0	0.22	B	11.3	0.32	-	13.5
		7.3			9.3			13.0
LIQ	299	9.7	0.160"	301	10.8	0.240"	301	13.1
		8.2	0.22		10.8	0.35		12.3
GAS	251	8.8		251	11.6		373	12.3
		8.4	0.380"		9.2	0.580"		12.3
TEMP	31.7	8.7	0.28	33.4	9.3	0.36	33.9	12.3
		8.5			10.4			12.3
PT		7.2	0.770"	16.05	9.2	0.910"	16.71	12.3
		8.8	0.28		9.0	0.33		12.7
PB	14.91			14.97	9.6		14.79	
		MEAN	1.030"		10.8	1.160"		MEAN
ΔPT		8.36	0.23	0.108	10.4	0.27	0.215	12.61
		DEV						DEV
ΔPB		0.70	1.080"	0.081	MEAN	CALC	0.202	0.42
			0.21		10.13	TOTAL		
VOID		TIME		.0206	DEV	79	.005	TIME
		45	1.130"		0.86			76
PT	237	58	0.20			EDGE		53
		103			TIME	0.089"		103
PB	234	87	CALC		77			87
		107	TOTAL		81			106
DRVD		91	59		104			53
		111			77			80
P11		88	EDGE	16.02	112		16.65	87
		62	0.095"		93			91
Δ11		132		0.107	77		0.213	57
		91			124			76
VRT		70		140.9	77		187.1	
					135			MEAN
P235	14.94	MEAN		15.00	112		14.87	79
		87			120			DEV
Δ235		DEV		0.081	131		0.204	18
		24						
DEN	.0724			.0721	MEAN		.0712	
					102			
VS	99.8			100.2	DEV		150.8	
					21			
VRB				146.0			199.1	
NRSL	462			482			486	

RUN	63
CAM	T
SAMP	C
LIQ	300
GAS	490
TEMP	31.3
PT	
PB	14.63
ΔPT	
ΔPB	
VOID	
FT	194
FB	
DRVD	
P11	
Δ11	
VRT	
P235	14.70
Δ235	
DEN	.0713
VS	197.9
VRB	
NREL	459

WAVES				CORE SAMPLE
VEL	16	12	24	
	12	16	12	0.153
11.8	12	12	20	0.34
10.3	16	16	12	
11.4	12	12	12	0.419"
9.7	16	16	12	0.32
11.4	16	12	12	
10.7	20	16	12	0.685"
11.8	16	16	12	0.29
10.7	12	24	16	
11.4	12	16	16	0.951"
11.0	12	16	12	0.36
11.4	16	16	12	
11.0	12	8	16	1.217"
11.8	16	12	16	0.41
10.0	12	12	20	
10.7	20	12	16	CALC
10.7	20	12	20	TOTAL
10.3	20	12	20	100
10.7	12	12	16	
	24	20	8	EDGE
MEAN	12	8	12	0.083"
10.93	16	12	12	
DEV	16	12	20	
0.61	16	12	16	
	12	24	8	
TIME	24	12	20	
12	16	8		
16	12	16	MEAN	
20	16	16	15	
12	16	16	DEV	
12	20	16	3.8	
16	12	16		
20				

RUN	64	WAVES		CORE SAMPLE	65	WAVES	
CAN	C	VEL	TIME		B	VEL	TIME
SAMP	B		39	0.080" 0.66	-	15.9	34
		10.8	44			15.8	42
LIQ	301	12.7	39	0.150"	300	15.9	27
		12.5	39	0.74		14.2	30
GAS	475	13.9	31		559	14.2	34
		12.3	35	0.230"		13.2	19
TEMP	31.2	12.7	26	0.82	32.1	15.0	34
		12.7	39			13.2	27
ΔT		11.9	22	0.380"	17.79	15.0	38
		13.9	35	0.82		13.6	46
PB	14.59	12.1	26		15.01	13.6	61
		12.7	22	0.750"		14.2	34
ΔPT		13.0	65	0.69	0.292	16.5	42
		12.3	44			13.2	34
ΔPB		12.3	22	1.000"	0.324		61
		12.3	35	0.66		MEAN	15
VOID		13.4	52		.004	14.54	57
		12.5	44	1.090"		DEV	34
PT	179	12.7	18	0.64		1.10	30
		12.3	52				30
PB	136	14.3	39	1.150"			19
		12.1	70	0.64			30
DRVD		13.0	57				34
			26	CALC			
P11		MEAN	57	TOTAL	17.71		MEAN
		12.65		172			35
Δ11		DEV	MEAN		0.289		DEV
		0.74	39	EDGE			12
VRT			DEV	0.083"	250.6		
			14				
P235	14.66				15.13		
Δ235					0.328		
DEN	.0711				.0731		
VB	192.3				220.2		
VRB					272.8		
NRLL	460				467		

RUN	66	CORE SAMPLE	675	WAVES	CORE SAMPLE
CAM	-		T	VEL	
		0.140"			0.075"
SAMP	T	0.20	T	6.8	1.16
				7.8	
LIQ	302	0.260"	301	8.1	0.150"
		0.115		8.1	1.04
GAS	501		510	8.9	
		0.580"		8.0	0.580"
TEMP	30.4	0.040	31.8	8.0	0.94
				8.3	
PT		0.920"		9.3	0.920"
		0.070			0.63
PB	14.90		14.85	MEAN	
		1.140"		8.14	1.060"
ΔPT		0.15		DEV	0.66
				0.66	
ΔPB		CALC			CALC
		TOTAL		TIME	TOTAL
VOID		49			215
				DIF-	
PT		EDGE		INTE	EDGE
		0.077"		WAVES	0.077"
PB				NOT	
				PRESENT	
DRVD					
				TIME	
P11				BETWEEN	
				"LUMPS"	
Δ11				OF	
				WATER	
VRT				ABOUT	
				15	
P235	15.02		14.94	MSECS	
Δ235					
DEN	.0731		.0723		
VS	197.3		203.1		
VRB					
MEL	454		466		

RUN	68S	WAVES		CORE SAMPLE	69S	WAVES		CORE SAMPLE
CAM	C	VEL	TIME		B	VEL	TIME	
				0.100"				0.100"
SAMP	C	12.0	25	0.69	B	14.0	28	1.24
		11.5	37			11.9	40	
LIQ	301	10.4	54	0.140"	300	11.9	20	0.250"
		11.9	33	0.67		15.1	52	1.08
GAS	510	10.7	21		493	13.1	40	
		11.5	50	0.380"		11.9	56	0.580"
TEMP	31.5	11.8	29	0.60	31.7	10.9	60	0.95
		12.4	33			13.3	67	
PT		11.5	29	0.770"	16.25	11.5	40	0.910"
		9.3	41	0.82		11.0	40	0.88
PB	14.54	10.7	41		14.45	11.0	20	
		11.5	46	1.020		10.9	71	1.160"
ΔPT		11.6	29	1.04	0.267	9.8	28	0.86
		9.8	37			12.4	28	
ΔPB		10.4	21	1.045"	0.250	13.1	56	CALC
		11.5	33	1.02		13.4	28	TOTAL
VOID		10.8	29		.0037	12.6	20	236
		12.4	50	1.110"		12.4	32	
FT	104	12.2	41	1.02			48	EDGE
		12.3	41			MEAN	36	0.083"
FB	113		33	1.150"		12.23	28	
		MEAN	33	1.00		DEV	44	
DRVD		11.31	33			1.27	24	
		DEV	45	CALC			36	
P11		0.85	66	TOTAL	16.17		48	
			58	195			36	
Δ 11			50		0.264		28	
			50	EDGE			24	
VRT			33	0.083	236.7		56	
			29				52	
P235	14.63		58		14.54		20	
							60	
Δ 235			MEAN		0.253		32	
			39				40	
DEN	.0709		DEV		.0704			
			11				MEAN	
VS	207.1				201.6		39	
							DEV	
VRB					250.7		14	
NREL	463				466			

RUN	705	CORE SAMPLE	71	WAVES	72	WAVES	
CAM	-		B	VEL	B	VEL	TIME
		0.100"		20.7		13.5	46
SAMP	B	0.84	-	19.8	-	12.4	30
				18.8		12.4	27
LIQ	300	0.140"	301	19.8	601	12.8	91
		0.93		19.4		11.6	49
GAS	513		847	18.8	380	13.3	84
		0.380"		20.2		12.0	53
TEM	29.0	0.93	33.4	19.4	36.3	12.9	46
				19.4		11.7	27
FT		0.770"	19.78		17.55	11.6	38
		0.80		MEAN		11.6	72
FB	14.64		14.84	19.59	14.81	12.8	42
		1.020"		DEV		13.9	49
ΔFT		0.72	0.290	0.58	0.320	13.3	49
						13.3	57
ΔFB		1.070"	0.650	TIME	0.293	14.3	68
		0.70				13.5	65
VOID			0	WAVES	.010	12.3	53
		1.110"		VERY		12.8	46
FT	81	0.67		DIFF-		12.5	30
				ICULT		12.0	61
FB	104	1.150"		TO		13.7	49
		0.64		FOLLOW		12.5	49
DRVD						12.9	46
		CALC		MEAN		13.3	46
P11		TOTAL	19.70	TIME	17.45	12.4	53
		196		ABOUT		12.4	61
Δ11			0.287	15	0.315	13.2	65
		EDGE		MSEC		13.3	61
VRT		0.083"	338.7		221.1	12.1	49
						13.3	76
P235	14.73		15.09		14.92	13.9	27
						13.9	
Δ235			0.668		0.297	13.9	MEAN
							52
DEN	.0721		.0725		.0708	MEAN	DEV
						12.86	16
VS	204.9		336.3		154.5	DEV	
						0.74	
VRB			391.3		240.6		
NREL	437		482		1020		

RUN	73	WAVES		74	WAVES	75	WAVES
CAM	B	VEL	TIME	B	VEL	B	VEL
SAMP	-	8.1	191	-	8.7	-	7.1
		8.7	244		8.7		7.1
LIQ	997	8.6	209	995	8.4	997	7.3
		7.9	278		8.2		7.1
GAS	0	7.2	174	25.3	7.9	50.8	6.7
		7.2	122		6.9		7.9
TEMP	40.4	8.4	174	40.4	7.1	40.0	7.8
		7.2	122		9.3		7.8
PT	14.89	8.7	157	14.80	9.0	14.80	8.0
		8.4	261		9.3		7.1
PB	14.89	7.2	174	14.85	7.9	14.83	7.6
		9.0	157		7.2		9.1
ΔPT	0.005	8.1	244	0.003	8.7	0.010	
		8.1	139				MEAN
ΔPB	0	7.9	209	0.007	MEAN	0.006	7.55
		6.8	261		8.25		DEV
VOID	.088	7.3	174	.087	DEV	.086	0.61
		7.3	313		0.78		
FT		8.1	209				TIME
		7.3	174		TIME		
FB		6.8	87				142
		6.8	313		235		142
DRVD		8.1	139		370		124
		8.4	104		269		212
P11	14.89	8.7	296	14.80	252	14.80	106
		8.4	226		235		195
Δ11	0.005			0.003	218	0.010	266
		MEAN	MEAN		134		71
VRT	11.0	7.87	198	60.2	269	87.3	89
		DEV	DEV		302		159
P235	14.89	0.66	63	14.85	202	14.83	354
					151		212
Δ235	0			0.007	218	0.006	248
DEN	.0693			.0692	MEAN	.0692	MEAN
					238		178
VS	0			10.5	DEV	21.1	DEV
					61		77
VRB	11.0			60.1		87.2	
NREL	1832			1829		1818	

RUN	76	WAVES		CORE SAMPLE	77	WAVES		CORE SAMPLE
CAN	T	VEL			C	VEL	TIME	
		7.3	43	0.153"		9.1	146	0.110"
SAMP	C	7.3	31	0.62	B	9.1	80	1.19
		6.6	67			9.7	46	
LIQ	1002	6.4	43	0.419	998	8.1	66	0.170"
		6.8	43	0.025		7.0	66	0.54
GAS	133.8	6.6	37		129	10.4	100	
		6.6	31	0.685		8.4	152	0.360"
TEMP	36.9	6.8	43	0.018	34.4	8.9	40	0.50
		7.3	55			8.8	126	
PT		6.8	43	0.951"		8.8	60	0.770"
		6.8	43	0.026		8.6	66	0.56
PB	15.05	6.6	43		14.86	9.7		
		6.8	55	1.217"		9.2	MEAN	1.000"
ΔPT		6.6	43	2.58		9.1	86	0.44
		6.8	31			8.2	DEV	
Δ PB		7.3	31	CALC		8.6	37	1.070"
			31	TOTAL		8.6		0.44
VOID		MEAN	55	55				
		6.84	37			MEAN		1.150"
FT		DEV	31	EDGE	946	8.84		0.58
		0.29	31	0.119"		DEV		
FB	881		31		914	0.73		CALC
		TIME	43					TOTAL
DRVD		55	67					101
		55	49					
P11		43	25					EDGE
		55	31					0.143"
Δ11		49	24					
		55	25					
VRT		43	61					
		43	49					
P235	15.07	55			14.88			
		55	MEAN					
Δ235		49	43					
			DEV					
DEN	.0713		11		.0711			
VS	54.0				52.2			
VRB								
NREL	1721				1630			

RUN	78	WAVES	79	CORE SAMPLE	80S	WAVES		CORE SAMPLE
CAM	B	VEL	-		T	VEL	36	
				0.160"			48	0.140"
SAMP	-	7.5	T	0.12	T	7.0	48	0.95
		7.0				7.0	54	
LIQ	995	7.4	990	0.250"	1008	6.8	36	0.260"
		4.2		0.007		6.6	36	0.82
GAS	127	6.0	129.8		128	7.5	42	
		7.0				6.8	48	0.580"
TEMP	37.1	7.1	34.8	0.580"	36.6	6.6	36	0.88
		4.6		0.012		7.5	24	
PT	15.34	6.6				7.0	42	0.920"
		7.0		1.140"		7.0	24	0.98
PB	14.89	6.9	15.47	0.051	15.00	6.4	36	
		6.5				7.0	42	1.140"
ΔPT	0.056	7.4		CALC		7.2	48	1.25
				TOTAL		6.8	42	
ΔPB	0.047	MEAN		38			42	CALC
		6.55				MEAN	42	TOTAL
VOID	.070	DEV		EDGE		6.94	24	238
		1.00		0.113"		DEV	30	
FT						0.30	30	EDGE
		TIME					54	0.107"
FB						TIME	30	
		110					30	
DRVD		72				24	36	
		110				24	36	
P11	15.32	105				36	36	
		39				36	42	
Δ11	0.056	94				48	36	
		93				42	24	
VRT	142.0	66				48	54	
		44				36		
P235	14.91	159	15.49		15.02	30	MEAN	
		148				48	37	
Δ235	0.047	39				36	DEV	
		MEAN				30	8.6	
DEN	.0705	90	.0739		.0711	24		
		DEV				42		
VS	51.9	38	50.6		51.8			
VRB	144.0							
NREL	1715		1630		1721			

RUN	81S	WAVES		CORE SAMPLE	82S	WAVES	CORE SAMPLE
CAM	C	VEL	TIME		B	VEL	
		8.8	71	0.130"		9.9	0.130"
LAMP	C	7.2	84	0.95	B	9.9	0.93
		8.7	90			9.8	
LIQ	1004	6.9	103	0.180"	1001	9.6	0.250"
		7.4	84	0.30		6.9	0.48
GAS	127	7.4	78		128	10.7	
		9.0	58	0.360"		10.3	0.580"
TEMP	34.8	8.2	78	0.15	34.7	9.6	0.58
		8.2	116			9.2	
PT		9.1	103	0.780"	15.34		0.910"
		7.1	97	0.13		MEAN	0.53
PB	14.89	6.7	97		14.85	9.54	
		7.6	65	1.090"		DEV	1.140"
ΔPT			90	0.17	0.058	1.02	0.55
		MEAN	129				
ΔPB		7.87	110	CALC		TIME	CALC
		DEV	103	TOTAL		97	TOTAL
VOID		0.81		82	.068	121	106
			MEAN			127	
FT	975		92	EDGE		170	EDGE
			DEV	0.113"		70	0.143"
FB	916		18			73	
						176	
DRVD						127	
						91	
P11					15.32		
						MEAN	
Δ11					0.058	120	
						DEV	
VR1					142.3	33	
P235	14.91				14.87		
Δ235					0.054		
DEN	.0712				.0710		
VS	51.4				51.9		
VRB					144.5		
NAEL	1653				1645		

RUN	83	WAVES			CORE SAMPLE	84	WAVES		CORE SAMPLE
CAM	T	VEL	25	32		C	VEL	TIME	
		10.7	38	25	0.153"		14.2	89	0.100"
CAMP	C	11.1	25	25	0.62	B	16.3	64	1.36
		9.5	25	32			14.3	72	
LIQ	1000	9.8	19	13	0.419"	1000	15.2	55	0.170"
		9.8	25	38	0.53		12.3	85	1.52
GAS	268	9.8	19	38		249	14.3	60	
		10.5	25	25	0.685"		12.1	51	0.370"
TEMP	35.3	10.5	38	25	0.54	35.6	13.8	47	2.02
		10.5	25	25			11.7	55	
PT		10.8	32	25	0.951"		12.4	59	0.760"
		10.1	19	25	0.53		12.3	64	1.95
PB	14.91	10.5	19	25		14.94	12.7	34	
		9.8	32	19	1.217"		12.1	34	0.910"
ΔPT		11.1	32	19	1.50		11.2	26	1.71
		9.5	19	19			11.2	68	
Δ PB		10.5	25	25	CALC		11.6	51	1.010"
		10.8	13	25	TOTAL		10.5	55	1.54
VOID		9.2	25	32	131		11.9	34	
		9.5	25	25			11.6	34	1.080"
FT	835	10.1	13	19	EDGE	858	11.3		1.42
			19	25	0.125"		14.3	MEAN	
FB		MEAN	32	32		698	12.7	55	1.150"
		10.21	19	19				DEV	1.28
DRVD		DEV	38	19			MEAN	17	
		0.56	32	19			12.73		CALC
P11			32	13			DEV		TOTAL
		TIME	32	32			1.46		333
Δ 11			25	19					
		19	25	38					EDGE
VRT		13	25	19					0.137"
		19	32	32					
P235	14.99	19	19	19		15.02			
		25	25	19					
Δ 235		32	38	19					
		38	13						
DEN	.0714	38	32	MEAN		.0714			
		25	25	26					
VS	108.0	32	32	DEV		100.4			
			32	7.0					
VRB									
WGT	1663					1673			

RUN	85	WAVES		86	CORE SAMPLE	87S	WAVES	
CAM	B	VEL	TIME	-		T	VEL	TIME
		13.6	66		0.140"		9.5	23
SAMP	-	13.4	33	T	0.70	-	7.7	53
		13.2	39				8.3	23
LIQ	999	14.4	66	991	0.250"	1002	7.6	23
		13.6	60		0.16		9.7	30
GAS	258	12.9	88	255		260	9.3	...
		12.9	61		0.580"		8.9	30
TEMP	35.9	12.9	55	32.3	0.095	34.2	8.6	38
		12.9	72				9.5	...
PT	16.71	13.4	60		0.920"		9.5	38
		13.5	61		0.106		9.2	23
PB	14.88	13.4	83	15.03		14.75		...
		13.9	110		1.140"		MEAN	15
ΔPT	0.178		66		0.34		8.89	30
		MEAN	77				DEV	30
ΔPB	0.202	13.38			CALC		0.71	30
		DEV	MEAN		TOTAL			30
VOID	.040	0.43	66		95			30
			DEV					30
FT			18		EDGE			23
					0.125"			23
FB								30
								38
DRVD								45
							MEAN	
P11	16.66						30	
							DEV	
Δ11	0.177						8.4	
VRT	207.3							
							SHUTTER LOOSE	
P235	14.96			15.11		14.83	SOME FRAMES WERE	
							UNINTELLIGIBLE	
Δ 235	0.204						REPEATED (88S)	
DEN	.0711			.0730		.0710		
VS	104.5			100.6		105.4		
VRB	219.8							
NREL	1682			1550		1630		

RUN	885	WAVES			CORE SAMPLE	895	WAVES		CORE SAMPLE
CAM	T	VEL	TIME	25		C	VEL	TIME	
		9.6	31	31	0.130"		13.1	42	0.120"
SAMP	T	10.2	18	31	1.05	C	11.3	47	0.91
		10.2	18	25			12.5	38	
LIQ	1000	9.6	12	18	0.260"	1002	15.8	25	0.160"
		9.6	25	18	0.955		10.9	34	0.62
GAS	263	9.9	18	31		257	12.3	47	
		10.2	31	24	0.580"		12.7	63	0.380"
TEMP	34.3	9.6	25	37	0.70	35.2	12.9	25	0.58
		9.6	25	37			11.8	38	
PT		9.6	37	25	0.920"		12.7	68	0.770"
		9.6	31	31	1.21		13.1	42	0.60
PB	14.69	8.8	37	31		14.65	13.6	72	
		8.8	12	18	1.140"		12.5	55	1.030"
ΔPT		10.2	31	37	1.40		11.3	42	0.54
		9.1	25	24			11.8	42	
ΔPB		9.6	24	37	CALC		10.0	59	1.080"
		9.1	43	31	TOTAL		12.1	38	0.52
VOID		9.0	31	25	238		12.1	55	
		9.1	25	31			11.3	38	1.130"
PT		10.2	24	24	EDGE	821		59	0.52
		9.6	18	31	0.113"		MEAN	30	
PB		9.0	18	25		699	12.29	51	CALC
		9.6	31	24			DEV	38	TOTAL
DRVD		9.3	31	18			1.20	34	123
		8.8	18						
P11		9.0	25	MEAN				MEAN	EDGE
			37	26				45	0.125"
Δ11		MEAN	24	DEV				DEV	
		9.50	31	7.5				12	
VRT		DEV	31						
		0.46							
P235	14.77					14.73			
Δ235									
DEN	.0706					.0702			
VS	107.3					105.4			
VRB									
HREL	1630					1663			

RUN	903	WAVES		CORE SAMPLE	918	CORE SAMPLE
CAN	B	VEL	TIME		-	
				0.130"		0.100"
SAMP	B	9.3	32	1.44	B	2.14
		11.1	47			
LIQ	995	13.2	31	0.250"	1002	0.140"
		10.1	63	2.06		2.75
GAS	229	12.3	71		253	
		11.6	32	0.580"		0.380"
TEMP	34.7	13.7	63	2.35	34.9	4.75
		12.1	75			
PT	16.46	13.2	91	0.910"		0.770"
		15.1	91	1.73		3.86
PB	14.86	9.8	31		14.79	
		12.3	32	1.140"		1.020"
ΔPT	0.199	12.9	75	1.29		1.89
		11.1	71			
ΔPB	0.219	12.3	43	CALC		1.070"
		11.9	87	TOTAL		1.55
VOID	.0415	12.9	99	368		
		13.8	55			1.110"
PT		12.6	87	EDGE	401	1.37
		9.4	87	0.131"		
PB		9.1	35		428	1.150"
			75			1.18
DRVD		MEAN	95			
		11.90				CALC
P11	16.40	DEV	MEAN			TOTAL
		1.59	64			618
Δ11	0.197		DEV			
			23			EDGE
VRT	193.2					0.131"
P235	14.94				14.87	
Δ235	0.221					
DEN	.0713				.0709	
VS	92.5				102.7	
VRB	203.6					
NREL	1635				1653	

RUN	92	WAVES		93	WAVES		
CAM	B	VEL	TIME	T	VEL	23	15
						12	23
SAMP	-	13.4	39	-	14.9	11	15
		13.5	32		14.9	12	15
LIQ	998	14.3	28	1010	14.2	11	15
		15.4	53		15.4	15	8
GAS	380	14.5	25	505	14.9	12	11
		14.7	28		14.5	11	12
TEMP	37.5	13.5	43	34.0	14.2	19	15
		13.5	39		13.4	12	11
PT	18.48	12.5	67		14.9	19	15
		15.1	60		13.4	8	12
PB	14.75	14.3	50	14.72	12.9	23	11
		13.4	57		14.5	12	8
ΔPT	0.408	13.4	36		14.5	11	12
		13.4	32		13.4	8	15
ΔPB	0.382	14.5	46		14.5	12	8
		13.4	25		15.8	11	11
VOID	.018	15.4	43		14.9	15	12
		12.5	25		13.4	12	15
FT		14.5	46		13.4	11	8
		15.4	32		15.3	12	11
FB		14.5	39		12.9	15	15
		13.4	25		13.7	11	12
DRVD		12.6	36		15.8	12	11
		14.3	32			19	12
P11	18.36	12.6	53		MEAN	19	11
		14.5	39		14.33	15	8
Δ11	0.401	14.5	53		DEV	11	15
		14.3			0.86	15	19
VRT	253.0		MEAN			19	12
		MEAN	40		TIME	8	15
P235	14.89	13.98	DEV	14.90		15	15
		DEV	12		19	19	15
Δ235	0.388	0.86			23	8	8
					15	8	
DEN	.0703			.0714	15	15	MEAN
					15	8	12.6
VS	155.7			203.6	19	15	DEV
					19	12	5.0
VRB	283.4						
NREL	1734			1636			

RUN	94
CAM	C
SAMP	B
LIQ	1000
GAS	497
TEMP	33.9
PT	
PB	14.44
Δ PT	
ΔPB	
VOID	
FT	653
FB	348
DRVD	
P11	
Δ11	
VRT	
P235	14.62
Δ235	
DEN	.0700
VS	204.4
VRB	
NREL	1617

WAVES		
VEL	TIME	42
14.9	25	25
15.6	17	17
15.6	34	33
14.9	17	34
15.5	17	21
14.9	38	34
14.9	34	25
14.3	17	33
15.5	25	46
15.5	38	54
15.5	29	21
14.9	29	42
16.2	29	42
13.9	25	29
15.4	34	42
14.9	46	46
13.9	17	67
15.5	17	34
13.8	38	17
14.9	38	
15.9	25	MEAN
15.6	17	32
13.3		DEV
		11
MEAN		
15.01		
DEV		
0.72		

CORE SAMPLE
0.090"
3.10
0.150"
3.75
0.360"
3.59
0.770"
2.69
0.980"
2.41
1.040"
2.46
1.090"
2.40
1.150"
2.43
CALC TOTAL
651
EDGE
0.119"

RUN	95	WAVES		96	CORE SAMPLE	97	CORE SAMPLE
CAM	B	VEL	TIME	-		-	
		14.2	32		0.140"		0.153"
SAMP	-	14.4	44	T	1.03	C	1.50
		14.0	24				
LIQ	997	14.8	32	1004	0.260"	993	0.419"
		13.6	40		0.64		1.31
GAS	506	15.0	56	508		511	
		13.8	56		0.580"		0.685"
TEMP	34.8	13.3	44	32.7	0.27	36.0	1.19
		13.5	32				
PT	19.36	15.0	48		0.920"	17.92	0.951"
		14.8	48		0.41		1.23
PB	15.00	14.0	68	14.85		14.55	
		14.6	64		1.140"		1.217"
ΔPT	0.394	13.4	44		0.76		1.45
		13.8	52				
ΔPB	0.466	14.6	44		CALC		CALC
		14.8	32		TOTAL		TOTAL
VOID	.016	15.3	68		176		303
			32				
PT		MEAN	36		EDGE		EDGE
		14.27	28		0.101"		0.107"
PB		DEV	28			565	
		0.60	32				
DRVD			60				
			52				
P11	19.25		28				
			44				
Δ11	0.388		44				
VRT	297.2		MEAN				
			43				
P235	15.18		DEV	15.03		14.83	
			12				
Δ235	0.475						
DEN	.0725			.0724		.0704	
VS	200.9			202.0		209.0	
VRB	338.0						
NREL	1642			1583		1675	

RUN	98S
CAM	T
SAMP	T
LIQ	1008
GAS	518
TEMP	33.9
PT	
PB	14.80
ΔPT	
ΔPB	
VOID	
FT	
FB	
DRVD	
P11	
Δ11	
VRT	
P235	14.97
Δ235	
DEN	.0717
VS	208.0
VRB	
NREL	1630

WAVES					
VEL	TIME	19	19	11	
		23	22	22	0.110"
11.5	19	11	19	15	1.58
12.3	19	22	19	19	
11.1	23	23	15	15	0.260"
11.8	19	15	19	23	3.27
12.1	11	19	19	30	
12.6	19	11	23	22	0.580"
11.1	19	19	11	23	1.37
11.8	34	11	19	11	
11.1	30	19	26	11	0.910"
10.5	22	11	22	22	4.14
11.8	19	15	23	15	
11.9	23	19	11	11	1.140"
10.8	26	15	11	19	6.19
10.8	15	22	15	19	
11.8	15	19	15	23	CALC
10.8	15	15	11	15	TOTAL
10.8	30	15	15	15	885
11.8	15	11	15	22	
12.3	11	23	11	23	EDGE
11.8	11	19	11	19	0.095"
12.2	22	15	11	11	
11.9	19	22	11	19	
12.2	15	19	19	15	
11.1	30	30	11	15	
11.8	19	26	19	15	
11.4	15	11	26	11	
11.1	26	19	22	19	
9.9	11	19	11	11	
11.9	23	15	11		
	15	23	11	MEAN	
MEAN	15	15	15	18	
11.52	22	15	11	DEV	
DEV	15	19	23	5.1	
0.62		15			

RUN	99S	WAVES	CORE SAMPLE	100S	WAVES	CORE SAMPLE
CAM	C	VEL 30		B	VEL TIME 39	
		15.9 39	0.100"		15.9 16 20	0.130"
CAMP	C	15.4 26	1.58	B	14.6 16 27	5.54
		14.9 26			16.7 16 12	
LIQ	1003	13.6 26	0.140"	999	11.6 20 20	0.250"
		15.9 22	1.21		14.0 24 16	4.38
GAS	511	12.4 17		506	13.6 27 27	
		13.6 43	0.380"		16.0 23 31	0.580"
TEMP	33.5	15.9 22	2.10	32.4	12.6 20 22	3.69
		13.2 17			13.9 39 12	
PT		16.8 30	0.770"	18.69	11.7 12 23	0.910"
		13.2 22	2.49		12.4 31 16	3.32
PB	14.40	14.0 13		14.77	13.7 20 20	
		13.9 30	1.020"		12.8 20 27	1.150"
ΔPT		14.9 26	1.38	0.512	14.6 12 16	2.14
		14.9 26			11.7 20 20	
ΔPB		16.3 26	1.070"	0.456	14.2 12 27	CALC
		16.0 26	1.34		13.0 20 27	TOTAL
VOID		14.4 22		.0076	20 27	767
		14.4 48	1.110"		MEAN 31 31	
PT	486	16.4 26	1.31		13.71 24 22	EDGE
		13.6 22			DEV 27 23	0.113"
PB	222	30	1.150"		1.49 12 35	
		MEAN 22	1.24		16 16	
DRVD		14.74 35			16	
		DEV 22	CALC		27 MEAN	
P11		1.22 30	TOTAL	18.54	12 22	
		17	362		27 DEV	
Δ11		TIME 22	EDGE	0.501	7.1	
VRT		30 MEAN	0.101"	301.8		
		17 26				
P235	14.57	26 DEV		14.94		
		26 7.3				
Δ235				0.465		
DEN	.0700			.0721		
VS	210.2			202.1		
VRB				339.2		
NREL	1608			1566		

RUN	101S	CORE SAMPLE	102	WAVES		103	WAVES	
CAM	-		B	VEL	11	B	VEL	TIME
		0.120"			8			
SAMP	B	5.57	-	19.5	11	-	15.0	25
				18.5	11		14.8	33
LIQ	998	0.160"	989	19.2	15	1502	13.9	29
		5.85		18.5	11		13.9	51
GAS	520		868	18.8	8	376	13.9	44
		0.380"		19.2	11		13.9	36
TEMP	34.3	4.51	33.2	18.5	8	38.4	13.9	33
				19.9	11		15.3	25
PT		0.770"	24.08	18.8	8	18.90	13.8	47
		3.91		18.5	11		13.9	44
PB	14.79		15.05	19.8	15	14.67	15.0	51
		1.030"		20.4	11		15.0	25
ΔPT		3.29	1.025	21.1	8	0.468	15.3	22
				18.9	11		12.9	29
ΔPB		1.080"	0.927	19.6	11	0.487	16.3	33
		2.85		19.5	11		12.9	29
VOID			.003	18.5	8	.028	14.8	51
		1.130"		19.5	8		14.1	40
FT	154	2.41		18.3	8			36
				18.8	8		MEAN	29
FB	170	CALC		17.1	11		14.37	
		TOTAL		18.2	8		DEV	MEAN
DRVD		860			8		0.85	36
				MEAN	11			DEV
P11		EDGE	23.79	19.05	8	18.77		9.1
		0.113"		DEV	8			
Δ11			0.991	0.83	11	0.459		
					8			
VRT			388.4	TIME	8	288.3		
				15	8			
P235	14.96		15.41	11	11	14.85		
				8	8			
Δ235			0.962	11	15	0.497		
				8	8			
DEN	.0716		.0741	11		.0698		
				11	MEAN			
VS	2091		337.2		9.7	155.1		
					DEV			
VRB			491.2		2.9	327.4		
NREL	1627		1576			2656		

RUN	104	WAVES		105	WAVES		106	WAVES	
		VEL	TIME		VEL	TIME		VEL	TIME
CAM	B	9.5	247	B	10.4	115	B	8.7	172
		8.8	285		11.8	307		10.2	172
SAMP	-	8.4	133	-	9.3	96	-	9.5	229
		9.1	266		10.6	211		10.8	229
LIQ	2011	11.2	304	2011	9.7	192	2021	12.5	191
		8.8	171		9.4	192		10.9	172
GAS	0	9.6	133	27.0	9.6	96	51.5	13.6	344
		10.4	266		10.8	230		13.6	287
TEMP	40.1	10.2	114	40.1	8.3	269	39.9	13.1	325
		9.5	323		11.1	173		12.7	344
PT	14.78	10.4	285	14.95	9.5	115	14.97	13.1	382
		9.5	114		9.5	269		12.0	115
PB	14.82	11.2	304	14.95	9.6	307	14.88	12.3	96
		10.2			9.5	154		12.3	
ΔPT	0.001		MEAN	0	9.6		0.003		MEAN
		MEAN	227		8.9	MEAN		MEAN	235
ΔPB	0	9.77	DEV	0		195	0.012	11.81	DEV
		DEV	77		MEAN	DEV		DEV	89
VOID	.134	0.83		.123	9.85	72	.121	1.49	
FT					DEV				
					0.84				
FB									
DRVD									
P11	14.78			14.95			14.97		
Δ11	0.001			0			0.003		
VRT	22.3			87.4			121.6		
P235	14.82			14.95			14.88		
Δ235	0			0			0.012		
DEN	.0691			.0697			.0695		
VS	0			11.20			21.3		
VRB	22.3			87.5			122.0		
NREL	3674			3674			3679		

RUN	107	WAVES		108	WAVES		109	WAVES	
CAM	B	VEL	TIME	B	VEL		B	VEL	TIME
		12.0	96		18.7			16.2	44
SAMP	-	12.0	96	-	18.0		-	14.2	44
		11.6	134		17.4			14.9	26
LIQ	2006	14.2	191	1989	18.7		2007	13.0	36
		13.6	153		15.6			14.9	44
GAS	126.8	10.9	76	250	17.4		377	14.5	40
		13.6	172		16.2			16.6	33
TEMP	39.3	14.2	134	38.5	15.8		38.6	14.9	44
		13.1	115		16.2			14.3	26
PT	15.98	14.2	210	17.61	16.5		19.46	16.2	33
		12.6	115		17.1			14.7	26
PB	14.94	13.1	172	14.97	18.7		14.58	15.7	40
		14.2	134					16.6	33
ΔPT	0.112	13.1	191	0.277	MEAN		0.518	15.8	36
		11.5	115		17.19			14.9	29
ΔPB	0.105	14.2	134	0.303	DEV		0.576	14.9	36
		12.6	115		1.10			13.0	29
VOID	.100	16.4	115	.067			.030	13.8	26
		14.7	95		TIME			16.3	36
PT		11.5	134		75			16.2	33
		12.0	172		64			13.8	40
PB		14.2	191		128			13.8	29
		13.6			70			13.8	36
DRVD		13.1	MEAN		75			13.7	33
		15.3	139		93				
P11	15.95	16.4	DEV	17.53	41		19.31	MEAN	MEAN
			37		70			14.86	34
Δ11	0.111	MEAN		0.274	46		0.507	DEV	DEV
		13.38			104			1.09	6.0
VRT	189.3	DEV		262.5	58		318.5		
		1.41			52				
P235	14.98			15.08	70		14.80		
Δ235	0.105			0.307	MEAN		0.590		
					73				
DEN	.0701			.0708	DEV		.0695		
					23				
VS	52.1			101.7			156.1		
VRS	196.0			284.7			367.7		
MREL	3610			3524			3549		

RUN	110	WAVES		111	WAVES		112	WAVES	
CAM	B	VEL	TIME	B	VEL		B	VEL	TIME
SAMP	-	19.4	20	-	22.2	12	-	18.2	51
		20.8	32		22.1	12		14.9	33
LIQ	2018	20.8	44	1984	22.1	16	2496	19.0	33
		15.7	44		19.6	8		15.7	26
GAS	475	19.4	40	861	17.4	12	373	16.6	44
		18.8	56		19.4	16		17.6	37
TEMP	37.3	18.3	40	34.7	19.4	8	39.1	14.0	40
		17.2	32		22.1	8		17.6	47
PT	21.16	17.4	24	27.01	21.4	8	19.85	18.1	25
		17.4	20		20.6	8		14.3	24
PB	14.89	18.5	40	14.42	21.4	12	14.55	15.3	25
		18.6	60		22.1	8		16.6	44
ΔPT	0.299	17.9	32	1.301	21.4	8	0.547	14.9	24
		17.9	48		19.8	12		16.6	69
ΔPB	0.716	17.9	60	1.680	22.1	8	0.649	12.9	36
		17.4	60		22.1	8		17.6	44
VOID	.032	16.9	24	.013	20.6	8	.046	14.3	40
		18.3	32		21.4	8		17.6	37
FT		18.6	32		18.7	12		16.6	40
		19.4	40		20.6	12		14.9	36
FB		19.1			21.4	16		15.2	37
			MEAN			12		16.6	33
DRVD		MEAN	39		MEAN	16		18.2	33
		18.37	DEV		20.85	8		16.6	47
P11	21.07	DEV	12.6	26.65	DEV	12	19.69	15.3	22
		1.19			1.31	8		16.1	36
Δ11	0.296			1.252		8	0.535	18.2	47
					TIME	12		MEAN	33
VRT	349.9			446.8	8	8	342.6	16.28	MEAN
					20			DEV	39
P235	15.16			15.10	8	MEAN	14.80	1.53	DEV
					20	10.6			6.8
Δ235	0.736			1.796		DEV	0.667		
						3.5			
DEN	.0716			.0721			.0693		
VS	190.9			343.7			155.0		
VRB	417.6			606.5			399.7		
NREL	3493			3260			4474		

RUN	113	WAVES		CORE SAMPLE	114	WAVES		CORE SAMPLE
CAM	T	VEL	72		C	VEL	TIME	
			85	0.180"				0.110"
SAMP	T	10.1	36	1.78	B	9.9	79	4.17
		8.5	60			10.3	46	
LIQ	2697	9.2	48	0.300"	2692	12.7	85	0.160"
		10.4	85	0.28		15.2	112	2.27
GAS	123.7	10.1	54		129	11.8	72	
		8.8	54	0.580"		11.5	66	0.360"
TEMP	33.7	9.2	91	0.19	37.4	14.0	79	2.10
		10.4	48			11.8	79	
PT		10.3	72	0.890"		12.7	131	0.770"
		8.6	48	0.23		11.9	79	2.69
PB	14.85	8.5	54		14.71	12.2	79	
		10.1	85	1.100"		11.8	118	1.000"
ΔPT		10.2	66	0.33		11.8	53	1.81
		9.5	54			12.7	46	
ΔPB		10.0	42	CALC		11.8	92	1.080"
		10.7	60	TOTAL		13.1	66	1.79
VOID		11.9	115	170		13.6	39	
		10.3	54			11.3	105	1.150"
PT		10.7	115	EDGE	2457	12.2	138	2.13
		8.9	42	0.137"		12.1		
PB		10.4	54		2569	10.4	MEAN	CALC
		9.7	84			11.8	82	TOTAL
DRVD		9.4	97			9.9	DEV	381
			79				27	
P11		MEAN	72			MEAN		EDGE
		9.82	91			12.02		0.161"
Δ11		DEV	60			DEV		
		0.83	60			1.23		
VRT			72					
		TIME						
P235	14.90	30	MEAN		14.76			
		48	64					
Δ235		42	DEV					
		42	21					
DRH	.0715	66			.0697			
		42						
VH	49.8				53.3			
VRH								
MRH	4342				4668			

RUN	115	CORE SAMPLE	1165	WAVES	CORE SAMPLE	1170	WAVES	CORE SAMPLE
CAM	-		T	VEL		T	VEL	
		0.153"			0.140"			0.140"
CAMP	C	4.10	T	10.3	10.78	T	11.2	4.20
				9.2			9.0	
LIQ	2712	0.419"	2705	10.3	0.260"	2708	11.6	0.260"
		0.24		10.3	2.86		12.9	1.69
GAS	126.1		120	10.3		123	11.6	
		0.685"			0.580"		10.4	0.580"
TEMP	38.3	0.21	39.1	MEAN	1.18	36.7		1.20
				10.08			MEAN	
PT		0.951"		DEV	0.920"		11.12	0.920"
		0.26		0.44	1.36		DEV	2.00
PB	14.87		14.74			14.95	1.20	
		1.217"		WAVES	1.140"			1.140"
ΔPT		9.21		VERY	2.63		WAVES	2.55
				DIFF-			VERY	
ΔPB		CALC		ICULT	CALC		DIFF-	CALC
		TOTAL		TO	TOTAL		ICULT	TOTAL
VOID		159		FOLLOW	521		TO	450
				VEL			FOLLOW	
PT	2250	EDGE		BASED	EDGE		VEL	EDGE
		0.149"		ON	0.131"		BASED	0.131"
PB				"LUMPS"			ON	
				OF			"LUMPS"	
DRVD				WATER			OF	
							WATER	
P11								
Δ11								
VRT								
P235	14.92		14.79			15.00		
Δ235								
DEN	.0701		.0693			.0710		
VS	51.8		49.9			49.9		
VRB								
NREL	4787		4849			4632		

RUN	1185	WAVES		CORE SAMPLE	1195	WAVES		CORE SAMPLE
CAM	C	VEL	TIME	0.130"	B	VEL	TIME	0.140"
SAMP	C	11.2	123	2.62	B	13.0	139	3.35
		10.2	68			12.1	41	
LIQ	2703	9.8	92	0.180"	2702	13.9	116	0.250"
		11.2	117	1.03		13.9	145	1.95
GAS	123	11.6	98		126	14.4	215	
		12.1	92	0.360"		14.4	93	0.580"
TEMP	36.7	11.7	68	0.44	35.6	12.8	133	3.02
		10.9	61			12.8	75	
PT		10.5	67	0.780"	15.93	13.0	87	0.900"
		10.2	61	0.40		11.6	128	2.42
PB	14.88	11.9			15.00	10.8	122	
		9.9	MEAN	1.090"		12.0	168	1.140"
ΔPT		12.4	85	0.45	0.090	15.4	110	1.92
		11.7	DEV			11.6	41	
ΔPB		11.9	22	CALC	0.129			CALC
		10.5		TOTAL		MEAN	MEAN	TOTAL
VOID		9.8		126	.1265	12.98	115	420
		11.0				DEV	DEV	
PT	2480	10.8		EDGE		1.25	45	EDGE
				0.143"				0.161"
PB	2350	MEAN						
		11.02						
DRVD		DEV						
		0.80						
P11					15.90			
Δ11					0.090			
VRT					214.6			
P235	14.93				15.05			
Δ235					0.130			
DEN	.0707				.0716			
VS	50.1				50 .7			
VRB					221.2			
NRSL	4623				4521			

RUN	120	WAVES			CORE SAMPLE	121	WAVES		CORE SAMPLE
CAN	T	VEL	TIME	36		C	VEL	TIME	
				30	0.160"				0.090"
SAMP	T	13.2	46	53	2.07	B	16.2	46	3.81
		13.7	53	38			15.0	54	
LIQ	2691	13.5	27	38	0.280"	2700	18.5	92	0.160"
		13.9	38	38	0.99		14.5	33	4.01
GAS	246.5	13.9	42	30		264	16.2	67	
		14.3	38	30	0.580"		19.1	58	0.360"
TEMP	37.7	12.9	42	27	0.54	36.8	15.6	71	8.29
		13.1	50	46			14.4	63	
PT		14.6	34	23	0.900"		16.9	33	0.760"
		15.9	38	61	0.56		16.1	46	6.11
PB	14.71	12.4	30	23		14.49	15.7	46	
		12.9	34	42	1.120"		16.8	38	0.990"
ΔPT		13.7	27	30	0.86		16.6	54	4.39
		13.5	30	30			17.9	46	
ΔPB		12.5	46	38	CALC		14.4	50	1.050"
		13.9	19	23	TOTAL		18.7	50	3.94
VOID		14.9	30	42	360		13.9	54	
		14.3	30	34			14.4	92	1.110"
FT		12.9	27	42	EDGE	1908	16.2	42	3.67
		13.2	38	27	0.125"		16.9	38	
FB		12.6	34	34		1444		71	1.150"
		13.5	38	50			MEAN	67	3.35
DRVD		14.6	30	46			16.20		
		14.6	27				DEV	MEAN	CALC
P11		13.3	53	MEA			1.49	56	TOTAL
		14.6	42	37				DEV	1121
Δ11		13.5	46	DEV				16	
		12.9		9.0					EDGE
VMT		15.5							0.137"
		15.5							
P235	14.48					14.62			
		MEAN							
Δ235		13.79							
		DEV							
DEN	.699	0.91				.0692			
VS	101.5					109.8			
VRB									
NREL	4694					4628			

RUN	122	CORE SAMPLE	1238	WAVES	CORE SAMPLE
CAM	-		T	VEL	
		0.153"			0.140"
CAMP	C	2.49	T	11.8	1.42
				13.2	
LIQ	2720	0.419"	2712	14.5	0.260"
		1.50		15.8	0.82
GAS	256		246	15.8	
		0.685"		15.8	0.580"
TEMP	37.9	1.43	38.3	MEAN	1.11
				14.48	
PT		0.951"		DEV	0.920"
		1.32		1.53	1.40
PB	14.75		14.63		
		1.217"		WAVES	1.140"
ΔPT		7.43		VERY	1.50
				DIFF-	
ΔPB		CALC		ICULT	CALC
		TOTAL		TO	TOTAL
VOID		431		FOLLOW	318
				VEL	
PT		EDGE		BASED	EDGE
		0.131"		ON	0.119"
PB				"LUMPS"	
				OF	
DRVD				WATER	
P11					
Δ11					
VRT					
P235	14.75		14.63		
Δ235					
DEN	.0701		.0694		
VL	105.1		102.1		
VRB					
NRSL	4764		4787		

RUN	1245	WAVES		CORE SAMPLE	1255	WAVES		CORE SAMPLE
CAM	C	VEL	TIME	0.120"	B	VEL	TIME	0.130"
CAMP	C	15.0	29	3.35	B	13.0	54	6.12
		18.1	25			17.6	54	
LIQ	2712	15.5	50	0.160"	2700	17.6	58	0.250"
		15.0	42	2.22		10.8	89	12.81
GAS	249	16.1	42		260	10.6	81	
		15.0	46	0.380"		12.8	69	0.580"
TEMP	37.1	14.5	54	2.75	33.2	10.1	97	11.29
		15.0	50			15.6	66	
PT		15.5	38	0.770"	18.10	15.6	50	0.900"
		12.7	50	1.64		15.6	31	7.40
PB	14.70	14.5	63		14.90	16.9	81	
		13.2	33	1.030"		11.3	58	1.140"
ΔPT		12.5	42	1.35	0.342	15.1	81	2.49
		14.5	50			16.8	31	
ΔPB		15.0	42	1.080"	0.377	11.6		CALC
		12.5	25	1.35			MEAN	TOTAL
VOID		15.0	38		.078	MEAN	64	1608
		14.6	29	1.130"		14.07	DEV	
PT	2270	11.4	50	1.25		DEV	19	EDGE
			29			2.62		0.149"
PB	1800	MEAN	46	CALC				
		14.51	58	TOTAL				
DAVD		DEV	46	418				
		1.48						
P11			MEAN	EDGE	18.00			
			42	0.137"				
Δ11			DEV		0.337			
			10					
VBT					298.3			
P235	14.70				15.04			
Δ235					0.383			
DEN	.0701				.0723			
VL	102.3				103.5			
VEB					328.2			
NUEL	4675				4303			

RUN	1265	CORE SAMPLE	127
CAN	-		T
		0.120"	
SAMP	B	6.35	T
LIQ	2704	0.170"	2703
		12.70	
GAS	258		502
		0.380"	
TEMP	37.1	14.78	35.4
PT		0.770"	
		11.05	
PB	14.52		14.95
		1.000"	
ΔPT		5.54	
ΔPB		1.080"	
		3.84	
VOID			
		1.150"	
FT	1268	2.87	
FB	1286	CALC TOTAL	
DRVD		1847	
P11		EDGE	
		0.149"	
Δ11			
VRT			
P235	14.66		15.19
Δ235			
DEN	.0693		.0723
VS	107.2		199.9
VRB			
NREL	4662		4505

WAVES			CORE SAMPLE
VEL	TIME	23	
		15	0.140"
16.5	23	19	2.89
17.6	15	19	
19.6	15	23	0.260"
19.0	15	23	1.27
19.6	15	11	
17.1	15	23	0.580"
18.2	19	19	0.73
17.7	27	19	
15.5	15	30	0.920"
16.0	30	15	0.80
18.2	26	19	
18.7	30	19	1.140"
17.6	30	23	1.49
18.3	15	15	
16.5	19	19	CALC
16.5	23	19	TOTAL
17.6	30	26	403
17.6	15	19	
17.1	23	19	EDGE
16.0	23	15	0.125"
17.1	19	19	
17.6	15	15	
18.2	19	19	
18.2	15	23	
17.1	19	15	
16.0	23	23	
18.7	30	27	
	27	19	
MEAN	30	26	
17.55	15	27	
DEV	15	23	
1.07	23	19	
	11	15	
	23		
		MEAN	
		20	
		DEV	
		5.0	

RUN	128	WAVES			CORE SAMPLE	129	CORE SAMPLE
CAM	C	VEL	TIME	33		-	
				29	0.080"		0.153"
SAMP	B	22.0	46	29	6.32	C	2.75
		23.4	37	37			
LIQ	2700	24.0	29	33	0.150"	2700	0.419"
		20.9	37	37	10.69		2.28
GAS	534	20.9	25	33		507	
		17.9	42	25	0.350"		0.685"
TEMP	36.7	21.7	29	21	10.59	38.1	2.20
		18.4	58	33			
PT		19.3	46	29	0.750"		0.951"
		21.7	33	29	7.29		2.22
PB	14.31	22.0	25	37		14.59	
		20.0	37	62	0.990"		1.217"
ΔPT		22.5	42	25	6.12		3.51
		25.0	33	37			
ΔPB		22.6	54	33	1.050"		CALC
		21.7	37	37	6.37		TOTAL
VOID		19.3	42	25			513
		24.0	42		1.100"		
PT	836	17.9	62	MEAN	6.26	1880	EDGE
		24.0	58	37			0.125"
PB	998	24.0	21	DEV	1.150"		
		17.9	50	10	5.92		
DRVD		20.9	33				
		20.0			CALC		
P11		21.7			TOTAL		
		22.5			1739		
Δ11		20.9					
		20.0			EDGE		
VRT		20.0			0.131"		
		MEAN					
P235	14.55	21.28				14.83	
		DEV					
Δ235		1.96					
DEN	.0689					.0698	
VS	223.1					209.1	
VRB							
MASL	4618					4747	

RUN	1308	WAVES				CORE SAMPLE
CAM	T	VEL	12	19	16	
			16	16	16	0.140"
SAMP	T	17.1	16	12	16	7.71
		14.0	23	19	16	
LIQ	2706	16 .1	19	12	16	0.260"
		13.4	16	19	16	8.06
GAS	496	16.1	23	12	16	
		14.6	19	19	16	0.580"
TEMP	37.3	15.1	23	12	12	10.15
		14.1	12	16	16	
PT		14.1	12	12	19	0.920"
		15.6	19	12	23	10.15
PB	14.90	15.4	16	19	12	
		14.6	16	23	12	1.140"
ΔPT		13.8	12	19	16	6.66
		15.6	19	8	12	
ΔPB		16.6	16	16	12	CALC
		16.0	16	19	12	TOTAL
VOID		14.3	19	19	16	1770
		16.0	16	12	16	
PT			16	19	19	EDGE
		MEAN	16	23	23	0.119"
PB		15.14	19	12	16	
		DEV	12	12	19	
DRVD		1.04	16	19	16	
			12	19	16	
P11		TIME	12	19	12	
			12	16		
Δ11		16	12	16	MEAN	
		12	16	12	15.6	
VRT		12	16	23	DEV	
		12	12	12	3.7	
P235	15.14	12	16	12		
Δ235						
DEN	.0715					
VS	199.7					
VRB						
PREL	4683					

RUN	1315	WAVES		CORE SAMPLE
CAM	C	VEL	25	
			25	0.100"
SAMP	C	16.7	33	3.96
		19.3	25	
LIQ	2700	17.6	25	0.140"
		18.2	33	5.06
GAS	521	16.9	25	
		15.1	17	0.380"
TEMP	36.7	13.7	21	5.10
		15.6	21	
PT		15.6	17	0.770"
		15.0	17	5.61
PB	14.63	16.7	29	
		15.2	33	1.020"
ΔPT		16.7	29	6.86
		15.6	29	
ΔPB		16.7	21	1.070"
		15.1	29	8.03
VOID		14.6	17	
		15.2	17	1.110"
FT	1340	16.9	37	7.06
			37	
FB	483	MEAN	42	1.150"
		16.13	17	4.94
DRVD		DEV	37	
		1.32	21	CALC
P11			29	TOTAL
		TIME	21	1165
Δ11			33	
		37	29	EDGE
VRT		29	25	0.119"
P235	14.87		MEAN	
			27	
Δ235			DEV	
			7.1	
DEN	.0704			
VS	213.1			
VRS				
NRML	4618			

1328	WAVES			CORE SAMPLE
B	VEL	TIME	20	
			12	0.130"
B	13.9	20	24	33.9
	13.9	20	20	
2700	12.7	28	35	0.260"
	12.0	12	20	16.18
514	11.6	24	20	
	10.5	12	24	0.580"
34.7	12.7	20	31	10.14
	11.5	16	28	
19.49	11.6	27	16	0.900"
	14.1	16	27	8.82
14.60	13.0	24	28	
	14.1	12	31	1.140"
0.852	10.5	28	35	4.58
	13.7	35	20	
	12.5	24	16	CALC
	13.7	27	24	TOTAL
.0185	12.9	20	27	2521
	12.6	20	28	
	14.1	24	20	EDGE
	13.3	24	20	0.125"
		20	24	
	MEAN	8	20	
	12.75	24	16	
	DEV	16		
	1.12	16	MEAN	
		16	22	
		12	DEV	
		16	6.1	
		20		
		20		
14.84		24		
		24		
		31		
		24		
.0709		20		
208.7				
493.5				
4437				

RUN	133B	CORE SAMPLE	134	WAVES		135	WAVES	
CAN	-		B	VEL	TIME	B	VEL	TIME
		0.100"						
CAN2	B	24.30	-	13.4	100	-	16.5	40
				15.0	184		18.8	29
LIQ	2702	0.150"	3026	16.2	167	2993	19.0	33
		23.99		17.5	284		17.1	22
GAS	529		120.3	17.5	167	375	19.9	33
		0.390"		16.2	117		15.6	33
TEMP	35.4	11.99	40.9	15.0	184	38.6	16.1	22
				16.2	200		17.7	59
PT		0.750"	16.07	16.9	84	20.40	17.6	26
		8.25		17.5	150		16.1	58
PB	14.41		14.77	18.1	117	14.52	16.1	47
		0.970"		12.5	234		15.8	26
APT		7.04	0.099	15.4	84	0.590	15.7	37
				17.5	117		17.6	29
APB		1.020"	0.144	16.9	200	0.743	17.1	22
		7.06		15.0	167		19.4	51
VOID			.129	17.5	84	.057	18.8	22
		1.080"		18.7	134		17.1	40
PT	434	6.04		18.7	234		17.6	29
				16.2	200		19.4	36
PB	191	1.150"		17.5	134		16.1	37
		4.27		19.4	167		14.2	22
DRVD				16.2	150		17.6	51
		CALC		15.0	100		19.4	44
P11		TOTAL	16.04	18.7	150	20.23	19.4	
		2349		17.5	167			MEAN
Δ11			0.099	14.6	MEAN	0.577	MEAN	35
		EDGE		16.9	157		17.43	DEV
VRT		0.125"	222.3	15.6	DEV	365.2	DEV	11
				MEAN	50		1.49	
P235	14.65		14.82	16.53		14.80		
				DEV				
Δ235			0.145	1.59		0.767		
DEN	.0697		.0688			.0695		
VS	218.5		50.3			155.4		
VAB			232.2			431.8		
NREL	4503		5614			5314		

RUN	136	WAVES		137	WAVES		138	WAVES	
CAM	B	VEL	TIME	B	VEL	TIME	B	VEL	TIME
SAMP	-	10.5	242	-	16.1	88	-	22.5	43
		10.3	190		14.8	88		21.2	38
LIQ	3362	10.8	242	3517	13.1	123	3476	23.2	49
		10.0	311		16.6	106		20.8	86
GAS	0	12.5	156	122.5	14.3	123	252	19.3	49
		9.4	277		14.8	88		19.3	76
TEMP	41.7	10.0	156	41.1	14.8	123	40.2	21.6	59
		12.9	156		15.4	158		18.6	81
PT	14.95	12.9	242	16.45	14.7	123	18.74	23.2	113
		11.2	260		16.6	106		21.2	27
PB	14.90	9.9	208	14.96	14.3	123	14.92	20.6	108
		10.3	138		16.6	88		19.3	49
ΔPT	0	12.0	138	0.094	17.8	158	0.285	21.6	38
		12.0	329		14.8	123			49
ΔPB	0	10.8	381	0.163	16.6	88	0.438	MEAN	113
		10.8	259		16.6	141		20.95	43
VOID	.183	10.4	121	.151	16.6	123	.097	DEV	54
		10.3	138		15.4	141		1.45	
FT		12.0	277		16.1	158			MEAN
		10.8	208		15.4	211			63
FB		11.1	225		14.3	123			DEV
					15.4	141			27
DRVD		MEAN	MEAN		14.3	194			
		11.00	222		15.4	194			
P11	14.95	DEV	DEV	16.42	16.6	176	18.66		
		0.99	69		14.3	158			
Δ11	0			0.094	17.2	88	0.282		
						158			
VRT	37.2			238.1	MEAN	106	326.0		
					15.51	141			
P235	14.90			15.02	DEV		15.08		
					1.11	MEAN			
Δ 235	0			0.164		132	0.446		
						DEV			
DEN	.0689			.0697		34	.0703		
VS	0			50.6			103.2		
VRB	37.3			249.8			365.7		
MREL	6332			6550			6364		

RUN	139	WAVES		140	WAVES	
CAM	B	VEL	TIME	B	VEL	TIME
SAMP	-	20.1	39	-	23.7	30
		18.3	43		22.8	27
LIQ	3515	20.7	43	3524	25.5	23
		20.1	47		24.1	34
GAS	490	21.4	51	702	21.9	27
		21.4	70		21.9	42
TEMP	39.0	18.7	27	38.5	21.9	27
		18.0	31		21.9	42
PT	23.03	18.3	43	27.12	24.1	38
		18.0	27		21.9	30
PB	14.14	17.2	55	14.97		42
		18.7	47		MEAN	27
ΔPT	0.857	16.8	59	1.266	22.97	30
		18.2	31		DEV	27
ΔPB	1.116	18.7	58	1.456	1.23	30
		16.0	59			19
VOID	0.049	20.3	62	.035		42
		18.7	31			30
FT		18.7	35			27
		18.3	51			19
FB		21.4	39			46
		22.9				57
DRVD			MEAN			19
		MEAN	45			38
P11	22.79	19.13	DEV	26.77		30
		DEV	12			27
Δ11	0.832	1.66		1.220		30
						46
VRT	428.1			486.4		
						MEAN
P235	14.58			15.55		32
						DEV
Δ235	1.170			1.541		9.0
DEN	.0683			.0730		
VS	206.4			276.7		
VRB	544.3			651.5		
NREL	6288			6244		

RUN	141	WAVES			142	WAVES	
CAN	B	VEL	11	19	B	VEL	TIME
			19	30			
SAMP	-	21.9	15	27	-	18.3	29
		23.0	15	30		19.5	29
LIQ	3383	20.6	19	23	3696	21.6	47
		21.9	11	15		18.3	47
GAS	813	21.9	11	15	369	16.2	51
		23.3	27	23		18.3	44
TEMP	38.0	23.3	19	19	38.6	15.8	47
		24.1	11	11		16.6	33
PT	29.23	23.0	11	15	21.05	18.2	33
		22.8	19	15		18.2	36
PB	14.39	24.1	15	19	14.48	17.2	40
		20.8	23	15		17.7	47
ΔPT	1.526	20.8	23	15	0.617	18.3	36
		23.0	15	19		17.2	25
ΔPB	2.058	21.9	27	19	0.789	21.0	36
		21.9	11	19		19.5	25
VOID	.034	21.9	15	23	.066	20.0	62
		24.6	8	15		16.6	36
FT		19.5	15	19		19.5	54
		21.9	15	19		19.7	36
FB		20.8	15	11		15.8	54
		21.9	27	11		17.2	58
DRVD		22.9	23	15			62
		23.1	15	11		MEAN	47
P11	28.81	24.7	19	19	20.87	17.76	40
			23	23		DEV	40
Δ11	1.463	MEAN	15	19	0.603	1.93	
		22.38	15	19			MEAN
VRT	503.5	DEV	19	15	389.7		42
		1.28	15	19			DEV
P235	15.23		15	15	14.78		10
		TIME	23				
Δ235	2.228		19	MEAN	0.816		
		11	19	18			
DEN	.0717	15	23	DEV	.0694		
		23	23	4.8			
VS	326.5	19	27		153.0		
			19				
VRB	708.6		11		468.5		
NREL	5937				6562		

RUN	143	WAVES	144	WAVES	145	WAVES
CAM	B	VEL	B	VEL	B	VEL
SAMP	-	4.4	-	5.1	-	6.6
		4.4		4.8		6.4
LIQ	98.5	4.2	100.3	4.0	99.4	6.4
		4.5		4.4		6.0
GAS	0		152.1	5.0	376	6.6
		MEAN				6.2
TEMP	23.1	4.38	24.7	MEAN	28.0	6.0
		DEV		4.66		5.8
PT	44.86	0.11	44.81	DEV	45.13	5.8
				0.40		6.2
PB	44.67	TIME	44.84		44.67	6.4
				TIME		
ΔPT	0	577	0		0.041	MEAN
		733		853		6.22
ΔPB	0	377	0.007	924	0.007	DEV
		955		498		0.28
VOID	.025		.025	284	.013	
		MEAN		711		TIME
PT		660				
		DEV		MEAN		64
PB		211		654		121
				DEV		83
DAVD				235		184
						210
P11	44.86		44.81		45.12	57
						133
Δ11	0		0		0.041	95
						83
VRT	1.1		42.4		92.4	171
P235	44.67		44.84		44.67	MEAN
						120
Δ235	0		0.007		0.007	DEV
						51
DEN	.2257		.2252		.2217	
VS	0		19.4		48.8	
VRB	1.1		42.4		92.9	
MRB	125.7		132.8		141.8	

RUN	146	WAVES		147	WAVES		148	WAVES	
CAM	B	VEL	TIME	B	VEL	TIME	B	VEL	TIME
SAMP	-	12.5	116	-	14.0	53	-	4.7	350
		12.5	34		13.6	28		5.3	250
LIQ	99.4	12.5	53	99.8	14.4	37	299	4.3	275
		12.5	34		14.4	37		4.7	150
GAS	797	12.5	52	1245	14.0	66	0	4.3	175
		12.5	90		13.2	66		4.7	450
TEMP	29.2	11.5	79	30.8	14.4	25	27.3	5.0	250
		11.1	49		14.0	21		5.3	225
PT	47.09	12.5	56	48.62	13.6	70	46.16	5.0	250
		10.7	45		13.6	20		4.7	325
PB	45.54	10.7	68	45.19	13.6	37	45.68	5.3	150
		12.0	41			61		5.3	475
ΔPT	0.153	10.2	75	0.230	MEAN	37	0	4.3	175
		12.0	34		13.89	37		5.3	
ΔPB	0.135	12.0	71	0.292	DEV	25	0.004		MEAN
		12.0	60		0.38	33		MEAN	269
VOID	.002	11.1	53	0			.049	4.87	DEV
		12.0	83			MEAN		DEV	102
FT		11.5	105			41		0.38	
		12.0	64			DEV			
FB						16			
		MEAN	MEAN						
DRVD		11.82	63						
		DEV	DEV						
P11	47.05	0.70	22	48.55			46.16		
Δ11	0.153			0.229			0		
VRT	121.6			265.7			5.3		
P235	45.59			45.30			45.68		
Δ235	0.135			0.293			0.004		
DEN	.2253			.2226			.2273		
VS	101.9			161.1			0		
VRB	184.7			284.9			3.3		
NREL	145.5			151.2			420		

RUN	149	WAVES		150	WAVES		
CAM	B	VEL.	TIME	T	VEL.	25	37
						19	19
SAMP	-	6.0	276	-	6.3	44	19
		6.4	248		5.6	25	31
LIQ	300	6.4	193	300	6.5	25	25
		5.5	580		6.7	37	37
GAS	156.0	5.7	221	396	6.1	44	50
		4.9	331		6.1	31	25
TEMP	28.7	6.0	221	31.8	6.9	37	37
		5.3	386		6.0	31	31
PT	45.12	6.4	331		6.7	37	31
		5.7	138		6.9	37	37
PB	45.05	6.2	386	44.92	6.5	31	37
		6.0	193		6.5	43	25
ΔPT	0.009	5.3	193		6.5	44	31
		5.1	331		6.3	37	25
ΔPB	0.007	4.7	166		6.0	19	37
		5.3	193		6.3	31	31
VOID	.039	6.4	497			25	31
		6.0	166		MEAN	25	44
FT		5.3	386		6.37	44	33
		4.7	110		DEV	43	25
FB		5.8	359		0.34	25	31
		5.7	524			31	25
DRVD		5.3	166		TIME	25	44
		4.9	221			31	43
P11	45.12	5.7	193		31	25	37
		5.3	166		37	31	19
Δ11	0.009	5.1	193		31	44	25
		5.7	359		25	25	50
VRT	57.0				31	37	37
		MEAN	MEAN		37	37	50
P235	45.05	5.60	276	44.95	37	44	31
		DEV	DEV		37	31	
Δ235	0.007	0.51	121		37	31	MEAN
					37	31	33
DEN	.2230			.2201	37	25	DEV
					19	43	7.9
VS	20.1			51.8		25	
VRB	57.1						
NREL	435			464			

RUN	151	WAVES		CORE SAMPLE	152	WAVES		153
CAM	C	VEL	TIME		B	VEL	TIME	-
				0.100"				
SAMP	B	7.5	97	0.15	-	8.4	128	-
		7.8	97			9.1	73	
LIQ	300	8.3	84	0.160"	304	8.9	122	300
		8.3	84	0.13		8.7	128	
GAS	397	7.8	71		394	8.7	37	391
		8.2	52	0.370"		8.4	73	
TEMP	30.9	7.8	45	0.14	29.0	9.4	98	34.4
		8.0	39			6.8	79	
PT		7.9	84	0.760"	46.37	9.4	73	
		7.4	45	0.14		8.9	116	
PB	44.97	8.6	84		45.31	8.7	92	44.81
		8.4	97	1.010"		8.9	55	
ΔPT		8.1	45	0.14	0.082	8.5	73	
		8.1	71			8.5	49	
ΔPB		8.0	71	1.090"	0.070	8.9	122	
		7.2	78	0.136		9.4	165	
VOID		7.2	110		.023			
		9.7	77	1.150"		MEAN	MEAN	
FT	256	8.6	45	0.125		8.73	93	270
		7.4	45			DEV	DEV	
FB	284	7.7	52	CALC		0.59	34	
		7.9	45	TOTAL				
DRVD		7.8		30				
		8.9	MEAN					
P11		7.8	69	EDGE	46.35			
			DEV	0.107"				
Δ11		MEAN	21		0.082			
		8.02						
VRT		DEV			112.1			
		0.54						
P235	45.00				45.34			44.84
Δ235					0.070			
DEN	.2211				.2242			.2175
VS	51.7				50.6			51.8
VRB					113.4			
NREL	455				443			490

RUN	154S	WAVES		CORE SAMPLE	155S	WAVES		CORE SAMPLE
CAM	T	VEL.	TIME		C	VEL.	TIME	
				0.120"				0.130"
SAMP	T	6.6	24	0.15	C	7.1	65	0.37
		6.9	56			6.9	33	
LIQ	301	6.6	56	0.280"	300	6.4	97	0.180"
		6.4	28	0.16		7.3	72	0.37
GAS	394	6.3	16		387	6.7	71	
		6.3	44	0.580"		7.1	117	0.360"
TEMP	36.0	5.4	32	0.38	33.0	7.4	78	0.34
		5.9	24			7.2	104	
PT		5.3	28	0.910"		5.2	111	0.780"
		5.5	60	0.355		5.9	98	0.29
PB	45.19	6.2	36		45.07	6.4	117	
			28	1.140"		6.6	72	1.090"
ΔPT		MEAN	36	0.36		5.3	97	0.34
		6.13	60			6.0	124	
ΔPB		DEV	64	CALC			162	CALC
		0.51	40	TOTAL		MEAN		TOTAL
VOID			44	61		6.54	MEAN	76
			44			DEV	94	
FT			40	EDGE	212	0.69	DEV	EDGE
			48	0.107"			30	0.107"
FB			60		243			
			40					
DRVD			40					
			52					
P11			64					
Δ11			MEAN					
			43					
VRT			DEV					
			14					
P235	45.22				45.10			
Δ235								
DEN	.2181				.2199			
VS	52.0				50.7			
VRB								
NRYL	508				476			

RUN	156S
CAM	B
SAMP	B
LIQ	301
GAS	396
TEMP	33.2
PT	46.08
PB	45.27
ΔPT	0.069
ΔPB	0.086
VOID	.0268
FT	
FB	
DRVD	
P11	46.06
Δ11	0.069
VRT	113.6
P235	45.30
Δ235	0.086
DEN	.2207
VS	51.7
VRB	114.6
NREL	480

WAVES	
VEL.	TIME
9.0	108
8.3	102
9.0	84
9.3	96
9.3	108
8.9	114
7.9	60
8.2	72
8.5	72
9.5	96
9.1	54
9.5	108
9.1	66
8.9	132
	90
MEAN	78
8.89	
DEV	MEAN
0.47	90
	DEV
	21

CORE SAMPLE
0.120"
0.21
0.240"
0.21
0.580"
0.22
0.920"
0.19
1.140"
0.18
CALC
TOTAL
44
EDGE
0.107"

RUN	157
CAM	T
SAMP	C
LIQ	299
GAS	770
TEMP	33.7
PT	
PB	44.94
ΔPT	
ΔPB	
VOID	
FT	251
FB	
DRVD	
P11	
Δ11	
VRT	
P235	45.01
Δ235	
DEN	.2188
VS	101.3
VRB	
NREL	481

WAVES				CORE SAMPLE
VEL	TIME			
		25	19	
		25	19	0.140"
11.2	12	25	19	0.25
10.7	25	31	19	
11.4	19	25	12	0.260"
10.7	19	19	12	0.225
11.5	12	12	19	
10.7	25	19	12	0.580"
11.1	12	12	12	0.17
9.8	12	19	19	
11.1	19	19	19	0.920"
9.8	12	19	12	0.19
10.0	19	25	12	
10.7	12	12	25	1.140"
11.5	19	19	19	0.23
10.7	19	19	19	
9.8	12	19	19	CALC
10.4	12	31	19	TOTAL
10.1	19	19	25	57
10.7	19	19	19	
	12	19	19	EDGE
MEAN	12	12	12	0.089"
10.66	19	19	25	
DEV	25	31	19	
0.56	19	19	25	
	12	25	19	
	25	25	12	
	19	25	25	
	19	12	12	
	19	19	25	
	19	12	19	
	19	19		
			MEAN 19	
			DEV 4.8	

RUN	158	WAVES		CORE SAMPLE	159	WAVES	
CAM	C	VEL	TIME		B	VEL	TIME
				0.090"			
SAMP	B	12.5	34	0.56	-	12.4	39
		11.6	51			12.9	59
LIQ	300	12.1	55	0.150"	302	12.9	51
		11.7	55	0.61		13.3	39
GAS	774	11.6	38		799	12.4	78
		11.7	51	0.350"		12.0	35
TEMP	30.3	12.7	38	0.65	29.9	12.9	43
		12.1	30			12.9	39
PT		11.4	30	0.760"	48.02	13.3	43
		11.2	42	0.56		12.0	63
PB	44.92	12.1	25		45.42	12.0	63
		12.5	63	0.990"		12.4	51
ΔPT		12.5	25	0.55	0.205	12.4	20
		11.4	42			12.0	35
ΔPB		11.6	21	1.050"	0.183	11.1	63
		12.1	47	0.55		11.5	47
VOID		12.3	21		.006	11.1	39
		10.9	34	1.100"		11.5	47
PT	227	11.7	25	0.55		10.6	27
		11.7	68			12.0	55
PB	147	11.2	21	1.150"		13.3	67
		11.2	30	0.54		10.6	31
DRVD		10.9	42			13.3	71
		11.6	34	CALC		12.0	39
P11		11.2	25	TOTAL	47.96	10.2	35
		11.7	34	146		12.4	63
Δ11			25		0.204	12.9	20
		MEAN	25	EDGE			24
VRT		11.73		0.083"	198.5	MEAN	51
		DEV	MEAN			12.16	
P235	44.99	0.50	37		45.49	DEV	MEAN
			DEV			0.87	46
Δ235			13		0.183		DEV
							15
DEN	.2215				.2243		
VS	100.6				102.6		
VRB					204.3		
NRSL	450				449		

NUB	160	CORE SAMPLE	1618	WAVES			CORE SAMPLE
CAM	-		T	VEL	TIME	32	
		0.120"				28	0.280"
SAMP	T	0.18	T	8.6	28	16	0.47
				8.3	24	24	
LIQ	298	0.240"	300	8.1	12	20	0.580"
		0.06		8.3	16	20	0.63
GAS	763		764	8.5	16	24	
		0.580"		8.5	20	16	0.920"
TEMP	32.2	0.012	36.9	8.1	20	24	0.76
				7.9	12	16	
PT		0.940"		8.4	16	28	1.140"
		0.024		8.1	16	24	0.71
PB	45.12		44.79	8.4	28	24	
		1.160"		9.0	20	24	CALC
APT		0.13		8.3	20	24	TOTAL
				7.6	28	24	144
APB		CALC		7.8	28	36	
		TOTAL		9.0	16	32	EDGE
VOID		29		8.1	24	32	0.089"
				9.0	24	20	
FT		EDGE		9.0	32	32	
		0.095"		8.4	20	32	
FB				8.3	32	28	
				7.7	28	40	
DRVD					16	24	
				MEAN	28	24	
P11				8.34	32	32	
				DEV	24	24	
A11				0.40	20	24	
					16	20	
VRT					28	32	
					20		
P235	45.20		44.88		20	MEAN	
					32	24	
A 235					20	DEV	
						5.4	
DEN	.2210		.2158				
VS	99.4		101.9				
VRB							
NREL	465		515				

RUN	162S	WAVES		CORE SAMPLE	163S	WAVES		CORE SAMPLE
CAM	C	VEL	TIME		B	VEL	31	
				0.120"			28	0.130"
SAMP	C	10.2	48	0.91	B	13.2	31	0.70
		9.5	48			14.1	31	
LIQ	300	9.9	26	0.160"	300	12.4	55	0.250"
		9.5	39	0.92		13.3	51	0.75
GAS	769	9.5	39		793	12.2	35	
		8.8	39	0.380"		14.2	31	0.580"
TEMP	33.5	8.3	66	0.92	34.9	12.6	27	0.66
		8.0	48			12.7	47	
PT		9.5	53	0.770"	47.34	12.6	39	0.910"
		10.3	44	0.85		12.1	35	0.61
PB	45.10	9.5	44		44.93	12.1	35	
		8.1	57	1.030"		12.1	20	1.140"
APT		7.2	39	0.66	0.182	12.5	51	0.59
		8.5	31			12.0	28	
APB		8.6	70	1.055"	0.238	13.1	27	CALC
		10.2	57	0.65		12.5	26	TOTAL
VOID		8.9	22		.0082	12.2	59	160
		9.5	61	1.130"		11.4	24	
PT	102	9.2	35	0.60		12.6	31	EDGE
			44			12.1	63	0.083"
PB	35	MEAN	22	CALC		12.1	31	
		9.12	66	TOTAL		11.3	28	
DRVD		DEV	66	190		12.0	43	
		0.82	39			12.9	20	
P11			57	EDGE	47.29		27	
			39	0.083"		MEAN	24	
A11					0.181	12.51	16	
			MEAN			DEV	39	
VAT			46		200.5	0.69	43	
			DEV				27	
P235	45.19		13		45.02	TIME		
							MEAN	
A235					0.239	28	34	
						43	DEV	
DSN	.2199				.2180		12	
VS	100.7				104.8			
VRB					205.8			
NREL	481				495			

RUN	164	WAVES				CORE SAMPLE
CAM	T	VEL	8	16	12	
			12	12	8	0.140"
SAMP	C	13.6	8	12	16	0.54
		14.3	8	12	12	
LIQ	302	14.0	12	12	8	0.260"
		13.6	8	12	8	0.454
GAS	1218	14.3	8	12	8	
		16.1	8	8	12	0.580"
TEMP	34.3	16.0	12	12	16	0.34
		15.2	8	8	12	
PT		13.8	8	12	16	0.920"
		14.7	8	12	8	0.394
PB	44.73	14.7	8	16	16	
		14.7	12	12	12	1.140"
ΔPT		14.0	12	16	12	0.49
		14.7	8	12	12	
ΔPB		14.7	16	16	19	CALC
		15.6	8	12	12	TOTAL
VOID		14.0	12	8	12	117
		13.4	8	12	12	
PT	168	13.2	8	16	8	EDGE
			12	12	12	0.077"
PB		MEAN	8	16	12	
		14.45	16	12	12	
DRVD		DEV	8	12	8	
		0.81	12	12	8	
P11			16	16	12	
		TIME	8	8		
Δ11			8	16	MEAN	
		12	8	19	10.9	
VRT		8	8	12	DEV	
		8	8	12	2.9	
P235	44.86	12	8	8		
Δ235						
DEN	.2177					
VS	161.1					
VRB						
MRAL	492					

RUN	165
CAM	C
SAMP	B
LIQ	300
GAS	1210
TEMP	30.2
PT	
PB	44.68
ΔPT	
ΔPB	
VOID	
FT	177
FB	94
DRVD	
P11	
Δ11	
VRT	
P235	44.81
Δ235	
DEN	.2207
VS	157.9
VRB	
NREL	449

WAVES		
VEL	13.2	23
	15.0	32
15.7	16.2	18
15.7		18
16.2	MEAN	37
15.5	15.45	32
17.2	DEV	27
16.7	0.95	23
13.2		14
14.1	TIME	23
15.4		32
15.5	18	18
16.2	18	23
16.7	9	27
15.4	23	28
15.7	41	14
14.5	23	23
14.6	18	32
15.7	14	18
15.7	14	23
15.0	32	14
15.7	37	18
15.0	14	23
15.9	18	14
14.1	32	9
15.7	28	18
15.2	18	
16.2	23	MEAN
15.7	27	23
15.9	28	DEV
15.2	18	7.3
15.7	23	
16.7	27	
15.7		
13.2		
17.1		
15.5		
15.0		

CORE SAMPLE	166
	B
0.080"	-
0.93	
0.150"	300
1.03	
	1232
0.350"	
0.94	31.1
0.740"	49.50
0.75	
	45.11
0.980"	
0.76	0.500
1.040"	0.362
0.79	
	.002
1.100"	
0.89	
1.150"	
0.91	
CALC	
TOTAL	49.36
142	
	0.496
EDGE	
0.077"	287.9
	45.24
	0.354
	.2221
	159.7
	301.6
	458

WAVES	
VEL	TIME
14.8	20
13.1	28
14.3	28
13.6	20
14.3	24
13.1	24
15.8	28
14.0	20
13.4	32
14.8	20
15.8	28
14.3	24
15.8	36
15.8	36
15.2	28
14.8	20
15.8	20
15.3	28
	20
MEAN	12
14.67	28
DEV	24
0.93	28
	36
	24
	40
	36
	28
	MEAN
	26
	DEV
	6.3

RUN	167	CORE SAMPLE	168S	WAVES			169S	CORE SAMPLE
CAM	-		T	VEL	8	16	-	
		0.120"			12	12		0.110"
SAMP	T	0.38	-	12.6	12	12	T	1.16
				14.3	20	8		
LIQ	301	0.250"	300	12.5	16	12	303	0.250"
		0.18		13.2	8	12		1.01
GAS	1202		1224	12.9	8	16	1222	
		0.580"		13.2	12	12		0.580"
TEMP	32.6	0.03	34.8	12.1	20	12	36.1	1.47
				12.8	12	16		
PT		0.930"		12.8	16	28		0.920"
		0.08		12.3	16	12		1.14
PB	44.78		44.67	10.5	12	12	45.15	
		1.160"		12.6	16	12		1.150"
ΔPT		0.30		11.5	12	16		0.87
				12.9	12	20		
ΔPB		CALC		11.8	12	12		CALC
		TOTAL		12.6	20	16		TOTAL
VOID		61			16	16		270
				MEAN	8	16		
PT		EDGE		12.54	16	16		EDGE
		0.077"		DEV	24	16		0.077"
PB				0.81	16	20		
					16	16		
DRVD				TIME	16	12		
					16	24		
P11				12	16	20		
				12	12	12		
Δ11				8	12	8		
				12	8	12		
VRT				12	12	8		
				8	8			
P235	44.92		44.82	8	20	MEAN	45.30	
					8	13.6		
Δ235						DEV		
						4.2		
DEN	.2193		.2171				.2184	
VC	157.8		162.3				161.1	
VRB								
NREL	474		494				512	

RUN	1703
CAM	0
SAMP	0
LIQ	299
GAS	1224
TEMP	33.6
PT	
PB	44.71
ΔPT	
ΔPB	
VOID	
PT	78
PB	23
DRVD	
P11	
Δ11	
VRT	
P235	44.86
Δ235	
DEN	.2182
VS	161.5
VRB	
MODL	480

WAVES

VEL	21	17
	17	13
12.3	8	17
10.7	13	17
11.2	13	13
11.3	8	21
10.7	13	17
11.6	8	17
11.6	8	25
10.3	17	17
10.3	17	21
10.7	13	21
11.1	13	21
10.7	21	13
11.2	13	17
11.2	21	13
10.7	21	17
10.7	21	25
11.6	17	17
10.2	17	8
9.8	17	30
12.8	17	17
11.2	21	30
10.6	12	25
9.8	17	13
10.7	21	21
	17	17
MEAN	17	8
10.96	30	13
DEV	13	15
0.69	13	8
	17	13
TIME	25	13
	17	
17	8	MEAN
21	21	17
17	13	DEV
		5.1

CORE SAMPLE

0.100"	
1.14	
0.140"	
1.14	
0.380"	
1.16	
0.770"	
0.99	
1.020"	
0.59	
1.070"	
0.57	
1.110"	
0.53	
1.150"	
0.51	
CALC	
TOTAL	
226	
EDGE	
0.077"	

RUN	1715	WAVES			CORE SAMPLE	1725	CORE SAMPLE
CAM	B	VEL	11	7		-	
			15	8	0.110"		0.100"
SAMP	B	14.9	11	11	1.08	B	1.07
		14.5	15	11			
LIQ	300	14.9	19	26	0.250"	301	0.140"
		12.2	8	11	0.95		1.14
GAS	1216	14.9	7	11		1215	
		12.7	15	11	0.580"		0.380"
TEMP	34.4	14.5	8	15	0.75	33.2	0.94
		14.3	15	15			
PT	47.92	14.9	15	19	0.910"		0.770"
		15.6	11	15	0.70		0.74
PB	44.70	14.7	11	11		44.66	
		16.1	7	11	1.160"		1.020"
ΔPT	0.287	15.1	11	15	0.76		0.79
		14.0	8	15			
ΔPB	0.412	14.5	7	15	CALC		1.070"
		14.0	8	11	TOTAL		0.80
VOID	.0025		15	15	143		
		MEAN	11	15			1.110"
PT		14.49	11	19	EDGE	81	0.80
		DEV	7	15	0.077"		
PB		0.93	11	11		99	1.150"
			8	22			0.81
DRVD		TIME	7	15			
			15	15			CALC
P11	47.84	19	19	11			TOTAL
		15	11	11			225
Δ11	0.286	11	22	11			
		22	11	11			EDGE
VRT	291.1	19	11	19			0.077"
		7	8	11			
P235	44.85	15	15	11		44.81	
		8	7	11			
Δ235	0.414	7	22	11			
		11	8				
DEN	.2176	8	22	MEAN		.2183	
		7	22	12.9			
VS	160.9		19	DEV		160.2	
				4.5			
VRB	301.3						
NREL	490					480	

RUN	173	WAVES		174	WAVES		
CAM	B	VEL	TIME	B	VEL	13.4	28
						13.4	32
SAMP	-	9.9	64	-	13.9	13.4	24
		9.2	51		13.0	14.2	28
LIQ	597	9.5	102	596	13.4		32
		10.1	83		14.2	MEAN	28
GAS	394	10.8	89	803	11.9	13.33	36
		10.9	127		12.8	DEV	36
TEMP	31.4	10.1	102	32.4	13.9	0.80	16
		10.9	76		14.3		48
PT	46.54	8.6	25	48.04	12.4	TIME	32
		9.8	70		13.4		24
PB	45.27	10.8	83	45.10	14.3	44	28
		9.8	64		13.4	24	44
ΔPT	0.114	10.1	96	0.341	11.9	48	40
		10.1	108		13.9	32	36
ΔPB	0.116	9.8	76	0.249	14.3	32	48
		10.5	70		12.4	16	20
VOID	.038	7.4	45	.015	12.8	36	48
		10.1	76		12.8	32	44
PT		10.9	115		14.3	44	20
					13.9	64	
PB		MEAN	MEAN		13.9	16	MEAN
		9.96	80		11.9	44	34
DRVD		DEV	DEV		12.4	16	DEV
		0.85	24		13.9	24	11
P11	46.51			47.94	11.9	48	
					13.4	36	
Δ11	0.114			0.339	14.3		
VRT	132.7			224.0			
P235	45.31			45.19			
Δ235	0.116			0.250			
DEN	.2222			.2208			
VB	51.1			104.7			
VRB	134.5			231.3			
NREL	916			934			

RUN	175	WAVES	176	WAVES		177	WAVES		CORE SAMPLE
CAM	B	VEL	B	VEL	TIME	T	VEL	32	
								45	0.140"
CAMP	-	6.9	-	7.2	193	C	8.6	19	0.675
		7.2		7.2	75		9.4	45	
LIQ	999	6.9	996	7.2	349	997	8.9	26	0.260"
		7.5		7.2	199		8.9	32	0.18
GAS	0	6.4	158.6	7.5	398	388	8.2	32	
		6.0		7.7	224		8.6	45	0.580"
TEMP	32.9	6.9	32.5	7.7	274	33.7	7.8	32	0.13
		7.2		7.7	299		8.9	39	
PT	45.40	6.9	45.31	7.2	125		8.3	32	0.920"
		6.7		6.7	249		7.4	26	0.15
PB	45.25	7.2	45.12	7.7	124	45.02	8.6	52	
				7.7	174		8.9	19	1.140"
ΔPT	0	MEAN	0.011	7.5	100		8.9	39	0.35
		6.89		7.7	100		8.9	32	
ΔPB	0	DEV	0.009	7.7	199		7.9	26	CALC
		0.40		8.1	224		9.1	26	TOTAL
VOID	.088		.077	7.2	249			32	76
		TIME		8.1	124		MEAN	19	
PT				8.3	199	849	8.62	26	EDGE
		508					DEV	19	0.125"
PB		194		MEAN	MEAN		0.52	26	
		363		7.54	204			26	
DRVD		242		DEV	DEV		TIME	32	
		315		0.38	85				
P11	45.40	169	45.31				32	MEAN	
		242					26	30	
Δ11	0	411	0.011				26	DEV	
		145					19	8.4	
VRT	11.1	169	90.1						
		194							
P235	45.25		45.12			45.07			
		MEAN							
Δ235	0	268	0.009						
		DEV							
DEN	.2207	111	.2204			.2192			
VS	0		20.7			51.0			
VRB	11.1		90.3						
NREL	1582		1564			1605			

RUN	178	WAVES		CORE SAMPLE
CAM	C	VEL	TIME	
				0.090"
SAMP	B	11.3	50	1.22
		11.3	43	
LIQ	1000	11.0	43	0.150"
		11.3	71	0.77
GAS	386	10.4	57	
		11.0	57	0.210"
TEMP	31.9	10.4	57	0.74
		11.7	85	
PT		10.1	43	0.280"
		10.4	57	0.75
PB	44.94	10.4	43	
		10.4	36	0.760"
ΔPT		10.1	36	0.85
		9.8	57	
ΔPB		10.7	78	0.940"
		10.4	64	0.77
VOID		11.7	50	
		9.7	36	1.080"
FT	913	10.7	85	0.75
		10.1	50	
FB	883	10.1	43	1.150"
		11.0	43	0.80
DRVD		12.1	64	
		10.9	64	CALC
P11		9.4	50	TOTAL
		12.4	43	150
Δ11		10.7	71	
		10.1	43	EDGE
VRT		10.1	57	0.137"
		10.4	50	
P235	44.99	10.7	43	
		10.4	71	
Δ^{235}		9.8	36	
		11.1	28	
DEN	.2202	10.6	57	
		10.1	43	
VS	50.5	9.8	64	
VRB		MEAN	MEAN	
		10.61	53	
NREL	1551			
		DEV	DEV	
		0.67	14	

RUN	179	WAVES		180	CORE SAMPLE
CAM	B	VEL	TIME	-	0.140"
SAMP	-	10.9	76	T	0.59
		10.2	70		
LIQ	994	10.9	64	999	0.240"
		10.2	95		0.044
GAS	392	10.5	76	382	
		10.5	89		0.580"
TEMP	31.9	11.3	63	32.9	0.006
		10.5	89		
PT	46.43	10.5	114		0.930"
		10.9	102		0.036
PB	44.99	10.9	70	45.13	
		11.3	83		1.140"
ΔPT	0.117	10.5	108		0.094
		10.2	70		
ΔPB	0.127	10.9	76		CALC TOTAL
		10.5			
VOID	.054		MEAN		46
		MEAN	83		
FT		10.67			EDGE
		DEV	DEV		0.125"
FB		0.34	15		
DRVD					
P11	46.40				
Δ11	0.117				
VRT	155.2				
P235	45.04			45.18	
Δ235	0.127				
DEN	.2205			.2204	
VS	51.1			49.9	
VRB	157.9				
NREL	1542			1582	

RUN	1813	WAVES			CORE SAMPLE	1823	WAVES		CORE SAMPLE
CAM	T	VEL	37	31		C	VEL	TIME	
			38	38	0.140"				0.130"
SAMP	T	7.5	37	19	1.33	C	7.8	72	2.88
		7.5	31	19			10.6	46	
LIQ	997	6.7	31	31	0.250"	1007	9.9	33	0.180"
		7.1	25	19	1.06		9.5	66	3.24
GAS	383	7.1	25	31		410	9.9	52	
		7.5	38	19	0.580"		8.8	59	0.360"
TEMP	37.9	7.4	31	56	0.98	34.4	7.8	59	2.18
		7.0	25	19			8.9	66	
PT		8.3	19	31	0.920"		9.5	46	0.780"
		6.7	25	19	0.92		6.6	66	2.02
PB	44.67		44	13		45.24	8.7	66	
		MEAN	44	25	1.150"		9.2	85	1.090"
ΔPT		7.28	31	19	1.12		9.9	33	2.98
		DEV	25	12			9.9	52	
ΔPB		0.45	25	19	CALC		8.6	33	CALC
			37	25	TOTAL		9.2	39	TOTAL
VOID		TIME	31	19	235		9.9	46	584
			25	37			8.1	39	
PT		19	38		EDGE	400	8.1	33	EDGE
		25	25	MEAN	0.119"		8.8	26	0.119"
PB		25	19	28		358	9.5	52	
		31	31	DEV			8.9	39	
DRVD			19	8.8				59	
			37				MEAN	39	
P11							9.00		
							DEV	MEAN	
Δ11							0.91	50	
								DEV	
VRT								15	
P235	44.73					45.30			
Δ235									
DEN	.2143					.2197			
VS	51.5					53.7			
VRB									
NRML	1746					1645			

RUN	1838
CAM	B
SAMP	B
LIQ	1002
G.S	386
TEMP	34.3
PT	46.47
PB	45.12
ΔPT	0.121
ΔPB	0.169
VOID	.052
PT	
PB	
DRVD	
P11	46.43
Δ11	0.121
VRT	155.0
P235	45.18
Δ235	0.169
DEN	.2192
VS	50.7
VRB	157.2
NRML	1633

WAVES	
VEL	TIME
9.5	65
12.4	47
11.4	59
11.4	71
11.9	82
8.4	94
12.4	94
11.0	65
11.4	65
11.1	76
7.9	65
13.2	41
12.8	76
12.4	88
13.3	82
11.0	47
9.8	71
11.5	41
11.9	76
10.6	76
11.0	100
11.5	47
MEAN	MEAN
11.26	69
DEV	DEV
1.36	17

CORE SAMPLE
0.110"
1.07
0.250"
0.85
0.580"
0.94
0.910"
0.86
1.160"
0.84
CALC TOTAL
174
EDGE
0.131"

RUN	184
CAM	T
LAMP	C
LIQ	994
GAS	769
TEMP	35.8
PT	
PB	45.07
ΔPT	
ΔPB	
VOID	
PT	662
PB	
DAVD	
P11	
Δ11	
VRT	
P235	45.21
Δ235	
DEN	.2182
VS	101.5
VRB	
ARRL	1670

WAVES				CORE SAMPLE
VEL	TIME			
		16	24	
		16	12	0.140"
13.3	20	16	20	0.97
13.7	20	16	16	
12.9	12	24	16	0.260"
13.5	12	28	20	0.93
13.5	12	16	16	
13.3	24	20	16	0.580"
12.9	24	24	16	0.74
14.4	24	16	20	
13.3	20	20	20	0.920"
12.9	16	16	20	0.83
13.9	16	16	12	
13.5	16	16	20	1.140"
12.7	28	16	20	0.91
12.0	20	16	20	
12.9	12	16	20	CALC
13.3	24	20	28	TOTAL
12.9	24	24	20	172
12.7	20	20	16	
13.3	16	16	20	EDGE
13.3	16	16	20	0.119"
12.5	8	20	12	
13.3	16	16	20	
12.9	12	16		
12.9	16	20	MEAN	
12.9	24	16	18	
13.3	12	16		
14.4	28	20	DEV	
	24	20	4.2	
MEAN				
13.20				
DEV				
0.51				

RUN	185	WAVES			CORE SAMPLE	186	WAVES	
CAM	C	VEL	TIME	44		B	VEL	TIME
				17	0.080"			
SAMP	B	14.4	30	22	2.20	-	14.7	41
		16.2	17	30			14.1	41
LIQ	998	16.4	30	35	0.140"	995	15.4	16
		13.3	30	22	2.59		14.5	28
GAS	798	13.8	22	22		800	15.4	45
		15.0	30	26	0.210"		13.9	29
TEMP	30.4	16.0	39	39	3.01	34.0	14.7	20
		14.4	44	26			12.8	20
PT		14.9	13	52	0.280"	48.85	14.7	37
		14.4	26	35	3.21		14.7	24
PB	44.71	15.6	26	43		44.92	15.4	45
		15.6	26	30	0.750"		14.1	57
ΔPT		13.9	35	31	2.36	0.438	14.7	20
		14.4	17	39			14.7	61
ΔPB		12.5	35	26	0.980"	0.356	15.4	24
		14.4	43	35	2.30		15.4	53
VOID		14.4	35	30		.027	14.7	41
		13.3	35	35	1.020"		13.9	24
FT	724	14.4	39	26	2.31		13.9	41
		14.4	30	30			14.1	33
FB	532	14.9	35	22	1.150"		15.4	20
		15.0	17	26	2.17		15.4	24
DRVD		15.4	52	44			14.7	45
		15.4	26	26	CALC		14.7	45
P11		13.8	35	30	TOTAL	48.72	13.9	49
		15.0	13	26	548		15.4	45
Δ11		14.4	22	35		0.435	13.7	45
		14.9	52	35	EDGE		13.9	57
VRT			35	13	0.125"	250.1	12.8	20
		MEAN	31				14.1	20
P235	44.85	14.66	39	MEAN		45.05	14.7	28
			26	31			14.7	33
Δ235		DEV	18			0.358		24
		0.88	39	DEV			MEAN	
DEN	.2207		39	9.1		.2188	14.52	MEAN
							DEV	35
VS	104.1					105.3	0.70	DEV
								13
VRB						260.9		
NREL	1499					1612		

RUN	187	CORE SAMPLE	188S
CAM	-		T
		0.130"	
SAMP	T	1.05	T
LIQ	1003	0.250"	997
		0.44	
GAS	755		788
		0.580"	
TEMP	34.1	0.19	39.1
PT		0.940"	
		0.27	
PB	45.24		44.07
		1.150"	
ΔPT		0.67	
ΔPB		CALC	
		TOTAL	
VOID		130	
FT		EDGE	
		0.119"	
FB			
DRVD			
P11			
Δ11			
VRT			
P235	45.38		44.21
Δ235			
DEN	.2204		.2109
VS	98.6		107.6
VRB			
NREL	1628		1787

WAVES				CORE SAMPLE
VEL	12	16	23	
	8	20	20	0.140"
13.0	16	20	24	1.51
10.6	12	12	20	
13.1	16	12	16	0.250"
13.6	12	8	20	2.12
12.6	12	16	16	
11.1	16	16	16	0.580"
11.4	8	8	12	1.23
11.1	16	20	16	
11.1	16	12	8	0.920"
11.7	12	20	16	1.33
12.2	16	20	27	
12.6	16	12	28	1.140"
11.6	16	20	20	1.76
11.1	8	20	16	
12.0	16	16	24	CALC
12.4	24	12	27	TOTAL
11.7	12	24	16	371
10.6	16	8	20	
11.8	16	20	28	EDGE
	12	24	16	0.113"
MEAN	16	20	12	
11.86	12	16	16	
	16	16	20	
DEV	16	20	16	
0.83	20	16	12	
	20	16		
TIME	12	16	MEAN	
	24	16	16	
16	16	16		
16	20	8	DEV	
16	16		4.6	

RUN	1898	WAVES		CORE SAMPLE	1900	WAVES		CORE SAMPLE
CAM	C	VEL	42		B	VEL	30	
			42	0.120"			19	0.100"
SAMP	C	10.8	42	3.93	B	13.6	31	2.63
		11.1	17			17.1	42	
LIQ	997	9.5	25	0.160"	1000	13.1	19	0.250"
		10.3	34	4.64		13.6	42	3.23
GAS	785	11.7	38		770	13.6	34	
		10.3	25	0.380"		13.3	27	0.580"
TEMP	34.6	10.6	29	3.79	34.4	15.2	30	2.57
		9.6	29			13.9	27	
FT		11.0	46	0.770"	48.11	12.0	19	0.910"
		9.6	34	3.78		14.2	34	2.29
FB	44.78	10.3	42		45.01	13.6	15	
		8.2	42	1.020"		15.3	27	1.160"
ΔFT		9.2	25	3.26	0.384	15.8	19	2.01
		8.9	46			13.3	38	
ΔFB		9.9	42	1.080"	0.384	14.3	38	CALC
		10.7	21	3.27		14.2	38	TOTAL
VOID		9.9	38		.026	15.0	42	545
		11.0	25	1.130"		13.3	53	
FT	234		34	3.29		13.3	34	EDGE
		MEAN	42			15.1	34	0.125"
FB	243	10.14	42	CALC		14.7	31	
		DEV	25	TOTAL		14.2	15	
DRVD		0.86	25	809			34	
			42			MEAN	27	
F11		TIME	34	EDGE	48.00	14.17	42	
			21	0.119"		DEV	30	
Δ11		21	42		0.382	1.08	38	
		13	46				34	
VRT		25	25		245.6	TIME	42	
		21	42				23	
F235	44.92	25			45.15	23	15	
		17	MEAN			27		
Δ235		34	32		0.386	23	MEAN	
			DEV			31	31	
DEN	.2177		9.5		.2190	19	DEV	
						46	9.2	
VS	103.8				101.2			
VRB					253.8			
KMEL	1635				1633			

RUN	1919	CORE SAMPLE	192
CAN	-		T
		0.120"	
SAMP	B	4.05	C
LIQ	1004	0.160"	995
		4.63	
GAS	789		1220
		0.380"	
TEMP	33.9	3.97	33.9
PT		0.770"	
		3.52	
PB	44.73		44.85
		1.030"	
ΔPT		3.21	
ΔPB		1.080"	
		2.88	
VOID			
		1.130"	
PT	295	2.56	561
PB	282	CALC TOTAL	
DRVD		740	
P11		EDGE	
		0.125"	
Δ11			
VRT			
P235	44.87		45.07
Δ235			
DEN	.2180		.2190
VS	104.2		160.4
VRB			
NRM	1623		1608

WAVES						CORE SAMPLE
VEL	TIME	8	12	8	16	
		8	12	8	8	0.140"
16.6	12	12	16	12	12	1.75
17.8	8	8	16	12	16	
17.6	12	16	16	12	8	0.260"
17.8	12	20	12	12	12	1.50
16.7	8	16	12	12	4	
15.6	12	12	4	12	16	0.580"
15.6	8	8	8	16	16	1.17
15.6	8	8	8	8	8	
16.6	8	12	8	16	12	0.920"
16.7	12	8	8	8	8	1.28
16.6	8	12	8	16	8	
17.3	8	4	12	8	12	1.140"
17.3	8	12	16	8	12	1.64
17.8	16	8	16	8	12	
16.6	8	12	12	8	12	CALC
17.1	8	8	12	8	12	TOTAL
17.1	12	8	8	8	12	360
16.6	12	8	16	12	16	
16.1	12	16	12	12	12	EDGE
15.6	12	8	12	8	16	0.101"
16.6	12	8	8	12	16	
16.6	16	8	12	12	8	
17.3	16	16	16	12	12	
16.1	8	12	8	16	12	
17.3	8	8	12	16	8	
15.6	12	8	12	8	16	
17.3	8	12	12	8		
17.3	12	12	8	12	MEAN	
	12	12	16	12	11.4	
MEAN	16	12	12	12		
16.74	12	12	16	12	DEV	
	12	12	12	8	3.1	
DEV	16	12	12	12		
0.70	12	12	8	12		
	8					

RUN	193	WAVES					CORE SAMPLE
CAM	C	VEL	TIME	4	9	13	
				17	13	13	0.070"
SAMP	B		9	9	13	9	3.42
			17	22	9	8	
LIQ	1003		13	9	13	9	0.130"
			9	9	13	13	4.39
GAS	1215	18.6	9	8	13	13	
		19.3	9	9	9	4	0.200"
TEMP	30.7	18.6	9	9	17	22	4.57
		18.5	13	17	17	17	
PT		16.6	9	17	13	13	0.280"
		16.9	13	9	22	13	4.20
PB	44.63	17.7	9	9	9	9	
		17.9	13	8	13	9	0.750"
ΔPT		15.7	13	9	13	17	4.20
		18.6	17	13	9	13	
ΔPB		16.1	17	17	17	13	0.980"
		18.6	13	13	17	17	2.78
VOID		17.9	13	17	17	13	
		18.6	17	13	13	13	1.030"
PT	553	17.9	22	13	17	9	2.78
		17.9	9	13	17	13	
PB	232	17.5	13	17	13	13	1.150"
		18.6	9	13	17	13	2.92
DRVD		18.5	9	13	22	13	
		19.3	9	13	17	9	CALC
P11		17.2	13	13	13	13	TOTAL
		18.5	9	9	13	13	824
Δ11		15.1	9	4	9	9	
			17	13	13		EDGE
VRT		MEAN	13	9	17	MEAN	0.107"
		17.83	17	17	9	12.7	
P235	44.85		9	9	13		
		DEV	17	17	13	DEV	
Δ235		1.09	17	13	22	3.9	
					13		
DEN	.2205						
VS	158.7						
VRB							
NREL	1517						

RUN	194	WAVES		195	CORE SAMPLE
CAM	B	VEL	TIME	-	
SAMP	-	15.3	16	T	0.130" 1.41
		16.2	24		
LIQ	1002	16.2	33	996	0.260"
		16.2	16		0.65
GAS	1241	16.3	12	1211	
		17.4	16		0.580"
TEMP	30.9	16.3	16	33.7	0.17
		15.3	16		
PT	50.76	15.3	24		0.920"
		16.3	20		0.35
PB	44.64	16.2	12	45.05	
		16.2	8		1.160"
ΔPT	0.666	15.3	16		1.09
		16.2	20		
ΔPB	0.584	16.3	20		CALC TOTAL
		16.2	16		180
VOID	.0087	15.3	12		
		16.2	12		
FT			16		EDGE
		MEAN	20		0.101"
FB		16.04	32		
		DEV	20		
DRVD		0.53	28		
			16		
P11	50.57		16		
			16		
11	0.659		20		
VRT	341.4		MEAN		
			19		
P235	44.86		DEV	45.28	
			5.8		
Δ235	0.589				
DEN	.2204			.2202	
VS	162.1			158.3	
VRB	363.9				
NREL	1522			1604	

RUN	1968
CAM	T
SAMP	T
LIQ	990
GAS	1208
TEMP	39.3
PT	
PB	44.15
ΔPT	
ΔPB	
VOID	
FT	
FB	
DRVD	
P11	
Δ11	
VRT	
P235	44.35
Δ235	
DEN	.2114
VS	164.5
VRB	
NREL	1781

WAVES					
VEL	TIME	8	12	8	
		8	8	8	0.140"
15.3	8	12	6	12	2.26
15.4	16	12	8	8	
14.2	8	12	8	8	0.260"
13.6	8	8	8	8	1.25
15.9	8	12	16	8	
16.0	8	4	12	8	0.580"
15.2	8	12	8	8	1.00
13.6	4	12	8	8	
17.4	4	12	12	8	0.920"
15.9	8	4	8	8	1.53
13.6	12	8	8	8	
16.0	4	8	8	12	1.140"
17.7	8	12	4	8	3.51
16.8	8	8	4	4	
13.0	8	16	4	8	CALC
13.0	12	12	16	8	TOTAL
13.3	12	12	8	8	527
11.8	8	8	12	8	
14.4	8	12	8	8	EDGE
15.2	4	16	8	16	0.095"
	8	4	16	8	
MEAN	8	4	4	8	
14.87	8	4	8	12	
DEV	8	12	8	12	
1.55	8	8	16	16	
	12	12	12	4	
	8	8	8	12	
	8	12	8	8	
	8	8	12	12	
	8	8	12	8	
	8	8	4	8	
	8	12	16		
	12	12	8	MEAN	
	12	12	16	9.2	
	8	16	8	DEV	
			12	3.0	

CORE SAMPLE

RUN	1978	WAVES				CORE SAMPLE	1983	CORE SAMPLE
CAM	C	VEL	TIME	13	13		-	
				9	17	0.100"		0.100"
SAMP	C	13.8	9	13	17	4.48	B	5.28
		15.5	13	13	13			
LIQ	1004	14.4	13	13	13	0.140"	1000	0.140"
		14.4	9	13	22	4.43		5.78
GAS	1215	13.8	17	17	26		1218	
		12.0	9	13	17	0.380"		0.380"
TEMP	33.9	14.4	9	22	9	4.37	33.6	3.86
		13.8	9	9	17			
PT		13.2	13	9	22	0.770"		0.770"
		14.4	17	9	13	3.75		3.36
PB	44.76	12.8	9	13	22		44.56	
		13.4	9	9	17	1.020"		1.020"
ΔPT		12.8	17	17	17	2.50		2.95
		12.8	17	13	9			
ΔPB		13.3	9	13	13	1.070"		1.070"
		12.5	13	9	17	2.36		2.88
VOID		12.9	17	17	13			
		13.8	13	9	13	1.110"		1.110"
FT	148	14.4	13	9	17	2.35	146	2.77
		12.9	9	9	17			
FB	141	11.8	13	13	13	1.150"	155	1.150"
		14.4	17	9	17	2.33		2.66
DRVD		13.5	9	17	26			
		12.8	13	9	26	CALC		CALC
P11		13.8	13	9		TOTAL		TOTAL
			9	9		795		820
Δ11		MEAN	9	9	MEAN			
		13.50	9	9	13.3	EDGE		EDGE
VRT		DEV	9	9	DEV	0.101"		0.107"
		0.85	9	17	4.6			
P235	44.96						44.76	
Δ 235								
DEN	.2185						.2178	
VS	160.1						161.0	
VRB								
NREL	1623						1607	

RUN	199S
CAM	B
SAMP	B
LIQ	990
GAS	1238
TEMP	34.1
PT	49.44
PB	45.06
ΔPT	0.405
ΔPB	0.549
VOID	.0052
FT	
FB	
DRVD	
P11	49.32
Δ11	0.402
VRT	346.6
P235	45.26
Δ 235	0.553
DEN	.2198
VS	162.2
VRB	362.8
NREL	1607

WAVES					CORE SAMPLE
VEL	8	4	16	4	
	8	8	8	8	0.100"
16.4	4	4	8	4	5.60
15.2	12	8	4	8	
15.2	8	8	8	8	0.250"
14.3	4	4	16	12	4.35
14.7	8	8	8	12	
16.3	12	8	4	12	0.580"
15.8	8	12	8	16	3.16
15.8	8	12	4	8	
15.2	8	4	12	8	0.910"
16.8	12	4	8	8	2.62
14.7	8	8	12	8	
15.8	12	8	8	12	1.160"
14.7	12	8	8	4	2.87
16.4	8	16	12	8	
15.8	4	12	12	12	CALC
15.8	12	4	12	8	TOTAL
	8	16	12	8	790
MEAN	12	4	12	4	
15.56	8	12	8	12	EDGE
	8	20	8	8	0.107"
DEV	12	8	8	8	
0.71	12	8	8	12	
	12	16	8	12	
TIME	16	16	8	12	
	4	8	12		
12	8	16	12	MEAN	
12	16	12	12	9.5	
8	8	20	4		
8	8	12	12	DEV	
	12	16		3.6	

RUN	200	WAVES		201	WAVES		202	WAVES
CAM	B	VEL	TIME	B	VEL	TIME	B	VEL
SAMP	-	12.2	52	-	15.9	29	-	9.0
		12.1	92		15.9	49		8.1
LIQ	1497	13.4	78	1498	16.6	33	1998	8.0
		10.6	59		15.8	29		8.4
GAS	396	11.1	33	816	16.6	33	0	8.1
		11.1	46		15.9	41		8.7
TEMP	31.6	12.7	26	31.7	17.4	37	33.3	8.4
		11.7	85		15.9	29		8.0
PT	46.64	12.1	92	49.57	15.8	25	45.39	7.7
		12.8	78		15.2	41		9.0
PB	44.77	12.7	79	44.88	15.2	25	45.22	
		12.1	65		15.2	37		MEAN
ΔPT	0.158	12.8	52	0.503	15.8	25	0.001	8.34
		12.2	105		15.9	41		
ΔPB	0.208	12.7	85	0.463	15.9	21	0	DEV
		12.2	46		15.2	41		0.42
VOID	.070	12.1	78	.038	15.2	37	.135	
		12.8	79		15.9	58		TIME
FT		10.8	65		15.9	37		
		12.7	92		14.6	41		224
FB		11.3	137		15.2	25		134
			39		15.9	45		224
DRVD		MEAN			15.9	25		224
		12.10	MEAN		15.2	21		269
P11	46.59		71	49.42	15.9	53	45.39	291
		DEV			15.2	37		358
Δ11	0.158	0.74	DEV	0.499	15.2	41	0.001	224
			25		16.6	45		202
VRT	180.5			281.2		49	22.1	246
					MEAN	45		157
P235	44.85			45.05	15.75	33	45.22	336
						49		134
Δ235	0.209			0.466	DEV	33	0	291
					0.57			
DEN	.2197			.2207		MEAN	.2202	MEAN
						37		237
VS	51.9			106.5			0	
						DEV		DEV
VRB	184.5			295.9		9.6	22.1	66
NREL	2307			2314			3190	

RUN	203	WAVES		204	WAVES			CORE SAMPLE
CAM	B	VEL	TIME	T	VEL	TIME	19	
							23	0.140"
SAMP	-	10.2	210	C	11.6	30	15	2.12
		9.6	162		11.1	19	23	
LIQ	2002	9.9	185	1985	11.6	30	26	0.260"
		9.9	162		11.5	23	23	0.57
GAS	156.7	9.5	162	381	10.4	19	19	
		9.9	139		11.5	15	30	0.580"
TEMP	33.9	9.9	231	37.0	10.1	19	30	0.47
		9.3	162		11.5	19	30	
PT	45.60	9.9	116		11.8	19	19	0.920"
		9.9	208		11.6	19	19	0.45
PB	45.24	10.4	208	45.11	11.6	15	11	
		10.4	162		11.6	15	19	1.140"
ΔPT	0.011	9.9	323		12.8	23	19	1.07
		9.9	139		11.5	27	15	
ΔPB	0.027	9.9	231		12.0	23	23	CALC
		10.4	231		10.4	23	38	TOTAL
VOID	.120	9.9	69		11.5	15	23	151
		9.5	231		12.4	38	19	
FT		9.9	162	1702		15	34	EDGE
		10.4	185		MEAN	27		0.131"
FB			115		11.47	30	MEAN	
		MEAN	185		DEV	15	22	
DRVD		9.93			0.64	19	DEV	
		DEV	MEAN			23	6.1	
P11	45.60	0.30	181			19		
			DEV			23		
Δ11	0.011		52					
VRT	121.4							
P235	45.25			45.20				
Δ235	0.027							
DEN	.2199			.2172				
VS	20.5			50.5				
VRB	121.9							
KRNL	3236			3415				

RUN	205	WAVES		CORE SAMPLE	206	WAVES	
CAS	C	VEL	74		B	VEL	TIME
			40	0.100"			
SAMP	B	13.6	60	2.59	-	13.0	109
		12.4	74			14.1	70
LIQ	2013	11.4	40	0.150"	1999	12.6	121
		12.4	47	1.80		13.1	102
GAS	409	11.9	34		395	13.0	70
		13.4	74	0.210"		13.6	64
TEMP	33.9	12.9	40	1.72	33.0	13.5	64
		17.4	67			13.6	51
PT		14.3	47	0.280"	47.24	12.5	89
		12.9	40	1.84		12.5	108
PB	44.99	13.4	60		45.13	13.0	64
		12.4	27	0.760"		14.1	45
APT		12.9	40	2.04	0.211	14.1	96
		14.9	27			13.1	115
APB		12.9	67	0.990"	0.228	13.6	45
		15.5	47	1.90		13.1	63
VOID		13.6	40		.082	14.0	51
		14.0	67	1.040"		14.0	51
PT	1905	11.5	60	1.89		14.4	140
		14.5	87			12.6	70
PB	1485	13.3	47	1.150"		13.0	77
		13.4	60	1.93		14.3	115
DRVD		11.4	47				
		12.9	81	CALC		MEAN	MEAN
P11		14.0	40	TOTAL	47.18	13.40	81
			74	367		DEV	DEV
A11		MEAN	40		0.210	0.60	27
		13.33	87	EDGE			
VRT		DEV	60	0.143"	201.3		
		1.32	101				
P235	45.08				45.21		
		TIME	MEAN				
A235			57		0.229		
		67	DEV				
DEN	.2191	60	18		.2204		
VS	53.8				51.6		
VRB					205.9		
NGNL	3254				3172		

RUN	207	CORE SAMPLE	2083	WAVES			CORE SAMPLE
CAM	-		T	VEL	12	20	
		0.140"			12	16	0.150"
SAMP	T	3.08	T	14.2	12	16	2.86
				12.0	20	16	
LIQ	2005	0.260"	2020	12.4	12	20	0.250"
		0.35		12.7	16	16	0.63
GAS	380		381	11.5	16	20	
		0.580"		13.4	16	20	0.380"
TEMP	36.1	0.23	38.0	13.0	20	16	0.58
				14.1	16	12	
PT		0.920"		13.9	16	12	0.580"
		0.21		13.4	12	12	0.62
PB	44.99		45.35	13.9	12	8	
		1.140"		13.0	12	20	0.900"
ΔPT		0.59		12.0	12	8	0.44
				15.0	20	20	
ΔPB		CALC		11.9	12	24	1.140"
		TOTAL		13.4	8	24	0.89
VOID		117		12.7	12	16	
				13.7	12	20	CALC
PT		EDGE			12	16	TOTAL
		0.131"		MEAN	20	20	182
PB				13.12	16	24	
				DEV	12	16	EDGE
DRVD				0.91	12	20	0.119"
					20	20	
P11				TIME	20	16	
					16	24	
Δ11				16	20	24	
				12	16	20	
VRT				12	12		
				12	16	MEAN	
P235	45.07		45.45	8	12	15.7	
				12	16	DEV	
A235				12	12	4.2	
					12		
DEN	.2173		.2177				
VS	50.3		50.4				
VRB							
NREL	3389		3545				

RUN	209S	WAVES		CORE SAMPLE	210S	WAVES		CORE SAMPLE
CAM	C	VEL	TIME	0.130"	B	VEL	TIME	0.130"
SAMP	C	12.8	40	2.43	B	13.0	83	2.66
		13.3	40			14.0	42	
LIQ	2024	13.3	47	0.180"	2002	15.7	83	0.260"
		10.8	40	1.18		15.7	113	2.30
GAS	379	11.9	47		385	13.5	113	
		12.8	34	0.360"		15.0	60	0.580"
TEMP	35.3	11.0	60	0.99	35.6	12.2	48	2.39
		12.0	60			12.2	78	
PT		13.4	60	0.780"	47.02	13.5	89	0.910"
		11.9	47	0.99		13.0	107	2.12
PB	44.96	12.3	40		45.07	14.5	77	
		13.5	60	1.090"		11.7	66	1.150"
ΔPT		12.4	40	0.99	0.142	13.1	113	3.11
		10.5	40			14.0	83	
ΔPB		12.9	47	CALC	0.269	12.7	60	CALC
		11.9	47	TOTAL		13.1	54	TOTAL
VOID		11.5	67	234	.084	14.0	95	458
		11.4	47			8.6	113	
FT	1747	12.3	40	EDGE		14.6	107	EDGE
		12.3	34	0.131"		13.5	113	0.143"
FB	1857	11.5	60			14.5	72	
		11.0	47				77	
DRVD		11.8	34			MEAN	66	
		11.0	40			13.43	83	
P11			74		46.98			
		MEAN	81			DEV	MEAN	
Δ11		12.06	34		0.142	1.51	83	
			47					
VRT		DEV	54		199.8		DEV	
		0.86					22	
P235	45.06		MEAN		45.17			
			49					
Δ235					0.270			
			DEV					
DEN	.2179		12		.2181			
VS	50.1				50.8			
VRB					204.0			
NREL	3366				3350			

RUN	211
CAM	T
SAMP	C
LIQ	2007
GAS	748
TEMP	37.8
PT	
PB	45.56
ΔPT	
ΔPB	
VOID	
PT	1333
PB	
DRVD	
P11	
Δ11	
VRT	
P235	45.75
Δ235	
DEN	.2192
VS	98.2
VRB	
NEEL	3508

WAVES

VEL	TIME	23
		15
15.0	19	23
15.5	23	15
16.0	23	11
15.1	30	19
14.2	11	19
15.0	15	15
15.0	15	15
17.0	15	15
16.0	15	15
19.5	11	23
16.0	15	27
16.0	11	26
15.5	11	27
16.0	19	23
15.0	15	15
17.0	27	15
15.5	19	23
15.1	8	30
14.4	23	15
15.5	11	15
13.3	30	15
15.1	15	23
15.1	23	19
15.0	11	15
14.6	19	19
14.4	23	15
14.6	23	15
16.0	27	15
14.6	11	30
MEAN	30	15
15.28	27	MEAN
DEV	26	19
0.78	11	DEV
	19	5.8
	27	
	26	

CORE SAMPLE

0.140"
1.87

0.260"
1.50

0.580"
1.34

0.920"
1.38

1.140"
1.61

CALC TOTAL
314

EDGE
0.125"

RUN	212
CAM	C
SAMP	B
LIQ	2000
GAS	794
TEMP	35.0
PT	
PB	44.85
ΔPT	
ΔPB	
VOID	
FT	1570
FB	1006
DRVD	
P11	
Δ11	
VRT	
P235	45.04
Δ235	
DEN	.2180
VS	104.9
VRB	
NREL	3307

WAVES		
VEL	TIME	55
		51
19.1	29	21
21.2	25	50
16.7	25	42
17.9	42	34
19.1	17	13
18.4	42	38
19.8	34	46
18.4	25	46
17.7	29	25
15.4	21	46
14.3	34	38
17.0	17	17
16.7	38	21
16.9	29	25
15.6	21	51
18.4	25	55
16.1	42	50
19.0	13	42
17.0	29	38
17.7	46	29
19.8	63	29
	25	
MEAN	59	MEAN
17.72	29	35
DEV	34	DEV
1.63	17	13
	29	
	67	

CORE SAMPLE
0.090"
3.99
0.150"
4.92
0.350"
6.29
0.750"
4.40
0.940"
4.32
1.020"
4.40
1.080"
4.49
1.150"
4.25
CALC TOTAL 1034
EDGE 0.131"

RUN	213	WAVES			214	CORE SAMPLE
CAM	B	VEL	16.3	24	-	
			14.7	44		0.140"
SAMP	-	15.5	15.5	28	T	2.21
		18.0	15.5	56		
LIQ	1999	15.5	16.1	36	2010	0.260"
		16.2	16.2	24		0.97
GAS	800	18.0	17.2	56	760	
		16.2		36		0.580"
TEMP	33.8	16.7	MEAN	20	35.0	0.48
		18.9	16.29	28		
PT	49.74	16.3		48		0.920"
		16.9	DEV	32		0.65
PB	44.81	16.2	1.03	32	45.14	
		16.2		20		1.140"
ΔPT	0.463	16.7	TIME	20		1.16
		17.7		24		
ΔPB	0.512	16.2	24	48		CALC
		16.9	24	32		TOTAL
VOID	.046	16.2	44	20		246
		14.8	20	36		
FT		18.9	16	24		EDGE
		16.3	28	40		0.125"
DRVD		15.5	32	36		
		16.3	69			
P11	49.61	16.3	24	MEAN		
		15.5	28	32		
Δ11	0.460	15.5	32			
		15.5	28	DEV		
VRT	305.8	14.7	20	12		
		16.7	36			
P235	45.00	14.8	28		45.33	
Δ235	0.516					
DEN	.2188				.2194	
VS	105.2				99.8	
VRB	322.0					
NREL	3225				3323	

RUN	215S
CAM	T
SAMP	T
LIQ	2007
GAS	782
TEMP	37.7
PT	
PB	44.80
APT	
ΔPB	
VOID	
FT	
FB	
DRVD	
P11	
Δ11	
VRT	
P235	45.01
Δ235	
DEN	.2157
VS	104.4
VRS	
NREL	3501

WAVES				
VEL	TIME	12	12	
		8	12	
13.6	12	20	16	
14.6	16	16	16	
15.1	16	16	12	
12.6	8	12	16	
11.9	8	16	16	
13.2	16	16	12	
13.6	12	16	12	
13.6	16	16	16	
12.1	12	12	20	
14.1	16	12	20	
16.6	12	12	12	
13.2	8	12	20	
12.1	8	16	12	
15.9	12	12	12	
13.2	8	20	16	
15.1	12	20	20	
12.9	12	16	20	
13.2	12	16	20	
14.5	8	12	16	
12.2	12	12	8	
	8	8	16	
MEAN	12	12	16	
13.66	16	12	12	
	16	12	16	
DEV	12	20	12	
1.27	12	16	20	
	16	12	12	
	12	8		
	24	12	MEAN	
	16	16	13.7	
	16	12		
	12	16	DEV	
			3.5	

CORE SAMPLE
0.150"
3.24
0.270"
3.64
0.580"
5.11
0.900"
2.89
1.140"
2.69
CALC
TOTAL
759
EDGE
0.107"

		WAVES			CORE SAMPLE
RUN	2168				
CAM	C	VEL	TIME	17	
				30	0.120"
CAMP	C	14.5	43	39	5.85
		15.1	26	34	
LIQ	2007	15.7	17	22	0.160"
		13.4	26	30	5.45
GAS	785	15.2	30	26	
		12.6	22	13	0.380"
TEMP	34.7	13.4	22	26	5.23
		14.5	43	17	
PT		13.9	26	26	0.770"
		15.0	43	26	4.25
PB	44.58	12.3	22	17	
		12.3	26	21	1.030"
ΔPT		13.9	22	22	4.77
		15.1	43	22	
ΔPB		12.9	39	35	1.080"
		12.9	26	30	5.40
VOID		12.5	21	34	
		14.0	39	22	1.130"
PT	673	14.5	17		5.73
		14.5	30	MEAN	
PB	471	13.4	17	26	CALC
		12.6	17	DEV	TOTAL
DRVD		13.5	17	8.2	1050
		14.2	17		
P11			22		EDGE
		MEAN			0.119"
Δ11		13.83			
		DEV			
VRT		1.00			
P235	44.79				
Δ235					
DSA	.2170				
VS	104.2				
VAB					
MBBL	3298				

RUN	217S	WAVES		CORE SAMPLE	218S	CORE SAMPLE
CAM	B	VEL	TIME		-	
				0.120"		0.120"
SAMP	B	15.3	20	5.56	B	6.58
		14.7	12			
LIQ	2000	16.4	12	0.250"	2005	0.160"
		15.8	24	6.63		8.82
GAS	774	15.8	16		800	
		16.4	28	0.580"		0.380"
TEMP	3513	15.2	20	4.62	34.7	7.75
		16.4	28			
PT	49.64	15.8	32	0.930"		0.770"
		15.2	16	4.43		6.51
PB	44.83	15.2	20		44.61	
		14.6	28	1.160"		1.030"
Δ PT	0.536	15.1	28	3.77		4.62
		14.2	20			
Δ PB	0.566	15.8	12	CALC		1.080"
		15.8	20	TOTAL		4.30
VOID	.0462	15.3	24	1031		
			40			1.130"
FT		MEAN	20	EDGE	1199	3.99
		15.47	32	0.131"		
FB			20		897	CALC
		DEV	16			TOTAL
DRVD		0.62	36			1299
			16			
P11	49.48		24			EDGE
			20			0.131"
Δ11	0.532		36			
			16			
VRT	300.5		28			
			32			
P235	45.04		20		44.82	
			28			
Δ235	0.571		40			
			20			
DEN	.2178		40		.2172	
			28			
VS	102.4		44		106.1	
			20			
VRB	315.9		40			
			32			
NREL	3326		28		3295	
			47			
			20			
			40			
			MEAN			
			26			
			DEV			
			9.1			

RUN	219
CAM	T
SAMP	C
LIQ	1999
GAS	1212
TEMP	36.9
PT	
PB	45.27
ΔPT	
ΔPB	
VOID	
FT	807
FB	
DRVD	
P11	
Δ11	
VRT	
P235	45.58
Δ235	
DEN	.2191
VS	159.2
VRB	
NREL	3433

WAVES

VEL	TIME					
20.7	15	11	11	15	15	11
23.7	11	15	15	11	11	11
20.3	11	15	15	8	8	15
20.3	11	19	11	15	11	19
18.4	8	11	15	8	19	15
20.7	11	11	11	8	15	11
22.1	8	15	15	11	8	11
21.4	4	11	15	11	11	15
21.4	8	8	11	15	19	15
20.3	15	11	19	15	15	11
20.7	11	11	15	8	11	15
20.7	15	15	8	15	8	19
21.4	8	11	11	8	8	8
21.4	11	11	8	15	15	8
19.7	8	15	8	8	19	15
20.3	19	11	11	19	19	11
20.7	23	11	8	11	11	19
20.3	11	8	11	15	8	15
20.7	15	11	15	15	11	15
20.3	15	11	8	8	11	19
19.0	11	11	15	11	15	19
22.1	15	11	8	8	11	15
20.7	15	11	15	8	19	15
20.3	19	15	11	11	15	15
21.4	8	15	11	8	11	11
20.9	15	15	11	15	11	8
20.7	15	8	11	8	19	11
20.0	15	11	8	8	11	11
19.0	11	11	11	19	11	15
20.7	19	8	15	15	15	11
	19	15	15	11	26	15
MEAN		19	11	11	19	
20.68		15	8	11	15	MEAN
		8	8	11	15	12.6
DEV						DEV
0.98						3.7

CORE SAMPLE

0.140"
2.83

0.260"
2.41

0.580"
2.07

0.920"
2.19

1.140"
2.51

CALC TOTAL
518

EDGE
0.119"

RUN	220
CAM	C
SAMP	B
LIQ	2000
GAS	1225
TEMP	31.4
PT	
PB	44.33
ΔPT	
ΔPB	
VOID	
PT	1264
PB	425
DRVD	
P11	
Δ11	
VRT	
P235	44.64
Δ235	
DEN	.2189
VS	161.1
VRB	
NREL	3069

WAVES

VEL	TIME		
		9	17
		9	13
17.6	13	13	9
21.4	17	13	13
18.7	13	9	26
18.0	13	13	13
21.5	13	9	13
21.0	13	9	17
18.0	13	13	13
21.0	9	13	17
21.0	13	13	21
19.4	4	17	17
20.8	9	17	21
20.1	13	17	9
20.1	21	17	17
20.1	21	13	9
23.5	13	9	9
21.8	17	9	17
17.0	13	9	13
21.0	9	13	17
20.2	13	17	13
20.1	13	13	9
20.2	17	9	13
21.8	21	13	17
21.0	17	17	21
	17	9	13
MEAN	9	9	17
20.23	13	9	9
DEV	13	9	13
1.51	9	4	13
	13	17	
	9	21	MEAN
	4	13	13.1
	13	17	DEV
	9	9	4.2
	13	13	

CORE SAMPLE

0.060"
5.91
0.120"
8.69
0.190"
9.48
0.280"
8.51
0.750"
5.71
0.980"
5.22
1.070"
5.44
1.150"
5.78
CALC
TOTAL
1487
EDGE
0.125"

RUN	221	WAVES			222	CORE SAMPLE
CAM	B	VEL	TIME	24	-	
				24		0.140"
SAMP	-	16.8	16	16	T	2.67
		18.7	12	16		
LIQ	2002	19.2	24	20	2004	0.260"
		18.0	16	32		1.37
GAS	1239	19.2	16	32	1235	
		18.9	32	24		0.580"
TEMP	33.1	18.8	16	16	35.7	0.54
		18.0	12	20		
PT	52.82	18.7	16	16		0.920"
		17.7	16	28		0.67
PB	44.80	18.0	16	8	44.68	
		17.5	20	28		1.140"
APT	0.808	17.5	8	20		1.70
		18.3	16	16		
APB	0.766	18.0	16			CALC
		16.5	16	MEAN		TOTAL
VOID	.0235	16.6	24	18.7		316
		15.8	15	DEV		
FT		17.5	24	6.6		EDGE
		17.5	24			0.119"
FB		17.5	16			
		17.5	20			
DRVD		19.2				
		17.5				
P11	52.59	19.2				
		17.8				
Δ11	0.798	18.4				
		18.3				
VRT	399.4	18.4				
P235	45.09	MEAN			44.99	
		17.97				
Δ235	0.774	DEV				
		0.85				
DEN	.2198				.2172	
VS	162.3				163.7	
VRB	433.3					
NREL	3184				3360	

RUN	223S
CAM	T
SAMP	T
LIQ	1989
GAS	1235
TEMP	36.5
PT	
PB	43.74
ΔPT	
ΔPB	
VOID	
FT	
FB	
DRVD	
P11	
Δ11	
VRT	
Δ235	44.00
Δ235	
DEN	.2118
VS	167.9
VRB	
NREL	3389

WAVES						
VEL	TIME	8	8	8	8	
		8	8	8	16	
15.2	12	8	8	4	8	
15.0	8	8	8	4	12	
15.0	4	8	8	8	12	
15.0	12	8	8	8	4	
15.0	4	12	12	8	4	
16.8	4	8	8	4	8	
13.4	4	4	8	16	12	
16.6	8	8	12	8	8	
16.5	12	4	4	12	8	
15.7	8	8	8	12	12	
15.8	12	8	8	8	12	
17.5	4	4	8	8	8	
17.8	8	4	12	8	12	
17.5	8	12	12	8	8	
16.8	8	12	12	12	12	
16.5	4	12	8	16	8	
16.6	8	8	12	4	8	
13.5	8	8	8	8	12	
15.8	4	12	12	8	8	
13.5	4	12	8	8	8	
	8	8	8	12	4	
MEAN	8	12	12	8	12	
15.77	8	12	8	8	8	
DEV	8	8	8	4	8	
1.29	12	4	8	16	16	
	12	8	4	8	8	
	8	8	8	8		
	4	8	4	16	MEAN	
	4	8	8	12	8.7	
	8	4	12	16	DEV	
	8	12	8	8	3.0	
	8	12	12	12		
	8	12	12			

CORE SAMPLE
0.140"
7.58
0.270"
5.96
0.580"
12.9
0.910"
9.05
1.140"
3.29
CALC TOTAL
1686
EDGE
0.095"

RUN	2248	WAVES			CORE SAMPLE	2258	CORE SAMPLE
CAM	C	VEL	13	13		-	
			9	13	0.100"		0.100"
SAMP	C	16.9	13	13	8.17	B	11.49
		14.5	9	13			
LIQ	2011	16.3	13	17	0.140"	1998	0.140"
		13.5	13	9	8.43		13.98
GAS	1242	15.7	9	17		1248	
		16.5	13	9	0.380"		0.380"
TEMP	33.3	15.1	9	17	6.73	34.2	9.56
		14.5	13	9			
PT		15.1	13	9	0.770"		0.770"
		15.0	17	9	7.49		5.96
PB	44.80	13.9	13	9		44.52	
		13.6	13	9	1.020"		1.020"
ΔPT		15.0	13	17	5.57		5.94
		15.0	13	13			
ΔPB		15.5	26	13	1.070"		1.070"
		15.1	17	9	5.00		5.02
VOID		15.2	9	9			
		14.5	9	17	1.110"		1.110"
FT	221	14.5	13	13	4.71	610	4.82
			9	17			
FB	152	MEAN	13	13	1.150"	209	1.150"
		15.02	9	13	3.67		4.61
DRVD		DEV	22	4			
		0.88	13	13	CALC		CALC
F11			17	9	TOTAL		TOTAL
		TIME	22	13	1435		1723
Δ11			9	13			
		13	13	4	EDGE		EDGE
VRT		13	17	9	0.107"		0.125"
		22	9	13			
F235	45.06	13	22			44.78	
		17	9	MEAN			
Δ235		13	9	12.5			
		9	13	DEV			
DEN	.2195	13	13	4.0		.2174	
		9	13				
VS	162.9					165.3	
VRB							
HREL	3211					3250	

RUN	2265
CAM	B
SAMP	B
LIQ	2001
GAS	1234
TEMP	35.1
PT	50.71
PB	44.64
ΔPT	0.556
ΔPB	0.706
VOID	.015
FT	
FB	
DRVD	
P11	50.55
Δ11	0.551
VRT	408.2
P235	44.90
Δ235	0.713
DEN	.2172
VS	163.6
VRB	434.8
NREL	3315

WAVES

VEL	TIME		
		8	16
		16	16
16.0	12	4	16
16.6	8	12	12
15.4	12	12	8
15.0	8	8	8
16.0	8	4	12
14.4	8	12	12
15.5	8	12	12
16.6	8	12	12
14.9	8	8	12
17.3	8	8	16
15.4	8	4	8
16.6	8	8	8
14.0	12	12	16
14.5	8	8	8
11.9	8	12	8
13.1	12	8	8
17.1	8	16	8
17.2	8	8	16
	12	12	8
MEAN	8	16	16
15.42	8	12	12
DEV	8	16	8
1.42	8	8	8
	4	8	8
	12	12	8
	4	16	12
	8	16	
	8	12	MEAN
	8	12	9.8
	8	12	DEV
	8	8	3.2
	4	12	

CORE SAMPLE

0.120"
14.00
0.250"
9.16
0.580"
11.89
0.920"
6.28
1.140"
4.93
CALC
TOTAL
1685
EDGE
0.125"

RUN	227	WAVES		228	WAVES		
CAN	B	VEL	TIME	B	VEL	18.7	29
SAMP	-	15.7	89	-		17.9	24
LIQ	2698	15.1	70		16.6	17.0	20
		15.7	89	2692	17.5	18.7	61
GAS	393	13.8	89		18.2	18.7	29
		15.0	70	807	18.9		37
TEMP	33.1	15.7	64		19.5	MEAN	33
		14.2	76	32.2	20.4	17.88	20
PT	46.93	14.2	76		17.9	DEV	33
		15.7	76	50.90	17.9	1.16	25
PB	44.84	16.4	76		17.0		57
		14.4	95	45.20	17.5	TIME	24
ΔPT	0.244	14.4	70		16.0		16
		13.8	127	0.537	16.8	25	41
ΔPB	0.244	13.8	38		18.2	29	49
		14.2	57	0.604	16.6	29	25
VOID	.102	15.3	76		20.4	33	20
		15.3	57	.058	17.9	33	41
FT		14.4	140		17.5	41	49
		13.7	146		18.7	24	37
FB		15.7	57		17.9	33	37
		15.7	51		16.2	33	25
DRVD			63		17.0	20	
		MEAN	140		16.6	20	MEAN
P11	46.86	14.87	63		17.9	25	31
		DEV		50.74	20.4	20	DEV
Δ11	0.243	0.81	MEAN		16.6	20	10
			81	0.533	17.9	33	
VRT	228.0		DEV		17.2		
			28	336.6			
P235	44.93			45.42			
Δ235	0.245			0.609			
DEN	.2189			.2221			
VS	51.7			104.6			
VHB	233.0			356.9			
NREL	4291			4201			

RUN	229	WAVES	230	WAVES	231	WAVES
CAM	B	VEL TIME	B	VEL TIME	B	VEL TIME
SAMP	-	7.2 259 7.7 130	-	10.2 221 9.4 123	-	16.2 141 17.1 114
LIQ	3475	8.0 389 7.2 259	3516	11.9 147 11.9 123	3511	14.9 94 16.3 87
GAS	0	8.8 389 7.8 181	156.1	11.0 245 11.0 220	397	15.5 34 17.6 101
TEMP	35.0	7.8 *803 8.4 233	34.7	10.2 147 11.5 122	33.8	17.6 100 15.5 94
PT	45.36	8.4 MEAN	45.69	11.9 123 11.0 74	47.53	16.6 80 15.5 54
PB	45.21	MEAN 263 7.92 DEV	45.01	11.9 147 11.0 343	44.75	16.6 94 16.6 80
ΔPT	0	DEV 90 0.51	0.026	11.5 245 10.6 171	0.262	17.1 134 17.6 80
ΔPB	0	BRIDGING	0.052	11.9 98 9.4 196	0.317	16.6 101 27
VOID	.201	TENDED TO OCCUR	.180	12.3 73 11.0 98	.123	MEAN 16.49 MEAN
FT		THE TEST SECTION		11.9 368 12.7 221		DEV 88 0.82 DEV
FB		COULD ONLY BE		11.0 172 269		30
DRVD		KEPT CLEAR BY USING		MEAN 11.20 MEAN		
P11	45.36	A SMALL GAS FLOW	45.68	DEV 179 0.86 DEV	47.45	
A11	0	OF ABOUT 2 FT/SEC	.026	79	0.261	
VRT	38.5	*PARTIAL	158.2		255.5	
P235	45.21	BRIDGING OCCURRED	45.03		44.87	
A235	0	FURTHER UP	0.052		0.318	
DEN	.2188	STREAM OMITTED	.2182		.2181	
VS	0	IN CALCULATING	20.6		52.4	
VRB	38.5	MEAN AND DEV	159.3		263.0	
NREL	5745		5777		5664	

RUN	232	WAVES			233	WAVES		
CAM	B	VEL			B	VEL	20.7	30
			15.8	17			18.2	26
SAMP	-	18.7	15.8	67	-	21.9	18.2	13
		16.2	16.6	63		21.9	21.9	21
LIQ	3510	18.5	18.3	29	3524	20.7	21.9	17
		17.4	18.3	29		20.7		17
GAS	812	17.4	20.8	21	1076	20.7	MEAN	43
		18.7	15.8	17		19.5	20.56	13
TEMP	33.9	18.5	15.8	33	34.1	19.4		17
		19.2	18.3	25		20.7	DEV	30
PT	51.81	15.7	21.2	58	53.76	25.5	2.23	30
		17.4		25		19.5		13
PB	44.58	18.3	MEAN	21	44.69	19.4	TIME	26
		18.0	18.05	21		18.2		26
ΔPT	0.758	18.1		29	1.031	20.7	13	43
		19.9	DEV	17		21.9	17	26
ΔPB	0.784	19.9	1.68	38	1.024	26.7	21	34
		19.9		42		20.7	21	21
VOID	.066	21.0	TIME	29	.047	19.5	21	21
		16.6		21		20.7	22	43
PT		17.4	29	29		18.2	21	17
		16.6	25	63		26.7	13	30
PB		19.1	33	38		17.0	17	
		16.6	25	25		21.9	22	MEAN
DRVD		19.1	33	42		19.4	17	23
		21.6	29	29		19.5	21	
P11	51.59	15.8	38	42	53.46	18.2	30	DEV
		15.8	71	29		19.4	22	7.9
Δ11	0.749	16.6	29		1.016	19.5	26	
		18.3	21	MEAN		19.4	21	
VRT	371.6	18.3	29	34	435.3		17	
		20.8	38					
P235	44.87		17	DEV	45.07			
				14				
Δ235	0.793				1.039			
DEN	.2180				.2189			
VS	107.2				141.5			
VRB	399.9				476.3			
NREL	5674				5720			

APPENDIX 2

PHYSICAL DATA

A2.1 TEST SECTION DIAMETER

Nominal diameter for calculations : 1.330".

Actual range at the end of glass sections : 1.325 - 1.340".

Porous wall injector bore 1.340".

∴ Worst variation from nominal = + 0.75% on diameter

= + 1.51% on area.

A2.2 WATER DENSITY

Temperature	Density		
°C	gm/cc	lb/ft^3	
20	0.99823	62.32	(Conversion
24	0.99733	62.26	factor :
28	0.99627	62.20	1 gm/cc = 62.43 lb/ft^3)
32	0.99506	62.12	
36	0.99371	62.04	
40	0.99225	61.95	
44	0.99066	61.85	

Source : Chemical Engineers' Handbook, 4th Edition.
(McGraw-Hill 1963). Table 3-46.

A2.3 MANOMETER FLUIDS

Absolute manometer : Water on Mercury

Differential manometers : Water on symmetrical Tetrabromoethane

Densities at 20°C (average manometer temperature) :

Water : 0.9982 gm/cc [1]

Mercury : 13.546 gm/cc [2]

s-Tetrabromoethane : specific gravity

= 2.964 at 20°C/4°C.

= density of 2.964 gm/cc at 20°C [3].

The tetrabromoethane used was checked and found to have a specific gravity of 2.927 at 25° C. This means that the tetrabromoethane probably contained small amounts of other impurities of lower specific gravity, for example, unsymmetrical tetrabromoethane.

∴ Net density of water - s-tetrabromoethane differential manometer at 20°C = 2.93 - 0.998 = 1.93 gm/cc.

Source : 1. Chemical Engineers' Handbook (4th Ed.) Table 3-46

2. Chemical Engineers' Handbook (4th Ed.) Table 3-47

3. Chemical Engineers' Handbook (4th Ed.) Table 3-2

A2.4 VISCOSITY OF WATER

The viscosity table for water over the range 17-41.8°C was constructed from the equation recommended by Bruges, Latto and Ray (1966). Their correlating equation can be written as:-

$$\mu = 0.02394 \times 10^{\frac{248.37}{TE-140}} \text{ centipoise}$$

where TE is in °K (273.15 + °C)

Viscosity of Liquid Water (centipoise)

TEMP °C	.0	.2	.4	.6	.8
17	1.0796	1.0742	1.0688	1.0634	1.0581
18	1.0527	1.0474	1.0422	1.0371	1.0320
19	1.0269	1.0219	1.0168	1.0118	1.0069
20	1.0020	0.9971	0.9923	0.9875	0.9828
21	0.9780	0.9733	0.9687	0.9641	0.9595
22	0.9549	0.9504	0.9459	0.9414	0.9370
23	0.9326	0.9283	0.9240	0.9197	0.9154
24	0.9112	0.9070	0.9028	0.8986	0.8945
25	0.8904	0.8864	0.8823	0.8783	0.8744
26	0.8704	0.8665	0.8626	0.8588	0.8549
27	0.8511	0.8473	0.8436	0.8398	0.8361
28	0.8325	0.8288	0.8252	0.8216	0.8180
29	0.8144	0.8109	0.8074	0.8039	0.8005
30	0.7970	0.7936	0.7902	0.7868	0.7835
31	0.7802	0.7769	0.7736	0.7703	0.7671
32	0.7639	0.7607	0.7575	0.7544	0.7513
33	0.7481	0.7450	0.7420	0.7389	0.7359
34	0.7329	0.7299	0.7269	0.7240	0.7210
35	0.7181	0.7152	0.7124	0.7095	0.7066
36	0.7038	0.7010	0.6982	0.6955	0.6927
37	0.6900	0.6873	0.6846	0.6819	0.6792
38	0.6765	0.6739	0.6713	0.6687	0.6661
39	0.6636	0.6610	0.6585	0.6560	0.6534
40	0.6510	0.6485	0.6460	0.6436	0.6411
41	0.6387	0.6363	0.6339	0.6316	0.6292

A 2.5 DENSITY OF AIR SATURATED WITH WATER VAPOUR (LB/FT^3).

TEMP °C	18	20	22	24	26	28	30
VAPOUR PRESSURE (PSIA)	0.2990	0.3386	0.3827	0.4316	0.4860	0.5463	0.6132
VAPOUR DENSITY (LB/FT^3)	.00096	.00108	.00121	.00136	.00152	.00170	.00189
6.70	0.0340	0.0337	0.0334	0.0330	0.0327	0.0324	0.0320
8.70	0.0443	0.0439	0.0435	0.0431	0.0428	0.0424	0.0420
10.70	0.0546	0.0542	0.0537	0.0533	0.0528	0.0523	0.0519
12.70	0.0649	0.0644	0.0639	0.0633	0.0628	0.0623	0.0618
14.70	0.0752	0.0747	0.0741	0.0734	0.0729	0.0723	0.0717
16.70	0.0856	0.0849	0.0842	0.0836	0.0829	0.0823	0.0816
19.70	0.1010	0.1003	0.0995	0.0987	0.0980	0.0972	0.0964
24.70	0.1268	0.1259	0.1249	0.1240	0.1231	0.1221	0.1212
40.00	0.2057	0.2043	0.2028	0.2013	0.1999	0.1984	0.1970
45.00	0.2315	0.2299	0.2282	0.2266	0.2250	0.2233	0.2218
50.00	0.2573	0.2555	0.2537	0.2519	0.2501	0.2483	0.2466
TOTAL PRESSURE (PSIA)							

TEMP °C	32	34	36	37.8	38	40	42
VAPOUR PRESSURE (PSIA)	0.6871	0.7687	0.8586	0.9471	0.9574	1.066	1.185
VAPOUR DENSITY (LB/FT^3)	.00211	.00235	.00260	.00285	.00288	.00319	.00353
6.70	0.0317	0.0313	0.0310	0.0306	0.0306	0.0302	0.0298
8.70	0.0415	0.0411	0.0407	0.0403	0.0403	0.0398	0.0393
10.70	0.0514	0.0509	0.0504	0.0500	0.0499	0.0494	0.0489
12.70	0.0612	0.0607	0.0601	0.0596	0.0596	0.0590	0.0584
14.70	0.0711	0.0704	0.0698	0.0693	0.0692	0.0686	0.0679
16.70	0.0809	0.0802	0.0796	0.0789	0.0789	0.0782	0.0775
19.70	0.0957	0.0949	0.0941	0.0934	0.0933	0.0926	0.0918
24.70	0.1203	0.1194	0.1184	0.1176	0.1175	0.1165	0.1156
40.00	0.1956	0.1942	0.1927	0.1915	0.1913	0.1899	0.1885
45.00	0.2202	0.2186	0.2170	0.2156	0.2155	0.2139	0.2123
50.00	0.2448	0.2431	0.2413	0.2398	0.2396	0.2379	0.2361
TOTAL PRESSURE (PSIA)							

The water vapour pressures and densities are taken from Weast (Editor) : Handbook of Physics and Chemistry 47th Edition (1966) (The Chemical Rubber Co.) pp E-11 and E-12.

Density values are calculated from :

$$\text{Density} = \frac{(P_T - P_W)}{14.696} \times \frac{273.15}{273.15 + T_C} \times 0.0808 + \rho_W$$

Where P_T is the total pressure, and P_W and ρ_W are the water vapour pressure and density respectively at temperature T_C °C. 0.0808 lb/ft^3 is the density of dry air at 1 atmosphere (14.696 psia) and 0°C.

APPENDIX 3.

GRAPHS OF EXPERIMENTAL RESULTS.

The graphs which were not included in the experimental results, Section 4, are included in this appendix. They are:-

Figures A3.1 - A3.7	Total pressure gradient versus reduced velocity.
Figures A3.8 - A3.11	Mean wave velocity versus dimensionless liquid flow rate.
Figures A3.12 - A3.17	Wave velocity standard deviation versus mean wave velocity.
Figures A3.18 - A3.21	Time interval between waves versus dimensionless liquid flow rate.
Figures A3.22 - A3.37	Droplet entrainment profiles.

A-118.

LEGEND

WATER RATE (LB/HR)	INJECTOR TYPE	SYSTEM PRESSURE	PRESSURE GRADIENT SYMBOL Δ11	PRESSURE GRADIENT SYMBOL Δ35	GRAPH Δ11	GRAPH Δ35
30	Porous Wall	Medium	◇	◆	-- ——	-·——
100	Porous Wall	Low	○	●	- ——	——
100	Porous Wall	Medium	□	■	- ——	——
100	Porous Wall	High	△	▲	- ——	——

Figure A3.1 TOTAL PRESSURE GRADIENT VERSUS REDUCED VELOCITY WATER RATES 30 AND 100 LB/HR.

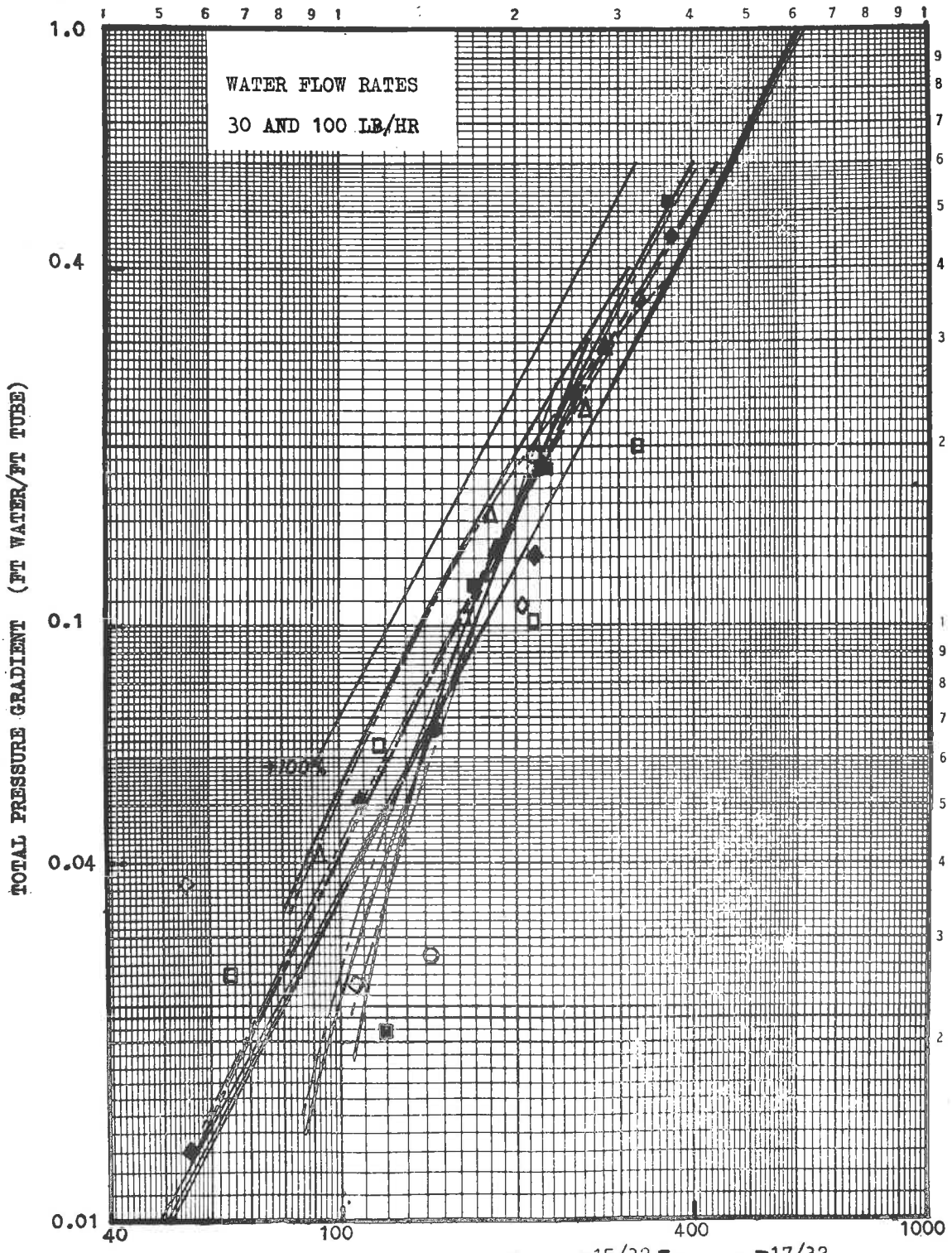

$$\text{REDUCED VELOCITY (FT/SEC)} = \frac{1}{3600}\left[\frac{G_L+G_G}{\rho_{ref}}\right]^{15/32}\left[\frac{G_L}{\rho_L}+\frac{G_G}{\rho_G}\right]^{17/32}$$

$\rho_{ref} = 0.0712$ LB/FT^3. G_L AND G_G IN LB/FT^{2}HR.

A-119.

LEGEND

WATER RATE (LB/HR)	INJECTOR TYPE	SYSTEM PRESSURE	PRESSURE GRADIENT SYMBOL Δ11	PRESSURE GRADIENT SYMBOL Δ235	GRAPH Δ11	GRAPH Δ235
300	Porous Wall	Low	○	●	- ——	——
300	Porous Wall	Medium	□	■	- ——	——
300	Spray	Medium	◇	◆	- - - -	- -
300	Porous Wall	High	△	▲	- ——	——
300	Spray	High	▽	▼	- - - -	- -

Figure A3.2 TOTAL PRESSURE GRADIENT VERSUS REDUCED VELOCITY WATER RATE 300 LB/HR.

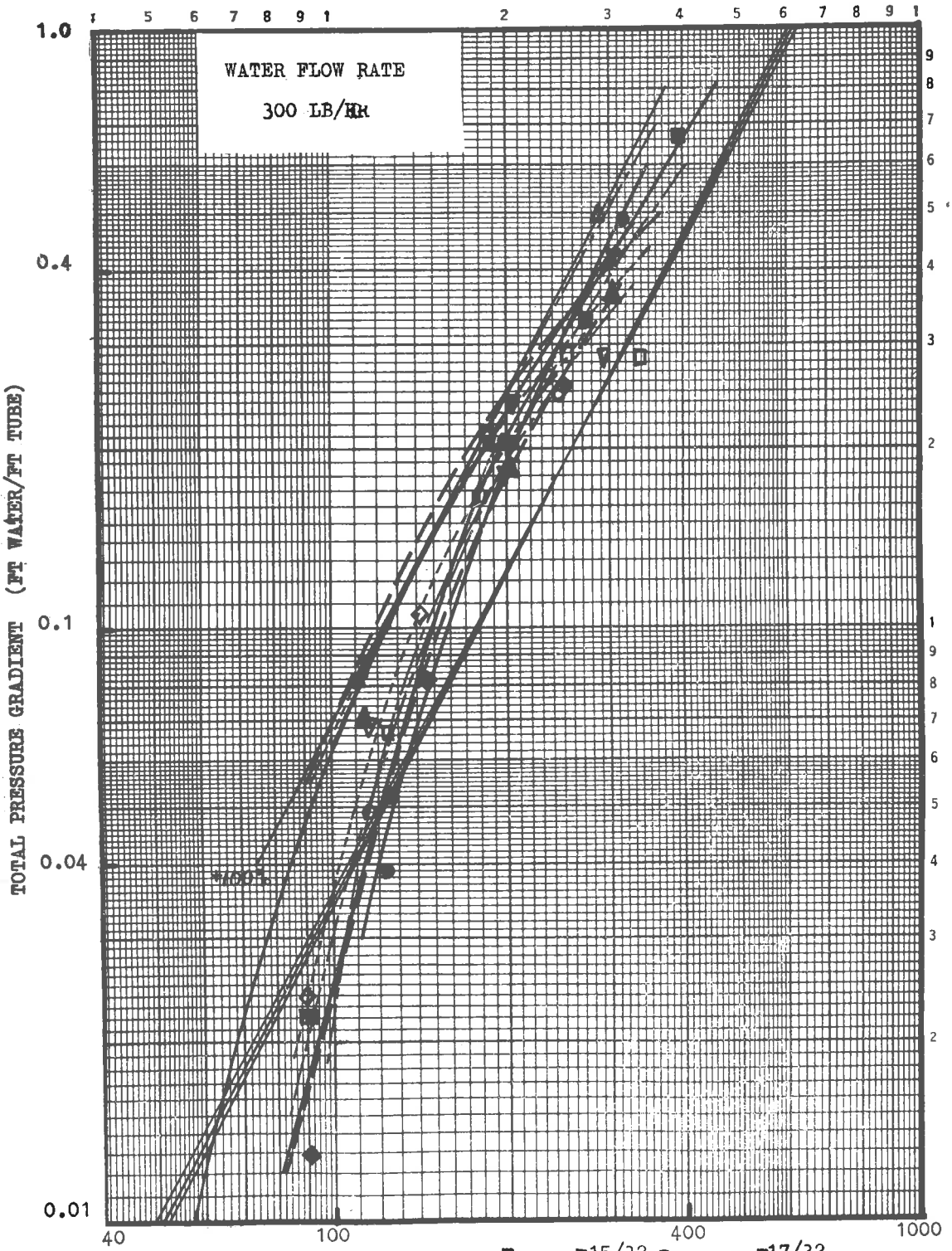

$$\text{REDUCED VELOCITY (FT/SEC)} = \frac{1}{3600}\left[\frac{G_L+G_G}{\rho_{ref}}\right]^{15/32}\left[\frac{G_L}{\rho_L}+\frac{G_G}{\rho_G}\right]^{17/32}$$

ρ_{ref} = 0.0712 LB/FT^3. G_L AND G_G IN LB/FT^{2}HR.

A-120.

WATER RATE (LB/HR)	INJECTOR TYPE	SYSTEM PRESSURE	PRESSURE GRADIENT SYMBOL A11	A235	GRAPH A11	A235
600	Porous Wall	Low	○	●	- ——	——
600	Porous Wall	Medium	□	■	- ——	——
600	Porous Wall	High	△	▲	- ——	——

Figure A3.3 TOTAL PRESSURE GRADIENT VERSUS REDUCED VELOCITY WATER RATE 600 LB/HR.

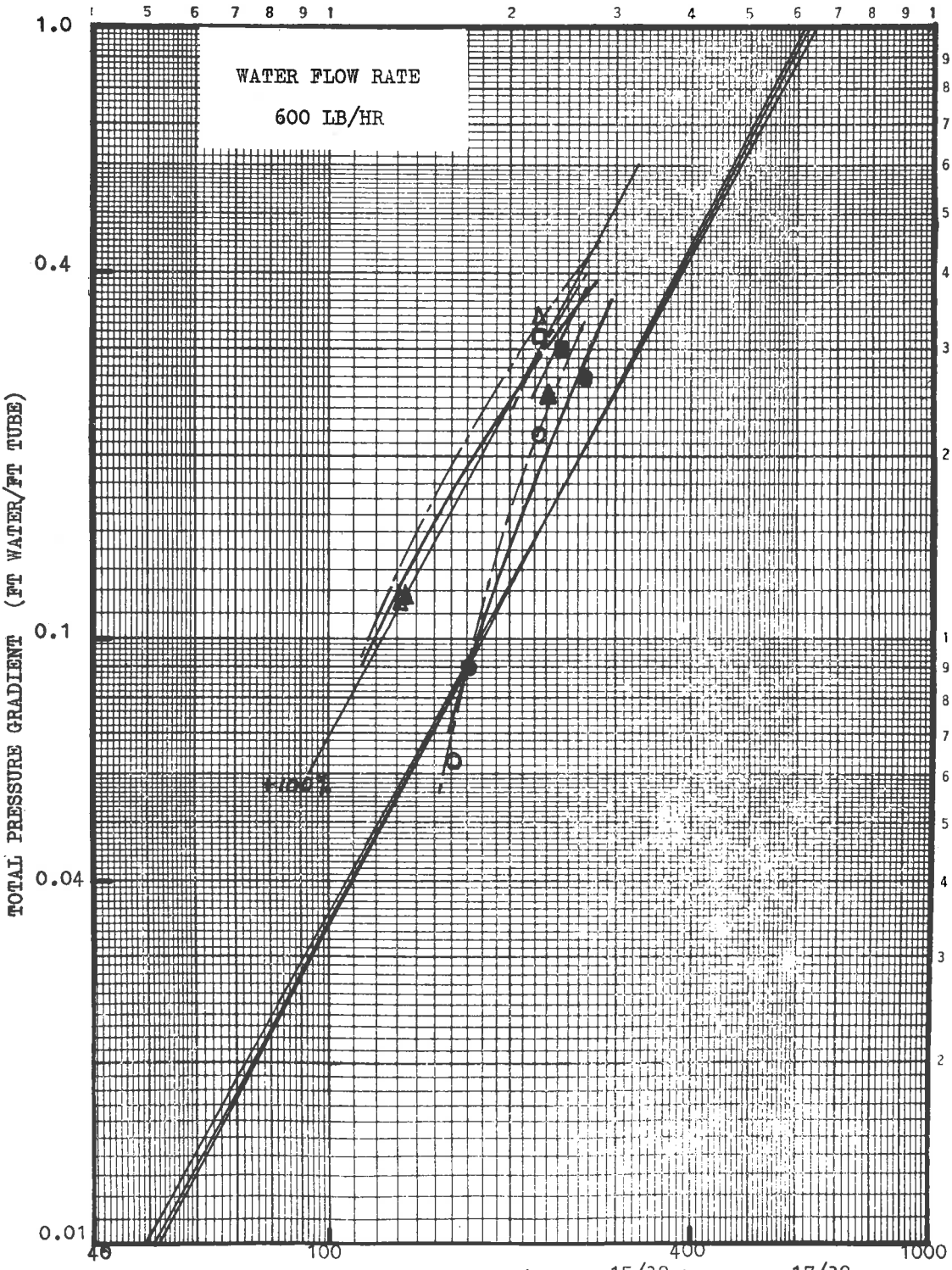
WATER FLOW RATE
600 LB/HR
TOTAL PRESSURE GRADIENT (FT WATER/FT TUBE)
1.0
0.4
0.1
0.04
0.01
40
100
400
1000
REDUCED VELOCITY (FT/SEC) = 1/3600 [(G_L+G_G)/ρ_ref]^15/32 [G_L/ρ_L + G_G/ρ_G]^17/32
ρ_ref = 0.0712 LB/FT^3 ; G_L AND G_G IN LB/FT^2 HR.

A-121.

LEGEND

WATER RATE (LB/HR)	INJECTOR TYPE	SYSTEM PRESSURE	PRESSURE GRADIENT SYMBOL Δ11	PRESSURE GRADIENT SYMBOL Δ235	PRESSURE GRADIENT GRAPH Δ11	PRESSURE GRADIENT GRAPH Δ235
1500	Porous Wall	Low	○	●	- ——	——
1500	Porous Wall	Medium	□	■	- ——	——
1500	Porous Wall	High	△	▲	- ——	——

Figure A3.4 TOTAL PRESSURE GRADIENT VERSUS REDUCED VELOCITY

WATER RATE 1500 LB/HR.

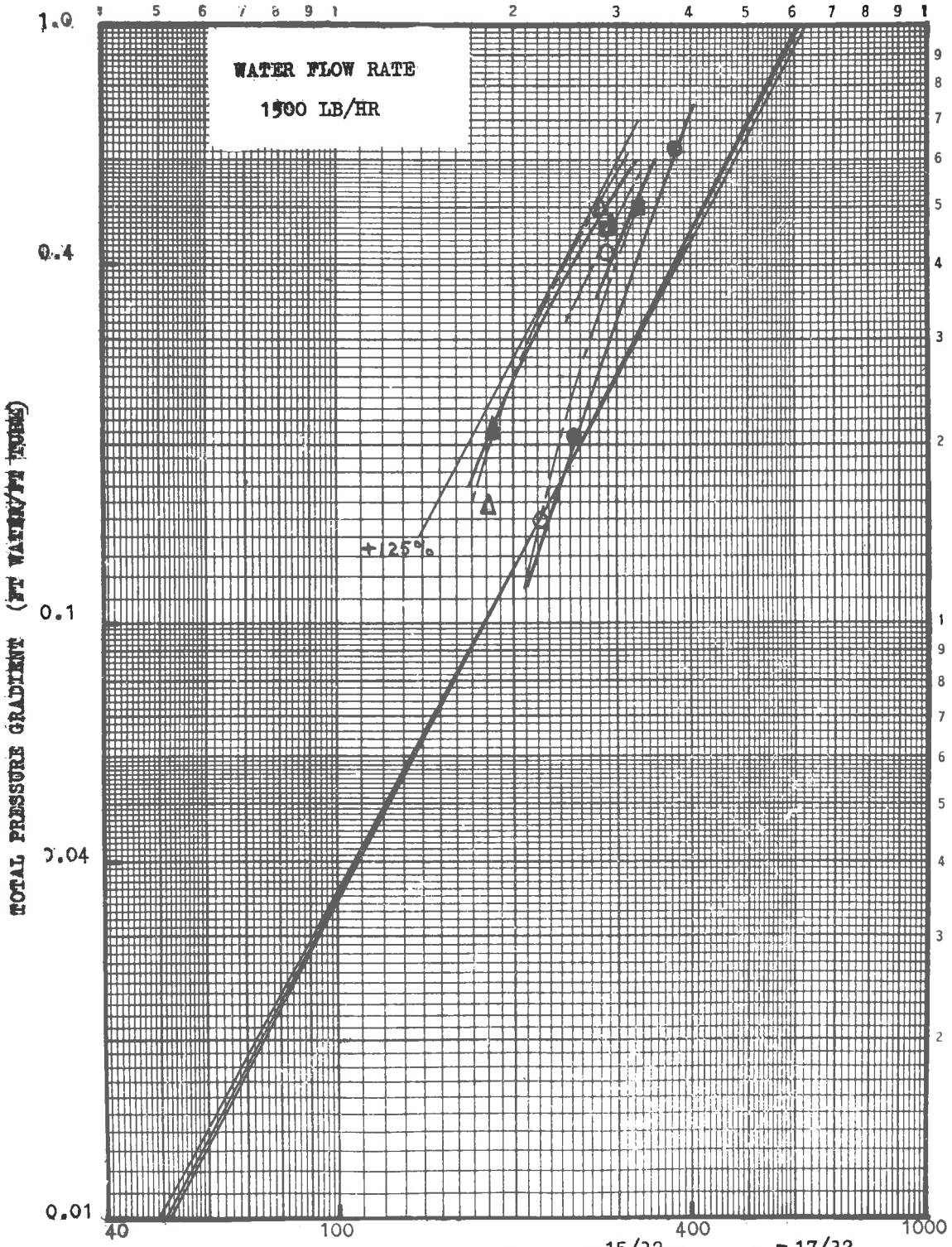

$$\text{REDUCED VELOCITY (FT/SEC)} = \frac{1}{3600}\left[\frac{G_L+G_G}{\rho_{ref}}\right]^{15/32}\left[\frac{G_L}{\rho_L}+\frac{G_G}{\rho_G}\right]^{17/32}$$

ρ_{ref} = 0.0712 LB/FT^3. G_L AND G_G IN LB/FT^{2}HR.

A-122.

LEGEND

WATER RATE (LB/HR)	INJECTOR TYPE	SYSTEM PRESSURE	PRESSURE GRADIENT SYMBOL Δ11	Δ235	GRADIENT GRAPH Δ11	Δ235
2000	Porous Wall	Low	○	●	- ——	——
2000	Porous Wall	Medium	□	■	- ——	——
2000	Porous Wall	High	△	▲	- ——	——
2000	Spray	High	▽	▼	— — —	— —

Figure A3.5 TOTAL PRESSURE GRADIENT VERSUS REDUCED VELOCITY WATER RATE 2000 LB/HR.

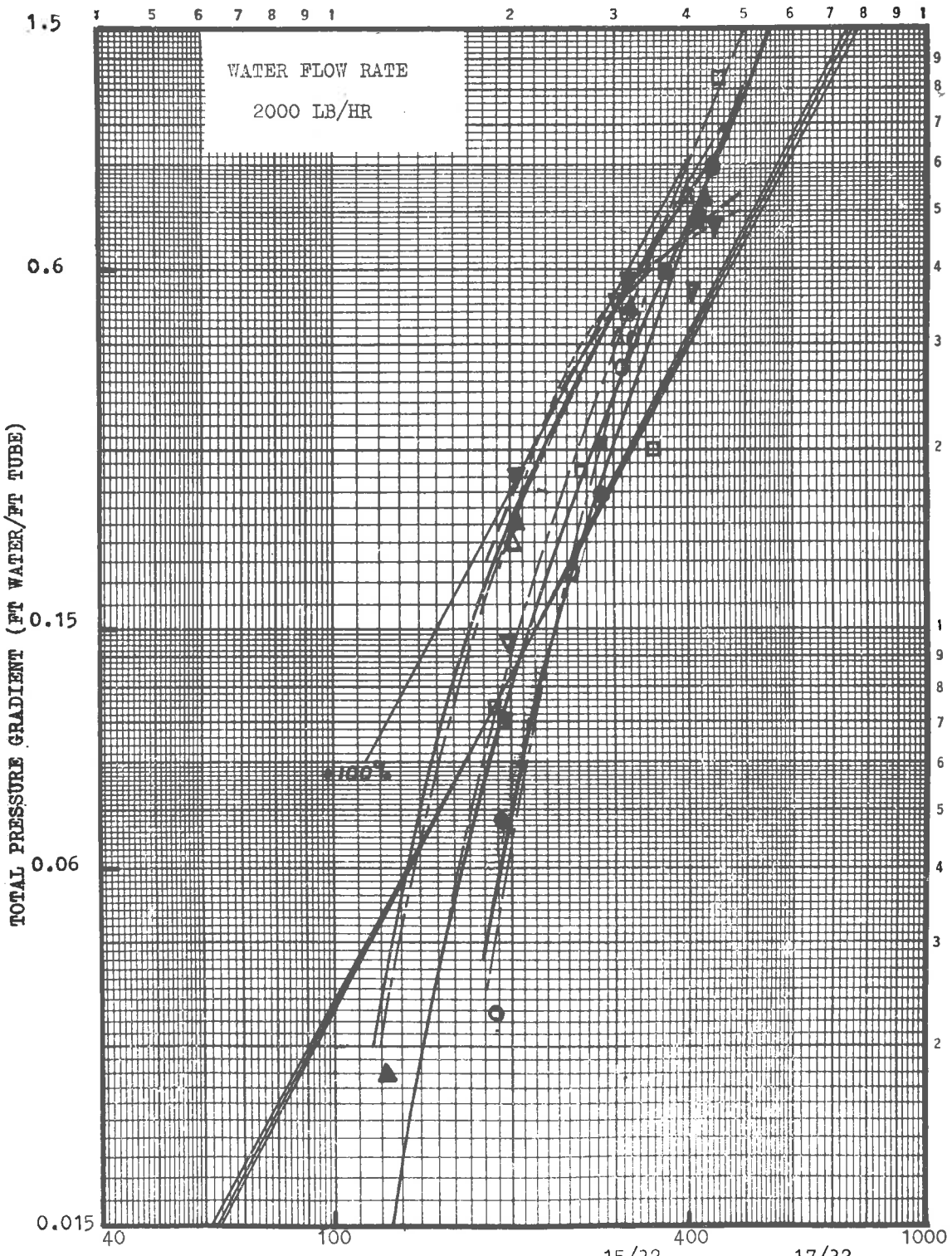
WATER FLOW RATE
2000 LB/HR
100%
TOTAL PRESSURE GRADIENT (FT WATER/FT TUBE)
1.5
0.6
0.15
0.06
0.015
40
100
400
1000
REDUCED VELOCITY (FT/SEC) = $\frac{1}{3600}\left[\frac{G_L+G_G}{\rho_{ref}}\right]^{15/32}\left[\frac{G_L}{\rho_L}+\frac{G_G}{\rho_G}\right]^{17/32}$
ρ_{ref} = 0.0712 LB/FT^3. G_L AND G_G IN LB/FT^{2}HR.

A-123.

LEGEND

WATER RATE (LB/HR)	INJECTOR TYPE	SYSTEM PRESSURE	PRESSURE GRADIENT SYMBOL Δ11	Δ235	GRAPH Δ11	Δ235
2500	Porous Wall	Medium	□	■	Common with 3000	
2700	Porous Wall	Low	○	●	– ———	———
2700	Spray	Medium	◇	◆	– – –	– –
2700	Porous Wall	High	△	▲	– ———	———
3000	Porous Wall	Medium	□	■	– ———	———

Figure A3.6 TOTAL PRESSURE GRADIENT VERSUS REDUCED VELOCITY WATER RATES 2500, 2700 AND 3000 LB/HR.

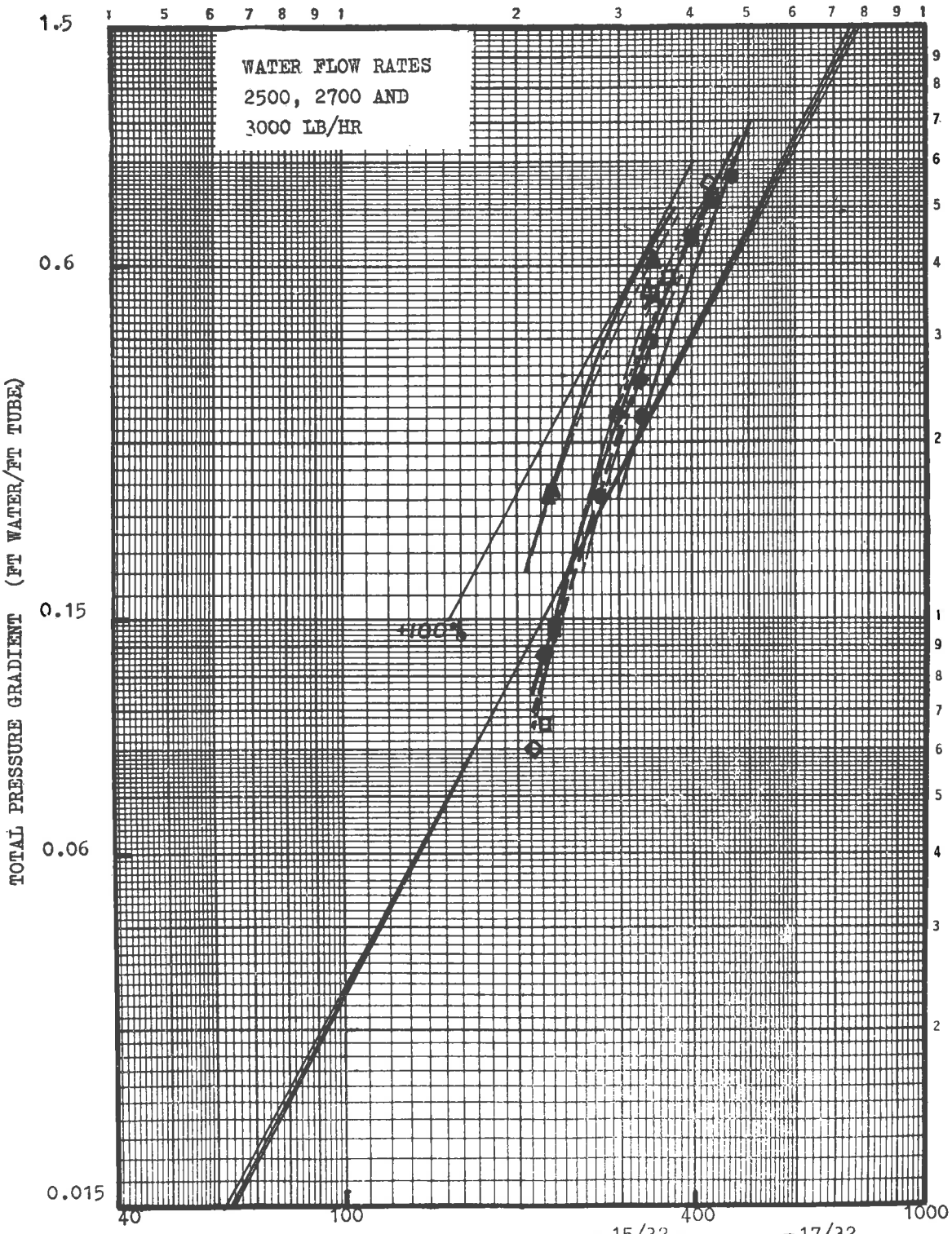
WATER FLOW RATES
2500, 2700 AND
3000 LB/HR
100%
TOTAL PRESSURE GRADIENT (FT WATER/FT TUBE)
1.5
0.6
0.15
0.06
0.015
40
100
400
1000
REDUCED VELOCITY (FT/SEC) = $\frac{1}{3600}\left[\frac{G_L+G_G}{\rho_{ref}}\right]^{15/32}\left[\frac{G_L}{\rho_L}+\frac{G_G}{\rho_G}\right]^{17/32}$
ρ_{ref} = 0.0712 LB/FT^3. G_L AND G_G IN LB/FT^{2}HR.

A-124.

LEGEND

WATER RATE (LB/HR)	INJECTOR TYPE	SYSTEM PRESSURE	PRESSURE GRADIENT SYMBOL Δ11	PRESSURE GRADIENT SYMBOL Δ235	GRAPH Δ11	GRAPH Δ235
3500	Porous Wall	Low	○	●	- ——	——
3500	Porous Wall	Medium	□	■	- ——	——
3500	Porous Wall	High	△	▲	- ——	——
3700	Porous Wall	Medium	⌑	◪	Common with 3500	

Figure A3.7 TOTAL PRESSURE GRADIENT VERSUS REDUCED VELOCITY WATER RATES 3500 AND 3700 LB/HR.

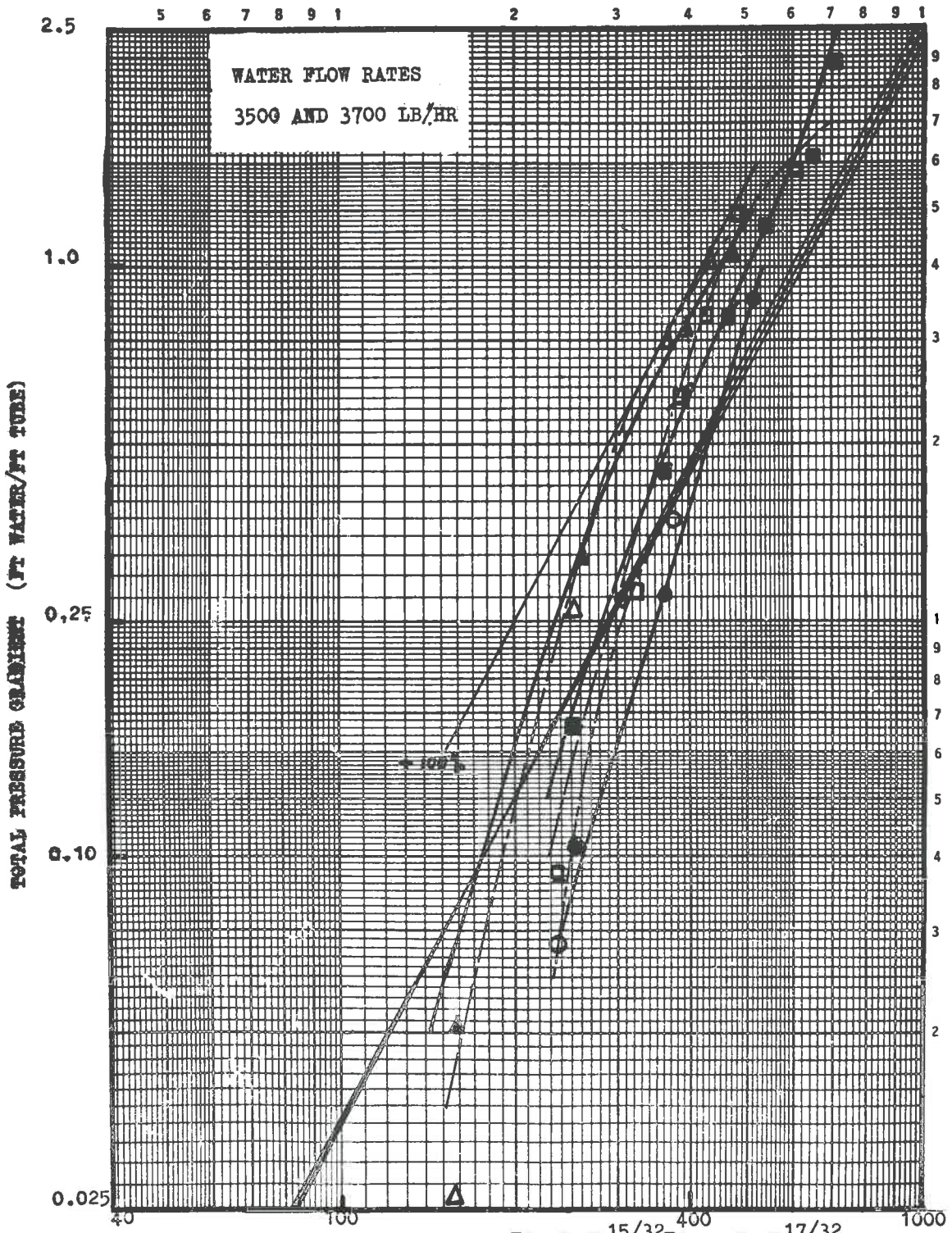

$$\text{REDUCED VELOCITY (FT/SEC)} = \frac{1}{3600}\left[\frac{G_L+G_G}{\rho_{ref}}\right]^{15/32}\left[\frac{G_L}{\rho_L}+\frac{G_G}{\rho_G}\right]^{17/32}$$

ρ_{ref} = 0.0712 LB/FT^3. G_L AND G_G IN LB/FT^{2}HR.

A-125.

LEGEND

MEAN SUPERFICIAL AIR VELOCITY AT 235 IN. LEVEL (FT/SEC)	MEAN AIR DENSITY AT 235 IN. LEVEL (LB/FT^3)	INJECTOR TYPE	WAVE VELOCITY SYMBOL	WAVE VELOCITY LINE DESIGNATED BY
0	0.0267	Porous Wall	●	L00
50.9	0.0269	Porous Wall	●	L51
104.5	0.0268	Porous Wall	●	L105
208.8	0.0268	Porous Wall	●	L209
(Point (2875, 17.05) is for 235 ft/sec, 0.0255 lb/ft^3)				
347.9	0.0268	Porous Wall	●	L348

Figure A3.8 MEAN WAVE VELOCITY VERSUS

DIMENSIONLESS LIQUID FLOW RATE, $N_{Re_L} = \frac{W_L}{\pi D \mu_L}$

LOW PRESSURE SERIES AND 235 INCH LEVEL.

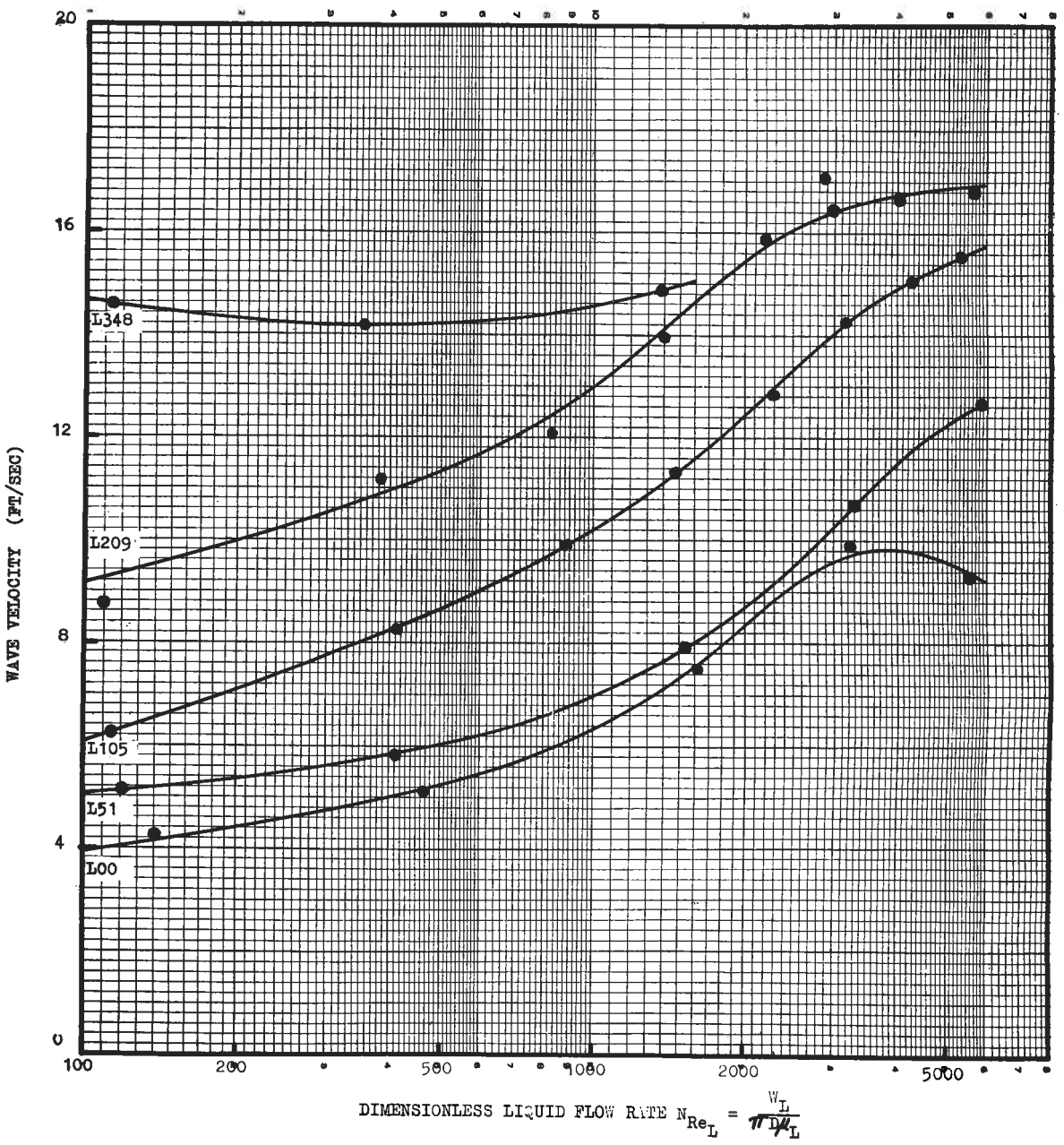
WAVE VELOCITY (FT/SEC)
20
16
12
8
4
0
L348
L209
L105
L51
L00
100
200
500
1000
2000
5000
DIMENSIONLESS LIQUID FLOW RATE $N_{Re_L} = \frac{W_L}{\pi D \mu_L}$

A-126.

LEGEND

MEAN SUPERFICIAL AIR VELOCITY AT 235 IN. LEVEL (FT/SEC)	MEAN AIR DENSITY AT 235 IN.LEVEL (LB/FT3)	INJECTOR TYPE	MEASUREMENT LEVEL	WAVE VELOCITY SYMBOL	WAVE VELOCITY LINE DESIGNATED BY
51.4	0.0721	Porous Wall	Top	□	M51
52.8	0.0708	Porous Wall	Centre	◧	M53
51.4	0.0715	Spray	Top	◇	MS51
50.4	0.0718	Spray	Centre	◆	MS50
100.6	0.0707	Porous Wall	Top	□	M101
105.8	0.0706	Porous Wall	Centre	◧	M106
102.2	0.0707	Spray	Top	◇	MS102
102.5	0.0709	Spray	Centre	◆	MS103
200.5	0.0717	Porous Wall	Top	□	M201
206.6	0.0700	Porous Wall	Centre	◧	M207
203.6	0.0720	Spray	Top	◇	MS204
210.1	0.0704	Spray	Centre	◆	MS210

Figure A3.9 MEAN WAVE VELOCITY VERSUS DIMENSIONLESS LIQUID FLOW RATE, $N_{Re_L} = \frac{W_L}{\pi D \mu_L}$.

MEDIUM PRESSURE SERIES, 11 INCH AND 56 INCH LEVELS.

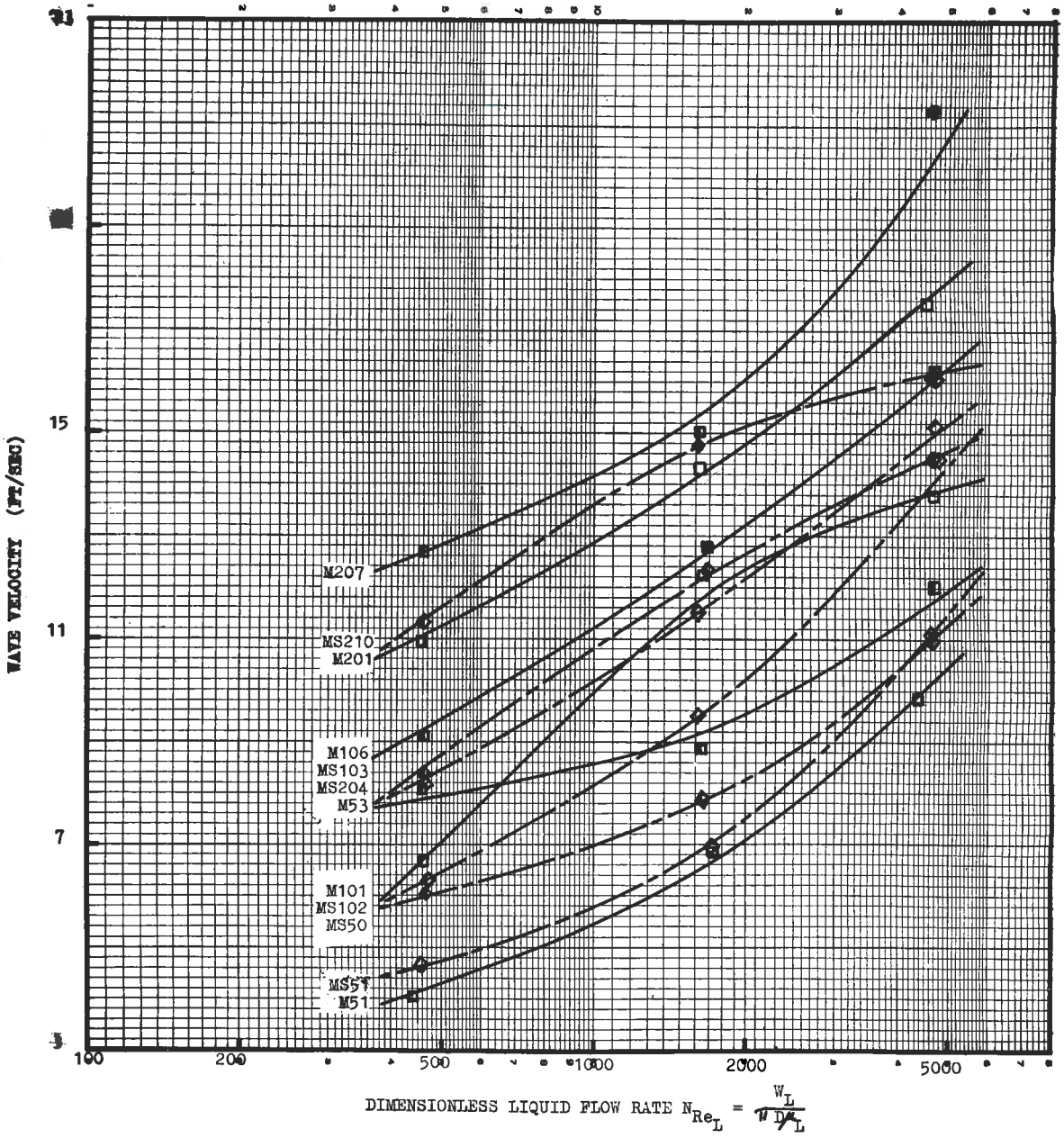
WAVE VELOCITY (FT/SEC)
21
15
11
7
5
100
200
500
1000
2000
5000
M207
MS210
M201
M106
MS103
MS204
M53
M101
MS102
MS50
MS51
M51
DIMENSIONLESS LIQUID FLOW RATE $N_{Re_L} = \frac{W_L}{\pi D \mu_L}$

A-127.

LEGEND

MEAN SUPERFICIAL AIR VELOCITY AT 235 IN. LEVEL (FT/SEC)	MEAN AIR DENSITY AT 235 IN. LEVEL (LB/FT^3)	INJECTOR TYPE	WAVE VELOCITY SYMBOL	WAVE VELOCITY LINE DESIGNATED BY
0	0.2225	Porous Wall	▲	H00
20.2	0.2213	Porous Wall	▲	H20
51.1	0.2207	Porous Wall	▲	H51
51.1	0.2193	Spray	▼	HS51
104.0	0.2211	Porous Wall	▲	H104
102.8	0.2183	Spray	▼	HS103
161.4	0.2208	Porous Wall	▲	H161
(Point (5720, 20.56) is for 142 ft/sec, 0.2189 lb/ft^3)				
162.2	0.2182	Spray	▼	HS162

Figure A3.10 MEAN WAVE VELOCITY VERSUS DIMENSIONLESS LIQUID FLOW RATE, $N_{Re_L} = \frac{W_L}{\pi D \mu_L}$.

HIGH PRESSURE SERIES AND 235 INCH LEVEL.

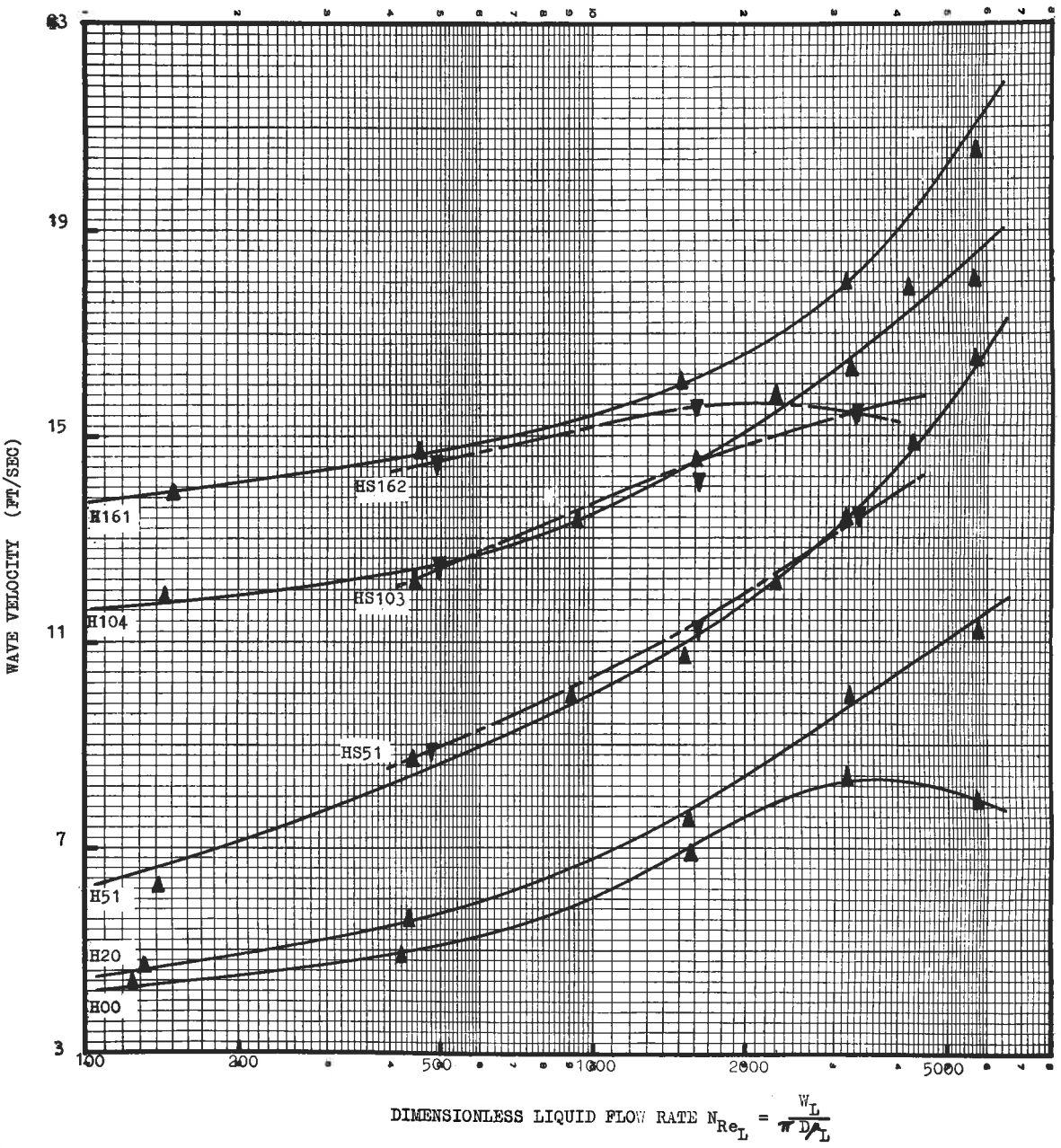
WAVE VELOCITY (FT/SEC)
23
19
15
11
7
3
100
200
500
1000
2000
5000
HS162
H161
HS103
H104
HS51
H51
H20
H00
DIMENSIONLESS LIQUID FLOW RATE $N_{Re_L} = \frac{W_L}{\pi D \mu_L}$

A-128.

LEGEND

MEAN SUPERFICIAL AIR VELOCITY AT 235 IN. LEVEL (FT/SEC)	MEAN AIR DENSITY AT 235 IN.LEVEL (LB/FT3)	INJECTOR TYPE	MEASUREMENT LEVEL	WAVE VELOCITY SYMBOL	WAVE VELOCITY LINE DESIGNATED BY
51.1	0.2188	Porous Wall	Top	Δ	H51
52.0	0.2201	Porous Wall	Centre	◭	H52
51.3	0.2167	Spray	Top	▽	HS51
51.5	0.2192	Spray	Centre	▼	HS52
100.3	0.2187	Porous Wall	Top	Δ	H100
103.2	0.2201	Porous Wall	Centre	◭	H103
104.6	0.2141	Spray	Top	▽	HS105
102.9	0.2182	Spray	Centre	▼	HS103
160.2	0.2183	Porous Wall	Top	Δ	H160
159.2	0.2201	Porous Wall	Centre	◭	H159
164.9	0.2134	Spray	Top	▽	HS165
161.5	0.2187	Spray	Centre	▼	HS162

Figure A3.11 MEAN WAVE VELOCITY VERSUS DIMENSIONLESS LIQUID FLOW RATE, $N_{Re_L} = \frac{W_L}{\pi D \mu_L}$.

HIGH PRESSURE SERIES, 11 INCH AND 56 INCH LEVELS.

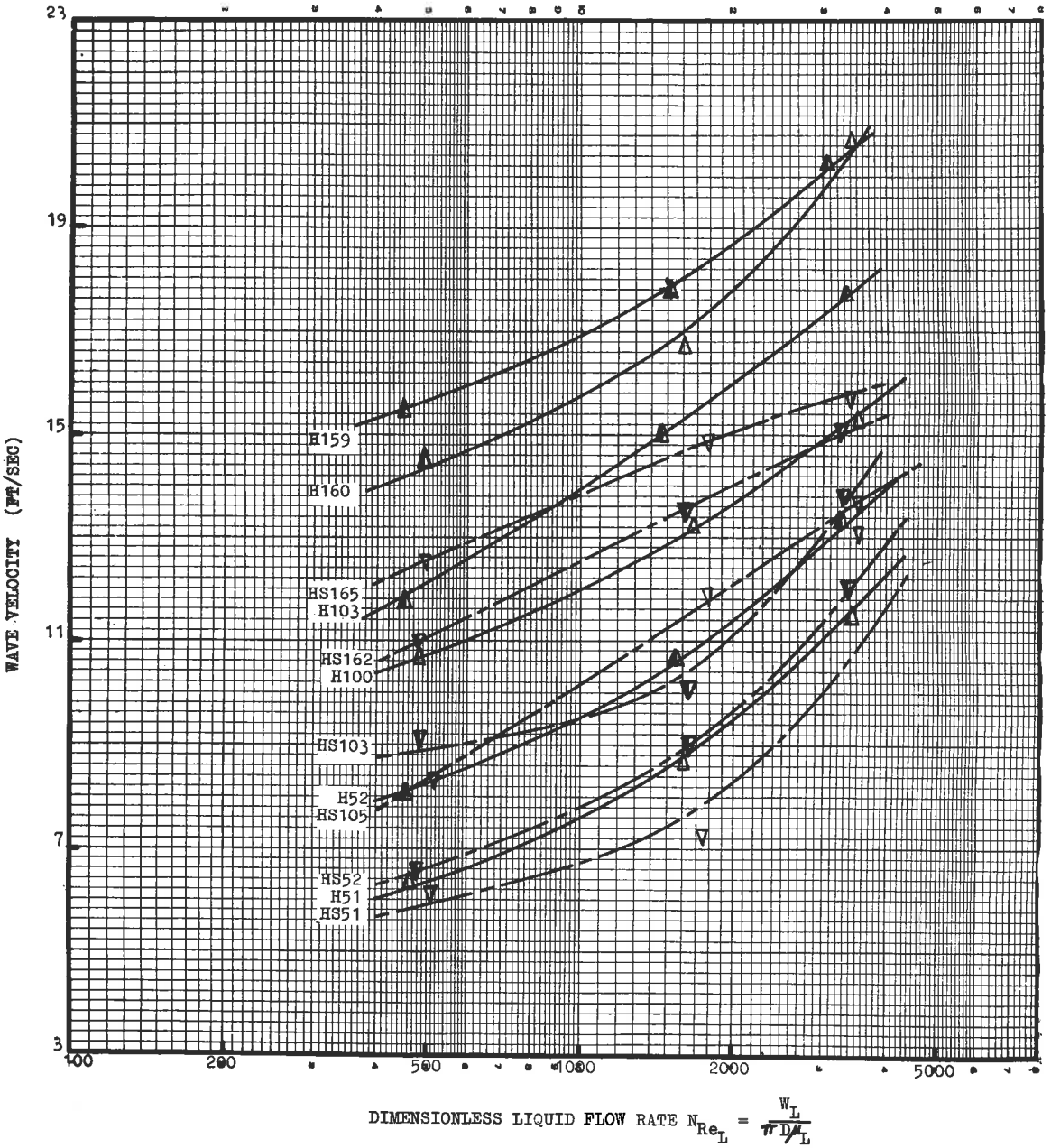
WAVE VELOCITY (FT/SEC)
23
19
15
11
7
3
100
200
500
1000
2000
5000
H159
H160
HS165
H103
HS162
H100
HS103
H52
HS105
HS52
H51
HS51
DIMENSIONLESS LIQUID FLOW RATE $N_{Re_L} = \frac{W_L}{\pi D \mu_L}$

A-129.

LEGEND

PRESSURE	INJECTOR TYPE	CAMERA LEVEL (INCH)	SYMBOL
Low	Porous Wall	235	●
Medium	Porous Wall	11	□
Medium	Spray	11	◇
Medium	Porous Wall	56	◧
Medium	Spray	56	◆
Medium	Porous Wall	235	■
Medium	Spray	235	◆
High	Porous Wall	11	△
High	Spray	11	▽
High	Porous Wall	56	◭
High	Spray	56	▼
High	Porous Wall	235	▲
High	Spray	235	▼

---- Line of best fit for points at 235 inch level.

——— Line of best fit for all points.

Figure A3.12 (TOP) WAVE VELOCITY STANDARD DEVIATION VERSUS MEAN WAVE VELOCITY. LIQUID RATE 100 LB/HR.

Figure A3.13 (BOTTOM) WAVE VELOCITY STANDARD DEVIATION VERSUS MEAN WAVE VELOCITY. LIQUID RATE 300LB/HR.

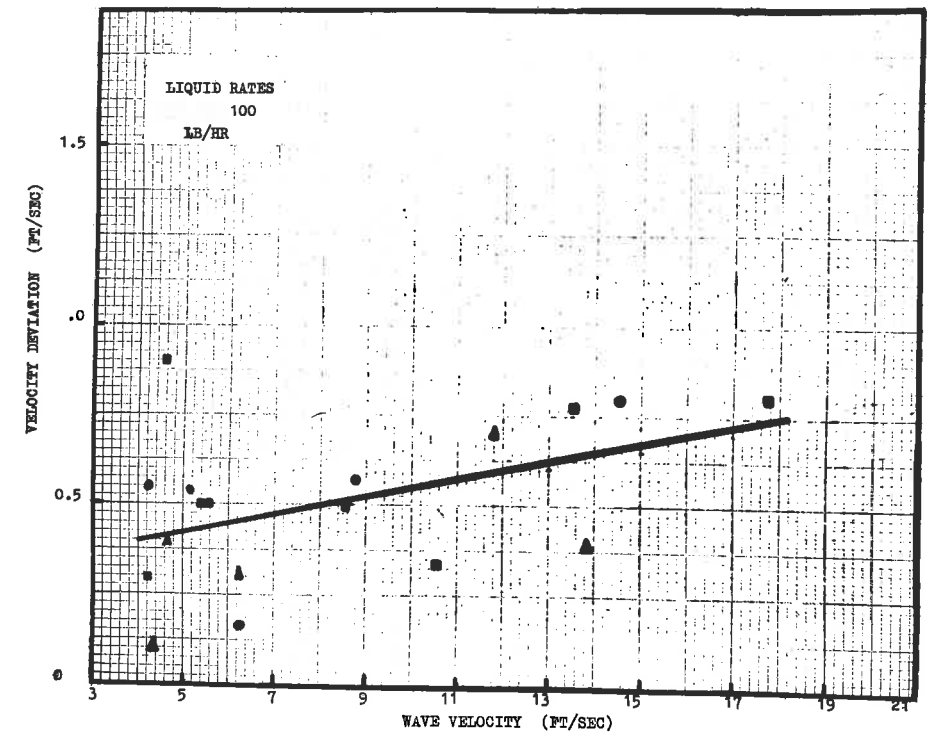
LIQUID RATES
100
LB/HR
VELOCITY DEVIATION (FT/SEC)
1.5
.0
0.5
0
3
5
7
9
11
13
15
17
19
21
WAVE VELOCITY (FT/SEC)

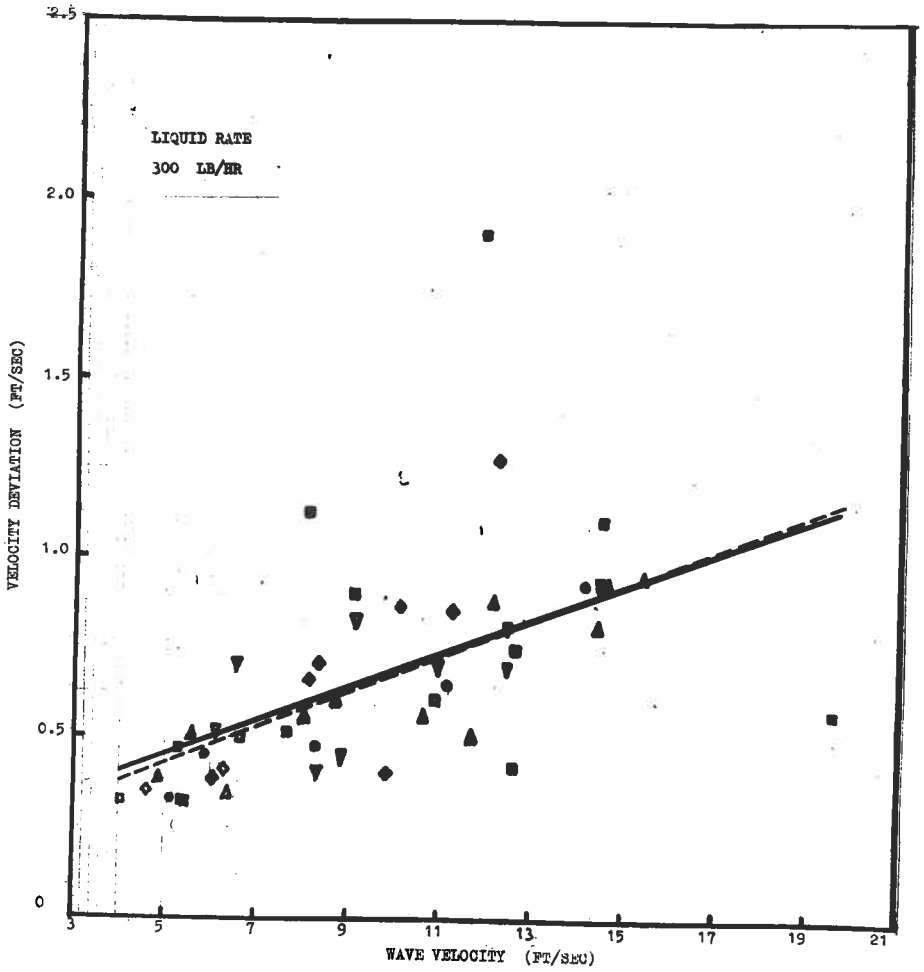
LIQUID RATE
300 LB/HR
VELOCITY DEVIATION (FT/SEC)
2.5
2.0
1.5
1.0
0.5
0
3
5
7
9
11
13
15
17
19
21
WAVE VELOCITY (FT/SEC)

A-130.

LEGEND

PRESSURE	INJECTOR TYPE	CAMERA LEVEL (INCH)	SYMBOL
Low	Porous Wall	235	●
Medium	Porous Wall	11	□
Medium	Spray	11	◇
Medium	Porous Wall	56	◧
Medium	Spray	56	◈
Medium	Porous Wall	235	■
Medium	Spray	235	◆
High	Porous Wall	11	△
High	Spray	11	▽
High	Porous Wall	56	◭
High	Spray	56	▽
High	Porous Wall	235	◭
High	Spray	235	▼

--- Line of best fit for points at 235 inch level.

——— Line of best fit for all points.

Figure A3.14 (TOP) WAVE VELOCITY STANDARD DEVIATION VERSUS MEAN WAVE VELOCITY. LIQUID RATE 1500 LB/HR.

Figure A3.15 (BOTTOM) WAVE VELOCITY STANDARD DEVIATION VERSUS MEAN WAVE VELOCITY. LIQUID RATE 2000 LB/HR.

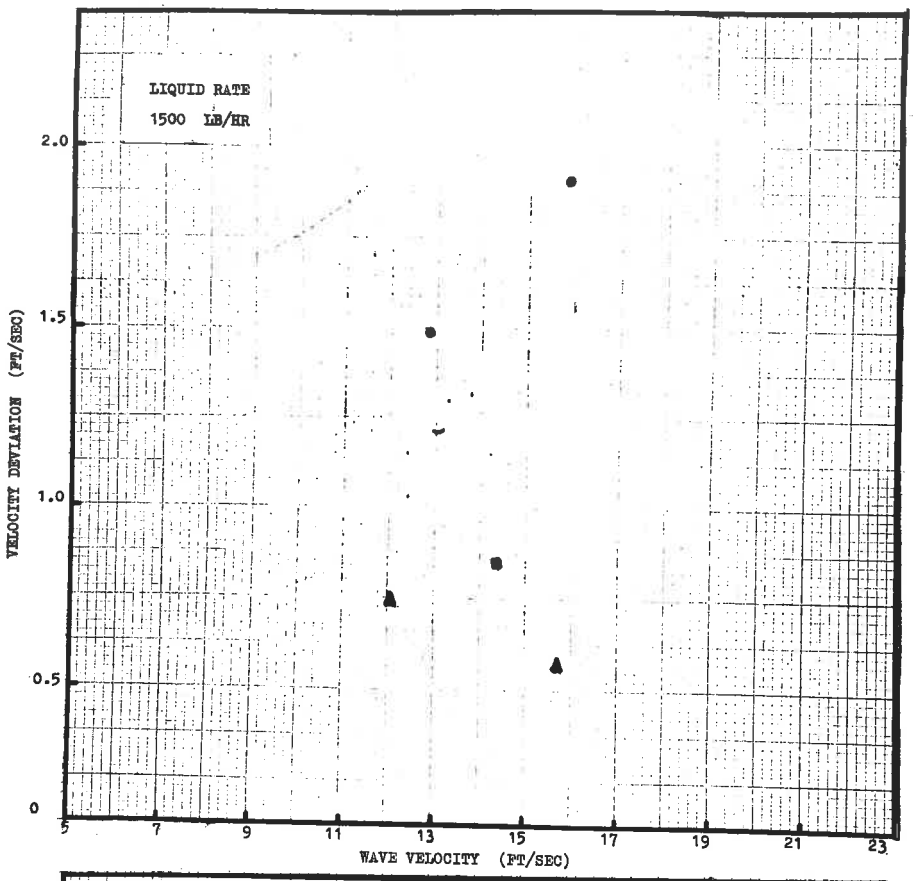
LIQUID RATE
1500 LB/HR
VELOCITY DEVIATION (FT/SEC)
2.0
1.5
1.0
0.5
0
5
7
9
11
13
15
17
19
21
23
WAVE VELOCITY (FT/SEC)

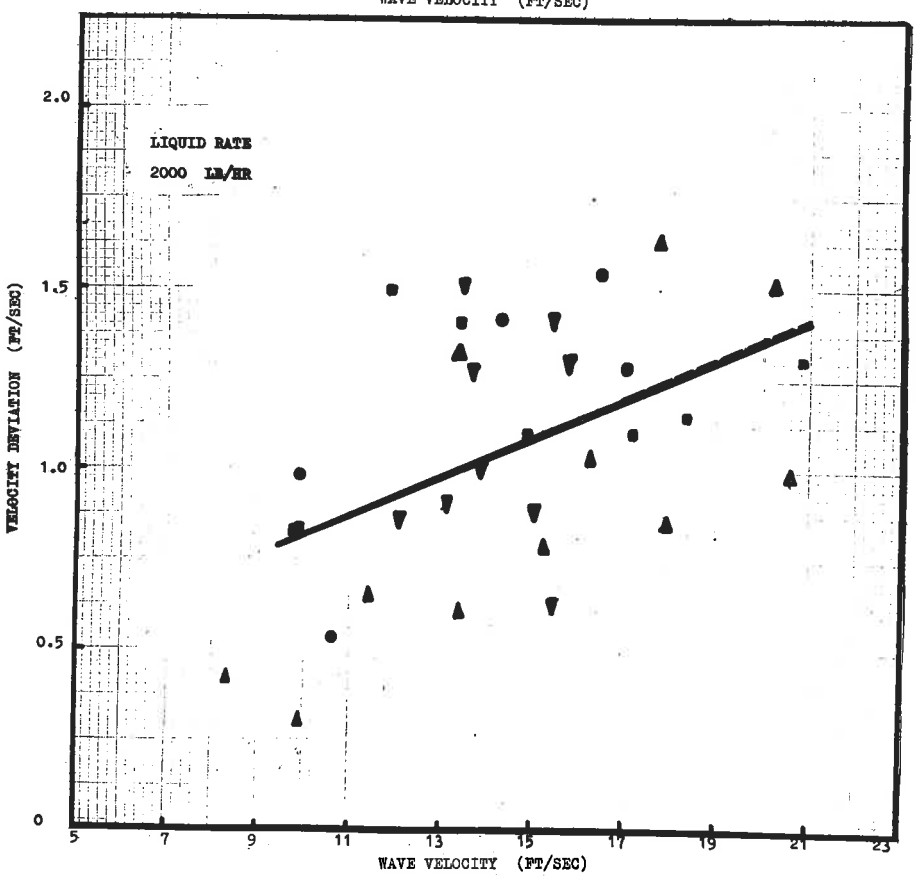
LIQUID RATE
2000 LB/HR
VELOCITY DEVIATION (FT/SEC)
2.0
1.5
1.0
0.5
0
5
7
9
11
13
15
17
19
21
23
WAVE VELOCITY (FT/SEC)

A-131.

LEGEND

PRESSURE	INJECTOR TYPE	CAMERA LEVEL (INCH)	SYMBOL
Low	Porous Wall	235	●
Medium	Porous Wall	11	□
Medium	Spray	11	◇
Medium	Porous Wall	56	◧
Medium	Spray	56	◈
Medium	Porous Wall	235	■
Medium	Spray	235	◆
High	Porous Wall	11	△
High	Spray	11	▽
High	Porous Wall	56	◭
High	Spray	56	▽
High	Porous Wall	235	▲
High	Spray	235	▼

--- Line of best fit for points at 235 inch level.

——— Line of best fit for all points.

Figure A3.16 (TOP) WAVE VELOCITY STANDARD DEVIATION VERSUS MEAN WAVE VELOCITY. LIQUID RATE 2700LB/HR.

Figure A3.17 (BOTTOM) WAVE VELOCITY STANDARD DEVIATION VERSUS MEAN WAVE VELOCITY LIQUID RATE 3500 LB/HR.

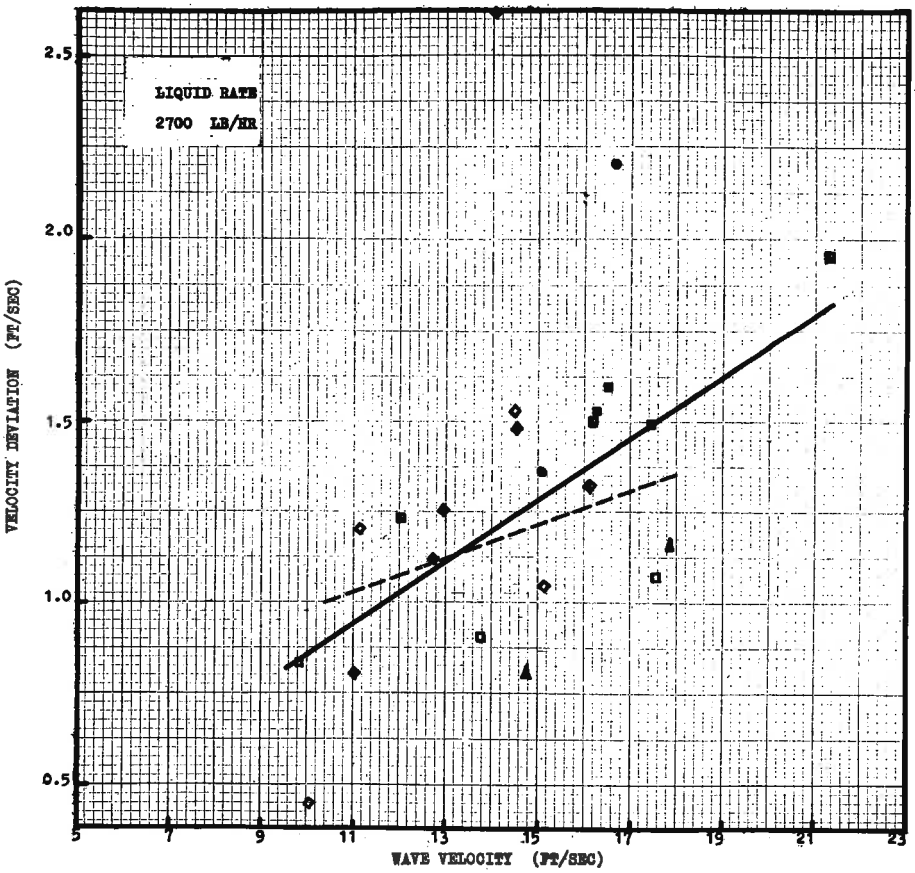
LIQUID RATE
2700 LB/HR
VELOCITY DEVIATION (FT/SEC)
WAVE VELOCITY (FT/SEC)
2.5
2.0
1.5
1.0
0.5
5
7
9
11
13
15
17
19
21
23

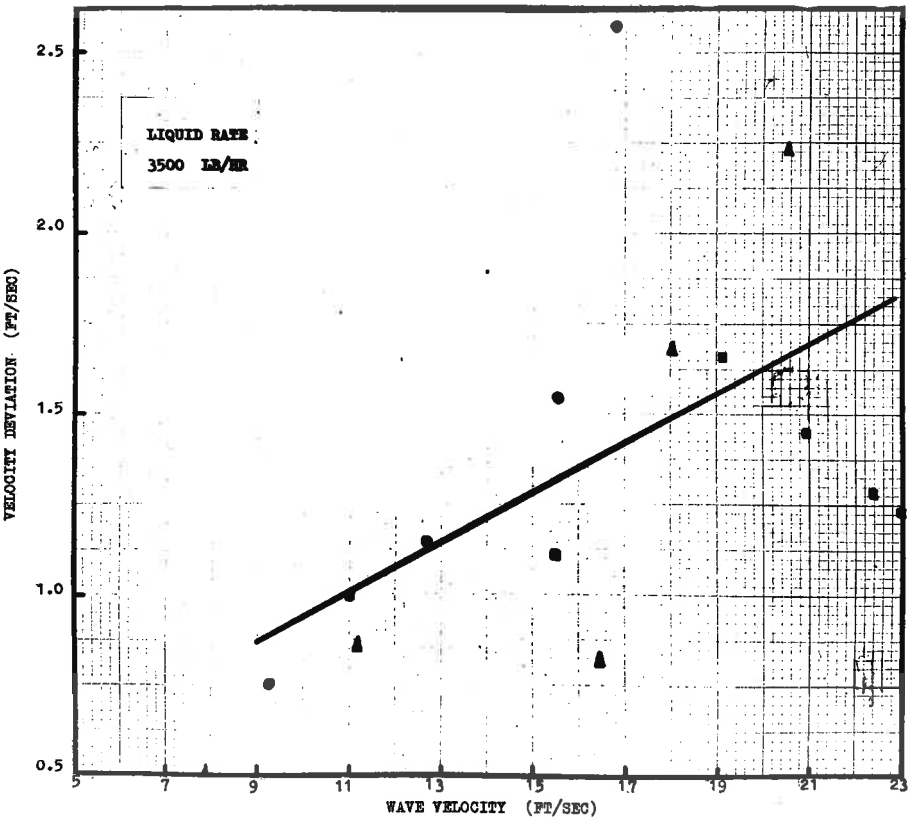
LIQUID RATE
3500 LB/HR
VELOCITY DEVIATION (FT/SEC)
WAVE VELOCITY (FT/SEC)
2.5
2.0
1.5
1.0
0.5
5
7
9
11
13
15
17
19
21
23

A-132.

LEGEND.

MEAN SUPERFICIAL AIR VELOCITY AT 235 IN. LEVEL (FT/SEC)	MEAN AIR DENSITY AT 235 IN. LEVEL (LB/FT^3)	INJECTOR TYPE	TIME BETWEEN WAVES SYMBOL	TIME BETWEEN WAVES LINES DESIGNATED BY
0	0.0267	Porous Wall	●	L00
50.9	0.0269	Porous Wall	●	L51
104.5	0.0268	Porous Wall	●	L105
208.8	0.0268	Porous Wall	●	L209

(Point (2875, 0.033) is for 235 ft/sec, 0.0255 lb/ft^3)

347.9	0.0268	Porous Wall	●	L348

Figure A3.18 MEAN TIME BETWEEN WAVES VERSUS DIMENSIONLESS LIQUID FLOW RATE, $N_{Re_L} = \frac{W_L}{\pi D_H \mu_L}$.

LOW PRESSURE SERIES AND 235 INCH LEVEL.

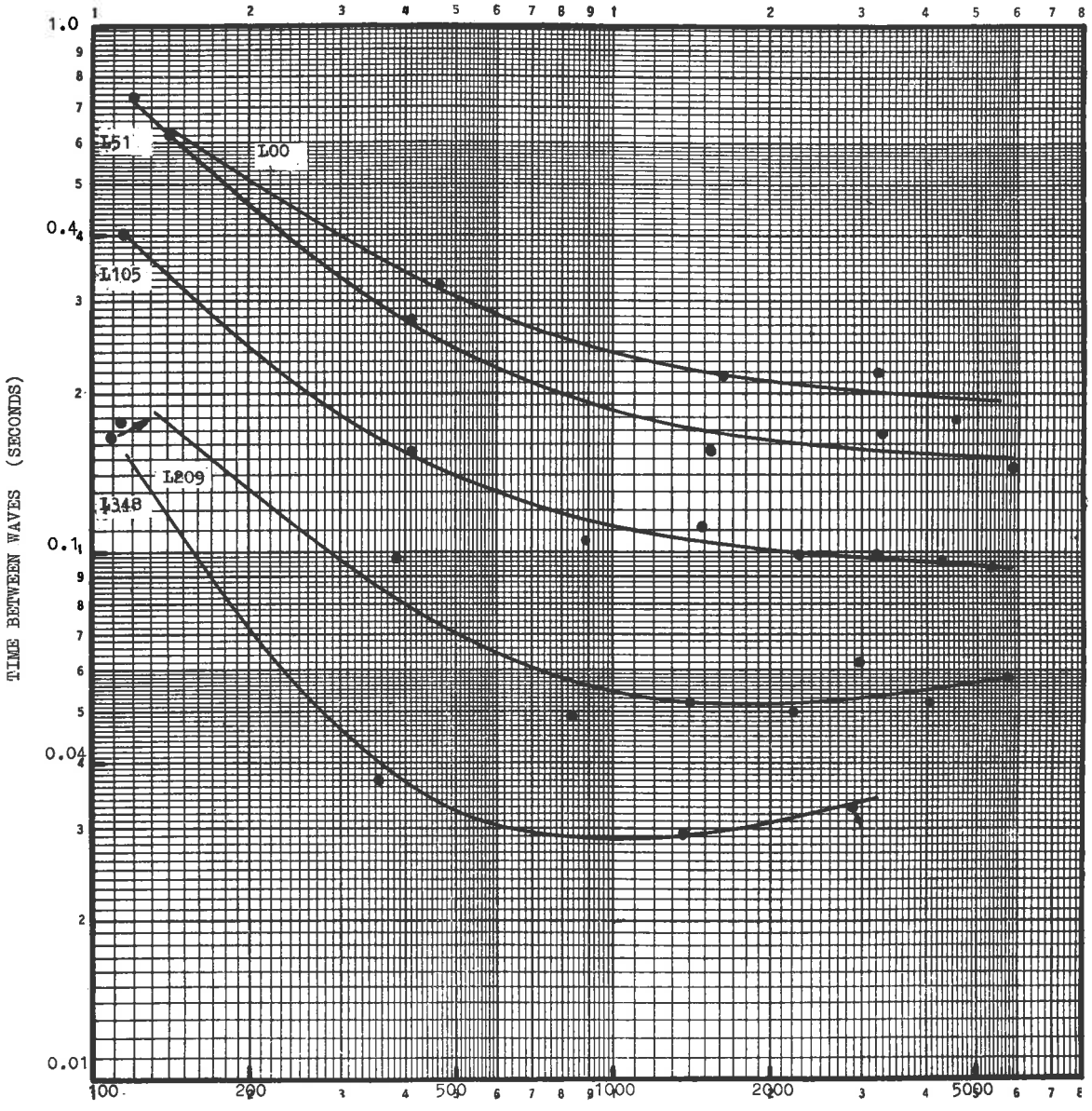
L51
L00
L105
L209
L348
TIME BETWEEN WAVES (SECONDS)
1.0
0.4
0.1
0.04
0.01
100
200
500
1000
2000
5000
DIMENSIONLESS LIQUID FLOW RATE $N_{Re_L} = \frac{W_L}{\pi D \mu_L}$

A-133.

LEGEND.

MEAN SUPERFICIAL AIR VELOCITY AT 235 IN. LEVEL (FT/SEC)	MEAN AIR DENSITY AT 235 IN. LEVEL (LB/FT^3)	INJECTOR TYPE	MEASUREMENT LEVEL	TIME BETWEEN WAVES SYMBOL	TIME BETWEEN WAVES LINE DESIGNATED BY
51.9	0.0714	Porous Wall	Top	□	M52
52.8	0.0708	Porous Wall	Centre	◧	M53
51.8	0.0711	Spray	Top	◇	MS52
50.4	0.0718	Spray	Centre	◈	MS50
100.6	0.0707	Porous Wall	Top	□	M101
105.8	0.0706	Porous Wall	Centre	◧	M106
102.3	0.0714	Spray	Top	◇	MS102
102.5	0.0709	Spray	Centre	◈	MS103
200.5	0.0717	Porous Wall	Top	□	M201
206.6	0.0700	Porous Wall	Centre	◧	M207
203.9	0.0718	Spray	Top	◇	MS204
210.1	0.0704	Spray	Centre	◈	MS210

Figure A3.19 MEAN TIME BETWEEN WAVES VERSUS DIMENSIONLESS LIQUID FLOW RATE, $N_{Re_L} = \frac{W_L}{\pi D \mu_L}$ MEDIUM PRESSURE SERIES, 11 INCH AND 56 INCH LEVELS.

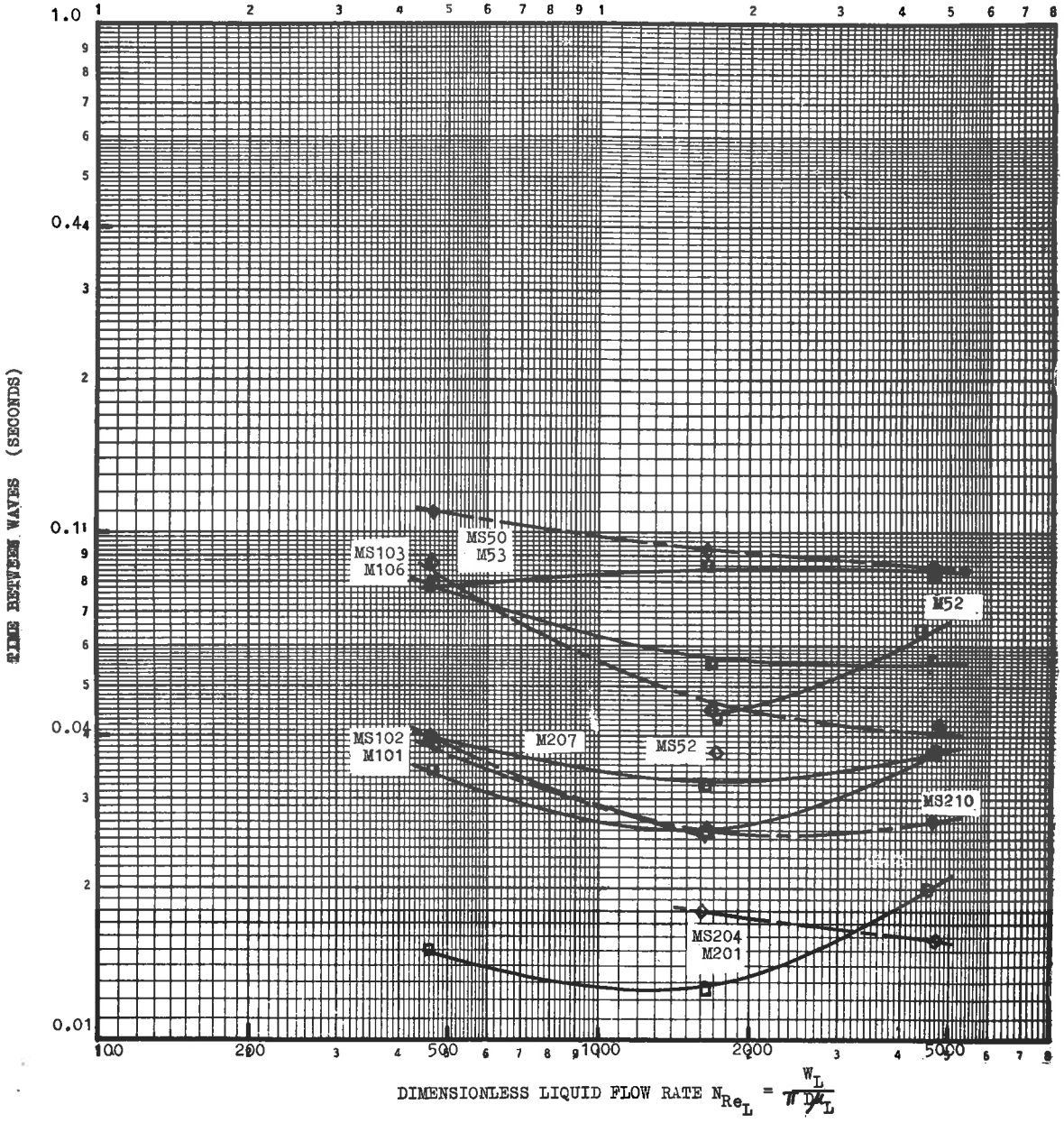
TIME BETWEEN WAVES (SECONDS)
1.0
0.4
0.1
0.04
0.01
100
200
500
1000
2000
5000
MS50
M53
MS103
M106
M52
MS102
M101
M207
MS52
MS210
MS204
M201
DIMENSIONLESS LIQUID FLOW RATE $N_{Re_L} = \frac{W_L}{\pi D \mu_L}$

A-134.

LEGEND

MEAN SUPERFICIAL AIR VELOCITY AT 235 IN. LEVEL (FT/SEC)	MEAN AIR DENSITY AT 235 IN. LEVEL (LB/FT^3)	INJECTOR TYPE	TIME BETWEEN WAVES SYMBOL	TIME BETWEEN WAVES LINE DESIGNATED BY
0	0.2225	Porous Wall	▲	H00
20.2	0.2213	Porous Wall	▲	H20
51.1	0.2207	Porous Wall	▲	H51
51.1	0.2193	Spray	▼	HS51
104.0	0.2211	Porous Wall	▲	H104
102.8	0.2183	Spray	▼	HS103
161.4	0.2208	Porous Wall	▲	H161
(Point (5720, 0.024) is for 142 ft/sec, 0.2189 lb/ft^3)				
162.2	0.2182	Spray	▼	HS162

Figure A3.20 MEAN TIME BETWEEN WAVES VERSUS DIMENSIONLESS LIQUID FLOW RATE, $N_{Re_L} = \frac{W_L}{\pi \mu_L}$.
HIGH PRESSURE SERIES AND 235 INCH LEVEL.

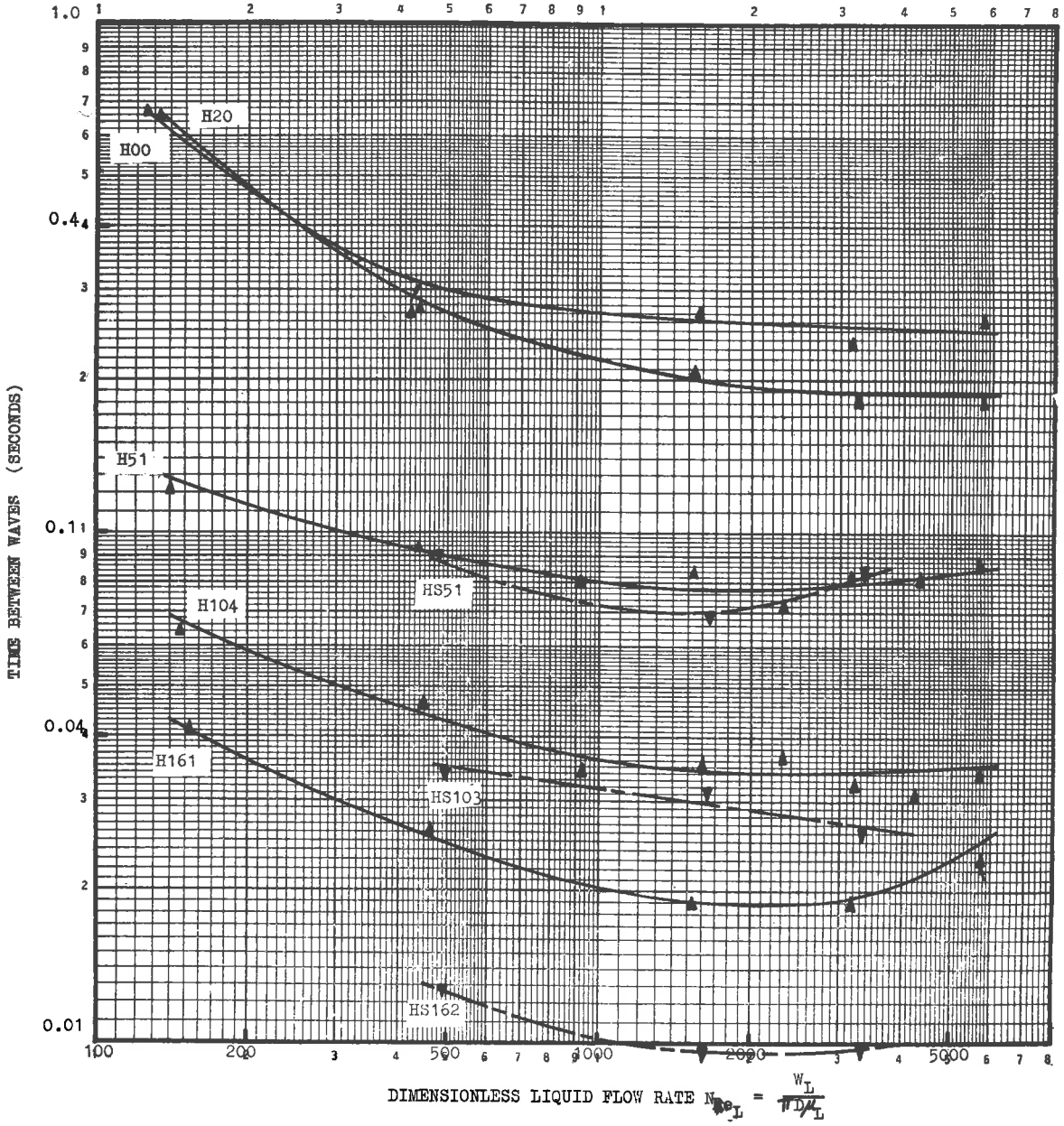
TIME BETWEEN WAVES (SECONDS)
1.0
0.4
0.1
0.04
0.01
H20
H00
H51
HS51
H104
H161
HS103
HS162
100
200
500
1000
2000
5000
DIMENSIONLESS LIQUID FLOW RATE $N_{Re_L} = \frac{W_L}{\pi D \mu_L}$

A-135.

LEGEND

MEAN SUPERFICIAL AIR VELOCITY AT 235 IN. LEVEL (FT/SEC)	MEAN AIR DENSITY AT 235 IN. LEVEL (LB/FT3)	INJECTOR TYPE	MEASUREMENT LEVEL	WAVE VELOCITY SYMBOL	WAVE VELOCITY LINE DESIGNATED BY
51.1	0.2188	Porous Wall	Top	Δ	H51
52.0	0.2201	Porous Wall	Centre	◭	H52
51.3	0.2167	Spray	Top	▽	HS51
51.5	0.2192	Spray	Centre	▼	HS52
100.3	0.2187	Porous Wall	Top	Δ	H100
103.2	0.2201	Porous Wall	Centre	◭	H103
104.6	0.2141	Spray	Top	▽	HS105
102.9	0.2182	Spray	Centre	▼	HS103
160.2	0.2183	Porous Wall	Top	Δ	H160
159.2	0.2201	Porous Wall	Centre	◭	H159
164.9	0.2134	Spray	Top	▽	HS165
161.5	0.2187	Spray	Centre	▼	HS162

Figure A3.21 MEAN TIME BETWEEN WAVES VERSUS DIMENSIONLESS LIQUID FLOW RATE, $N_{Re_L} = \frac{W_L}{\pi D \mu_L}$ HIGH PRESSURE SERIES, 11 INCH AND 56 INCH LEVELS.

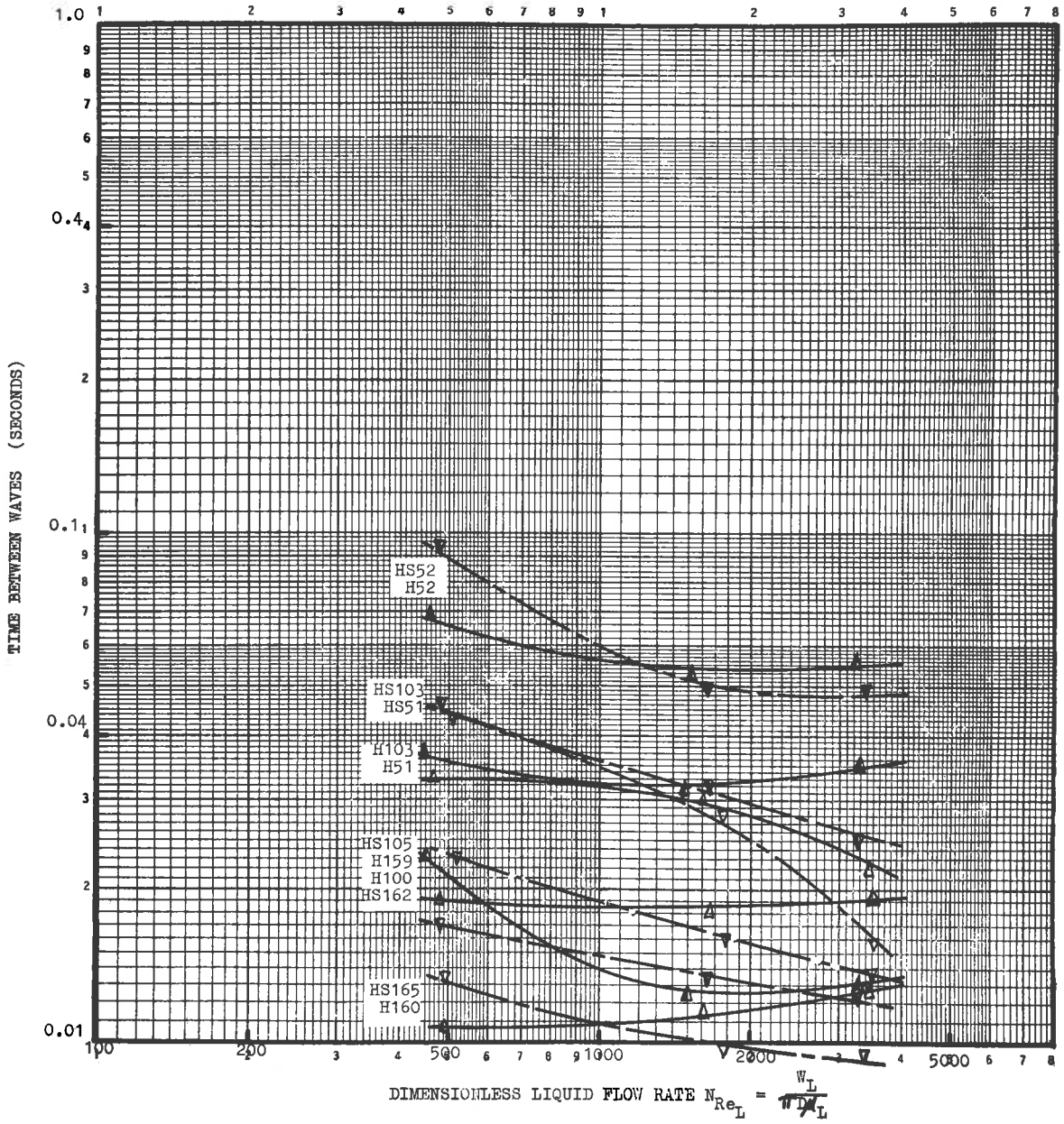
TIME BETWEEN WAVES (SECONDS)
1.0
0.4
0.1
0.04
0.01
HS52
H52
HS103
HS51
H103
H51
HS105
H159
H100
HS162
HS165
H160
100
200
500
1000
2000
5000
DIMENSIONLESS LIQUID FLOW RATE $N_{Re_L} = \frac{W_L}{\pi D \mu_L}$

LEGEND; DROPLET ENTRAINMENT PROFILES

RUN NO.	WATER FLOW RATE (LB/HR)	SUPERFICIAL AIR VELOCITY AT 235 IN.LEVEL (FT/SEC)	AIR DENSITY AT 235 IN. LEVEL (LB/FT^3)	INJECTOR TYPE	DROPLET FLOW THROUGH PROBE POSITION, IN.BELOW INJECTOR	SYMBOL	LINE
49	297	50.3	0.0734	Porous Wall	60.8	Nil Flow	not plotted
50	301	53.0	0.0717	Porous Wall	244.8	■	———
52	301	52.5	0.0724	Spray	15.9	◇	-------
53	301	49.7	0.0736	Spray	60.8	◈	— — —
54	301	50.7	0.0727	Spray	244.8	◆	——— .

Figure A3.22 MEDIUM PRESSURE SERIES MEAN AIR RATE 51.5 FT/SEC MEAN WATER RATE 300 LB/HR

151	300	51.7	0.2211	Porous Wall	244.8	▲	———
154	301	52.0	0.2181	Spray	15.9	▽	------
155	300	50.7	0.2199	Spray	60.8	▼	— — —
156	301	51.7	0.2207	Spray	244.8	▼	——— .

Figure A3.23 HIGH PRESSURE SERIES MEAN AIR RATE 51.5 FT/SEC MEAN WATER RATE 300.5 LB/HR

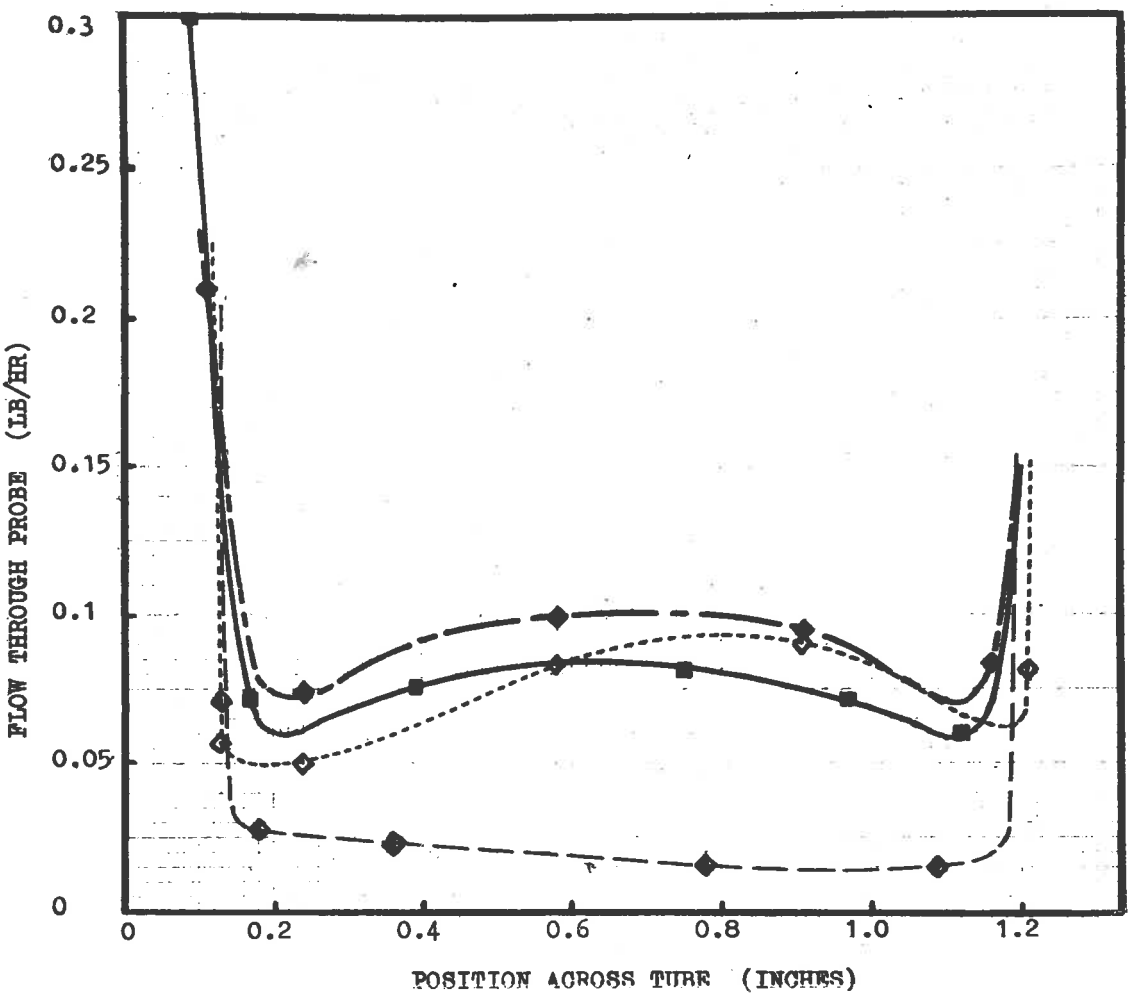
0.3
0.25
0.2
0.15
0.1
0.05
0
FLOW THROUGH PROBE (LB/HR)
0
0.2
0.4
0.6
0.8
1.0
1.2
POSITION ACROSS TUBE (INCHES)

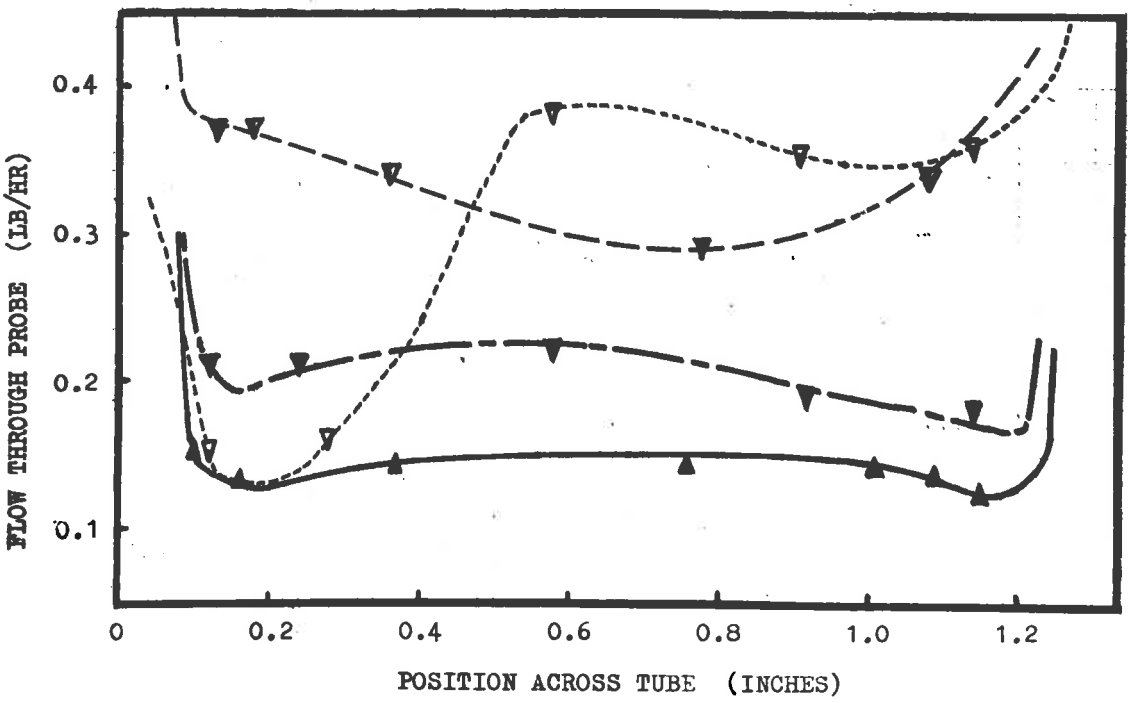
0.4
0.3
0.2
0.1
FLOW THROUGH PROBE (LB/HR)
0
0.2
0.4
0.6
0.8
1.0
1.2
POSITION ACROSS TUBE (INCHES)

LEGEND; DROPLET ENTRAINMENT PROFILES

RUN NO.	WATER FLOW RATE (LB/HR)	SUPERFICIAL AIR VELOCITY AT 235 IN.LEVEL (FT/SEC)	AIR DENSITY AT 235 IN. LEVEL (LB/FT^3)	INJECTOR TYPE	DROPLET FLOW THROUGH PROBE POSITION, IN.BELOW INJECTOR	SYMBOL	LINE
79	990	50.6	0.0739	Porous Wall	15.9	□	.....
76	1002	54.0	0.0713	Porous Wall	60.8	◧	------
77	998	52.2	0.0711	Porous Wall	244.8	■	———
80	1008	51.8	0.0711	Spray	15.9	◇	---.---
81	1004	51.4	0.0712	Spray	60.8	◈	—— —
82	1001	51.9	0.0710	Spray	244.8	◆	——.—

Figure A3.24 MEDIUM PRESSURE SERIES MEAN AIR RATE 52.0 FT/SEC MEAN WATER RATE 1001 LB/HR

180	999	49.9	0.2204	Porous Wall	15.9	△	.....
177	997	51.0	0.2192	Porous Wall	60.8	◭	------
178	1000	50.5	0.2202	Porous Wall	244.8	▲	———
181	997	51.5	0.2143	Spray	15.9	▽	---.---
182	1007	53.7	0.2197	Spray	60.8	▼	—— —
183	1002	50.7	0.2192	Spray	244.8	▼	——.—

Figure A3.25 HIGH PRESSURE SERIES MEAN AIR RATE 51.2 FT/SEC MEAN WATER RATE 1000 LB/HR

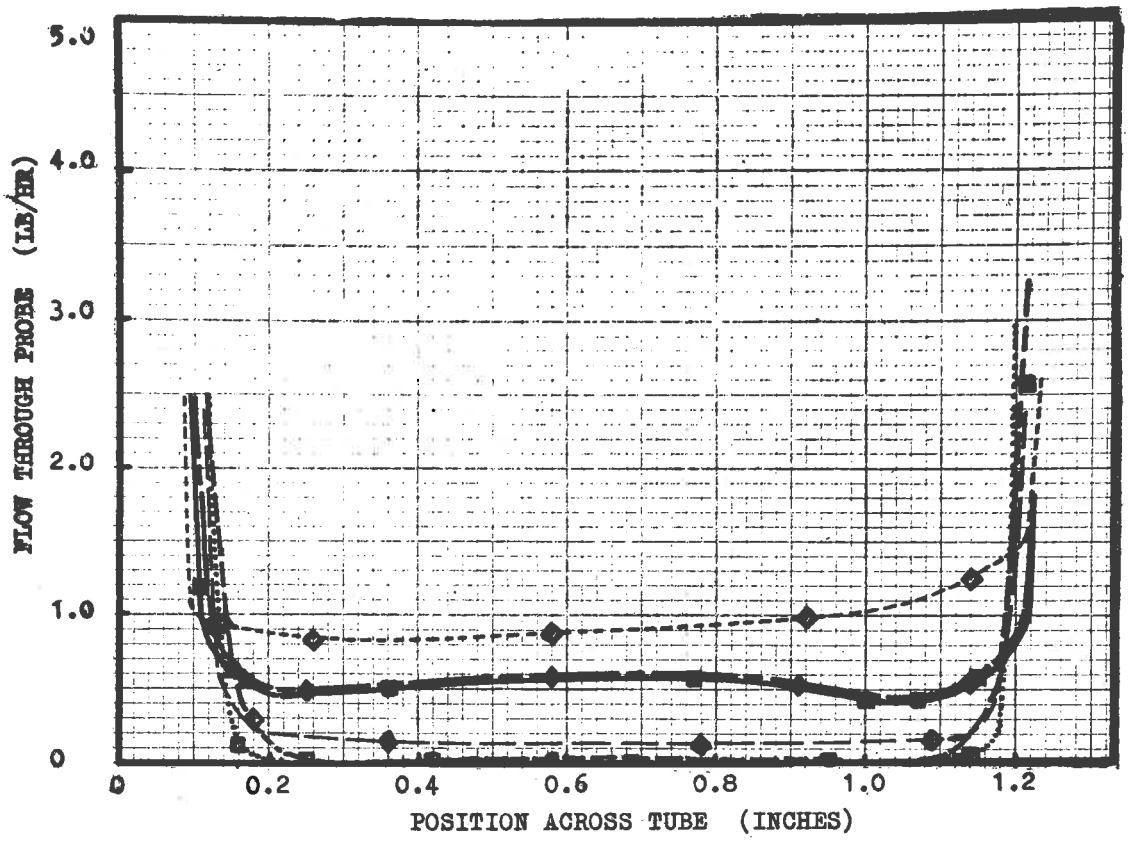
FLOW THROUGH PROBE (LB/HR)
5.0
4.0
3.0
2.0
1.0
0
0
0.2
0.4
0.6
0.8
1.0
1.2
POSITION ACROSS TUBE (INCHES)

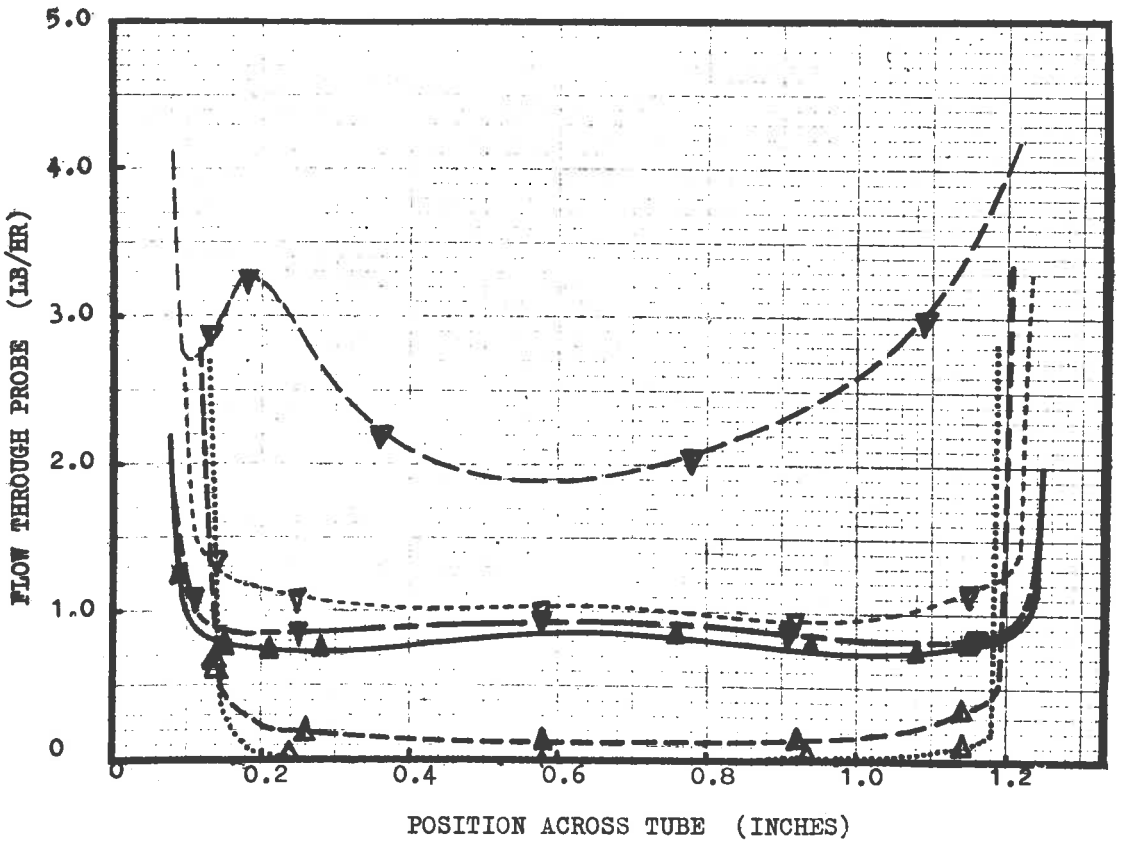
FLOW THROUGH PROBE (LB/HR)
5.0
4.0
3.0
2.0
1.0
0
0
0.2
0.4
0.6
0.8
1.0
1.2
POSITION ACROSS TUBE (INCHES)

LEGEND: DROPLET ENTRAINMENT PROFILES

RUN NO.	WATER FLOW RATE (LB/HR)	SUPERFICIAL AIR VELOCITY AT 235 IN.LEVEL (FT/SEC)	AIR DENSITY AT 235 IN. LEVEL (LB/FT^3)	INJECTOR TYPE	DROPLET FLOW THROUGH PROBE POSITION, IN.BELOW INJECTOR	SYMBOL	LINE
113	2697	49.8	0.0715	Porous Wall	15.9	□	·····
115	2712	51.8	0.0701	Porous Wall	60.8	▯	- - - - -
114	2692	53.3	0.0697	Porous Wall	244.8	■	———
116	2705	49.9	0.0693	Spray	15.9	◇	·····
117	2708	49.9	0.0710	Spray	15.9	◇	——— —
118	2703	50.1	0.0707	Spray	60.8	◈	— — —
119	2702	50.7	0.0716	Spray	244.8	◆	——— -

Figure A3.26 MEDIUM PRESSURE SERIES MEAN AIR RATE 50.8 FT/SEC MEAN WATER RATE 2703 LB/HR

207	2005	50.3	0.2173	Porous Wall	15.9	△	·····
204	1985	50.5	0.2172	Porous Wall	60.8	▲	- - - - -
205	2013	53.8	0.2191	Porous Wall	244.8	▲	———
208	2020	50.4	0.2177	Spray	15.9	▽	·····
209	2024	50.1	0.2179	Spray	60.8	▼	——— —
210	2002	50.8	0.2181	Spray	244.8	▼	——— -

Figure A3.27 HIGH PRESSURE SERIES MEAN AIR RATE 51.0 FT/SEC MEAN WATER RATE 2005 LB/HR

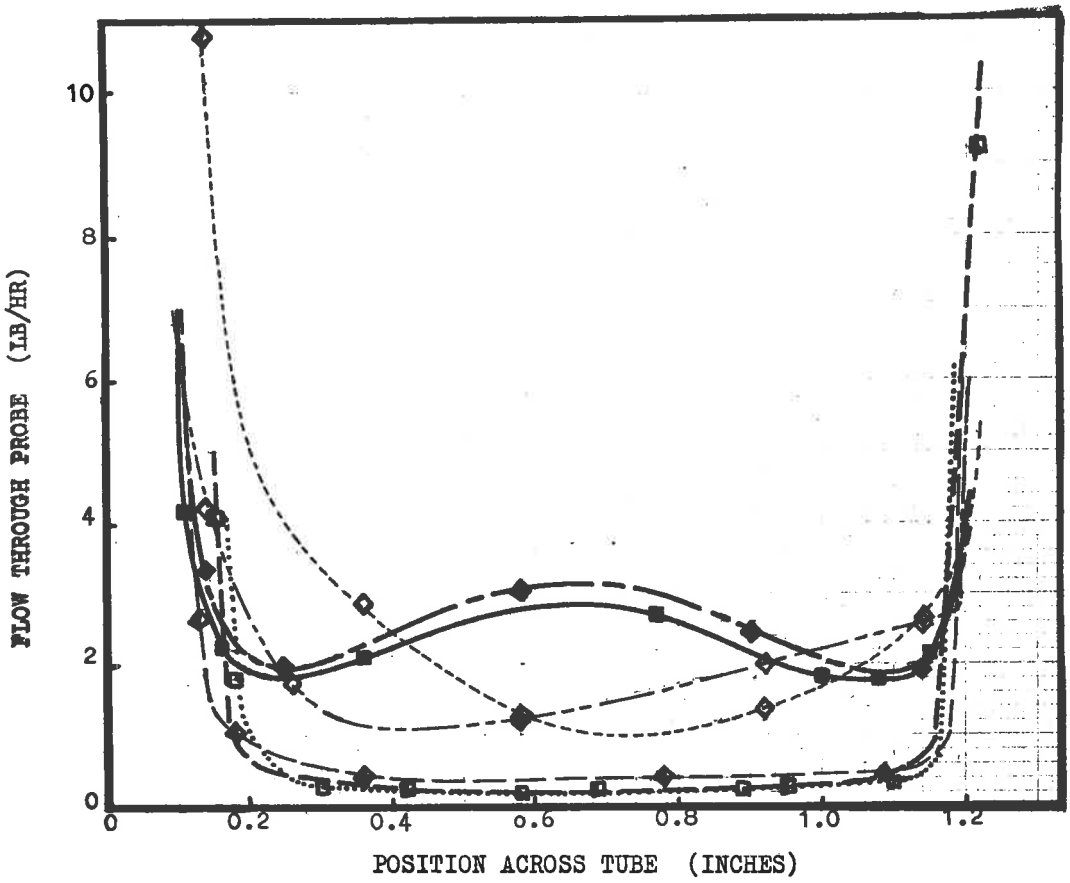
FLOW THROUGH PROBE (LB/HR)
10
8
6
4
2
0
0
0.2
0.4
0.6
0.8
1.0
1.2
POSITION ACROSS TUBE (INCHES)

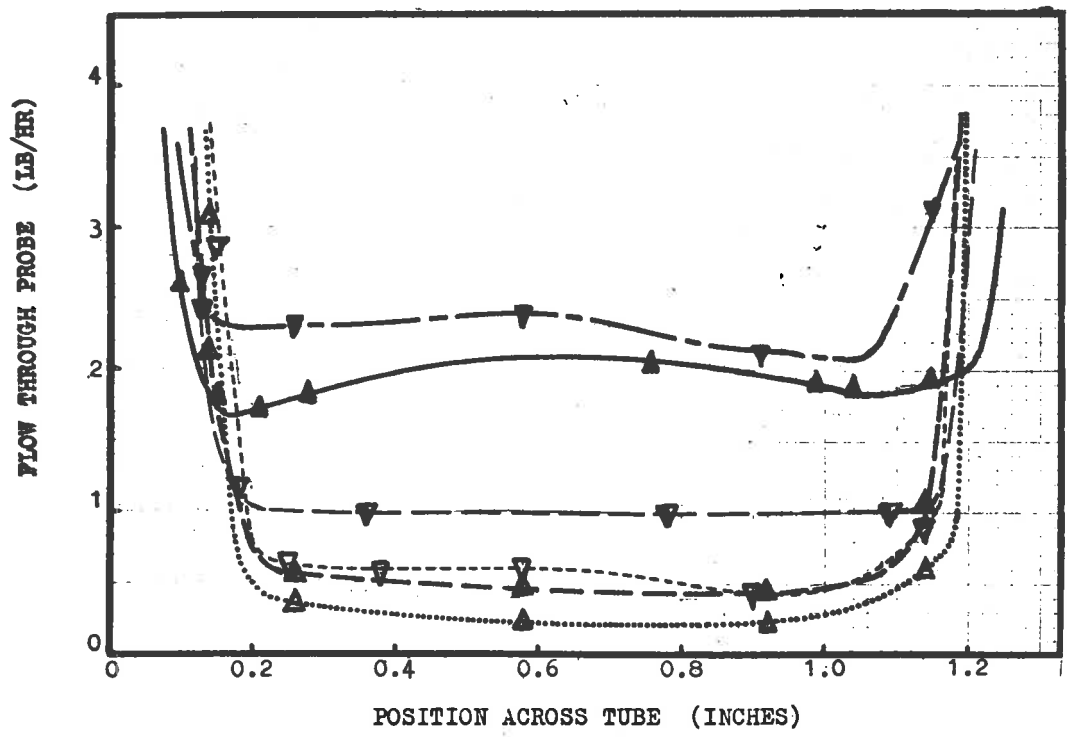
FLOW THROUGH PROBE (LB/HR)
4
3
2
1
0
0
0.2
0.4
0.6
0.8
1.0
1.2
POSITION ACROSS TUBE (INCHES)

LEGEND; DROPLET ENTRAINMENT PROFILES

RUN NO.	WATER FLOW RATE (LB/HR)	SUPERFICIAL AIR VELOCITY AT 235 IN. LEVEL (FT/SEC)	AIR DENSITY AT 235 IN. LEVEL (LB/FT^3)	INJECTOR TYPE	DROPLET FLOW THROUGH PROBE POSITION, IN. BELOW INJECTOR	SYMBOL	LINE
58	301	97.9	0.0729	Porous Wall	15.9	□	.....
55	300	92.4	0.0707	Porous Wall	60.8	◧	- - - -
56	301	107.3	0.0711	Porous Wall	244.8	■	———
59	299	97.3	0.0722	Spray	15.9	◇	------
60	299	99.8	0.0724	Spray	60.8	◆	— — —
61	301	100.2	0.0721	Spray	244.8	◆	———

Figure A3.28 MEDIUM PRESSURE SERIES MEAN AIR RATE 99.1 FT/SEC MEAN WATER RATE 300 LB/HR

160	298	99.4	0.2210	Porous Wall	15.9	△	.....
157	299	101.3	0.2188	Porous Wall	60.8	◭	- - - -
158	300	100.6	0.2215	Porous Wall	244.8	▲	———
161	300	101.9	0.2158	Spray	15.9	▽	------
162	300	100.7	0.2199	Spray	60.8	▼	— — —
163	300	104.8	0.2180	Spray	244.8	▼	———

Figure A3.29 HIGH PRESSURE SERIES MEAN AIR RATE 101.5 FT/SEC MEAN WATER RATE 299.5 LB/HR

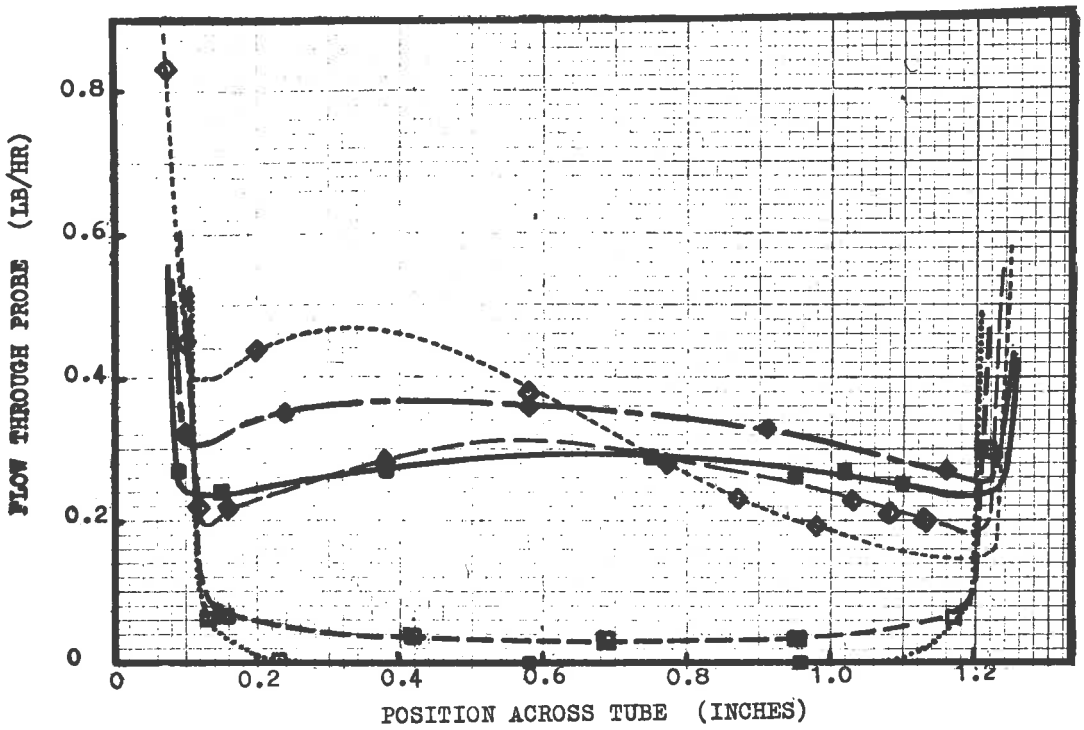
FLOW THROUGH PROBE (LB/HR)
0.8
0.6
0.4
0.2
0
0
0.2
0.4
0.6
0.8
1.0
1.2
POSITION ACROSS TUBE (INCHES)

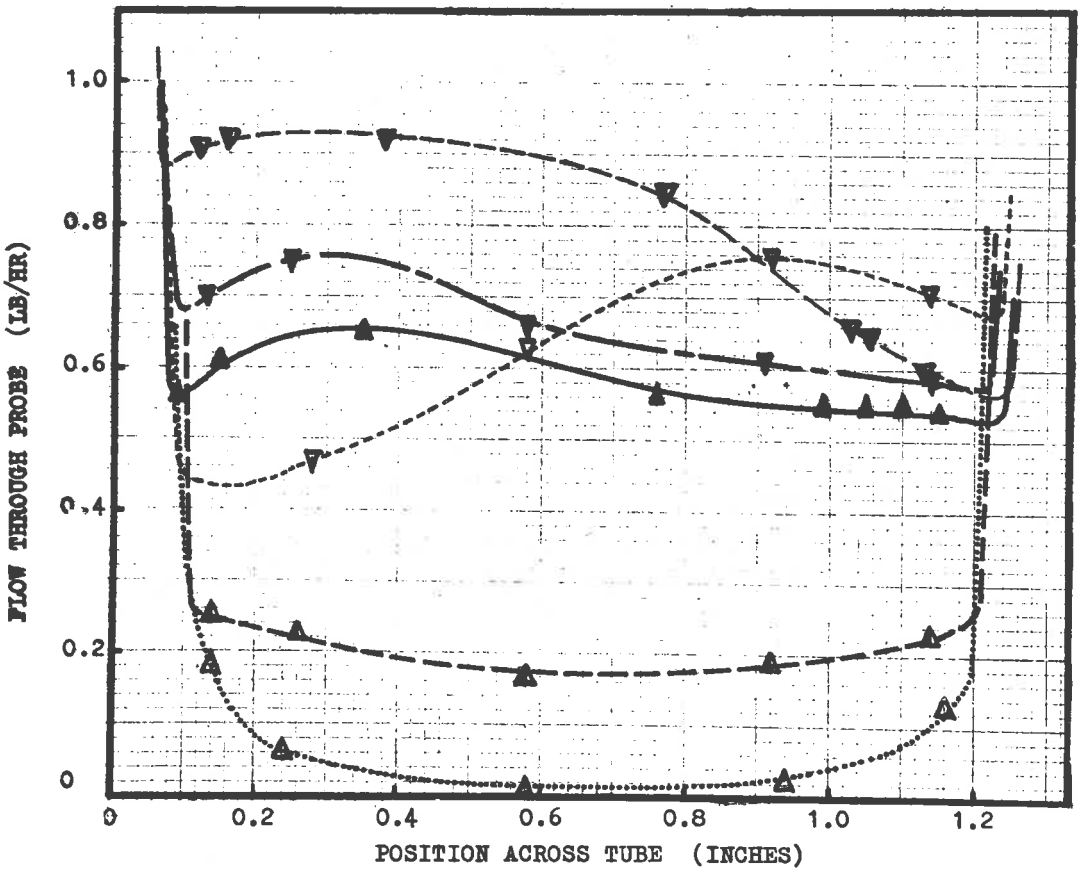
FLOW THROUGH PROBE (LB/HR)
1.0
0.8
0.6
0.4
0.2
0
0
0.2
0.4
0.6
0.8
1.0
1.2
POSITION ACROSS TUBE (INCHES)

LEGEND; DROPLET ENTRAINMENT PROFILES

RUN NO.	WATER FLOW RATE (LB/HR)	SUPERFICIAL AIR VELOCITY AT 235 IN.LEVEL (FT/SEC)	AIR DENSITY AT 235 IN. LEVEL (LB/FT^3)	INJECTOR TYPE	DROPLET FLOW THROUGH PROBE POSITION, IN.BELOW INJECTOR	SYMBOL	LINE
120	2691	101.5	0.0699	Porous Wall	15.9	□	·····
122	2720	101.5	0.0701	Porous Wall	60.8	◧	– – – –
121	2700	109.8	0.0692	Porous Wall	244.8	■	———
123	2712	102.1	0.0694	Spray	15.9	◇	- - - - -
124	2712	102.3	0.0701	Spray	60.8	◐	— — —
125	2700	103.5	0.0723	Spray	244.8	◆	———–
126	2704	107.2	0.0693	Spray	244.8	◆	——— – –

Figure A3.30 MEDIUM PRESSURE SERIES MEAN AIR RATE 104.5 FT/SEC MEAN WATER RATE 2706 LB/HR

214	2010	99.8	0.2194	Porous Wall	15.9	△	·····
211	2007	98.2	0.2192	Porous Wall	60.8	◭	– – – –
212	2000	104.9	0.2180	Porous Wall	244.8	▲	———
215	2007	104.4	0.2157	Spray	15.9	▽	- - - - -
216	2007	104.2	0.2170	Spray	60.8	▽	— — —
217	2000	102.4	0.2178	Spray	244.8	▼	———–
218	2005	106.1	0.2172	Spray	244.8	▼	——— – –

Figure A3.31 HIGH PRESSURE SERIES MEAN AIR RATE 102.9 FT/SEC MEAN WATER RATE 2005 LB/HR

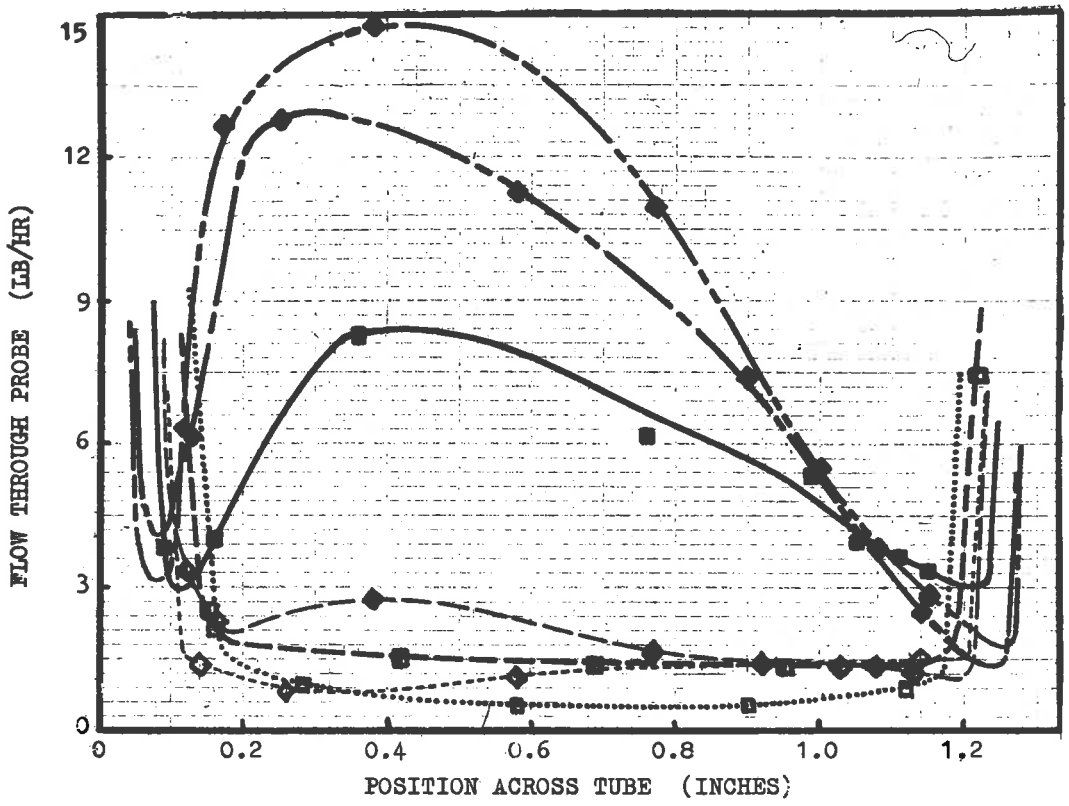
FLOW THROUGH PROBE (LB/HR)
15
12
9
6
3
0
0
0.2
0.4
0.6
0.8
1.0
1.2
POSITION ACROSS TUBE (INCHES)

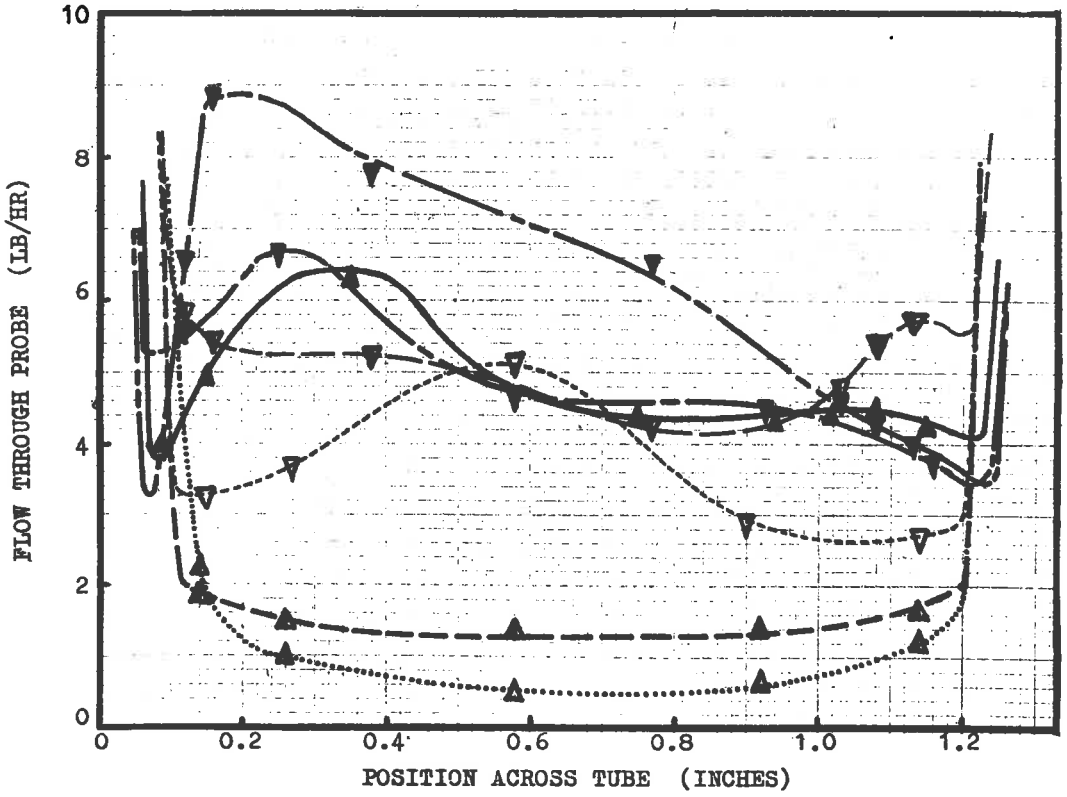
FLOW THROUGH PROBE (LB/HR)
10
8
6
4
2
0
0
0.2
0.4
0.6
0.8
1.0
1.2
POSITION ACROSS TUBE (INCHES)

LEGEND: DROPLET ENTRAINMENT PROFILES

RUN NO.	WATER FLOW RATE (LB/HR)	SUPERFICIAL AIR VELOCITY AT 235 IN. LEVEL (FT/SEC)	AIR DENSITY AT 235 IN. LEVEL (LB/FT^3)	INJECTOR TYPE	DROPLET FLOW THROUGH PROBE POSITION, IN. BELOW INJECTOR	SYMBOL	LINE
66	302	197.3	0.0731	Porous Wall	15.9	□	·····
63	300	197.9	0.0713	Porous Wall	60.8	◧	– – –
64	301	192.3	0.0711	Porous Wall	244.8	■	———
67	301	203.1	0.0723	Spray	15.9	◇	·····
68	301	207.1	0.0709	Spray	60.8	◈	— – —
69	300	201.6	0.0704	Spray	244.8	◆	——— –
70	300	204.9	0.0721	Spray	244.8	◆	——— – –

Figure A3.32 MEDIUM PRESSURE SERIES MEAN AIR RATE 210.1 FT/SEC MEAN WATER RATE 301 LB/HR

167	301	157.8	0.2193	Porous Wall	15.9	△	·····
164	302	161	0.2177	Porous Wall	60.8	◭	– – – –
165	300	157.9	0.2207	Porous Wall	244.8	▲	———
169	303	161.1	0.2184	Spray	15.9	▽	·····
170	299	161.5	0.2182	Spray	60.8	▼	— – —
171	300	160.9	0.2176	Spray	244.8	▼	——— –
172	301	160.2	0.2183	Spray	244.8	▼	——— – –

Figure A3.33 HIGH PRESSURE SERIES MEAN AIR RATE 161.0 FT/SEC MEAN WATER RATE 301 LB/HR

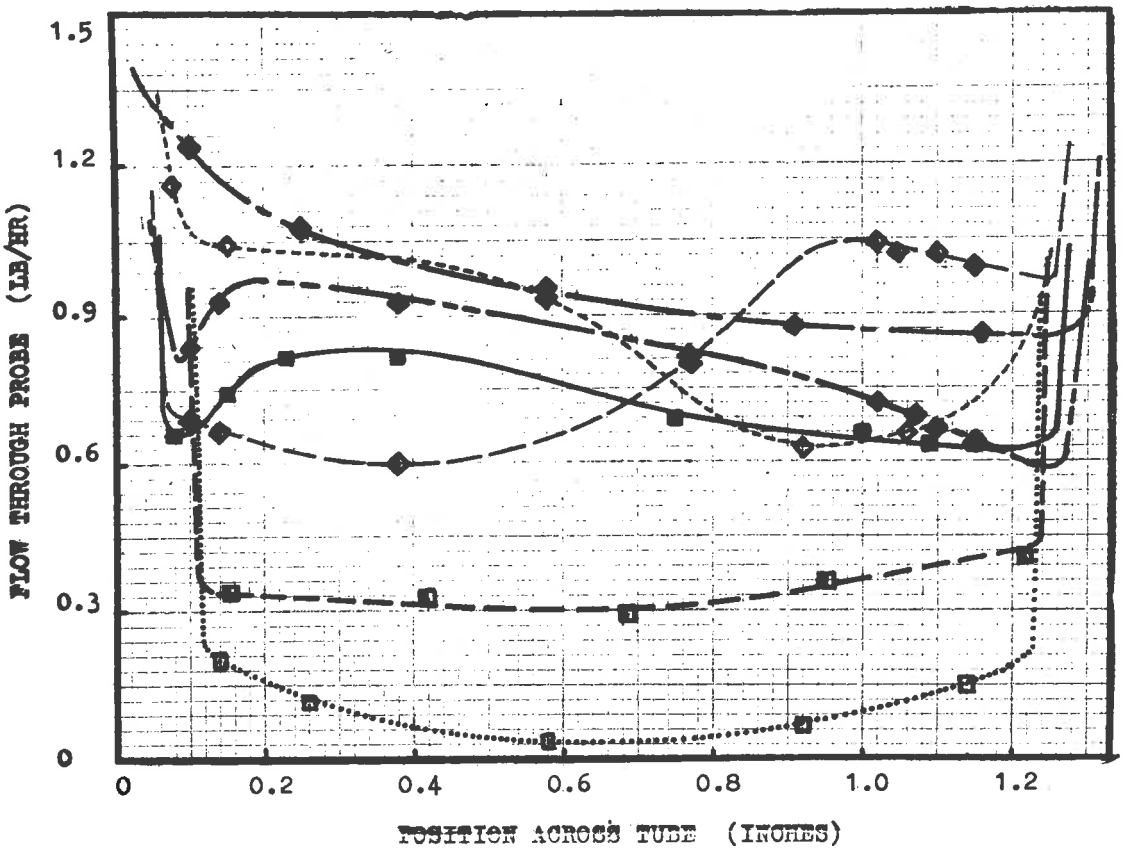
FLOW THROUGH PROBE (LB/HR)
1.5
1.2
0.9
0.6
0.3
0
0
0.2
0.4
0.6
0.8
1.0
1.2
POSITION ACROSS TUBE (INCHES)

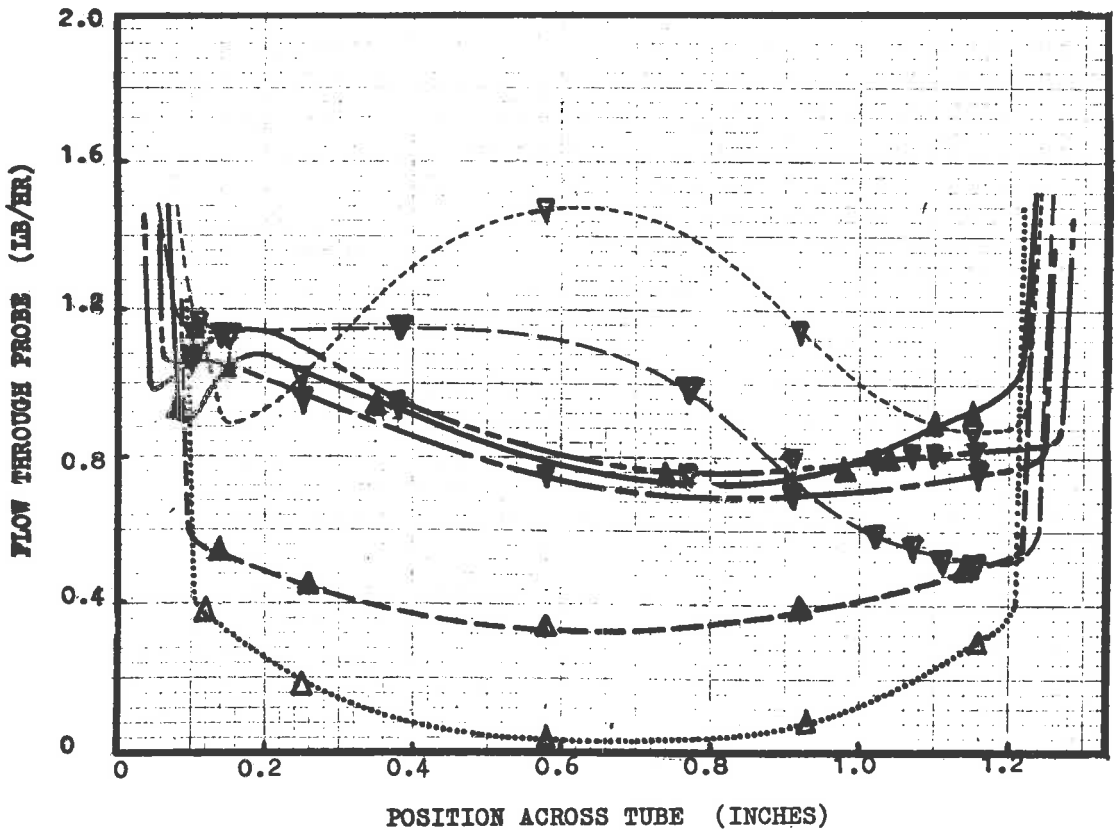
FLOW THROUGH PROBE (LB/HR)
2.0
1.6
1.2
0.8
0.4
0
0
0.2
0.4
0.6
0.8
1.0
1.2
POSITION ACROSS TUBE (INCHES)

LEGEND: DROPLET ENTRAINMENT PROFILES

RUN NO.	WATER FLOW RATE (LB/HR)	SUPERFICIAL AIR VELOCITY AT 235 IN. LEVEL (FT/SEC)	AIR DENSITY AT 235 IN. LEVEL (LB/FT^3)	INJECTOR TYPE	DROPLET FLOW THROUGH PROBE POSITION, IN. BELOW INJECTOR	SYMBOL	LINE
96	1004	202.0	0.0724	Porous Wall	15.9	□	·····
97	993	209.0	0.0704	Porous Wall	60.8	◧	- - - -
94	1000	204.4	0.0700	Porous Wall	244.8	■	———
98	1008	208.0	0.0717	Spray	15.9	◇	- - - -
99	1003	210.2	0.0700	Spray	60.8	◈	— — —
100	999	202.1	0.0721	Spray	244.8	◆	——— -
101	998	209.1	0.0716	Spray	244.8	◆	——— - -

Figure A3.34 MEDIUM PRESSURE SERIES MEAN AIR RATE 206.4 FT/SEC MEAN WATER RATE 1000 LB/HR

195	996	158.3	0.2202	Porous Wall	15.9	△	·····
192	995	160.4	0.2190	Porous Wall	60.8	◭	- - - -
193	1003	158.7	0.2205	Porous Wall	244.8	▲	———
196	990	164.5	0.2114	Spray	15.9	▽	- - - -
197	1004	160.1	0.2185	Spray	60.8	▼	— — —
198	1000	161.0	0.2178	Spray	244.8	▼	——— -
199	990	162.2	0.2198	Spray	244.8	▼	——— - -

Figure A3.35 HIGH PRESSURE SERIES MEAN AIR RATE 160.7 FT/SEC MEAN WATER RATE 997 LB/HR

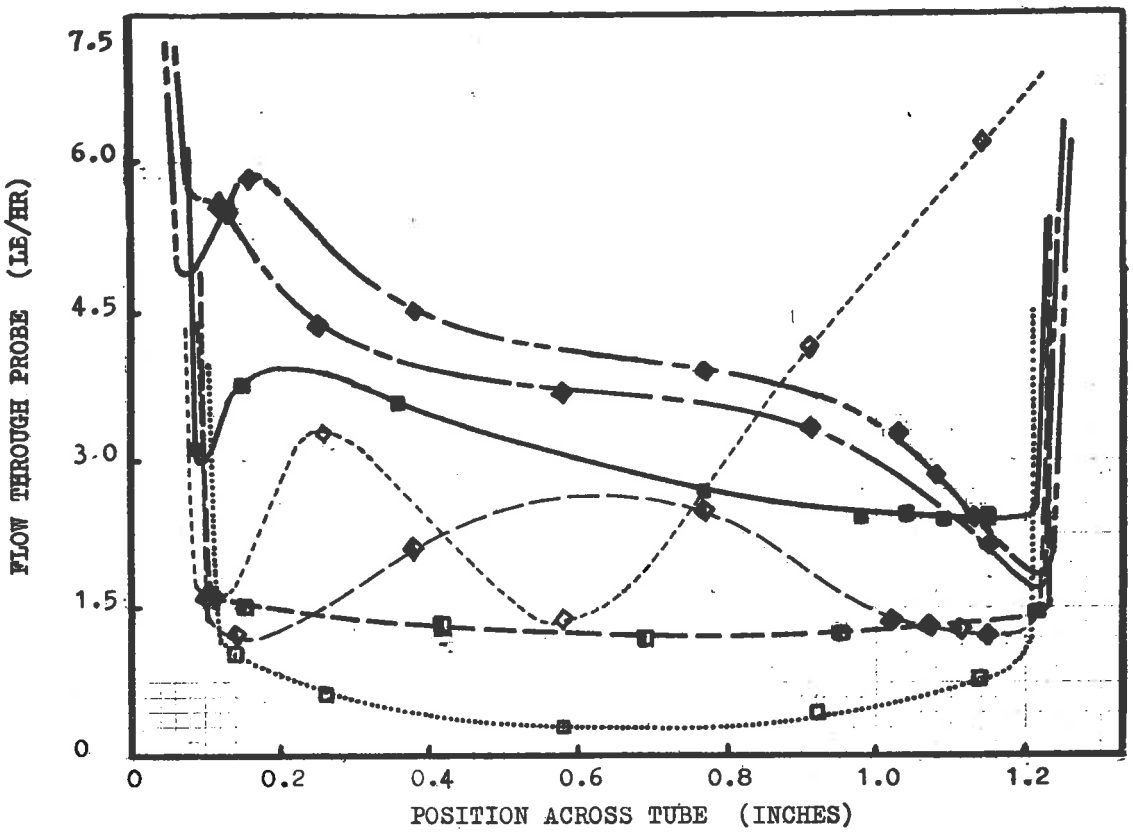
FLOW THROUGH PROBE (LB/HR)
7.5
6.0
4.5
3.0
1.5
0
0
0.2
0.4
0.6
0.8
1.0
1.2
POSITION ACROSS TUBE (INCHES)

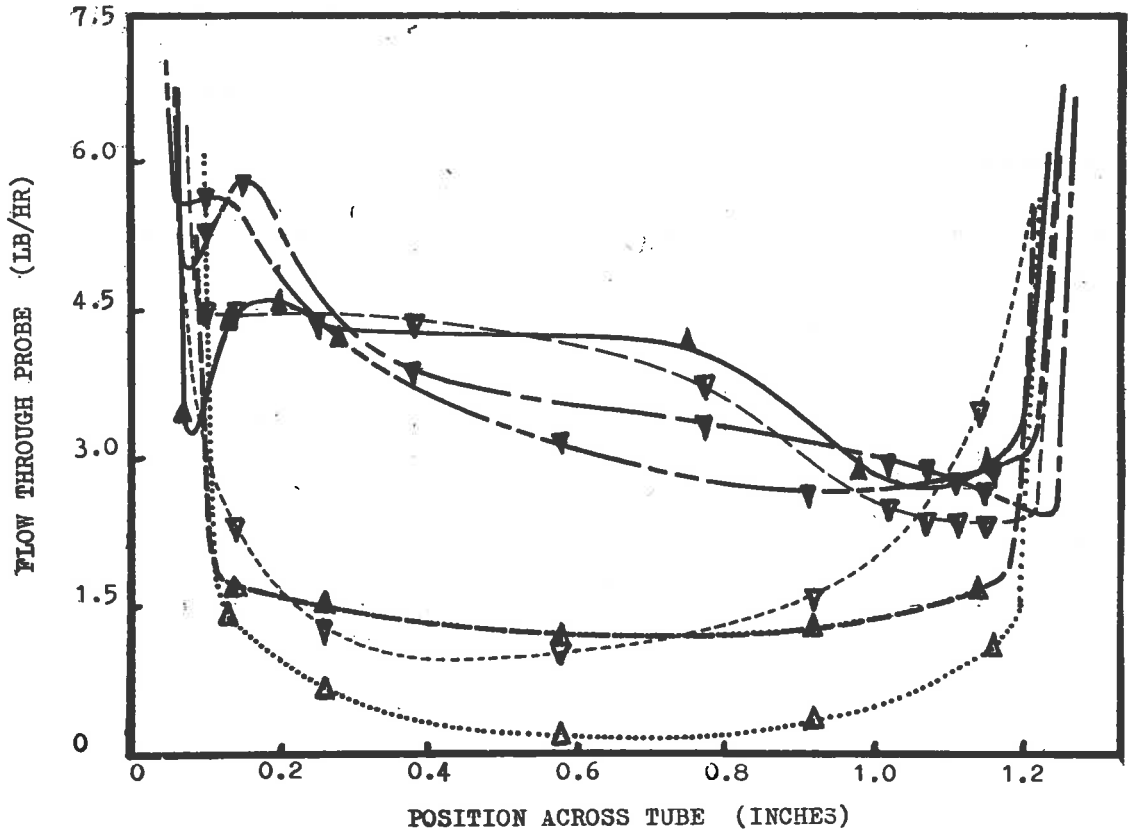
FLOW THROUGH PROBE (LB/HR)
7.5
6.0
4.5
3.0
1.5
0
0
0.2
0.4
0.6
0.8
1.0
1.2
POSITION ACROSS TUBE (INCHES)

LEGEND; DROPLET ENTRAINMENT PROFILES

RUN NO.	WATER FLOW RATE (LB/HR)	SUPERFICIAL AIR VELOCITY AT 235 IN. LEVEL (FT/SEC)	AIR DENSITY AT 235 IN. LEVEL (LB/FT^3)	INJECTOR TYPE	DROPLET FLOW THROUGH PROBE POSITION, IN. BELOW INJECTOR	SYMBOL	LINE
127	2703	199.9	0.0723	Porous Wall	15.9	□	.....
129	2700	209.1	0.0698	Porous Wall	60.8	▯	- - - -
128	2700	223.1	0.0689	Porous Wall	244.8	■	———
130	2706	199.7	0.0715	Spray	15.9	◇	- - - -
131	2700	213.1	0.0704	Spray	60.8	◈	— — —
132	2700	208.7	0.0709	Spray	244.8	◆	——— -
133	2702	218.5	0.0697	Spray	244.8	◆	——— - -

Figure A3.36 MEDIUM PRESSURE SERIES MEAN AIR RATE 208.9 FT/SEC MEAN WATER RATE 2702 LB/HR

222	2004	163.7	0.2172	Porous Wall	15.9	△	.....
219	1999	159.2	0.2191	Porous Wall	60.8	▲	- - - -
220	2000	161.1	0.2189	Porous Wall	244.8	▲	———
223	1989	167.9	0.2118	Spray	15.9	▽	- - - -
224	2011	162.9	0.2195	Spray	60.8	▽	— — —
225	1998	165.3	0.2174	Spray	244.8	▼	——— -
226	2001	163.6	0.2172	Spray	244.8	▼	——— - -

Figure A3.37 HIGH PRESSURE SERIES MEAN AIR RATE 163.4 FT/SEC MEAN WATER RATE 2000 LB/HR

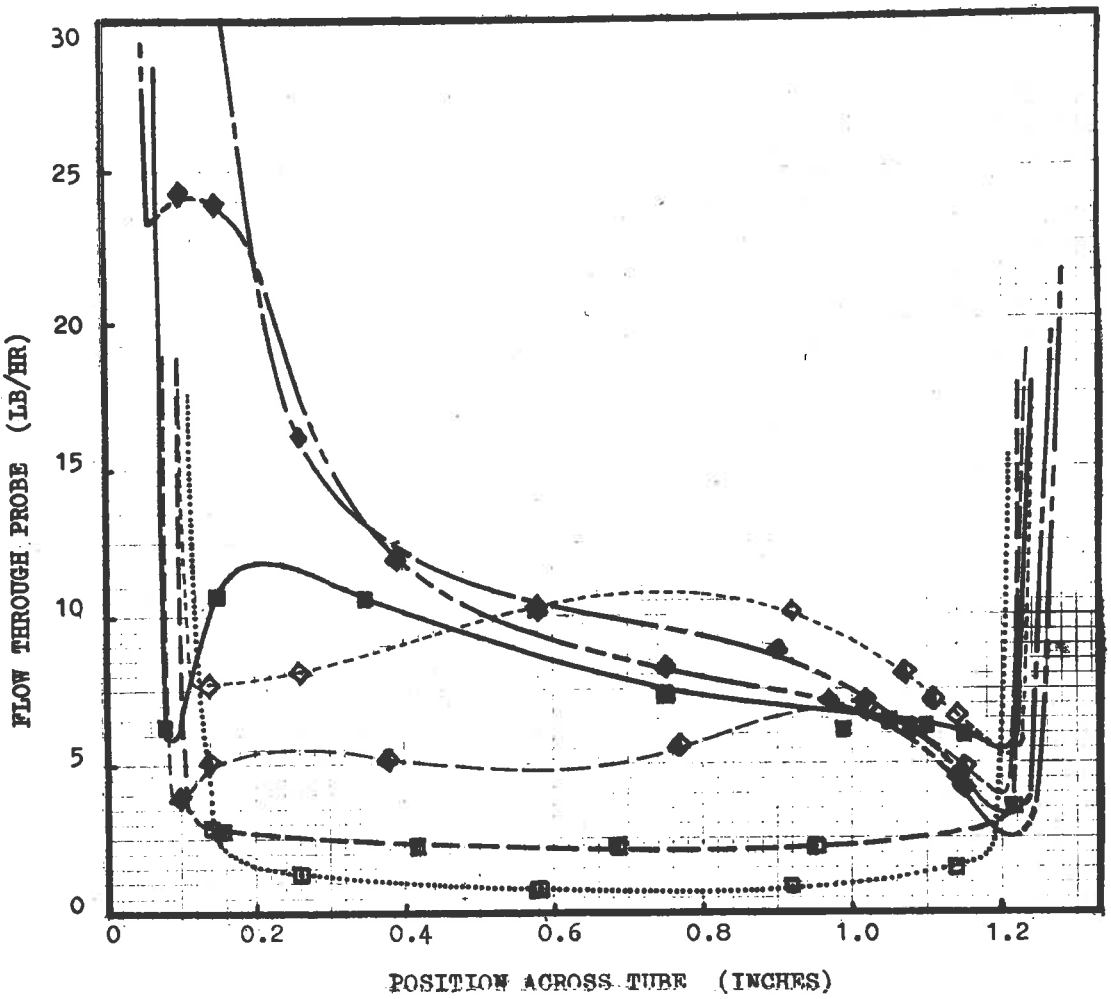
FLOW THROUGH PROBE (LB/HR)
30
25
20
15
10
5
0
0
0.2
0.4
0.6
0.8
1.0
1.2
POSITION ACROSS TUBE (INCHES)

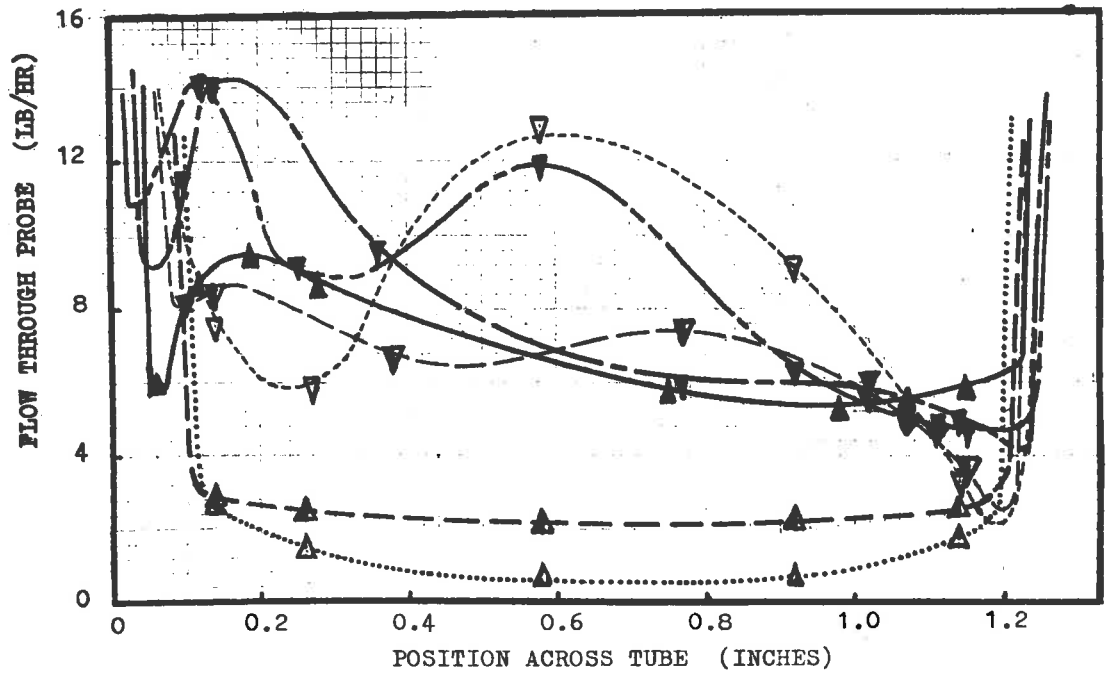
FLOW THROUGH PROBE (LB/HR)
16
12
8
4
0
0
0.2
0.4
0.6
0.8
1.0
1.2
POSITION ACROSS TUBE (INCHES)

APPENDIX 4

SAMPLING PROBE CHARACTERISTICS

Probe capture efficiency.

The probe internal diameter was 0.075 inches. The table below is drawn up from the work of Doussourd and Shapiro (1955) and its discussion in Gill, Hewitt, Hitchon and Lacey (1963). It is for the extremes of the sampling conditions, and shows the minimum droplet sizes which would be captured with 99% efficiency by a probe with no gas flow through the probe mouth.

Air Velocity (ft/sec)	Air Density (lb/ft^3)	Minimum size of water droplet captured with 99% efficiency (microns)
50	0.2183	52 μ
160	0.2183	38 μ
50	0.0712	30 μ
200	0.0712	25 μ

Comparison with the droplet size measurement data of Cousins and Hewitt (1968b) shows that the high velocity - high density case is the least favourable situation because of the smaller droplets present at high velocities. They found that for an air velocity of 160 ft/sec and an air density of 0.16 lb/ft^3 in a $^3/_8$ inch diameter tube the volume mean droplet diameter ($\sqrt[3]{\bar{d}^3}$) was 45-50 microns. About 10% by weight of the droplets were less than 25 microns in diameter. In a tube $3\frac{1}{2}$ times larger in diameter and

therefore with a much lower pressure gradient and a much less steep air velocity profile it seems reasonable to expect that even at the higher air density of 0.22 lb/ft^3 the droplets would be at least 20% larger in diameter.

In fact the probe was operated with an air flow through the probe mouth of about 80-90% of the isokinetic velocity. Under these conditions it seems reasonable to expect that the 99% capture efficiency droplet size would be extended from 38 microns down to about 25 microns. In the 1.330 inch tube it is likely that less than 10% of the droplet mass flow is smaller than 25 microns in diameter. Hence, the overall mass capture efficiency for the whole range of droplet sizes should exceed 99% even in this worst case. This is dependent on the under 25 micron sizes being a representative part of the whole droplet size distribution. If the smaller droplets are formed by a separate mechanism from the main mass of droplets this might not be so.

The effect of variation in the gas take-off rate on the liquid collection rate.

Gill, Hewitt, Hitchon and Lacey (1963) found that variations in the gas take-off rate from 25% to 115% of the isokinetic velocity had practically no effect on the liquid collection rate. This is not unexpected because of the high capture efficiency of a static system. The decrease in

collection rate at low take-off rates could be due to partial filling of the probe mouth with liquid. At gas velocities greater than the isokinetic velocity the probe would be expected to collect too much liquid because some of the droplets stopped by the probe rim would be dragged into the probe mouth by the excess gas. In the data of Gill et al. this increase became noticeable at 115% of the isokinetic velocity.

It follows that the safest region in which to operate a non-isokinetic probe is, as was done by Gill et al., at gas take-off rates somewhat less than the isokinetic velocity. In this investigation the range 80-90% of the isokinetic velocity was used. The actual gas rate was calculated from the total gas rate, the ratio of the probe area to the tube area and the position of the sampling probe, assuming that the gas velocity profiles were similar to those of Gill et al.

Sampling with an isokinetic probe.

Isokinetic sampling probes have been used by Adorni et al. (1961) and also in the more recent studies of the Harwell group (Cousins and Hewitt, 1968a). An isokinetic probe has a two channel construction. One channel is the sampling probe proper. The second channel is used to measure the static pressure at the sampling probe mouth. This pressure is compared with the static

pressure on the tube wall at the same level by means of a differential manometer. The pressure differential is zero when the extraction velocity at the probe mouth is equal to the local mainstream velocity which is the isokinetic velocity.

Gill, Hewitt, Hitchon and Lacey (1963) point out that it is difficult to design an isokinetic probe so that the true static pressure at the probe mouth is measured. Alternatively, if the static tapping is not at the probe mouth then it is difficult to decide what is the proper correction factor for a two phase mixture. Because of these known difficulties in using an isokinetic sampling probe no attempt was made to construct such a probe for this investigation.

APPENDIX 5.

COLLISIONS BETWEEN DROPLETS IN THE CORE

1. The Mean Free Path

We assume that all the droplets have the same diameter d and move at the same velocity $\bar{u}_d$ but move in random directions. The mean free path of a droplet is unaltered if the field of droplets is made stationary and the droplet moves at the average value of its own velocity plus the field velocity. In the diagram below $\overline{OR}$ represents the object droplet velocity and $\overline{RP}$ the field droplet velocity. Then P can lie anywhere on the surface

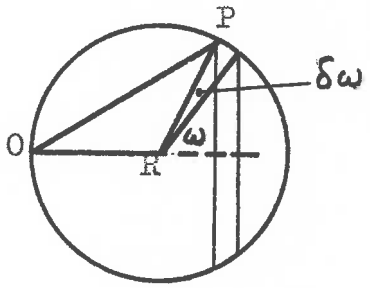

of a sphere centre R and radius RP. If the angle between the directions of motion of the droplets is ω then the sum of their velocities is $2\,\bar{u}_d \cos\frac{\omega}{2}$. The probability of the angle being between ω and $\omega+\delta\omega$ is equal to the ratio of the surface area of the sphere lying between these limits to the surface area of the whole sphere. It is

$$\frac{2\pi \sin\omega\delta\omega}{4\pi} = \tfrac{1}{2}\sin\omega\delta\omega .$$

$\therefore$ Average value of (droplet velocity + field velocity)

$$= \bar{u}_d \int_0^{\pi} \sin\omega \cos\frac{\omega}{2}\, d\omega = \frac{4}{3}\bar{u}_d \qquad \text{.....(A5.1)}$$

This result was first obtained by Clausius in his work on the kinetic theory of gases.

If the volume fraction of the droplets is γ, then:-

$$\text{Number in unit volume} = \frac{6\gamma}{\pi d^3} \qquad \text{.....(A5.2)}$$

The object droplet, which can be considered to move at a velocity $\frac{4}{3}\bar{u}_d$ with reference to a stationary field, sweeps out the path of a "collision sphere" of diameter d.
A collision occurs when this collision sphere passes through the centre of another droplet.

$\therefore$ Effective volume swept per unit time $= \pi d^2 \cdot \frac{4}{3}\bar{u}_d$.

$\therefore$ Mean free path $= \dfrac{\text{Actual velocity}}{\text{Effective volume swept} \times \text{Number of droplets per unit volume}}$

$$= \frac{d}{8\gamma} \qquad \text{.....(A5.3)}$$

2. <u>The Average Velocity Of The Centre Of Mass Of A Group Of Droplets</u>

The velocity of the centre of mass of a group of droplets is unaltered if they collide with each other. The total momentum of the group is not changed by collisions.

(1) <u>The two droplet group</u>

For droplets which all have the same mass adding momenta is equivalent to adding velocities. Therefore, from equation (A5.1), the total momentum of a two droplet group has

a mean value of $\frac{4}{3}$ times the momentum of a single droplet. But the mass is doubled and so the mean velocity of the centre of mass of a two droplet group is $\frac{2}{3}$ times that of a single droplet.

(2) The three droplet group and the four droplet group

We consider the sum of the momenta of two groups of droplets each of arbitary momentum. Then, using the same sketch as was used for the mean free path analysis, we let $\overline{OR}$ represent the momentum of one group and $\overline{RP}$ represent the momentum of the other group. We let $z = \frac{\overline{RP}}{\overline{OR}}$. Then

$$\overline{OP} = \overline{OR}\sqrt{(1 + z\cos\omega)^2 + z^2\sin^2\omega} \quad \text{.....(A5.4)}$$

The probability of $\overline{RP}$ lying between the angles ω and $\omega + \delta\omega$ in relation to $\overline{OR}$ is $\frac{1}{2}\sin\omega\delta\omega$ as before.

∴ Average momentum of the two groups of droplets

$$= \overline{OR}\int_0^{\pi}\frac{1}{2}\sin\omega\sqrt{1 + z^2 + 2z\cos\omega}\,d\omega$$

$$= \overline{OR}\left[1 + \frac{1}{3}z^2\right] \text{ or } \overline{OR}\left[\frac{1}{3}z + z\right] \quad \text{.....(A5.5)}$$

This gives:-

Average momentum of the two groups of droplets

$$\left.\begin{aligned} &= \overline{OR} + \frac{\overline{RP}^2}{3\,\overline{OR}} \quad \text{if } \overline{OR} \geq \overline{RP} \quad \text{or} \\ &= \frac{\overline{OR}^2}{3\,\overline{RP}} + \overline{RP} \quad \text{if } \overline{OR} \leq \overline{RP} \end{aligned}\right\} \text{.....(A5.6)}$$

If $\overline{RP}$ represents the momentum of a group of two droplets then it can be represented by the sum of two unit vectors at an angle ω' to one another. Hence $\overline{RP} = 2\,\overline{UN}\cos\frac{\omega'}{2}$

where $\overline{UN}$ is the momentum of a single droplet. The probability of the angle lying between ω' and $\omega'+\delta\omega'$ is $\frac{1}{2}\sin\omega'\delta\omega'$

$\therefore$ average momentum =

$$\int_0^Z \left[\frac{\overline{OR}^2}{6\,\overline{UN}\cos\frac{\omega'}{2}} + 2\,\overline{UN}\cos\frac{\omega'}{2}\right]\frac{1}{2}\sin\omega' d\omega' \quad \left[\overline{OR} \leqslant \overline{RP}\right]$$

$$+\int_Z^\pi \left[\overline{OR} + \frac{4\,\overline{UN}^2\cos^2\frac{\omega'}{2}}{3\,\overline{OR}}\right]\frac{1}{2}\sin\omega' d\omega' \quad \left[\overline{OR} \geqslant \overline{RP}\right]$$

and $\overline{OR} = 2\,\overline{UN}\cos\frac{\omega'}{2}$ at the point Z.

$\therefore$ Average momentum $= \frac{4}{3}\overline{UN} + \frac{1}{3}\frac{\overline{OR}^2}{\overline{UN}} - \frac{1}{24}\frac{\overline{OR}^3}{\overline{UN}^2}$ .....(A5.7)

Putting $\overline{OR} = \overline{UN}$ shows that the average momentum of a three droplet group is $\frac{13}{8}$ times the momentum of a single droplet. Hence the mean velocity of the centre of mass of the group is $\frac{13}{24}$ times the velocity of a single droplet.

If we put $\overline{OR} = 2\,\overline{UN}\cos\frac{\omega''}{2}$ with probability $\frac{1}{2}\sin\omega''\delta\omega''$ then equation (A5.7) can be integrated to show that the average momentum of a group of 4 droplets is $\frac{28}{15}$ times the momentum of a single droplet. Hence the mean velocity of the centre of mass of the group is $\frac{7}{15}$ times the velocity of a single droplet.

(3) <u>The asymptotic solution - a large number of droplets</u>

An examination of the results for up to four droplets indicates that the average momentum of a group

of (m+1) droplets is slightly less than $\sqrt{1+\frac{1}{m}}$ times the average momentum of a group of m droplets. As m is increased the approximation becomes more and more accurate.

The average momentum of a group of m droplets is approximately $\sqrt{m}$ times the momentum of a single droplet. This approximation becomes relatively more accurate as m increases, but the true value of the average momentum of the group does not asymptote to $\sqrt{m}$.

Hence for large values of m the average velocity of a group of droplets is approximately $\frac{1}{\sqrt{m}}$ times the velocity of a single droplet.

REFERENCES

Adorni, N., Casagrande, I., Cravarolo, L., Hassid, A., and Silvestri, M., CISE Report R.35 (1961).

Alexander, L.G., and Coldren, C.L., Ind. Eng. Chem., 43, 1325-1331 (1951).

Anderson, G.H., and Mantzouranis, B.G., Chem. Eng. Sci., 12, 109-126 (1960a); 12, 233-242 (1960b).

Arnold, C.R., and Hewitt, G.F., U.K.A.E.A. Report No. AERE -R5318 (1967).

Benjamin, T.B., J. Fluid Mech., 2, 554-574 (1957).

Benjamin, T.B., J. Fluid Mech., 6, 161-205 (1959).

Bennett, J.A.R., and Thornton, J.D., Trans. Instn. Chem. Engrs. (London), 39, 101-112 (1961).

Bird, R.B., Stewart, W.E., and Lightfoot, E.N., "Transport Phenomena", Wiley (1960).

Brauer, H., V.D.I. - Forschungsheft, 457 (1956).

Brötz, W., Chem.- Ing.- Tech., 26, 470-478 (1954).

Bruges, E.A., Latto, B., and Ray, A.K., Int. J. Heat Mass Transfer, 9, 465-480 (1966).

Bushmanov, V.K., Zhur. Eksper. Teor Fiz., 39, 1251-1257 (1960) English Transl. Soviet Phys.- JETP., 12, 873-877 (1961).

Butterworth, D., Chem. Eng. Sci., 22, 911-924 (1967) see also U.K.A.E.A. Report No. AERE -R5284 (1966).

Calvert, S., and Williams, B., A.I.Ch.E. Journal 1, 78-86 (1955).

Chang, F.W., and Dukler, A.E., Int. J. Heat Mass Transfer, 7, 1395-1404 (1964).

Charvonia, D.A., Interim Report No. I-59-1, Jet Propulsion Center, Purdue Univ. (1959).

Chien, S.F., and Ibele, W., Trans. A.S.M.E., Series C, J. Heat Transfer, 86, 89-96 (1964).

Clegg, M.J., Ph.D. Thesis, University of Adelaide (1966).

Collier, J.G., and Hewitt, G.F., Trans. Instn. Chem. Engrs. (London), 39, 127-136 (1961) see also U.K.A.E.A. Report No. AERE -R3455 (1960).

Cooper, K.D., Hewitt, G.F., and Pinchin, B., J. Photographic Science, 12, 269 (1964) see also U.K.A.E.A. Report No. AERE -R4301 (1963).

Cousins, L.B., Denton, W.H., and Hewitt, G.F., Proc. Symp. on Two Phase Flow, Vol. II, Paper C4, University of Exeter, United Kingdom (1965) see also U.K.A.E.A. Report No. AERE -R4926 (1965).

Cousins, L.B., and Hewitt, G.F., U.K.A.E.A. Report No. AERE -R5693 (1968a).

Cousins, L.B., and Hewitt, G.F., U.K.A.E.A. Report No. AERE -R5657 (1968b).

Deissler, R.G., NACA TN 2129 (1950); TN 2138 (1952); TN 3145 (1959).

Deissler, R.G., NACA TR 1210 (1955).

Doig, I.D., and Roper, G.H., Ind. Eng. Chem. Fund., 6, 247-256 (1967).

Dombrowski, N., Hasson, D., and Ward, D.E., Chem. Eng. Sci., 12, 35-50 (1960).

Doussard, J.L., and Shapiro, A.H., Part XX, Heat Transfer and Fluid Mechanics Institute, University of California, (1955).

Dressler, R.F., Commun. Pure Appl. Math., 2, 149-194 (1949).

Dukler, A.E., and Bergelin, O.P., Chem. Eng. Progress, 48, 557-563 (1952).

Dukler, A.E., Chem. Eng. Progress, 55, 62-67 (1959).

Dukler, A.E., Chem. Eng. Progress Symposium Series, 56, No. 30, 1-10 (1960).

Dukler, A.E., Petro/Chem. Engr., 33, 9, 52-54 (1961); 33, 11, 46-53 (1961).

Dukler, A.E., and Magiros, P.G., Developments in Mechanics, 1, 532-553, Plenum Press; New York (1961).

Dukler, A.E., Wicks, M., and Cleveland, R.G., A.I.Ch.E. Journal, 10, 38-43 (1964a); 10, 44-51 (1964b).

Foust, A.S., Wenzel, L.A., Clump, C.W., Maus, L., and Andersen, L.B., "Principles of Unit Operations" p. 544 Wiley (1960).

Fraser, R.P., Eisenklam, P., Dombrowski, N., and Hasson, D., A.I.Ch.E. Journal, 8, 672-680 (1962).

Fraser, R.P., Dombrowski, N., and Routley, J.H., Chem. Eng. Sci., 18, 315-321 (1963); 18, 323-337 (1963).

Fulford, G.D., Advances in Chemical Engineering, 5, 151-236, Academic Press, New York (1964).

Gill, L.E., Hewitt, G.F., Hitchon, J.W., and Lacey, P.M.C., Chem. Eng. Sci., 18, 525-535 (1963) see also U.K.A.E.A. Report No. AERE -R3954 (1962).

Gill, L.E., Hewitt, G.F., and Lacey, P.M.C., Chem. Eng. Sci., 19, 665-682, (1964) see also U.K.A.E.A. Report No. AERE -R3955 (1963).

Gill, L.E., Hewitt, G.F., and Lacey, P.M.C., Chem.Eng. Sci., 20, 71-88, (1965) see also U.K.A.E.A. Report No. AERE -R3935 (1962).

Gill, L.E., and Hewitt, G.F., Chem. Eng. Sci., 23, 667-687 (1968) see also U.K.A.E.A. Report No. AERE M1202 (1967).

Haas, F.C., A.I.Ch.E. Journal, 10, 920-924 (1964).

Haenlein, A., Forsch. Ing. Wes., 2, 139 (1931) English Transl. NACA TM 659 (1932).

Hagerty, W.W., and Shea, J.F., A.S.M.E., J. Appl. Mech., 22, 509-514 (1955).

Hall Taylor, N., Hewitt, G.F., and Lacey, P.M.C., Chem. Eng. Sci., 18, 537-552 (1963) see also U.K.A.E.A. Report No. AERE -R3953 (1962).

Hall Taylor, N.S., and Nedderman, R.M., Chem. Eng. Sci., 23, 551-564 (1968).

Hanratty, T.J., and Lillelehet, L.U., J. Fluid Mech., 11, 65-81 (1961).

Hanratty, T.J., and Lillelehet, L.U., A.I.Ch.E. Journal, 7, 548-550 (1961).

Hanratty, T.J., and Hershmann, A., A.I.Ch.E. Journal, 7, 488-497 (1961).

Hanratty, T.J., and Woodmansee, D.E., Proc. Symp. on Two Phase Flow, Vol. I, Paper A1, University of Exeter, United Kingdom (1965).

Hartley, D.E., and Roberts, D.C., Nuclear Research Memorandum Q6, Queen Mary College, University of London (1961).

Hewitt, G.F., U.K.A.E.A. Report No. AERE -R3680 (1961).

Hinze, J.O., A.I.Ch.E. Journal, 1, 289-295 (1955).

Hoogendoorn, C.J., and Welling, W.A., Proc. Symp. on Two Phase Flow, Vol. I, Paper C3, University of Exeter, United Kingdom (1965).

Hopf, L., Ann. Physik, 4 , 32, 777-808 (1910).

Houze, N., and Dukler, A.E., Proc. Symp. on Two Phase Flow, Vol. I, Paper C1, University of Exeter, United Kingdom (1965).

Hughmark, G.A., and Pressburg, G.S., A.I.Ch.E. Journal, 7, 677-682 (1961).

Huyghe, J., and Truong, Q.M., Comptes Rendus, 260, 2405-2408 (1965).

Ishihara, T., Iwagaki, Y., and Iwasa, Y., Trans. Am. Soc. Civil Engrs., 126, Pt. 1, 548-563 (1961).

Kapitza, P.L., Zhur. Eksper. Teor Fiz., 18, 3-18 (1948).

von Kármán, T., Trans. A.S.M.E., 61, 705-710 (1939).

Kelvin, Lord (1871) Mathematical and Physical Papers, 4, 76-85. Cambridge University Press (1910).

Knuth, E.H., Jet Propuls., 24, 359-365 (1954); 25, 16-25 (1955).

Lacey, P.M.C., Hewitt, G.F., and Collier, J.G., Proc. Symp. Two Phase Fluid Flow, Instn. Mech. Engrs., London (1962) see also U.K.A.E.A. Report No. AERE -R3962 (1962).

Laird, A.D.K., Trans. A.S.M.E., 76, 1005-1010 (1954).

Lamb, H., "Hydrodynamics" 6th Ed. Dover (1945).

Lee, J., A.I.Ch.E. Journal, 10, 540-544 (1964).

Levich, V.G., Zhur. Fiz. Kim., 22, 721 (1948).

Levich, V.G., "Fiziko-Khimicheskaya Gidrodinamika", 2nd Ed., Fizmatgiz, Moscow (1959); English Transl. "Physico-Chemical Hydrodynamics", Prentice-Hall, Englewood Cliffs, New Jersey (1962).

Levy, S., GEAP-4193, General Electric Co., San Jose, California (1963).

Levy, S., Int. J. Heat Mass Transfer, 9, 171-188 (1966).

Lighthill, M.J., and Whitham, G.B., Proc. Roy. Soc., Series A, 229, 281-316 (1955).

Longwell, J.P., and Weiss, M.A., Ind. Eng. Chem., 45, 667-677 (1953).

Martinelli, R.C., and Lockhart, R.W., Chem. Eng. Prog., 45, 39-50 (1949).

Massot, C., Irani, F., and Lightfoot, E.N., A.I.Ch.E. Journal, 12, 445-455 (1966).

Messenger, M.J., Ph.D. Thesis, University of Adelaide (1964).

Michell, J.H., Phil. Mag., 5th Series, 36, 430-437 (1893).

Miles, J.W., J. Fluid Mech., 3, 185-204 (1957).

Miles, J.W., J. Fluid Mech., 6, 568-582 (1959a); 583-598 (1959b).

Miles, J.W., J. Fluid Mech., 13, 433-448 (1962).

Mugele, R.A., and Evans, H.D., Ind. Eng. Chem., 43, 1317-1324 (1951).

Nedderman, R.M., and Shearer, C.J., Chem. Eng. Sci., 18, 661-670 (1963).

Nelson, P.A., and Stevens, W.F., A.I.Ch.E. Journal, 7, 80-86 (1961).

Nusselt, W., Z. Ver. Deut. Ing., 60, 27, 541-546 (1916); 60, 28, 569-575 (1916).

Ostrach, S., and Koestel, A., A.I.Ch.E. Journal, 11, 294-303 (1965).

Paleev, I.I., and Filippovich, B.S., Int. J. Heat Mass Transfer, 9, 1089-1093 (1966).

Parker, J.D., and Grosh, J.L., Argonne National Laboratory Report, ANL-6291 (1961).

Pletcher, R.H., and McManus, H.N., Int. J. Heat Mass Transfer, 11, 1087-1104 (1968).

Portalski, S., Ph.D. Thesis, University of London (1960).

Portalski, S., Chem. Eng. Sci., 18, 787-804 (1963); 19, 575-582 (1964).

Quandt, E.R., A.I.Ch.E. Journal, 11, 311-318 (1965) see also U.S. Atomic Energy Commission WAPD-T-1507 (1962)

Rayleigh, Lord, Proc. London Math. Soc., 10, 4-13 (1879). see also Theory of Sound, Vol. II, 351-362, Dover, New York (1945)

van Rossum, J.J., Chem. Eng. Sci., 11, 35-52 (1959).

Shearer, C.J., Ph.D. Thesis, University of Cambridge (1964).

Shearer, C.J., and Nedderman, R.M., Chem. Eng. Sci., 20, 671-683 (1965).

Smith, T.N., Ph.D. Thesis, University of Adelaide (1964).

Squire, H.B., Brit. J. App. Phys., 4, 167-169 (1953).

Truong, Q.M., and Huyghe, J., Proc. Symp. on Two Phase Flow, Vol. I, Paper C2, University of Exeter, United Kingdom (1965).

Wallis, G.B., A.S.M.E., 1961 International Heat Transfer Conference, Part II, 38, 319-340, Boulder, Colorado.

Wallis, G.B., General Electric Report No. 62 GL127 (1962).

Wallis, G.B., U.S. Atomic Energy Commission Report No. NYO 3114-14 (1966).

Wallis, G.B., Int. J. Heat Mass Transfer, 11, 783-785 (1968).

Weber, C., Z. Augen. Math. Mech., 11, 136 (1931).

Whitaker, S., Ind. Eng. Chem. Fundamentals, 3, 132-142 (1964).

Wicks, M., and Dukler, A.E., A.I.Ch.E. Journal, 6, 463-468 (1960).

Wicks, M., Ph.D., Dissertation, University of Houston (1967).

Wicks, M., Int. J. Heat Mass Transfer, 11, 785-786 (1968).

Wilkes, J.O., and Nedderman, R.M., Chem. Eng. Sci., 17, 177-187 (1962).

York, J.L., Stubbs, H.E., and Tek, M.R., Trans. A.S.M.E. 75, 1279-1286 (1953).